Metabolic rewiring compensates for the loss of amino acid biosynthesis in *Bacillus subtilis*

Dissertation to obtain the doctoral degree of Natural Sciences (Dr. rer. nat.)

Faculty of Natural Sciences

University of Hohenheim

Institute of Biology

submitted by

Mohammad Saba Yousef Mardoukhi

from *Sanandaj*

2024

Examination board

Supervisor

Prof. Dr. Fabian M. Commichau / Department of Molecular Microbiology (190 h)

The examination committee

Prof. Dr. Fabian M. Commichau / Department of Molecular Microbiology (190 h)

Prof. Dr. Julia Fritz-Steuber / Department of Cellular Microbiology (190 i)

Prof. Dr. Florian Fricke / Department of Microbiome and Applied Bioinformatics (140 d)

Dean of the Faculty of Natural Sciences

Prof. Dr. Jan Frank

Date of the oral examination:

May 12th, 2025

علم علم بر برین بالا

تا برو چون علم شوی والا

علم نورست و جهل تاریکی

علم راهت برد به باریکی

اوحدی

Seek knowledge, rise to the highest height,
Through it, you'll shine like a beacon bright

Knowledge is light, ignorance but despair,
Knowledge will guide you with utmost care

Ohadi

Acknowledgments

First and foremost, I would like to express my deepest gratitude to my supervisor, Fabian. Thank you for giving me the opportunity to pursue my PhD under your guidance and for your unwavering support throughout this journey. Your kindness, patience, and encouragement during both the highs and the lows of my doctoral career have been invaluable. Without your mentorship, I would not have reached this stage. You consistently pushed me forward and guided me through challenges with remarkable understanding and care, embracing my cultural differences and calmly addressing my mistakes. I am truly honored to have taken this important step under your supervision.

I am also deeply thankful to my colleagues from our previous lab in Senftenberg: Robert, Katarina, Carolin, and Kerstin. Your warmth and support created a sense of belonging that felt like home. Robert, your friendly advice and encouragement inspired me to keep going, and I learned something new every time we met.

To my fellow PhD colleagues—Mengyi, Inge, Katharina, and Sabrina—thank you for your kindness, support, and for helping me grow personally and professionally. You introduced me to German culture, guided me through regulations, and offered constructive criticism that greatly improved my work.

I extend my heartfelt thanks to Gisela, Simone, Renate, Doro, Betty, and Lutz for your support during this chapter of my life. Gisela and Renate, you were like older sisters to me, always willing to listen and provide comfort during difficult times. Simone, despite our language barrier, your patience and warm smile made tackling official challenges much easier. Thank you all for your invaluable support.

A special thanks to my exceptional students—Janina, Renato, Nils, and Lucca—who played a significant role in shaping my thesis. I wish each of you great success in both your professional and personal endeavors.

I would also like to acknowledge Julia, Günter, and their team. Our joint seminars were intellectually enriching, and the discussions we had contributed significantly to the development of my research.

I cannot adequately express my gratitude to my late uncle, whose belief in my potential and encouragement to pursue a brighter future laid the foundation for my journey to Germany. His wisdom and vision have been a guiding light. May he rest in peace.

To my family—Dad, Mom, Sina, and Sana—thank you for being my constant source of strength and encouragement. Despite the physical distance over the past few years, your unwavering belief in me and pride in my achievements kept me going. I am profoundly grateful for your love and support, which have shaped who I am today.

Finally, to my beloved wife, Mohadese. From the moment you entered my life, everything changed for the better. You helped me overcome my weaknesses, believed in me, and stood by my side through every challenge. Your unwavering love, support, and faith have been the cornerstone of my success. Words cannot fully capture my gratitude for your presence in my life. I dedicate this dissertation to you, as this accomplishment is as much yours as it is mine.

Table of Contents

List of Abbreviations

General abbreviations

% (w/v)	% (weight/volume)
ABC transporters	ATP binding cassette transporters
ATP	Adenosine triphosphate
BHI	Brain Heart Infusion
CAA	Casamino acids
CAF	Ammonium iron citrate
Cit	Citrate
DNA	Deoxyribonucleic acid
et al.	*et alii*
$FADH_2$/FAD	Flavin adenine dinucleotide
Fig.	Figure
GDH	Glutamate dehydrogenase
Glc	Glucose
GOGAT	Glutamine oxoglutarate aminotransferase
GS	Glutamine Synthetase
kbp	Kilo base pairs
Km	Michaelis-Menten constant (enzyme activity)
LB	Lysogeny broth
Mal	Malate
mRNA	Messenger RNA
$NADH/NAD^+$	Nicotinamide adenine dinucleotide
$NADPH/NADP^+$	Nicotinamide adenine dinucleotide phosphate
ONPG	o-Nitrophenol-β-D-galactopyranosid
PAGE	Polyacrylamide gel electrophoresis
PAP	6x SDS loading dye
PCR	Polymerase chain reaction
pH	Potential of hydrogen
RNA	Ribonucleic acid
SDS	Sodium dodecyl sulfate
Suc	Succinate
Tab.	Table
TCA cycle	Tricarboxylic Acid cycle
TEMED	N,N,N´,N´-tetramethylethylendiamine
Tm	Melting temperature
TRIS	Tris-(hydroxymethyl)-aminomethane
tRNA	Transfer RNA
WT	Wild type
X-gal	5-bromo-4-chloro-3-indolyl-β-D-galactopyranoside
Δ*gene*	Deletion of the gene

Nucleotides

A	Adenine
C	Cytosine
G	Guanine
T	Thymine
U	Uracil

Units

°C	Degree centigrade
Bar	Bar
bp	Base pairs
Da	Dalton
g	Gram
h	Hour
l	Liter
M	Molar
min	Minute
OD	Optical density
rpm	Rounds per minute
sec	Seconds

Prefix

m	milli (10^{-3})
µ	micro (10^{-6})
n	nano (10^{-9})
p	pico (10^{-11})

Amino acids

A	Alanine (Ala)
C	Cysteine (Cys)
D	Aspartic acid (Asp)
E	Glutamic acid (Glu)
F	Phenylalanine (Phe)
G	Glycine (Gly)
H	Histidine (His)
I	Isoleucine (Ile)
K	Lysine (Lys)
L	Leucine (Leu)
M	Methionine (Met)
N	Asparagine (Asn)
P	Proline (Pro)
Q	Glutamine (Gln)
R	Arginine (Arg)
S	Serine (Ser)
T	Threonine (Thr)
V	Valine (Val)
W	Tryptophan (Trp)
Y	Tyrosine (Tyr)

Publications

Mardoukhi MSY, Rapp J, Irisarri I, Gunka K, Link H, Marienhagen J, de Vries J, Stülke J, Commichau FM (2024). Metabolic rewiring enables ammonium assimilation via a non-canonical fumarate-based pathway. *Microb Biotechnol*. 17(3):e14429. doi: 10.1111/1751-7915.14429.

Riedel R, Commichau FM, Benndorf D, Hertel R, Holzer K, Hoelzle LE, **Mardoukhi MSY**, Noack LE, Martienssen M (2024). Biodegradation of selected aminophosphonates by the bacterial isolate *Ochrobactrum* sp. BTU1. *Microbiol Res*. 280:127600. doi: 10.1016/j.micres.2024.127600.

Meißner J, Königshof M, Wrede K, Warneke R, **Mardoukhi MSY**, Commichau FM, Stülke J (2024). Control of asparagine homeostasis in *Bacillus subtilis*: identification of promiscuous amino acid importers and exporters. *J Bacteriol*. 206(2):e0042023. doi: 10.1128/jb.00420-23.

Ahmadi S, **Mardoukhi MSY**, Salehi M, Saijadi S, Keihan AH (2019) Molecular dynamics simulation of lactate dehydrogenase adsorption onto pristine and carboxylic-functionalized graphene. *Molecular Simulation*. 45(16), 1305–1311. doi: 10.1080/08927022.2019.1632447.

Conference contributions

21st International Conference on *Bacilli* and Gram-positive Bacteria 14 - 17 June 2022: **poster presentation**
Prague, Czech Republic
Saba Mardoukhi, Fabian M. Commichau. Metabolic rewiring compensates for the loss of glutamate biosynthesis in *Bacillus subtilis*.

BACELL Meeting 19 - 20 June 2023: **talk**
Stuttgart, Germany
Saba Mardoukhi, Johanna Rapp, Hannes Link, Fabian M. Commichau. Metabolic rewiring compensates for the loss of glutamate and aspartate/asparagine biosynthesis in *Bacillus subtilis*.

VAAM annual conference 10 - 13 September 2023: **poster presentation**
Göttingen, Germany
Saba Mardoukhi, Fabian M. Commichau. Establishment of an interspecies cross-feeding community to identify novel players in vitamin B6 metabolism.

Summary

Amino acids are considered as some of the earliest organic molecules to form on Earth. Serving as the building blocks of proteins, they are intricately connected to nearly every life process. Therefore, amino acid metabolism needs to be precisely regulated in any living organism. Amino acid metabolism includes the biochemical pathways responsible for the synthesis, degradation, and utilization of amino acids. Most of the bacteria, particularly the Gram-positive model bacterium *Bacillus subtilis*, have the capability to synthesize all proteinogenic amino acids or, if available, import them from the environment. Throughout evolution, different metabolic pathways have emerged to maintain metabolites level inside the cells. Some biosynthetic pathways are unknown as they are not primary routes or are typically inactive under normal conditions. However, they may become active under specific circumstances. Two very important pathways, previously not known to be substituted by alternative routes, involve *de novo* biosynthesis of glutamate, which is an essential amino group donor in every cell. Many bacteria can synthesize glutamate using a NADPH + H^+-dependent glutamate dehydrogenase (GDH). Alternatively, glutamate can be produced by the combined action of the ATP-dependent glutamine synthetase (GS) and the NADPH + H^+-dependent glutamate synthase (GOGAT). *B. subtilis* only employs the GS-GOGAT pathway for *de novo* synthesis of glutamate. In the context of this work, it was shown that a *B. subtilis* deficient for the GS-GOGAT pathway may employ the aspartase AnsB and aspartate transaminase AspB for the synthesis of glutamate in biologically significant amounts. Genetic analyses revealed that the aspartase AnsB converts ammonium and the tricarboxylic acid cycle intermediate fumarate to aspartate. Subsequently, the aspartate transaminase AspB transfers the amino group from aspartate to α-ketoglutarate, resulting in the production of L-glutamate and oxaloacetate. This observation challenges the well-established point of view of whether the GS-GOGAT-dependent pathway is indeed the only route for *de novo* synthesis of glutamate in nature. It was also set out to explore which amino acids could serve as the sole sources of carbon and nitrogen in the background of a *B. subtilis* strain that is a genetically stable glutamate auxotroph. The aim was to understand the conversion of the amino acids into glutamate and further to α-ketoglutarate, a reaction that is facilitated by the enzymatic activity of the GDHs RocG/GudB. It turned out that some of the amino acids are toxic for *B. subtilis*. However, *B. subtilis* can quickly develop resistance by the acquisition of mutations that result in reduced and enhanced amino acid uptake and export, respectively. Moreover, the toxicity of some amino acids may be reduced by increased degradation of glutamate. Furthermore, with focus on the toxicity of asparagine, it could be demonstrated that AimA, which has been characterized as a general amino acid importer, serves as a low affinity asparagine transporter in *B. subtilis*. Finally, AzlCD, which was previously described as an exporter for histidine and branched-chain amino acids, also exports asparagine. Thus, *B. subtilis* can adapt to amino acid toxicity in various ways.

Zusammenfassung

Aminosäuren gehören zu ersten organischen Molekülen, die sich auf der Erde gebildet haben. Als Bausteine von Proteinen sind sie eng mit nahezu jedem Lebensprozess verbunden. Daher muss der Aminosäurestoffwechsel in jedem lebenden Organismus genau reguliert werden. Der Aminosäurestoffwechsel umfasst die biochemischen Wege, die für die Synthese, den Abbau und die Nutzung von Aminosäuren verantwortlich sind. Die meisten Bakterien, insbesondere das Gram-positive Modellbakterium *Bacillus subtilis*, besitzen die Fähigkeit, alle proteinogenen Aminosäuren zu synthetisieren oder, sofern verfügbar, aus der Umwelt zu importieren. Im Laufe der Evolution haben sich verschiedene Stoffwechselwege herausgebildet, um den Metabolitenspiegel in den Zellen aufrechtzuerhalten. Einige Biosynthesewege sind unbekannt, da sie keine primären Wege sind oder unter normalen Bedingungen typischerweise inaktiv sind. Unter bestimmten Umständen können sie jedoch aktiv werden. Zwei sehr wichtige Wege, von denen bisher nicht bekannt war, dass sie durch alternative Wege ersetzt werden können, umfassen die *de novo*-Biosynthese von Glutamat, einem essenziellen Aminogruppendonor in jeder Zelle. Viele Bakterien können Glutamat mithilfe einer NADPH + H^+-abhängigen Glutamatdehydrogenase (GDH) synthetisieren. Alternativ kann Glutamat durch die Zusammenarbeit der ATP-abhängigen Glutamin-Synthetase (GS) und der NADPH + H^+-abhängigen Glutamat-Synthase (GOGAT) hergestellt werden. *B. subtilis* nutzt ausschließlich den GS-GOGAT-Weg für die *de novo*-Synthese von Glutamat. Im Rahmen dieser Arbeit wurde gezeigt, dass ein *B. subtilis*, dem der GS-GOGAT-Weg fehlt, die Aspartase AnsB und die Aspartat-Transaminase AspB für die Synthese von Glutamat in biologisch signifikanten Mengen nutzen kann. Genetische Analysen ergaben, dass die Aspartase AnsB Ammonium und das Zwischenprodukt des Tricarbonsäurezyklus, Fumarat, in Aspartat umwandelt. Anschließend überträgt die Aspartat-Transaminase AspB die Aminogruppe von Aspartat auf α-Ketoglutarat, was zur Produktion von L-Glutamat und Oxalacetat führt. Diese Beobachtung stellt die etablierte Sichtweise in Frage, ob der GS-GOGAT-abhängige Weg tatsächlich der einzige Weg für die *de novo*-Synthese von Glutamat in der Natur ist. Außerdem sollte untersucht werden, welche Aminosäuren als einzige Kohlenstoff- und Stickstoffquellen für eine genetisch stabilen Glutamat-bedürftigen *B. subtilis*-Stamm dienen. Ziel war es, die Umwandlung der Aminosäuren in Glutamat und weiter in α-Ketoglutarat zu verstehen, eine Reaktion, die durch die enzymatische Aktivität der GDHs RocG/GudB katalysiert wird. Es stellte sich heraus, dass einige der Aminosäuren für *B. subtilis* toxisch sind. Allerdings kann *B. subtilis* durch den Erwerb von Mutationen, die zu einer verringerten Aminosäureaufnahme bzw. einem verstärkten Aminosäureexport führen, schnell eine Resistenz entwickeln. Darüber hinaus kann die Toxizität einiger Aminosäuren durch einen erhöhten Glutamat-Abbau verringert werden. Darüber hinaus konnte mit Fokus auf die Toxizität von Asparagin gezeigt werden, dass AimA, das als allgemeiner Aminosäureimporteur charakterisiert wurde, in *B. subtilis* als Asparagin-Transporter mit niedriger Affinität fungiert. Schließlich exportiert der AzlCD-Komplex, der zuvor als

Exporter für Histidin und verzweigtkettige Aminosäuren beschrieben wurde, auch Asparagin. Somit kann sich *B. subtilis* auf verschiedene Weise an die Aminosäuretoxizität anpassen.

Introduction

Amino acids were among the initial organic molecules to emerge on Earth (Kvenvolden et al., 1970), and they are fundamental components of macronutrients, alongside carbohydrates and fatty acids, in all living organisms. They serve as the building blocks of proteins, which are critical to the structure and function of cells and tissues. Beyond their role in protein synthesis, amino acids participate in various metabolic pathways, influencing growth, repair, and overall physiological homeostasis (Wu, 2009). Among the amino acids, L-glutamate stands out due to its multifunctional roles in all life kingdoms, especially in all organisms. While it is best known for being a key player in protein synthesis, L-glutamate also acts as a pivotal neurotransmitter in the central nervous system and plays a significant role in cellular metabolism and the regulation of nitrogen balance (Meldrum, 2000, Brosnan, 2003). L-Glutamate is classified as a non-essential amino acid in human, as it can be synthesized endogenously through transamination reactions; However, its demand can rise under certain physiological conditions such as rapid growth or stress, making dietary intake beneficial (Reeds, 2000). L-Glutamate-rich foods, including meat, fish, and certain fermented products, contribute significantly to dietary protein quality and flavor enhancement, as this amino acid is also recognized for its role as a flavoring agent due to its umami taste (Yamaguchi & Ninomiya, 2000). The increasing global population necessitates sustainable and efficient methods for producing amino acids like L-glutamate to meet rising nutritional and industrial demands. Advances in biotechnology, particularly microbial fermentation, have revolutionized L-glutamate production, enabling large-scale synthesis with reduced environmental impact compared to chemical methods (Ikeda, 2003; Wendisch, 2016). Microbial production, predominantly utilizing strains of *Corynebacterium glutamicum*, is now a cornerstone of the amino acid industry, and lots of worldwide researches focus on optimizing metabolic pathways to further improve yields and sustainability (Eggeling & Bott, 2005; Becker et al., 2013).

The model bacterium *Bacillus subtilis*

B. subtilis, a Gram-positive bacterium, holds a prominent position as one of the most extensively studied organisms after *Escherichia coli* (Sonenshein et al., 2002). The ease of cultivation and well-characterized genetics of *B. subtilis* have established it as an invaluable model organism for studying various biological processes (Stülke et al., 2023). *B. subtilis* which was initially described as *Vibrio subtilis* by Christian Gottfried Ehrenberg in 1835, was later renamed to *Bacillus subtilis* by Ferdinand Julius Cohn in 1872 (Ehrenberg, 1833; Hoppe, 1983). This bacterium gained scientific interest due to several reasons: Primarily, the sporulation cycle, initially documented by Cohn, offers a straightforward model for investigating processes related to cell differentiation and development. Secondly, the nonpathogenic nature, versatile metabolism, and ease of

cultivation of *B. subtilis* render it valuable for various applications (L. Sonenshein et al., 1993). These applications span from the traditional food production in Asia through the fermentation of soybeans, such as Natto in Japan, to the synthesis of vitamins, amino acids, and enzymes for detergent formulations (Moir, 1990; Stülke et al., 2023). Thirdly, *B. subtilis* shares lineage with several important Gram-positive pathogens, including *Bacillus anthracis*, *Staphylococcus aureus*, and *Listeria monocytogenes*. *B. subtilis* serves as the prototype organism for these pathogens and all other Firmicutes (Nakamura, 1989; Ivanova et al., 2003). Lastly, *B. subtilis* exhibits rapid growth and is amenable to genetic manipulation, facilitated by its capacity to uptake foreign DNA and integrate it into its own genome (Borriss et al., 2018).

Also, *B. subtilis*'s adaptability and resistance to elevated temperatures happens through the formation of spores (Hoppe, 1983). Cohn's pioneering work on *B. subtilis* and its ability to form spores played a pivotal role in the establishment of pasteurization, a critical method in the food industry for ensuring food safety (Stülke et al., 2023).

Ecology of *B. subtilis*

B. subtilis is also known as the hay bacillus or grass bacillus because of its historical association with hay and its common occurrence in hay and straw (Priest, 2014; Stülke, 2023). It can be frequently found in decomposing plant material, including haystacks, silage, and soil rich in organic matter (Ehrenberg, 1833). The term "hay bacillus" was likely used informally by early microbiologists and researchers to describe *B. subtilis* based on its common occurrence in hay and straw samples. However, the specific individual who first used this term is not well-documented in scientific literature. *B. subtilis* is not limited to environmental sources such as hay and straw; it can also be found and isolated from the gastrointestinal tracts of diverse organisms, including ruminants, humans, and marine sponges (Rahman et al., 2020; Paul et al., 2021). In a study conducted in 2009, the density of *B. subtilis* spores in soil was compared to that in human feces. The findings revealed approximately 106 spores per gram in soil, contrasting with approximately 104 spores per gram in human feces (Hong et al., 2009). However, it is categorized as a non-pathogenic bacterium with a low likelihood of causing disease in humans (N. K. Lee et al., 2019). Interestingly, in certain bee habitats, scientists could also find and isolate *B. subtilis* from the gut flora of honeybees (Sudhagar et al., 2017).

Morphology of *B. subtilis*

The morphology of *B. subtilis* is characterized by its rod-shaped appearance, which resembles a symmetrical cylinder with rounded ends. The bacterium typically measures around 4–10 µm in length and 0.25–1.0 µm in diameter (Liu et al., 2022). *B. subtilis* possesses a thick cell wall, primarily composed of a dense peptidoglycan layer. During the Gram staining process, the bacterium retains the crystal violet dye even after the

washing step then appears purple under optical microscope. This retention of the dye is a characteristic feature of Gram-positive bacteria (Hoppe, 1983).

Lifestyle of *B. subtilis*

B. subtilis exhibits two modes of division: symmetrical division, yielding two daughter cells through binary fission, and asymmetrical division, resulting in a single endospore (Errington & Wu, 2017). These endospores have the remarkable ability to remain viable for extended periods, enduring adverse environmental conditions such as drought, salinity, extreme pH, radiation, and exposure to solvents. Endospore formation occurs during periods of nutritional stress, facilitated by hydrolysis, enabling the organism to endure in the environment until conditions become favorable once again (Stephens, 1998; Higgins & Dworkin, 2012; Riley et al., 2021;). While sporulation in *B. subtilis* is triggered by nutrient deprivation, the initiation of the sporulation developmental program does not occur immediately when growth slows due to a lack of nutrients (Riley et al., 2021). Various alternative responses may unfold, such as activating flagellar motility to search for new food sources through chemotaxis, producing antibiotics to eliminate competing soil microbes, secreting hydrolytic enzymes to scavenge extracellular proteins and polysaccharides, or inducing 'competence' for the uptake of external DNA, occasionally resulting in the stable integration of new genetic information (Dubnau, 1991; Aizawa, 2001; Schallmey et al., 2004; Stein, 2005; López & Kolter, 2010). Sporulation, serving as a last-resort response to starvation, remains suppressed until alternative responses are deemed insufficient (Stephens, 1998; Higgins & Dworkin, 2012; Riley et al., 2021).

The genome of *B. subtilis*

In the nascent stages of the genomic revolution during the 1990s, there arose a considerable interest in the comprehensive sequencing of the *B. subtilis* genome. This monumental endeavor was undertaken through a robust collaboration between European and Japanese laboratories (Kunst et al., 1997). After this pivotal achievement, the focus shifted towards the delineation of a core ensemble of essential genes. This initiative aimed to ascertain the expression dynamics of the complete spectrum of *B. subtilis* genes across an expansive array of 104 distinct conditions (Nicolas et al., 2012) and also, contributing to the formulation of an initial genome-reduced strain that was devoid of all prophages (Kobayashi et al., 2003). The genome of *B. subtilis* encompasses an estimated 4.2 kilo base pairs, encompassing a repertoire of 4,100 protein-coding genes (Kunst et al., 1997). Characterized by a low GC content, this bacterium's genome constitutes 43.5% GC content (Piggot, 2009). Out of 4,100 protein-coding genes, only 192 coding genes were proven to be indispensable, while an additional 79 were anticipated to be essential. Most of these essential genes were concentrated in a relatively small number of cell metabolism domains. Approximately half of them were

associated with information processing, one-fifth were engaged in the synthesis of the cell envelope and the regulation of cell shape and division, and one-tenth were linked to cell energetics (Barbe et al., 2009; Reuß et al., 2017).

Amino acids

Amino acids are organic compounds which possess two functional groups: amino and carboxylic acid (Boyle, 2005). Among more than 500 discovered amino acids in nature, only 22 of them exclusively manifests within the universal genetic code (or genetically encoded) which they are called “proteinogenic” (Koonin & Novozhilov, 2009).

In the early 1800s, French chemists Louis-Nicolas Vauquelin and Pierre Jean Robiquet made a groundbreaking discovery by extracting the first amino acids from asparagus. This newly identified compound was subsequently named asparagine (Vickery & Schmidt, 1931). After that, cystine was discovered in 1810 (Wollaston, 1810), although its monomer, cysteine, remained undiscovered until 1884 (Baumann, 1884). The final one among the 20 common amino acids, threonine, was discovered in 1935 by William Cumming Rose (Simoni et al., 2002).

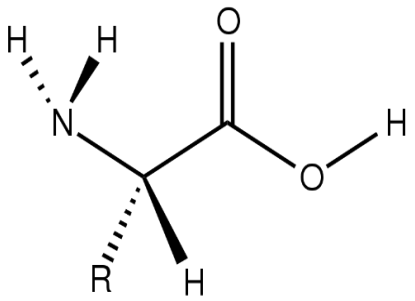

Figure 1. General structure of L-α-amino acids.

Amino acids typically exhibit a generic formula of $H_2NCHRCOOH$, where R denotes an organic substituent referred to as a "side chain" (Fig. 1). Classification of amino acids is contingent upon the location of this side chain, resulting in designations such as alpha (α-), beta (β-), gamma (γ-) amino acids, etc. Furthermore, their categorization is influenced by factors like polarity, ionization, and the type of side chain group like aliphatic, acyclic, aromatic, polar, etc. (Boyle, 2005).

Concerning the stereoisomers of the alpha carbon, all chiral proteogenic amino acids exhibit the “L” configuration, signifying "left-handed" enantiomers (McNaught & Wilkinson, 1997). However, there are exceptions, with a limited number of D-amino acids ("right-handed") observed in nature. Instances include their presence in bacterial envelopes (Thorne et al., 1955; Van Heijenoort, 2001; Leiman et al., 2013), as a neuromodulator (D-serine) (Wolosker et al., 2008), and in certain antibiotics (Michal & Schomburg, 2013). On rare occasions, D-amino acid residues are identified in proteins, typically arising through post-translational modifications from the L-amino acid form (Genchi, 2017).

Amino acids are monomers of proteins

Standard or *canonical* amino acids encompass a set of 20 amino acids directly encoded by the codons within the universal genetic code. In certain biological contexts, a modified form of methionine known as *N-formylmethionine* is commonly used as the initial amino acid in proteins, especially in bacteria, mitochondria, and chloroplasts (Arnold, 1977; Pelley, 2012). Beyond this standard set, there exists another category termed *nonstandard* or *non-canonical* amino acids. The majority of these are non-proteinogenic, meaning they cannot be incorporated into proteins during the translation process. However, it is noteworthy that two among this group are proteinogenic, indicating their ability to be translationally integrated into proteins by utilizing information not explicitly encoded in the universal genetic code (Boyle, 2005). Selenocysteine, which is found in many non-eukaryotes as well as most eukaryotes but is not directly coded by DNA (Johansson et al., 2005), and pyrrolysine, which is present in certain archaea and some bacteria (Rother & Krzycki, 2010), are the two nonstandard proteinogenic amino acids. For instance, selenocysteine is present in the primary structure of 25 proteins from human body (Johansson et al., 2005). Pyrrolysine and selenocysteine are encoded through variant codons. Notably, selenocysteine is encoded by a stop codon and a SECIS element. The SECIS element is an RNA element approximately 60 nucleotides long, adopting a stem-loop structure. This structural motif guides the cell to translate the stop codon UGA as selenocysteines (Walczak et al., 1996; Xie & Schultz, 2005; Elzanowski & Andrzej, 2010).

Non-protein functions of amino acids

Amino acids serve not only as precursors for proteins but also fulfill various other biological functions, encompassing both proteinogenic and non-proteinogenic amino acids. In many bacteria, such as *B. subtilis*, amino acids can function as the sole sources of carbon, nitrogen, and even energy (Meißner et al., 2022; Warneke et al., 2023). To uphold osmotic balance under hyperosmotic conditions, certain archaea and bacteria, such as *B. subtilis*, generate elevated quantities of proline as an osmoprotectant (Gunka & Commichau, 2012; Hoffmann et al., 2017). Within the human body, specific amino acids like tryptophan and tyrosine (along with its precursor phenylalanine) play roles as precursors for neurotransmitters. Tryptophan contributes to the synthesis of serotonin, while tyrosine participates in the production of dopamine, epinephrine, and norepinephrine (Cuevas, 2019). Furthermore, gamma-aminobutyric acid (GABA), a nonstandard amino acid, and glutamate serve as neurotransmitters in the human brain (Petroff, 2002). Additionally, nucleotides, vital components of nucleic acids, are synthesized from aspartate, glycine, and glutamine (Berg et al., 2002). Another noteworthy application is the use of L-dihydroxyphenylalanine (L-DOPA), derived from phenylalanine, in the treatment of Parkinson's disease (Kostrzewa et al., 2005).

Application of amino acids in industry

On an industrial scale, amino acids have long been utilized across various sectors, spanning from human and animal nutrition to pharmaceuticals and cosmetics. Within this multibillion-dollar market, the production of amino acids from the L-glutamate family (GFAAs), including L-glutamate, L-arginine, L-citrulline, L-ornithine, L-proline, L-hydroxyproline, γ-aminobutyric acid, and 5-aminolevulinic acid, predominantly relies on microbial fermentation. This process involves the use of genetically modified strains of *Corynebacterium glutamicum* and its related subspecies, *Corynebacterium crenatum* (Sheng et al., 2021).

In the animal feed industry, amino acids are incorporated into feed formulations to compensate for the depletion of essential amino acids like tryptophan, threonine, lysine, or methionine (Leuchtenberger et al., 2005). Amino acids have also been employed extensively in the production of herbicides and pesticides. For instance, glyphosate, the most widely known and used herbicide globally, is originally synthesized from glycine (Chenier, 2002). Furthermore, aztreonam, a β-lactam antibiotic with selective activity against Gram-negative aerobic bacteria, can be derived from threonine (Floyd et al., 1982; Slusarchyk et al., 1984).

It comes as no surprise that the primary consumption of amino acids occurs in the food industry, with particular emphasis on glutamic acid. This amino acid is widely utilized as a flavor enhancer (Garattini, 2000). Additionally, the well-known artificial sweetener Aspartame (aspartylphenylalanine 1-methyl ester) is a major player in the beverage industry. Aspartame, approximately 200 times sweeter than sucrose but significantly lower in calories, is derived from a combination of aspartic acid and phenylalanine (Magnuson et al., 2007). Amino acids also find common use as preservatives in various food and beverage products. Cysteine, for instance, is frequently employed as an antioxidant in fruit juices (Montgomery, 1983; Iyidoğan & Bayindirli, 2004). Furthermore, in the context of extending the shelf life of milk powder, a combination of tryptophan and histidine is utilized as an antioxidant compound (Samtiya et al., 2022). One of the interesting utilizations of arginine involves its incorporation as an additive in toothpaste and various dental products to alleviate tooth sensitivity. Arginine, functioning similar to dentin (a crucial regulator of tooth sensitivity), serves as a mineral with the potential to provide relief in this context (Chakraborty & Burne, 2017; Ayad et al., 2018).

Chemical synthesis of amino acids

The commercial-scale production of amino acids typically involves the use of engineered bacteria, which consume glucose as a carbon source to produce individual amino acids. However, some amino acids are manufactured through the conversion of synthetic intermediates utilizing enzymes. For example, the production of aspartic acid entails the addition of an ammonium group to the carbon backbone of fumarate, facilitated by a

lyase enzyme (Tosa et al., 1974). Another illustration involves the industrial utilization of 2-aminothiazoline-4-carboxylic acid to produce L-cysteine (Takumi et al., 2017).

Biosynthesis of amino acids

Organisms have the capability to internally synthesize amino acids, rendering them "prototrophic" for those specific amino acids. In contrast, if an organism lacks the ability to synthesize certain amino acids, it is termed "auxotrophic". The majority of members in the plant and bacterial kingdoms exemplify prototrophic organisms, proficient in synthesizing all 22 amino acids utilizing glucose as a carbon source and ammonium as a nitrogen source. Conversely, mammalian cells are classified as essential amino acid consumers, necessitating the uptake of specific amino acids from their dietary intake (Naylor et al., 1976; Seif et al., 2020). Most plants and bacteria exhibit the capacity to assimilate ammonia into amino acids via the reductive amination of α-ketoglutarate and producing glutamate (Gunka & Commichau, 2012). Conversely, ammonia poses a considerable toxicity risk to mammalian cells. Therefore, glutamine assumes a pivotal role as the carrier molecule for ammonia in this context (Amorim & Blanchard, 2017).

Biosynthesis of amino acids in *B. subtilis*

The majority of bacterial species exhibit the capability to uptake all 22 amino acids from the environment if available, employing an array of specific and non-specific transporters developed over the course of evolution. Additionally, they possess the ability to digest or degrade amino acids from external sources such as peptides and proteins. Furthermore, in environments devoid of amino acids, such as minimal media, many bacteria, including *B. subtilis*, demonstrate the capacity to systematically utilize glucose and ammonium as the sole sources of carbon and nitrogen, respectively, to synthesize all 22 proteinogenic amino acids (Reuß et al., 2016; Warneke et al., 2023; Meißner et al., 2024).

Biosynthesis of glutamate in *B. subtilis*

Across all life kingdoms, glutamate assumes the most critical role as a primary nitrogen contributor, constituting approximately 80 to 88 percent of the nitrogen allocated for the biosynthesis of the entire biomass, encompassing other amino acids, as well as building blocks for DNA and RNA. Also, it can be directly integrated into proteins. In contrast, glutamine, another significant amino donor, contributes only around 20 percent of the nitrogen supply (Magasanik, 2003; Oh et al., 2007; He et al., 2023). From an anabolism perspective, in *B. subtilis*, glutamate serves as an amino group donor in more than 37 cellular reactions (Gunka & Commichau, 2012). This is particularly significant because the standard free energy for these transamination reactions is almost zero. Therefore, to

propel these reactions forward, it is imperative to maintain a high intracellular glutamate concentration (Goelzer et al., 2008; Oh et al., 2007; Bennett et al., 2009). Despite the significant role of glutamate in anabolism, it also plays a crucial role as an osmoprotectant in some archaea and bacteria. In hyperosmotic environments, cells produce a substantial amount of glutamate, on a molar scale, to prevent the outflow of intracellular water (Csonka et al., 1994; Saum et al., 2006; Frank et al., 2021). In *B. subtilis*, proline assumes the role of an osmoprotectant, originating from the conversion of glutamate to proline while cells sense a hyperosmotic condition (Gunka & Commichau, 2012; Bremer & Krämer, 2019; Stecker et al., 2022). Furthermore, to uphold electric neutrality within the intracellular space, glutamate, with its negative charge, acts as a counterion for potassium, the most positively charged ion inside the cells (McLaggan et al., 1994; Epstein, 2003; Gundlach et al., 2018; Krüger et al., 2020, 2021).

Given the numerous crucial functions of glutamate, maintaining high levels of this compound within the cell is essential. To achieve this, bacteria primarily attempt to uptake glutamate from their surroundings if available. Through evolution, *B. subtilis* has developed two specific glutamate transporters, GltT and GltP, both characterized as glutamate symporters. GltT serves as the primary high-affinity Na^+-coupled glutamate/aspartate symport protein, playing a role in the uptake of glyphosate[1] as well (Zaprasis et al., 2015). On the other hand, GltP functions similarly to an H^+/glutamate symporter and serves as a minor transporter for glyphosate but is not necessary for glutamate transport (Tolner et al., 1995). Furthermore, there exists a nonspecific transporter known as AimA, which, besides facilitating the import of other amino acids such as serine and asparagine, also functions as a low-affinity symporter for glutamate. (Krüger et al., 2021; Meißner et al., 2024).

Nevertheless, in a medium devoid of glutamate or any other amino acids convertible to glutamate, bacteria, including *B. subtilis*, endeavor to synthesize glutamate autonomously. In nature, two prominent glutamate biosynthesis pathways have been documented: 1) the conversion of α-ketoglutarate to glutamate via GDH, involving an $NADPH_2$-dependent ammonium reduction reaction, and 2) the amino transformation from glutamine to α-ketoglutarate facilitated by the Glutamine Oxoglutarate Aminotransferase (GOGAT), yielding one molecule of L-glutamate. The required glutamine for this reaction is derived from an ATP-dependent process that incorporates ammonium into glutamate through the activity of GS (Commichau, et al., 2006; Sonenshein, 2007). It is intriguing to consider that the reason many bacteria maintain both distinct pathways for glutamate synthesis lies in the fact that the GS–GOGAT-dependent pathway necessitates ATP, while the GDH reaction does not. Specifically, GS exhibits a higher affinity for ammonia compared to GDH (Reitzer, 2003; Rehm & Burkovski, 2011). This implies that GDH is only active at high intracellular ammonia concentrations (Reitzer, 2003). Consequently, bacteria retain the advantage of synthesizing glutamate in diverse media with varying nitrogen concentrations; In

[1] glyphosate is the most frequently used herbicide worldwide (O Duke & B Powles, 2008).

nitrogen-limited conditions, bacteria prefer the GS–GOGAT pathway, despite the energy expenditure of breaking an ATP molecule in each reaction. Conversely, in energy-poor environments with high external ammonia concentrations, the bacteria favor the GDH pathway for glutamate synthesis due to its greater energy efficiency (Helling, 1998; Reitzer, 2003; Gunka & Commichau, 2012). In summary, the presence of two distinct glutamate biosynthesis pathways provides bacteria with the flexibility to maintain a high glutamate pool, subsequently high growth rate, in various environmental conditions.

Although, many bacterial species are able to employ both pathways to synthesize glutamate, *B. subtilis* exclusively uses the ATP-dependent GS-GOGAT cycle to assimilate ammonium to L-glutamate due to the low affinity of the GDH enzymes GudB/RocG to ammonium (Commichau et al., 2008). The entire process of L-glutamate biosynthesis in *B. subtilis* involves the proficient conversion of glucose to pyruvate through the glycolysis pathway, followed by the entry of acetyl-CoA into the TCA cycle to generate α-ketoglutarate, the precursor to L-glutamate. Subsequently, in an amino transformation reaction independent of energy consumption, α-ketoglutarate acquires an amino group from one molecule of glutamine through the action of GOGAT. This complex enzyme comprises two subunits encoded by an operon consisting of *gltA*, *gltB*, and a transcription activator, *gltC* (Bohannon & Sonenshein, 1989; Belitsky & Sonenshein, 1995; Jayaraman et al., 2022). This reaction results in the production of two molecules of glutamate, one of which is utilized by GS (encoded by *glnA*) to synthesize a molecule of L-glutamine. In this process, one molecule of ammonium is assimilated into L-glutamate to produce one molecule of L-glutamine, requiring energy for its execution. This energy is derived from the conversion of ATP to ADP (Schreier et al., 1989; Travis et al., 2022). In conclusion, a cycle is established through the collaboration between GOGAT and GS, referred to as the GS-GOGAT cycle. Also, it can be asserted that glutamate biosynthesis serves as a crucial metabolic intersection, functioning as a bridge between carbon metabolism and nitrogen metabolism (Fig. 2; Sonenshein, 2007; Commichau et al., 2008; Gunka & Commichau, 2012). It is important to note that all enzymes involved in the biosynthesis and degradation of L-glutamate in *B. subtilis* exhibit bifunctionality. This dual functionality allows these enzymes to contribute to the dynamic regulation of glutamate homeostasis (Commichau, Forchhammer, et al., 2006b; Commichau, Wacker, et al., 2006; Gunka & Commichau, 2012; Stannek et al., 2015).

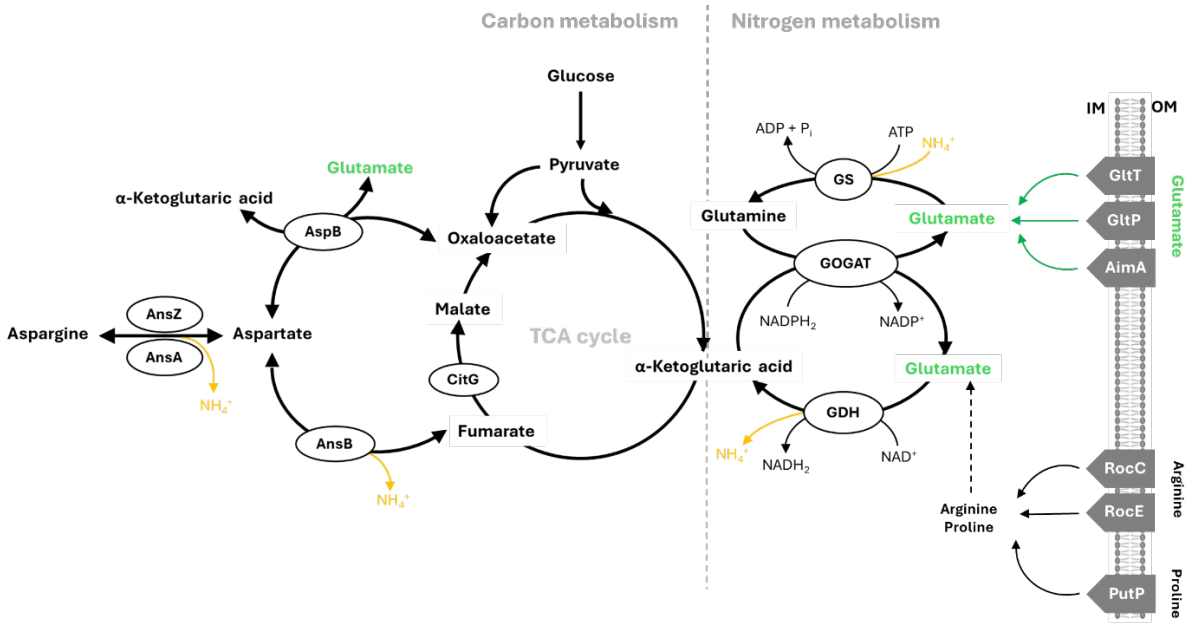

Figure 2. L-Glutamate biosynthesis pathways in *B. subtilis* linking carbon and nitrogen metabolism.
L-Glutamate biosynthesis occurs through two main pathways: the GS-GOGAT pathway and the AnsB-AspB route (discovered in this study). In the GS-GOGAT pathway, L-glutamine acts as the amino group donor, while in the AnsB-AspB route, L-aspartate fulfills this role. GDH enzymes RocG and GudB in *B. subtilis* are strictly catabolically active. L-Glutamate can be transported into the cell through various L-glutamate transporters such as GltT, GltP, and AimA. Alternatively, it can be generated through the degradation of other amino acids in the glutamate family, such as L-arginine and L-proline. These amino acids are transported into the cell via specific transporters: RocC and RocE for L-arginine, and PutP for L-proline. AnsA and AnsZ, asparaginases; AnsB, aspartase; AspB, aspartate transaminase; CitG, fumarase; GDH, glutamate dehydrogenase encoded by *gudB* or *rocG*; GOGAT, glutamate synthase encoded by *gltAB*; GS, glutamine synthetase encoded by *glnA*; TCA, tricarboxylic acid (Figure adapted from Mardoukhi et al., 2024)

Mechanisms of controlling L-glutamate metabolism in *B. subtilis*

As elaborated in the preceding section, the GOGAT-GS cycle stands as the primary and fundamental pathway for glutamate synthesis in *B. subtilis*. The expression of the *gltAB* genes, which encode for GOGAT, is regulated by signals originating from carbon and nitrogen metabolism. These signals are mediated by the LysR-type transcription activator GltC and the global regulatory protein TnrA, respectively (Belitsky et al., 2000; Belitsky & Sonenshein, 2004; Bohannon & Sonenshein, 1989). The *gltC* gene encodes for GltC, which serves as both a transcriptional activator and repressor of the *gltAB* operon (Bohannon & Sonenshein, 1989; Picossi et al., 2007; Gunka & Commichau, 2012). In the presence of glucose, GltC activates the transcription of *gltAB* genes to facilitate glutamate production and satisfy the glutamate demand. Conversely, in the absence of glucose and when glutamate serves as the sole carbon source, GltC represses the *gltAB* operon (Fig. 3A, B; Belitsky et al., 2004; Commichau et al., 2007; Picossi et al., 2007).

The regulation of *gltAB* expression via the ammonium metabolism signal, mediated by TnrA, relies on the availability of glutamine or glutamate and ammonium, which can be converted to glutamine through the enzymatic activity of GS, GlnA (Wray et al., 2001; Fedorova et al., 2013). In the absence of glutamine, GOGAT becomes unnecessary since the ammonium required to combine with α-ketoglutarate for the production of two glutamate molecules is absent (Fig. 2). Consequently, GltC is unable to activate the transcription of *gltAB* genes because TnrA binds to and obstructs the downstream region of the *gltAB* promoter (Belitsky et al., 2000; Commichau et al., 2006b). However, in the presence of excess nitrogen, GlnA deactivates TnrA, thereby restoring the expression of the *gltAB* genes (Wray et al., 1996, 2001). Thus, it can be deduced that GOGAT synthesis is contingent upon the availability of both of its substrates: α-ketoglutarate derived from glucose catabolism and glutamine (Gunka & Commichau, 2012).

B. subtilis harbors two $NADPH_2$-dependent GDHs, GudB and RocG, encoded by the *gudB* and *rocG* genes, respectively. In the commonly used laboratory strains, 168 and SP1, which are specifically employed in this study, only RocG exhibits enzymatic activity (Belitsky & Sonenshein, 1998). GudB remains cryptic due to the presence of a perfect direct repeat of 9 base pairs (G279-C287), resulting in the duplication of 3 amino acids within its active site. This duplication induces instability in its structure, leading to rapid proteolytic degradation (Gunka et al., 2012). When *B. subtilis* 168 or SP1 strains lacking functional RocG are cultured on either a complex medium or a minimal medium supplemented solely with L-glutamate or amino acids, such as L-proline and L-arginine, which can be catabolized to L-glutamate, a pronounced growth impairment is observed (Commichau, et al., 2006; Gunka et al., 2012). These strains swiftly acquire activating mutations in the *gudB* gene at a remarkably high frequency, approximately 10^{-4} (Gunka et al., 2012). This mutational event leads to the expression of GudB1 protein, an active variant of the GDH GudB. GudB1 plays a crucial role in preventing the accumulation of glutamate to potentially toxic levels by catalyzing its conversion to α-ketoglutarate, thereby restoring metabolite homeostasis (Fig. 3A, B; Commichau, et al., 2006; Gunka et al., 2012).

Both GDH enzymes possess a notably low affinity for ammonium in the low intracellular ammonium concentrations, rendering them strictly catabolically active (Commichau et al., 2008; Noda-Garcia et al., 2017). The activity of RocG, the sole active GDH in *B. subtilis* 168/SP1, is subject to intricate regulation stemming from signals originating in carbon and nitrogen metabolism (Belitsky & Sonenshein, 1998; Commichau et al., 2007). In the presence of amino acids or other nitrogen sources that can be metabolized to glutamate, such as arginine and proline, the transcription factors RocR and AhrC activate the expression of RocG (Fig. 3B; Gardan et al., 1997; Miller et al., 1997; Commichau et al., 2007).

Furthermore, for the expression of the *rocG* gene, the RNA polymerase depends on another type of sigma factor known as sigma factor σ^L, encoded by the *sigL* gene (Débarbouillé et al., 1991). However, in the presence of glucose in the media, the

pleiotropic transcription factor CcpA strongly represses the *rocG* promoter and the *sigL* gene (Belitsky et al., 2004; Choi & Saier, 2005). This meticulous and complex regulation of the *rocG* gene ensures that the catabolic activity of the GDH RocG, involved in glutamate degradation, is only activated when metabolic demands necessitate glutamate degradation (Fig. 3A; Gunka & Commichau, 2012).

A recent study, conducted *in vivo* and *in vitro*, has revealed that under conditions of glutamate limitation, the GOGAT, GltAB, associates with GDH, GudB to form a counter-enzyme complex. This complex effectively inhibits the activity of GudB, thereby preventing depletion of the glutamate pool (Fig. 3A). In this configuration, six monomers of GudB are being covered by six monomers of GltA and GltB. This arrangement prevents the active site of GudB from interacting with free glutamate (Jayaraman et al., 2022).

In the wild-type *B. subtilis* strains like *B. subtilis* NCIB 3610, which expresses both GDHs, GudB and RocG, in their active version, under conditions where glutamate serves as the sole carbon and nitrogen source, GudB interacts with GltC, inhibiting its ability to activate the transcription of GOGAT, *gltAB* genes. This inhibition leads to a metabolic shift in the cell from glutamate anabolism to catabolism, resulting in the degradation of glutamate to α-ketoglutarate and its subsequent utilization in carbon catabolism pathways (Fig. 3A). In *B. subtilis* 168 and SP1 strains, which express the RocG as the only active GDH enzyme, it has been reported that RocG, like GudB, can also deactivate the GltC protein (Commichau et al., 2007; Stannek et al., 2015).

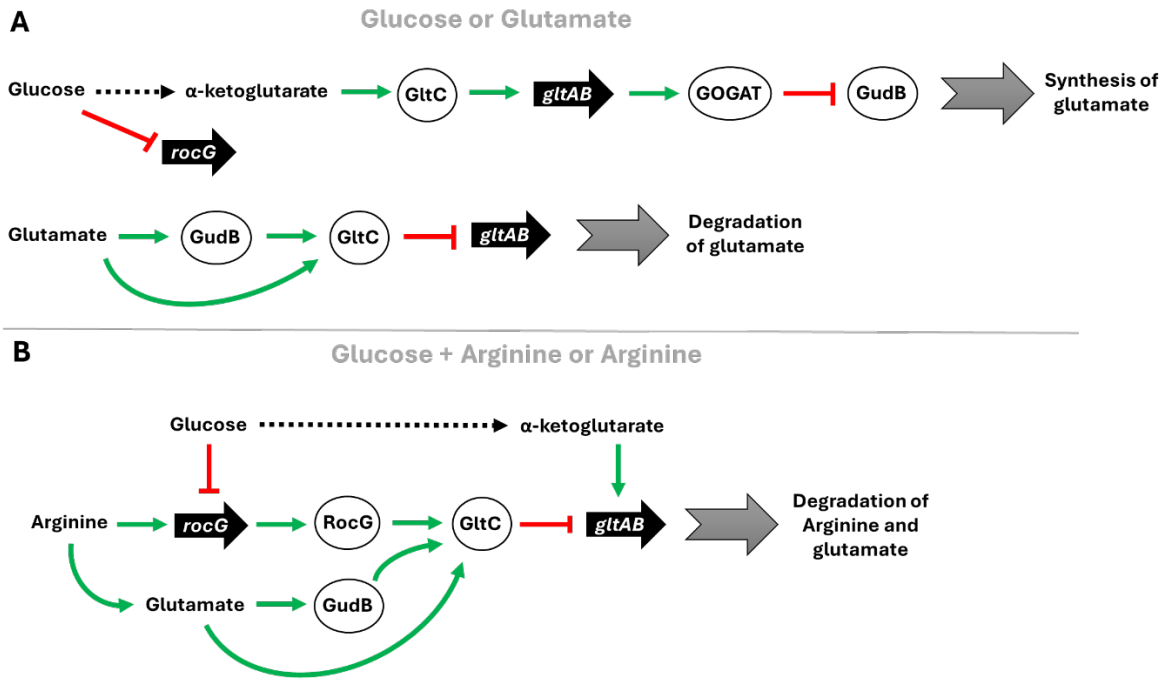

Figure 3. Regulation of L-glutamate biosynthesis in *B. subtilis*.

A) Induction and repression of the GOGAT, *gltAB* genes, by glucose and glutamate, respectively. **B)** Repression of the GOGAT, *gltAB* genes, by arginine. (Figure adapted from Mardoukhi et al., 2024)

Mechanisms of controlling L-arginine metabolism in *B. subtilis*

In *B. subtilis*, L-arginine transport is primarily mediated by two types of transport systems: the ATP-binding cassette (ABC) transporters and amino acid-polyamine-organocation (APC) superfamily. These transporters facilitate the uptake of L-arginine across the bacterial membrane (Lorca et al., 2007). The ABC transporters responsible for L-arginine uptake in *B. subtilis* comprise ArtP, ArtQ, and ArtR, which exhibit a high affinity for L-arginine and harness the energy derived from ATP hydrolysis for its uptake (Quentin et al., 1999; Yu et al., 2015). Conversely, within the APC superfamily, L-arginine uptake is facilitated by RocC and RocE, selective symport systems capable of transporting arginine, ornithine, and citrulline alongside protons (Gardan et al., 1995; Klingel et al., 1995).

The *rocC* and *rocE* genes, encoding the permeases RocC and RocE respectively, are integral components of the *rocABC* and *rocDEF* operons, which play pivotal roles in the uptake and metabolic utilization of arginine, ornithine, and citrulline. Within the *rocABC* operon, in addition to the permease RocC, RocA is encoded, facilitating the final conversion step of arginine degradation from L-glutamate-semialdehyde to glutamate (Calogero et al., 1994). Furthermore, RocB, which was recently characterized, serves as an enzyme catalyzing the conversion of citrulline to ornithine (Warneke et al., 2023). In parallel, the *rocDEF* operon, beside coding for the permease RocE, encodes enzymes responsible for the initial steps of arginine utilization. Specifically, RocF mediates the conversion of arginine to ornithine, while RocD catalyzes the subsequent conversion of ornithine to L-glutamate-semialdehyde (Gardan et al., 1995).

Both arginine degradation operons, *rocABC* and *rocDEF*, are under the control of two transcriptional regulators, RocR and AhrC (Calogero et al., 1994; Gardan et al., 1995; Klingel et al., 1995; Miller et al., 1997). The initiation of transcription for these operons is orchestrated by the RNA polymerase employing an alternative sigma factor SigL which relies on the ATP-hydrolyzing transcription activators RocR and AhrC. In the presence of ornithine or L-arginine, with the latter being converted into ornithine through a single enzymatic step, RocR stimulates the expression of both operons (Gardan et al., 1997; Warneke et al., 2023). Additionally, AhrC, in the presence of L-arginine, serves as a transcriptional activator for genes involved in arginine degradation while simultaneously acting as a repressor for genes associated with arginine biosynthesis (Garnett et al., 2007). The allocation of diverse types and a multitude of transporters and genes dedicated to arginine uptake and degradation underscores its pivotal role in numerous cellular processes, peptide and protein production and etc. Furthermore, the degradation of arginine yields reducing power in the form of NADH + H^+, which can be

harnessed for ATP synthesis during cellular respiration (Warneke et al., 2023). This dual functionality highlights the multifaceted significance of arginine metabolism in cellular energetics and metabolic homeostasis.

Mechanisms of controlling L-proline metabolism in *B. subtilis*

PutP serves as a high-affinity proline permease, facilitating the uptake of proline coupled with the influx of sodium ions. This transporter is encoded by the *putP* gene, which resides within the *putBCP* operon (Fig. 4; Atkinson et al., 1990; Belitsky, 2011; Moses et al., 2012). Alongside PutP, this operon encodes two additional enzymes, PutB and PutC, crucial for L-proline degradation. PutB functions as a FAD-dependent proline dehydrogenase, catalyzing the conversion of L-proline into Δ^1-pyrroline-5-carboxylate and alongside producing one molecule of $FADH_2$. This intermediate is highly unstable and spontaneously undergoes conversion to γ-glutamate-5-semialdehyde. Subsequently, γ-glutamate-5-semialdehyde undergoes enzymatic transformation to L-glutamate with the aid of 1-pyrroline-5-carboxylate dehydrogenase PutC. This enzyme relies on NAD^+ as a cofactor for its activity, facilitating the conversion of the intermediate to L-glutamate and production of one NADH, thereby completing the degradation pathway of L-proline. Indeed, the catabolism of proline serves dual purposes, contributing not only to metabolic homeostasis but also to energy production within the cell. During the hydrolase of one molecule of L-proline to one molecule of L-glutamate, the enzymatic reactions involved generate one molecule of $FADH_2$ and NADH (Fig. 4; Belitsky, 2011; Huang et al., 2011; Moses et al., 2012).

The expression of the L-proline utilization *putBCP* operon is facilitated by a SigA-type promoter and depends on the presence of the proline-responsive activator protein PutR. Even at very low concentrations external sources of L-proline (submillimolar levels), PutR triggers the activation of *putBCP* transcription. However, this activation can be counteracted by an active form of the negatively acting CodY regulatory protein, particularly in medium containing a mixture of other amino acids. CodY, a global transcriptional regulator in *B. subtilis*, responds to branched-chain amino acids such as isoleucine, leucine, and valine. Its regulatory influence extends to genes involved in amino acid and nitrogen metabolism. Acting as a master regulator, CodY governs cellular metabolism, particularly under conditions of nutrient excess. The PutR binding site is positioned within the promoter region of the *putB* gene, overlapping with the CodY-binding site. In the repression of the *putBCP* operon, CodY's role involves diminishing operon activation by competitively inhibiting PutR from binding to the *putB* promoter. Thus, CodY plays a pivotal role in modulating the expression of *putBCP* in response to environmental nutrient availability (Belitsky, 2011; Huang et al., 2011; Moses et al., 2012).

Osmotically controlled synthesis of the compatible solute proline in *B. subtilis*

In response to high osmolarity environments, *B. subtilis* employs cellular defense mechanisms, including the accumulation of specific water-attracting ions, primarily potassium (Holtmann et al., 2003; Whatmore & Reed, 1990), and organic compounds referred to as compatible solutes (Bremer, 2014; Kempf & Bremer, 1998). Among these solutes, L-proline stands out as the sole compatible solute that *B. subtilis* can synthesize *de novo* (Kuhlmann & Bremer, 2002; Whatmore et al., 1990). Its osmotically regulated production plays a pivotal role in enabling effective cellular adaptation to sustained high-osmolarity conditions (Hoffmann et al., 2012, 2017).

To maintain physiological hydration levels within the cytoplasm, *B. subtilis* employs three distinct strategies involving L-proline: Firstly, it imports L-proline via the OpuE transporter, an osmotically inducible symporter that facilitates the co-transport of L-proline alongside sodium ions (Fig. 4; Spiegelhalter & Bremer, 1998; Von Blohn et al., 1997). Expression of *opuE* which codes for OpuE transporter is induced by glucose via the global regulator CcpA (carbon catabolite protein A) and recognized by the sigma factor A and B (Marciniak et al., 2012; Spiegelhalter & Bremer, 1998). Secondly, *B. subtilis* synthesizes L-proline *de novo* through the osmostress adaptive L-proline biosynthetic pathway, involving the sequential action of ProJ, ProA, and ProH enzymes (Brill et al., 2011). It's noteworthy that *B. subtilis* has evolved an additional anabolic pathway for L-proline synthesis, facilitated by the ProB-ProA-ProI enzymes. However, unlike the osmostress adaptation response system, this pathway is not directly involved in the cellular response to osmotic stress due to differences in the mechanisms governing their expression (Fig. 4; Brill et al., 2011). Thirdly, *B. subtilis* facilitates the generation of free proline by uptaking proline-containing peptides and subsequently breaking them down through proteolysis. This process involves several ABC-type peptide transporters, including App, Dpp, and Opp (Koide & Hoch, 1994; Mathiopoulos et al., 1991; Perego et al., 1991; Rudner et al., 1991), as well as DtpT, which is a predicted peptide uptake system (Caldwell et al., 2001).

As discussed above, the *de novo* synthesis of L-proline entails two distinct pathways: ProB-ProA-ProI and ProJ-ProA-ProH, which share an identical enzymatic cascade for the conversion of L-glutamate to L-proline (Brill et al., 2011; Hoffmann et al., 2012; Kuhlmann & Bremer, 2002; Stecker et al., 2022). Notably, ProA plays a pivotal role in both pathways, while the final step of the pathway is executed by different enzymes, ProI, ProH, and ProG, in response to varying environmental conditions. The genes *proB* and *proA* are typically co-located within a single operon, while *proJ* and *proH* genes reside in another operon. The *proI* and *proG* genes, on the other hand, are typically single genes. In each pathway, the initial conversion is catalyzed by glutamate 5-kinase, ProB or ProJ, utilizing L-glutamate and ATP to yield L-glutamyl 5-phosphate and ADP. Subsequently, L-glutamyl 5-phosphate undergoes transformation into L-glutamate 5-semialdehyde through the enzymatic activity of glutamate-5-semialdehyde dehydrogenase, ProA. L-glutamate 5-semialdehyde, being an unstable intermediate, spontaneously converts to 1-pyrroline-5-carboxylate, serving as the substrate for the final step in L-proline

synthesis. In this last step, pyrroline-5-carboxylate reductase, ProI, ProH or ProG, catalyzes the conversion of 1-pyrroline-5-carboxylate to L-proline (Fig. 4; Forlani et al., 2017; Hoffmann et al., 2012). Indeed, ProG and ProI contribute to providing the necessary building blocks for protein synthesis, whereas ProH facilitates the enhanced production of proline as a compatible solute (Forlani et al., 2017). It's noteworthy that the last two conversion steps to synthesis L-proline require one NADPH molecule as a cofactor for each step (Hoffmann et al., 2012).

The regulation of the *proAB* operon and *proI* gene is under the control of the T-box element. When L-proline is absent, uncharged tRNA molecules engage with the T-box region situated within the leader sequence of the mRNA of the regulated gene or operon, thereby impeding the formation of a transcription terminator (Brill et al., 2011). Consequently, gene expression proceeds for the target gene even in the absence of L-proline. Conversely, the *proHJ* operon's expression mechanism diverges, lacking a T-box element. Instead, its transcription is initiated by the sigma factor A, and it undergoes robust upregulation in response to heightened osmolarity/salinity, and antibiotic stress (Brill et al., 2011; Morawska et al., 2022).

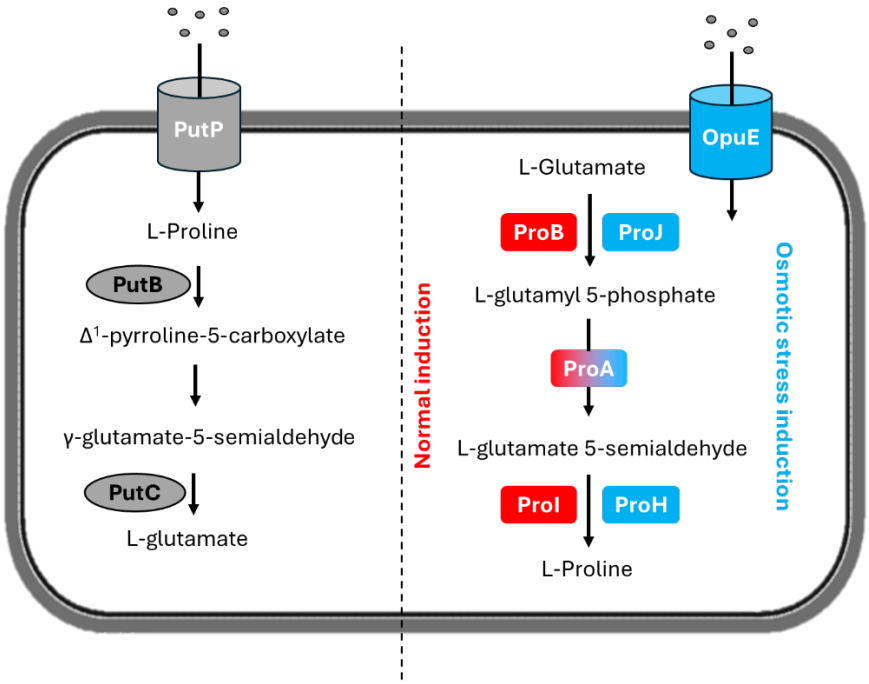

Figure 4. L-Proline metabolism in *B. subtilis* in normal environment and osmotic stress. *B. subtilis* employs HutP to facilitate the uptake of L-proline, subsequently metabolizing it to L-glutamate through the sequential action of PutB and PutC enzymes (highlighted in gray). Under normal conditions and in environments devoid of salinity stress, *B. subtilis* synthesizes L-proline from L-glutamate via the enzymatic cascade involving ProB, ProA, and ProI enzymes (highlighted in red). In high salinity environment, *B. subtilis* elevates the intracellular concentration of L-proline, serving as a compatible solute to maintain cellular hydration. This can be achieved either by uptaking L-proline from the medium, if available, through the OpuE transporter, or by endogenously synthesizing it via the ProJ-ProA-ProH enzymatic pathway (highlighted in blue).

Mechanisms of controlling L-aspartate/asparagine metabolism in *B. subtilis*

L-Aspartate and L-asparagine are both amino acids belonging to the glutamate family. L-aspartate can be directly converted into L-glutamate, while the conversion of L-asparagine to L-glutamate requires an intermediate step, where L-asparagine is first converted into L-aspartate before being further transformed into L-glutamate. When L-aspartate is present in the growth medium, *B. subtilis* exhibits a preference for its uptake via GltT, the primary high-affinity Na^+-coupled glutamate/aspartate symport protein. A previous study has revealed that elevated levels of L-glutamate in the medium can impede the uptake of L-aspartate, predominantly through competitive inhibition mechanisms. This inhibition arises because GltT exhibits comparable affinities for both amino acids (Zhao et al., 2018). Specifically, the K_m values of GltT for L-glutamate is approximately 37 +/- 5 µM and for L-aspartate, it is about 41 +/- 9 µM (Zaprasis et al., 2015). L-aspartate can be subsequently converted to L-glutamate through a reversible pyridoxal 5´-phosphate (PLP)-dependent transamination reaction facilitated by aspartate transaminase AspB. In this process, an amino group from L-aspartate is transferred to 2-oxoglutarate, yielding L-glutamate and oxaloacetate (Dajnowicz et al., 2017). Oxaloacetate will later enter the TCA cycle. Despite the auxotrophy of *B. subtilis* AspB mutant for L-aspartate and L-asparagine, this study will later elucidate that this dependency can be circumvented. This bypass can be achieved either through the derepression of the *ansA-ansB* operon (by inactivating of the *ansR* gene), or by the amplification of the *ansA-ansB* operon (Mardoukhi et al., 2024). Additionally, it has been reported that the *ansR* mutation enables the utilization of L-glutamate as a carbon source in a *B. subtilis rocG gudB* mutant. This serves as further evidence for the degradation pathway of L-glutamate to L-aspartate and subsequently to fumarate (Flórez et al., 2011).

In *B. subtilis*, L-aspartate can also be synthesized via nitrogen assimilation, involving the enzymatic conversion of fumarate and NH_4^+ to L-aspartate by L-aspartase AnsB. The *ansB* gene encodes L-aspartase AnsB and is situated within an operon upstream of *ansA*. This operon, *ansA-ansB*, is under the control of the transcriptional repressor AnsR, encoded by the *ansR* gene, which is located upstream of the *ansA-ansB* operon with a shared promoter region in the reverse direction (Sun & Setlow, 1991). In the presence of L-asparagine, AnsR disengages from the promoter site of the *ansAB* operon, consequently leading to the transcriptional activation of *ansA* and *ansB* genes (Fisher & Wray, 2002). This regulatory mechanism helps maintain the homeostasis of L-asparagine by degrading L-asparagine to L-aspartate, which is further converted to fumarate and utilized in the TCA cycle as a carbon source.

Despite various strategies employed to identify specific L-asparagine transporters, only the broad-spectrum amino acid importers AimA and BcaP have been reported to be responsible for the uptake of L-asparagine. Additionally, in the same study, which encompasses a portion of the results discussed herein later, it was demonstrated that

at toxic concentrations of L-asparagine, AzlCD, known as an amino acid exporter for L-histidine and 4-azaleucine, also functions as an exporter for L-asparagine (Meißner et al., 2022, 2024). Subsequently, L-asparagine undergoes degradation into L-aspartate, facilitated primarily by the pivotal enzyme AnsZ, alongside AnsA serving as a secondary L-asparaginase, releasing a single ammonia molecule. Although this reaction is reversible, the catabolism of L-asparagine exhibits a higher K_m. Expression of *ansZ* is elicited by TnrA under conditions devoid of favorable nitrogen sources, such as L-glutamine or ammonium, highlighting its role in nitrogen metabolism regulation (Fisher & Wray, 2002). Conversely, the expression of *ansA* is subject to negative regulation by the transcriptional repressor AnsR, whose activity is contingent upon the presence of L-asparagine (Sun & Setlow, 1993, Fisher & Wray, 2002; Mardoukhi et al., 2024;).

Asparagine biosynthesis occurs in *B. subtilis*, as evidenced by its ability to thrive in a minimal medium without the supplementation of L-asparagine, indicating efficient biosynthesis of L-asparagine (Meißner et al., 2024). In nature, asparagine biosynthesis involves enzymatic reactions catalyzed by asparagine synthetase enzymes, utilizing either free ammonium or L-glutamine as a nitrogen source to convert L-aspartate to L-asparagine. The reactions can be described as follows: 1) L-aspartate + ATP + H_2O + NH_4^+ → L-asparagine + AMP + PP_i + H^+ and, 2) L-aspartate + L-glutamine + ATP + H_2O → L-asparagine + L-glutamate + AMP + PP_i + H^+. The first reaction, which utilizes ammonia as a nitrogen source, is found in prokaryotes such as *E. coli* and *Klebsiella aerogenes* (Humbert & Simoni, 1980; L. J. Reitzer & Magasanik, 1982). The second reaction, which employs L-glutamine as a nitrogen source, is found in both prokaryotes and eukaryotes (Van Heeke & Schuster, 1989; Scofield et al., 1990; Hughes et al., 1997;). *B. subtilis*, a natural prototroph for L-asparagine, possesses three asparagine synthetases AsnO, AsnB, and AsnH, all of which are glutamine-dependent (Yoshida et al., 1999).

B. subtilis exhibits a remarkable capacity for L-asparagine synthesis throughout various stages of growth, facilitated by the presence of three asparagine synthetases (Yoshida et al., 1999). The expression of the *asnB* gene predominates during the exponential growth phase. Conversely, during the transition from exponential growth to stationary phase, heightened expression of the *asnH* gene is noted. Notably, expression of the *asnO* gene becomes evident exclusively during the sporulation stage. This orchestrated regulation of enzyme expression underscores the adaptability and resilience of *B. subtilis* in ensuring continuous L-asparagine synthesis across diverse growth stages (Yoshida et al., 1999).

Mechanisms of controlling L-histidine metabolism in *B. subtilis*

In *B. subtilis*, the transport of L-histidine is facilitated by the histidine permease HutM. Notably, all components responsible for both the uptake and degradation of L-histidine are encompassed within a single operon, HutPHUIGM (Wray & Fisher, 1994). Given the pivotal role of histidine, its catabolic pathway exhibits a remarkable degree of

conservation across bacterial species. The initial three enzymatic steps involved in the conversion of L-histidine to formiminoglutamate constitute a fundamental sequence: histidase HutH catalyzes the deamination reaction to produce urocanate, which is subsequently hydrated to imidazolone propionate by urocanase HutU. Following this, imidazolone-5-propionate hydrolase HutI facilitates the cleavage of the imidazolone propionate ring, yielding formiminoglutamate (Wray & Fisher, 1994; Bender, 2012;). This triadic process appears to be universal among bacterial taxa. Subsequently, the fate of formiminoglutamate diverges among bacterial genera. In certain bacteria such as *Bacillus* and *Klebsiella*, formiminoglutamate undergoes direct hydrolysis to L-glutamate and formamide via the enzymatic action of formiminoglutamate hydrolase HutG, with formamide subsequently excreted as a metabolic waste product (Magasanik & Bowser, 1955; Kaminskas et al., 1970). Conversely, in other bacteria such as *Pseudomonas* and *Streptomyces*, an additional step takes place, wherein an additional ammonium group is released from formiminoglutamate to yield formylglutamate, which is then converted to glutamate (Tabor & Hayaishi, 1952; Kendrick & Wheelis, 1982).

The regulation of the HutPHUIGM operon is under the control of HutP, an RNA-binding protein encoded by the *hutP* gene and acts as an anti-terminator by attaching to the *hutP* acting site located between *hutP* and *hutH* genes (Oda et al., 1988; Wray & Fisher, 1994; Yoshida et al., 1995). In conditions of low L-histidine concentration, an intrinsic stem-loop configuration emerges within the RNA transcript, particularly within a CG-rich domain area between *hutP* and *hutH* genes, functioning as a terminator and impeding the progression of RNA polymerase through the rest of the operon. Additionally, under low L-histidine levels, residual expression (uninduced) of histidase HutH degrades histidine availability, thereby does not allow significant induction of the *hut* operon (Fig. 5). Conversely, abundant and sustained L-histidine presence prompts operon induction. X-ray crystallography elucidates that six monomers of HutP aggregate to form a hexameric structure. Upon binding with L-histidine and a magnesium ion, this complex undergoes a conformational alteration. The resultant 6xHutP-His-Mg^{2+} complex then interfaces with the stem-loop structure (terminator) of the RNA transcript situated between the *hutP* and *hutH* genes. This interaction facilitates the progression of RNA polymerase, enabling uninterrupted transcription throughout the *hut* operon (Fig. 5; (Wray & Fisher, 1994; Oda et al., 1988, 2000; Bender, 2012; Babitzke et al., 2019).

The operation of the *hut* operon expression is intricately governed by two distinct global regulators: CodY, responsible for monitoring amino acid availability and overall nutritional status (Slack et al., 1995), and CcpA, tasked with assessing the quality of the carbon source (Henkin, 1996). Positioned just downstream of the *hutP* gene within its promoter site lies a binding site for CodY (Fig. 5). In response to fluctuations in amino acid levels, CodY binds to this site, thereby exerting repression on the transcriptional initiation of the *hut* operon. Concurrently, located within the midsection of the *hutP* gene resides a *cre* site, serving as a recognition site for CcpA, particularly in the presence of glucose (Fig. 5). Upon CcpA's binding to the *cre* site, a block is imposed upon the

transcriptional machinery, impeding the full expression of HutP as well as the remaining components of the *hut* operon (Oda et al., 2000; Bender, 2012).

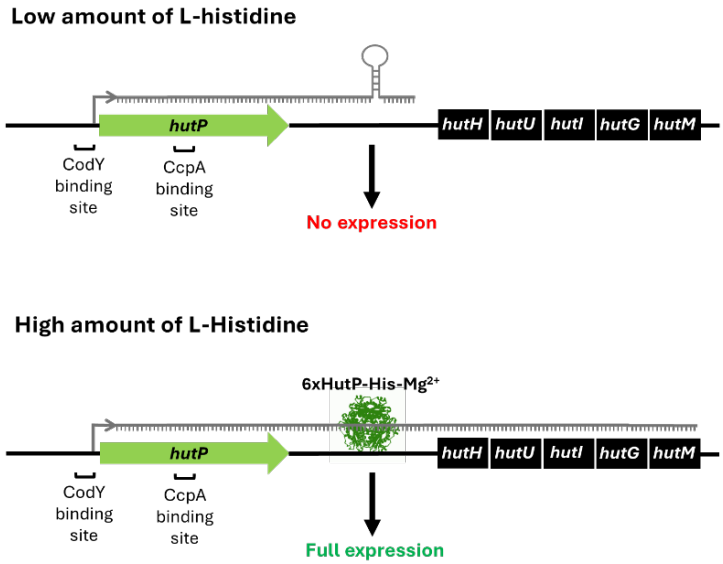

Figure 5. L-Histidine metabolism in *B. subtilis*.
In presence of low concentration of L-histidine, a stem-loop structure forms in the RNA transcript in the noncoding region between *hutP* and *hutH* genes functioning as a terminator and blocking the progression of RNA polymerase through the rest of the operon. In the presence of high concentration of L-histidine, a complex of 6xHutP-His-Mg^{2+} binds to the stem-loop structure and allows the RNA polymerase to read through the rest of the operon. CodY and CcpA binding site also is depicted within the promoter site and middle region of *hutP* gene, respectively.

While amino acids are indispensable for cellular growth, maintaining their concentration within a precise range is crucial, as excessive levels can prove toxic to cells. Amino acids can exert toxicity through various mechanisms, including misloading onto non-specific tRNAs, resulting in their erroneous incorporation into proteins, or interference with enzymatic pathways due to chemical and structural similarities among amino acids (de Lorenzo et al., 2015; Meißner et al., 2022). To address these challenges, bacteria have evolved specific or serendipitous solutions, often through mutations, to uphold amino acid homeostasis. For instance, mutations in uptake systems for certain amino acids (e.g., glutamate, threonine, alanine, proline, serine) and non-amino acid compounds (e.g., glyphosate) have been observed in *B. subtilis*, preventing or reducing their uptake when grown in media supplemented with toxic levels of these substances (Zaprasis et al., 2014; Belitsky, 2015; Commichau et al., 2015; Wicke et al., 2019; Klewing et al., 2020; Krüger et al., 2021; Sidiq et al., 2021;). Additionally, enhancing the activity of export systems, as demonstrated for glutamate and 4-azaleucine, offers another mechanism to counteract amino acid toxicity (Ward & Zahler, 1973; Krüger et al., 2021). Furthermore, mutations facilitating the degradation or detoxification of toxic amino acids to non-toxic

metabolites have been documented, particularly for glutamate and serine (Belitsky & Sonenshein, 1998; Commichau et al., 2008; Klewing et al., 2020; Krüger et al., 2021). Alterations in target proteins via mutations leading to the protein modification confer potential resistance against some compounds like glyphosate (Comai et al., 1983). Lastly, increasing the expression levels of target proteins can mitigate inactivation or suppression by toxic amino acids or compounds, as evidenced for serine and glyphosate (Wicke et al., 2019; Klewing et al., 2020).

Numerous studies have documented the inhibitory effect of histidine on the growth of *B. subtilis* (Comai et al., 1983; Lachowicz et al., 1996; Klewing et al., 2020; Meißner et al., 2022). Notably, research indicates that inactivation mutations in the *azlB* gene confer tolerance to histidine toxicity. The AzlB protein serves as a transcriptional repressor of the *azlB-azlC-azlD-brnQ-yrdK* operon, encoded by the *azlB* gene. Within this operon, the *azlCD* genes encode the branched-chain amino acid exporter, comprising the large subunit AzlC and the small subunit AzlD. Inactivation of AzlB leads to a significant upregulation of *azlCD* gene expression, facilitating the detoxification of histidine by translocating it out of the cell (Meißner et al., 2022). Interestingly, our study reveals that AzlCD is also capable of exporting L-asparagine, aiding *B. subtilis* in detoxifying elevated concentrations of this amino acid (Meißner et al., 2024). Additionally, we demonstrate another strategy for mitigating histidine toxicity: decriptification of the *gudB* gene, resulting in enhanced degradation of glutamate, a byproduct of histidine degradation, by the GDH GudB1.

Degradation pathways of other amino acids

Given the lower emphasis and fewer experiments conducted with other amino acids in this study, their degradation pathways are presented in tabular form. It is worth noting that there is limited information regarding the degradation of certain amino acids in *B. subtilis*. Additionally, for some amino acids such as L-tryptophan, L-tyrosine, L-phenylalanine, and L-methionine, there is no available data to confirm whether *B. subtilis* can degrade them.

Table 1. Degradation pathway of other amino acids

Amino acid	Enzymes	Degradation pathway	Reference
L-Glutamine	GlsA, YlaM	H_2O + L-glutamine → L-glutamate + NH_4^+	(Satomura et al., 2005; Brown et al., 2008)
L-Serine	SdaAA-SdaAB	L-serine → NH_4^+ + pyruvate	(S. Chen et al., 2012; X. L. Xu & Grant, 2013)
L-Alanine	Ald	H_2O + L-alanine + NAD^+ → H^+ + NADH + NH_4^+ + pyruvate	(Siranosian et al., 1993)

L-Glycine	GcvH GcvPA-GcvPB-GcvT	glycine + H+ + N^6-lipoyl-L-lysyl → (6R)-5,10-methylene-5,6,7,8-tetrahydrofolate + (R)-N^6-dihydrolipoyl-L-lysyl + NH_4^+	(Mandal et al., 2004; Abendroth et al., 2010)
L-Valine	IlvE/IlvK, Bcd, BkdB/BkdAA/ BkdAB/LpdV	L-valine → methylacrylyl-CoA + NADH + CO_2	(Debarbouille et al., 1999)
L-Leucine	IlvE/IlvK, Bcd, BkdB/BkdAA/ BkdAB/LpdV	L-leucine → 3-methylcrotonyl-CoA + NADH + CO_2	(Debarbouille et al., 1999)
L-Isoleucine	IlvE/IlvK, Bcd, BkdB/BkdAA/ BkdAB/LpdV	L-isoleucine → (E)-2-methylcrotonoyl-CoA + NADH + CO_2	(Debarbouille et al., 1999)
L-Threonine	Tdh, Kbl	L-threonine + NAD^+ → glycine + acetyl-CoA + NADH	(Schmidt et al., 2001; Zhang et al., 2019)
L-Lysine	KamA	L-lysine → (3S)-3,6-diaminohexanoate	(Chen et al., 2000)
Cysteine	MetI, MetC/PatB	L-cysteine + H_2O → Homocysteine + pyruvate + NH_4^+	(Oudega et al., 1997; Auger et al., 2002, 2005)
L-Tryptophane		Unknown	
L-Methionine		Unknown	
L-Phenylalanine		Unknown	
L-Tyrosine		Unknown	

Aim of this study

The primary objective of this study was to investigate the unexpected emergence of suppressor mutations in *B. subtilis gltAB* mutants, which were presumed incapable of growing on minimal medium without external L-glutamate supplementation due to their glutamate auxotrophy. This study aimed to explore how this genetic lesion, widely believed for more than eight decades to be insurmountable, could be bypassed.

To achieve this, the following main steps were undertaken:

1. Genome Sequencing of Suppressor Mutants: The first step was to perform genome sequencing of the suppressor mutants to identify the genetic basis of this phenomenon.

2. Verification of Bypassing Route: After identifying the genetic alterations responsible for the bypass, gene deletions were conducted to verify the possible bypassing routes.

3. Metabolome Analysis: To gain a deeper understanding of the potential pathways and compare metabolite levels with wild-type conditions, metabolome analysis was performed.

4. Ammonium Dependency Assessment: The study also aimed to compare the ammonium dependency of the new possible pathway with the general glutamate biosynthesis pathway to understand the efficiency of ammonium assimilation.

5. Response to Hyperosmotic Conditions: It was important to evaluate how the new glutamate pathway responds to hyperosmotic conditions, particularly in producing sufficient proline (derived from glutamate) as an osmoprotectant.

6. Adaptation to Toxic Levels of Amino Acids: Another objective was to investigate whether the new pathway can adapt to toxic levels of amino acids, such as L-arginine, which can be degraded to glutamate, or to complex media like LB, which contains all amino acids.

7. Conversion of Other Amino Acids: Finally, the study aimed to determine whether a *B. subtilis* strain, with both glutamate biosynthesis pathways inactivated and ensured to be a genetically stable auxotroph for glutamate, can convert other amino acids into glutamate and restore growth.

These main steps were designed to provide comprehensive insights into the characterization, metabolic flexibility and regulatory mechanisms underlying the new possible glutamate biosynthesis pathway in *B. subtilis*.

Materials and Methods

Materials

All chemicals, utilities, equipment, commercial systems, enzymes, and oligonucleotides utilized in the study are listed in the appendix.

Bacterial strains and plasmids

Bacterial strains and plasmids are detailed in the appendix.

Growth media

The media were dissolved in deionized water and autoclaved for 20 minutes at 121°C. Chemicals that are not thermostable were dissolved and filtered. Agar plates were obtained by supplementing the media with agar to a final concentration of 1.5% (w/v).

LB medium	10 g	Tryptone
	5 g	Yeast extract
	10 g	NaCl
	Ad to 1000 ml	H_2O
BHI medium	37 g	BHI powder
	Ad to 1000 ml	H_2O
C medium	20 ml	5x C salt
	1 ml	III´ salts
	1 ml	Iron Ferric Ammonium Citrate (CAF; 2.2 mg/ml)
	Ad to 100 ml	H_2O
C-Glc medium		C medium
	Final con. 0.5% w/v	Glucose
CE medium	20 ml	5x C salt
	1 ml	III´ salts
	1 ml	Iron Ferric Ammonium Citrate (CAF; 2.2 mg/ml)
	2 ml	Potassium Glutamate (40 % w/v)
	1 ml	Tryptophan (5 mg/ml)
	Ad to 100 ml	H_2O
5x C salts	0.232 g	$MnSO_4 \cdot 4\ H_2O$
	12.3 g	$MgSO_4 \cdot 7\ H_2O$

	Ad to 1000 ml	H_2O
III´ salts	20 g	KH_2PO_4
	80 g	$K_2HPO_4 \cdot 3\ H_2O$
	16.5 g	$(NH_4)_2SO_4$
	Ad to 1000 ml	H_2O
SM medium	200 ml	5x SM base medium
	10 ml	100x Trace element solution
	10 ml	100x Fe-Citrate-Solution
	10 ml	Glucose (50% w/v)
	10 ml	$(NH_4)_2SO_4$ (20% w/v)
	Ad to 1000 ml	H_2O
5x SM base medium	175 g	K_2HPO_4
	75 g	KH_2PO_4
	12.5 g	Na_3-Citrate $\cdot 2\ H_2O$
	2.5 g	$MgSO_4 \cdot 7\ H_2O$
	Adjust the pH to 7.0	
	Ad to 2000 ml	H_2O
100x Trace elements	0.55 g	$CaCl_2$
	0.1 g	$MnCl_2 \cdot 4\ H_2O$
	0.17 g	$ZnCl_2$
	0.033 g	$CuCl_2 \cdot 2\ H_2O$
	0.06 g	$CoCl_2 \cdot 6\ H_2O$
	0.06 g	$Na_2MoO_4 \cdot 2\ H_2O$
	Ad to 1000 ml	H_2O
	Sterile filtration!	
100x Iron-Citrate	0.0135 g	$FeCl_3 \cdot 6\ H_2O$
	0.1 g	Na_3-Citrate $\cdot 2\ H_2O$
	Ad to 100 ml	H_2O
	Sterile filtration!	
10x MN	136 g	$K_2HPO_4 \times 3\ H_2O$
	60 g	KH_2PO_4
	10 g	Sodium citrate $\cdot 2\ H_2O$
	Ad to 1000 ml	H_2O
1x MNGE medium	1 ml	10x MN medium
	400 µl	Glucose (50% w/v)
	50 µl	Potassium glutamate (40% w/v)

	50 µl	Iron Ferric Ammonium Citrate (CAF; 2.2 mg/ml)
	100 µl	Tryptophane (5 mg/ml)
	30 µl	MgSO4 (1 M)
	100 µl	Casaminoacids (10% w/v)
	Ad to 10 ml	H_2O
Expression mix	500 µl	Yeast extract (5%)
	250 µl	Casaminoacids (10% w/v)
	50 µl	Tryptophan (5 mg/ml)
	250 µl	H_2O
	Can be used for 10 samples	
CGXII medium	1 ml	MgSO4 · 7 H2O (12.5 g/50 ml dH_2O)
	1 ml	$CaCl_2$ · 2 H_2O (665 mg/ 50 ml dH_2O)
	1 ml	PCA 300 mg/10 ml (dissolve 300 mg in 3 ml of 1 M NaOH, add H_2O to 10 ml)
	1 ml	Biotin 0.02g/100 ml dH_2O
	1 ml	Trace elements solution
	40 ml	Glucose (50% w/v)
	Ad to 1000 ml with CGXII Basic Solution	
CGXII Basic solution	20 g	$(NH_4)_2SO_4$
	5 g	Urea
	1 g	KH_2PO_4
	1 g	K_2HPO_4
	42 g	MOPS
	Adjust the pH to 7 with KOH or NaOH	
	Ad to 1000 ml	H_2O
	Autoclave!	
Trace elements solution	1 g	$FeSO_4$ · 7 H_2O
	1 g	$MnSO_4$ · H_2O
	0.1 g	$ZnSO_4$ · 7 H_2O
	0.02 g	$CuSO_4$
	0.002 g	NiCl · 6 H_2O
	Adjust the pH to 1 with concentrated HCl	
	Ad to 100 ml	H_2O
	Sterile filtration!	
Starch medium	7.5 g	Nutrient broth
	5 g	Starch
	15 g	Agar-agar / Bacto-agar
	Ad to 1000 ml	H_2O

Antibiotics

To select for bacterial strains or plasmids, antibiotics were prepared as 1000-fold stock solutions, sterile-filtered (0.22 µm pore size), and stored at -20°C. After cooling down the autoclaved medium to approximately 50°C, the antibiotics were added.

			Selective concentration (µg/ml)	
Antibiotic	**Solvent**	**Stock (mg/ml)**	***E. coli***	***B. subtilis***
Ampicillin	H_2O	100	100	-
Kanamycin	H_2O	10	50	10
Lincomycin[1]	H_2O	25	-	25
Spectinomycin	H_2O	150	100	150 (250 for LB)
Tetracycline	70% ethanol	12.5	-	12.5
Erythromycin[1]	70% ethanol	2	5	2
Chloramphenicol	70% ethanol	5	15	5

[1] A mixture of erythromycin and lincomycin is used for selection of strains carrying *ermC* cassette (L. J. Griffith et al., 1965).

Other buffers and solutions

Saline	0.9 %	NaCl in deionized H_2O
X-Gal	80 mg/ml	5-Bromo-4-Chloro-3-Indoxyl-β-D-Galactopyranoside
	Ad to 1 ml	DMF (N, N-Dimethylformamide)
	Stored in the dark, covered by aluminum foil and frozen in -20°C!	
5x Lugol solution	100 g	K-Iodide
	50 g	Iodine
	Ad to 1000 ml	H_2O
RNase A	20 mg/ml	dissolved in deionized H_2O
Lysis Buffer	50 mg/ml	Lysozyme
	50 µl	Tris-HCl pH 8.0 (1 M)
	10 µl	$Na_2EDTA \cdot 2\ H_2O$, pH 8.0 (0.5 M)
	Ad to 2.5 ml	H_2O
Tris-HCl pH 8.0 (1 M)	121.14 g	Tris-base

	Add 800 ml	deionized H_2O
	Adjust the pH to 8.0 with HCl	
	Ad to 1000 ml	deionized H_2O
50x TAE buffer	242 g	Tris-Base (2 M)
	57.1 ml	Acetic Acid (100%)
	100 ml	Na_2EDTA x 2 H_2O pH 8 (0.5 M)
	Ad to 1000 ml	H_2O
5x DNA loading dye	5 ml	Glycerol (100%)
	0.2 ml	TAE buffer (50x)
	10 mg	Bromophenol blue
	4.8 ml	H_2O
Agarose	1 %	In 1x TAE buffer
6x SDS loading dye	3.15 ml	Tris-HCl pH 6.8 (1 M)
	600 µl	β-Mercaptoethanol
	1.2 g	SDS
	6 ml	Glycerol
	6 mg	Bromophenol blue
	0.25 ml	H_2O
10x ZAP	60.57 g	Tris-base
	116.9 g	NaCl
	Adjust the pH to 7.5 with HCl	
	Ad to 1000 ml	H_2O
10x Buffer W	121.14 g	Tris-base
	87.7 g	NaCl
	3.72 g	$Na_2EDTA \cdot 2\ H_2O$
	Adjust the pH to 8 with HCl	
	Ad to 1000 ml	H_2O
Buffer E	0.027 g	D-Desthiobiotin
	50 ml	Buffer W (1x)
10x Buffer R	121.14 g	Tris-base
	87.7 g	NaCl
	3.72 g	$Na_2EDTA \cdot 2\ H_2O$
	2.42 g	HABA
	Adjust the pH to 8 with HCl	

	Ad to 1000 ml	H_2O
10x Phosphate-buffered saline (PBS)	80 g	NaCl
	2 g	KCl
	14.24 g	Na_2HPO_4
	2.72 g	KH_2PO_4
	Adjust the pH to 6.5 with HCl	
	Ad to 1000 ml	H_2O
10x PAGE Buffer	144 g	L-Glycine
	30.3 g	Tris-base
	10 g	SDS
	pH should be 8.3 without adjustment	
	Ad to 1000 ml	H_2O
Fixation solution	10 %	Acetic acid
	50%	Methanol
	Ad to 1000 ml	H_2O
Staining solution	5 g	Coomassie Brilliant blue R-250
	10%	Acetic Acid
	45%	Methanol
De-staining solution	5%	Acetic acid
	20%	Ethanol
Silver-Fixation	50%	Methanol
	12%	Acetic acid
	100 µl	Formaldehyde (37%)
Silver-Developer	6 g	Na_2CO_3
	2 ml	Thiosulfate solution
	50 µl	Formaldehyde (37%)
	Ad to 100 ml	H_2O
Silver-Impregnator	0.2 g	$AgNO_3$
	37 µl	Formaldehyde (37%)
	Ad to 100 ml	H_2O
De-staining solution	20 mg	$Na_2S_2O_3 \cdot 5\ H_2O$
	Ad to 100 ml	H_2O

Silver-Stop solution	18.612 g	$Na_2EDTA \cdot 2\ H_2O$
	pH should be 8.0 without adjustment	
	Ad to 1000 ml	H_2O
LD-Mix	100 mg	Lysozyme
	10 mg	DNase I
	Ad to 10 ml	H_2O
	Store 500 µl aliquots at -20°C	
Z buffer (freshly prepared)	0.534 g	$Na_2HPO_4 \cdot 2\ H_2O$
	0.276 g	NaH_2PO_4
	0.037 g	KCl
	50 µl	$MgSO_4$ (1 M)
	175 µl	β-Mercaptoethanol
	Ad to 50 ml	H_2O
ONPG	4 mg	o-Nitrophenyl-β-D-Galactopyranoside (ONPG)
	Ad 1 ml Z buffer without β-Mercaptoethanol	
PNPX	4 mg	*p*-Nitrophenyl-β-D-Xylopyranoside (PNPG)
	Ad 1 ml Z buffer without β-Mercaptoethanol	
Stop solution	26.5 g	Na_2CO_3
	Ad to 250 ml	H_2O
Quenching solution	40% V	Acetonitrile
	40% V	Methanol
	20% V	H2O
Storage buffer	35 ml	$CaCl_2$ (120 mM)
	10 ml	Glycerol (50%)

Methods

The basic methods were taken, and some parts are adapted from the method collection of Sambrook, Fritsch, and Maniatis 1989.

Cultivation of Bacteria

To start bacteria cultivation, a fresh colony from a plate or material from a cryo-culture were used for inoculation. If not otherwise specified, *E. coli* and *B. subtilis* strains were cultivated in Lysogeny Broth (LB) medium (Sezonov et al., 2007), while *C. glutamicum* was cultured in Brain Heart Infusion (BHI) (Rosenow, 1919), all at 30°C with agitation (160 rpm).

To monitor and analyze bacterial growth in liquid media, a fresh colony was used to inoculate 4 ml of LB or BHI medium supplemented with appropriate antibiotics. After overnight incubation, the cell material was collected by centrifugation for 2 min at 13,000 rpm and washed twice with saline solution to remove any remaining traces from the complex medium. Subsequently, a pre-culture was established in the desired medium and grown until the OD_{600} reached approximately 0.5 to 0.8. Then, 200 µl of fresh medium with a starting OD_{600} of 0.1 was inoculated into a 96-well plate reader. The growth was monitored by measuring OD_{600} at 10 to 15 min intervals at 37°C with medium orbital shaking at 237 cpm (4 mm) using a Synergy H1 plate reader (Agilent, USA) equipped with Gen5 software (version 3.12.2008; BioTek).

To evaluate growth on solid plates, two distinct methods were employed depending on the experiment's objectives. Initially, an overnight culture underwent centrifugation at 13,000 rpm for 2 minutes and was subsequently resuspended in saline solution, followed by two washes. After this washing step, the OD_{600} was adjusted to 1, and 100 µl of the cell material was spread onto plates using a sterile inoculating loop. Alternatively, bacterial strains obtained from either cryo-culture or a colony from a plate were streaked onto fresh plates. Lastly, the cultivated plates were incubated at 37°C for up to two days for typical strains exhibiting normal growth, and for additional days to allow for the emergence of suppressor mutants in unfavorable media conditions.

Images of bacterial strains were captured using either the EPSON scanner (EPSON PERFECTION V700 PHOTO) or smartphone camera iPhone 12.

Storage of bacteria

For long-term storage, 700 µl of liquid bacterial culture were mixed with 300 µl of glycerol (50% w/v) and stored at -80°C. Additionally, since *B. subtilis* produces spores, it can be preserved on SP agar at room temperature. *E. coli*, on the other hand, can be stored for up to 4 weeks on agar plates at 4°C.

Transformation of *E. coli*

Preparation of competent cells

The $CaCl_2$ method was employed to prepare competent *E. coli* cells. Initially, 50 ml of LB medium were inoculated with an overnight LB culture in a 500 ml shake flask, starting with an OD_{600} of approximately 0.1. The culture was then grown at 37°C with agitation until reaching an OD_{600} of around 0.6 – 0.8. Following cell harvest at 5000 rpm at 4°C for 8 minutes in a 50 ml Falcon tube, the cells were resuspended in 25 ml of ice-cold $CaCl_2$ solution (100 mM). Subsequently, the cells underwent another round of harvest at 4°C, 5000 rpm for 8 minutes, followed by resuspension in 6 ml of ice-cold storage buffer. The cells were then ready for transformation or could be aliquoted into 1 ml Eppendorf tubes (220 µl each) and stored at -80°C for future use.

Transformation

To initiate the transformation process, 100 µl of competent *E. coli* cells were combined with 5 ng of DNA and placed on ice for 10 minutes. Following this incubation, the cells underwent heat shock at 42°C for 60 seconds, after which they were promptly returned to ice for an additional 10 minutes to facilitate the uptake of DNA induced by heat shock. Subsequently, 800 µl of LB medium were added to the cells, which were then incubated for 30 minutes at 37°C with agitation. Finally, the transformed cells were plated onto LB-agar plates containing appropriate antibiotics for selection.

Transformation of *B. subtilis*

Preparation of competent cells

An overnight culture of the desired *B. subtilis* strain was first grown in LB medium. Then, 10 ml of MNGE medium, supplemented with 0.1% CAA, was inoculated with the overnight culture to achieve an initial OD_{600} of approximately 0.1. The culture was allowed to grow in 37°C with agitation until the OD_{600} reached approximately 1.3. To induce competence gene expression in *B. subtilis*, a nutritional starvation step (Hamoen et al., 2003) was initiated by diluting the culture 1:1 with 10 ml of MNGE medium (without CAA). After 1 hour of further incubation at 37°C, the cells were ready for transformation or long-term storage. For long-term storage, 15 ml of the culture was harvested by centrifugation at 5000 rpm for 5 minutes. The resulting pellet was resuspended in 1.8 ml of the supernatant and mixed with 1.2 ml of glycerol (50% w/v). The competent cells were then aliquoted into 300 µl portions and stored at -80°C.

Transformation

To begin the transformation process, a 300 µl aliquot of competent cells was thawed on ice. Subsequently, it was mixed with 1.7 ml of MN-medium (1x), which was supplemented with 43 µl of glucose (20% w/v) and 34 µl of $MgSO_4$ (1 M). Following this, either 0.1 - 1 µg of genomic DNA or 2 µg of plasmid DNA was added to 400 µl of the competent cell mixture. The mixture was then incubated for 30 minutes at 37°C. After incubation, 100 µl of expression mix was added to the cells, and they were further incubated at 37°C with agitation for 1 hour. Finally, the transformed cells were plated on LB plates containing appropriate antibiotics.

Isolation of plasmid DNA from *E. coli*

To prepare the plasmid DNA, 3 - 5 ml of bacterial overnight culture were first harvested at 13000 rpm. The harvested cells were then treated according to the manufacturer's manual using the Monarch™ Plasmid Miniprep Kit from New England Biolabs (NEB). After the appropriate treatment steps, the plasmid DNA was eluted using deionized water instead of an elution buffer. This eluted plasmid DNA was subsequently used in the transformation process described earlier.

Isolation of chromosomal DNA from *B. subtilis*

To prepare the chromosomal DNA, 3 - 5 ml of an overnight culture of the target strain were first harvested by centrifugation at 13000 rpm for 2 minutes. The resulting pellet was then resuspended in 100 µl of TE buffer mixed with 10 µl of Lysozyme (10 mg/ml). This mixture was incubated at 37°C for 30 minutes and then centrifuged again for 2 minutes at 13000 rpm. Following this, 100 µl of TL Buffer and 20 µL of Proteinase K Solution (20 mg/ml) were added to the pellet, and the mixture was thoroughly mixed by vortexing. Subsequently, the mixture was incubated at 55°C in a shaking water bath for 1 hour to complete bacterial lysis. After incubation, 5 µL of RNase A (20 mg/ml) was added to the tube, and it was inverted several times to mix. The tube was then allowed to sit at room temperature for 20 minutes to remove RNA. Following another centrifugation step at 13000 rpm for 2 minutes, the supernatant was treated with BL buffer and ethanol in two different steps to inactivate all enzymes and remove any residues remaining from cell debris. Finally, cDNA was eluted from a spinning column using deionized water instead of an elution buffer, following the instructions provided in the manufacturer's manual for the peqGOLD Bacterial DNA Kit from VWR, which includes all the materials and solutions mentioned above.

Determining DNA concentrations

To determine the DNA concentration of a sample, one can utilize a UV-Vis Spectrophotometer (Nanodrop), which requires only very small volumes, typically 1 - 2 µl. This device measures the optical density at wavelengths of 260 nm (OD_{260}), 280 nm (OD_{280}), and 230 nm (OD_{230}) relative to the solvent in which the sample is diluted (as a blank). The accompanying software then calculates the DNA concentration and assesses the purity of the DNA, taking into account potential contamination from RNA, proteins, and other impurities that may remain from the DNA extraction process. The spectrophotometer used in this study is the NanoDrop™ 2000/2000c spectrophotometer from ThermoFischer Scientific™.

Agarose gel electrophoresis

Agarose gel electrophoresis is a technique used to separate DNA and RNA molecules based on their size. Agarose, a polysaccharide made up of D-galactose and 3,6-anhydro-L-galactose monomers, forms a gel matrix that acts as a molecular sieve for nucleic acids. Samples are loaded into wells on the gel, and when an electric field is applied, negatively charged nucleic acid molecules migrate through the gel towards the positive electrode. Smaller molecules move faster, resulting in separation by size. The concentration of agarose in the gel is critical for achieving optimal resolution. Typically, 1% (w/v) agarose gels are used, capable of separating molecules ranging from 0.2 to 10,000 kbp in size. Agarose powder is dissolved in 1x TAE buffer, boiled briefly, and supplemented with a DNA stain such as Ethidium Bromide (EtBr) from ThermoFischer Scientific™. The mixture is then poured into a gel chamber, and as it cools, hydrogen bonds form between agarose monomers, solidifying the gel. A comb is inserted into the gel before solidification to create wells for sample loading, and a mixture of sample and loading dye is added to each well. Additionally, a DNA ladder marker is loaded to provide reference sizes. Once the gel is set, it is covered with 1x TAE buffer, and an electric field is applied (~120 V) to induce nucleic acid migration. As the samples migrate through the gel, they separate according to size. After sufficient separation, the gel is visualized using a GelDoc™ XR system (Biorad). The Ethidium Bromide in the gel binds to nucleic acid molecules, allowing for detection under UV light which fluoresces in orange-red range in the wavelength of 590 nm (P. Y. Lee et al., 2012).

Polymerase chain reaction (PCR)

The polymerase chain reaction (PCR) is a technique used to amplify DNA fragments exponentially in a short period of time (Saiki et al., 1985). This process requires two primers that define the region to be replicated. PCR consists of three main steps, each occurring at different temperatures in a thermocycler. Firstly, during the denaturation step, the DNA strands are separated by breaking the hydrogen bonds between the bases.

This step typically occurs at temperatures between 95 and 98°C. Subsequently, during the annealing step at approximately 60°C, the primers bind to their complementary sequences on the DNA strands. The annealing temperature is determined based on the primers' characteristics, particularly their length and GC content. Usually, an annealing temperature is chosen that is 5°C below the primer's melting temperature (Tm). Once the primers are bound, the temperature is raised to around 72°C for the elongation step, allowing the DNA polymerase to synthesize the complementary strand. These three steps are repeated in cycles until the desired amount of DNA product is obtained. Additional steps are often included in the PCR program to optimize its efficiency. These include an initial denaturation step to melt the cDNA, a final elongation step to complete polymerase activity, and a "hold" step to terminate the reaction and protect the product from degradation. For cloning purposes, it is crucial to ensure that the PCR product is identical to the template DNA to avoid mutations. Therefore, a high-fidelity polymerase such as Phusion® polymerase (ThermoScientific), derived from *Pyrococcus furiosus* and engineered for low error rates, is used. Additionally, the PCR products are cleaned and purified using the Monarch® PCR & DNA Cleanup Kit (NEB) to remove contaminants and ensure high-quality DNA for downstream applications.

Table 1. Pipetting scheme of a Phusion®-PCR (50 µl)

Volume [µl]	Compound
10	5x Phusion®HF Buffer
1	dNTPs (10 mM)
1.5	DMSO (100%)
1	Fwd primer (5 pmol)
1	Rev primer (5 pmol)
2	Template DNA (1 ng/µl)
0.25	DNA Phusion® Polymerase (2 U/µl)
33.25	H_2O

Table 2. Cycler program Pfusion® PCR

Step	Temp. [°C]	Time [s]	
Initial denaturation	98	180	
Denaturation	98	30	x 35
Annealing	Primer Tm – 5°C	35	
Elongation	72	30 / kbp	
Final elongation	72	600	
Hold	20	∞	

Colony PCR with *B. subtilis*

Gram-positive bacteria such as *B. subtilis* possess a thicker cell wall compared to Gram-negatives, necessitating cell lysis through a process involving detergent (Triton X-100) and heat to release the free DNA template prior to PCR amplification.

Initially, a fresh single colony or 10 µl of an overnight culture is combined with 30 µl of Triton buffer (0.5% w/v Triton X-100) and subjected to boiling at 99°C for 10 minutes. Subsequently, the mixture is centrifuged for 10 minutes at 13,000 rpm, after which 10 µl of the supernatant is utilized for a 50 µl PCR reaction.

Table 3. Pipetting scheme of a B. subtilis colony PCR (50 µl)

Volume [µl]	Compound
5	5x Phusion®HF Buffer
2	dNTPs (10 mM)
2	Fwd primer (5 pmol)
2	Rev primer (5 pmol)
10	Cell mix as template
0.25	DNA Phusion® Polymerase (2 U/µl)
27.75	H_2O

Table 4. Cycler program B. subtilis colony PCR

Step	Temp. [°C]	Time [s]	
Initial denaturation	98	180	
Denaturation	98	30	x 30 - 35
Annealing	Primer Tm – 5°C	35	
Elongation	72	30 / kbp	
Final elongation	72	600	
Hold	20	∞	

Long-flanking homology PCR

The Long-flanking homology (LFH) PCR is a method used to generate gene mutations or deletions, which can then be introduced into *B. subtilis*. This method originated from cloning in *Saccharomyces cerevisiae* and is employed to amplify deletion cassettes, facilitating gene knockouts through homologous recombination (Wach, 1996). To delete a gene, it is replaced by a deletion cassette containing an antibiotic resistance marker. This process involves two main steps: Firstly, the deletion cassette and upstream/downstream fragments are amplified from a plasmid or chromosomal DNA, respectively. The upstream and downstream fragments are approximately 1 kbp in length, flanking regions of the gene of interest, thereby enabling double homologous

recombination in the bacterium. It is essential that the inner primers of the upstream/downstream fragments have a complementary region with the ends of the deletion cassette, typically around 25 bp long. This ensures that in a second PCR step, all three fragments align to each other, allowing them to be fused together. To facilitate this, the LFH-PCR mixture is prepared, but the oligos are added after a brief pause, allowing for better mixing and pre-annealing of the fragments. Following verification of the product by gel electrophoresis, it is used for transformation of *B. subtilis*.

Table 5. Pipetting scheme for a LFH PCR (100 µl)

Volume [µl]	Compound
20	5x Phusion®HF Buffer
4	dNTPs (10 mM)
8	Fwd primer (5 pmol)[1]
8	Rev primer (5 pmol)
x	100 ng upstream fragment
x	100 ng downstream fragment
x	150 ng resistance cassette
2	DNA Phusion® Polymerase (2 U/µl)
Ad to 100	H_2O

Table 6. Cycler program Pfusion® PCR

Step	Temp. [°C]	Time [s]	
Initial denaturation	98	180	
Denaturation	98	30	x 10
Annealing	Primer Tm – 5°C	35	
Elongation	72	30 / kbp	
Hold	15	600	
Addition of oligos			
Denaturation	98	30	x 25
Annealing	Primer Tm – 5°C	35	
Elongation	72	30 / kbp	
Final elongation	72	600	
Hold	20	∞	

[1] Do not add until the hold step!

Restriction digestion of DNA

The DNA digestion is performed using FastDigest restriction endonucleases (ThermoFischer), which recognize a 4 - 10 bp palindromic sequence and cleave it in a specific manner. The resulting ends can then be ligated with a vector backbone (which is plasmids here) that has been cut with the same enzymes. The reaction utilizes buffers and concentrations specified in the manufacturer's manual.

Table 7. Pipetting scheme for DNA digestion

Volume [µl]	Compound
4	10x FD buffer
4	Enzyme 1
4	Enzyme 2
x	DNA (1 µg)
Ad to 40	H_2O

Ligation of DNA

After digesting the insertion segment and the vector, the DNA fragments were cleaned and purified using a PCR purification Kit (NEB) and subsequently, ligated using T4 DNA ligase (ThermoFischer). After ligating the fragments for two hours at room temperature or overnight on ice, the entire sample was used for transformation of the competent bacteria.

Table 8. Pipetting scheme for a ligation

Volume [µl]	Compound
1	T4 DNA ligase (5 U/µl)
2	10x ligation buffer
x	150 ng insert
x	50 ng plasmid
Ad to 20	H_2O

DNA sequencing

DNA sequencing is a method used to determine the base sequence of a DNA strand. This process is outsourced and performed by Microsynth Seqlab GmbH in Göttingen, Germany. At SeqLab, the DNA sequence is determined using the chain termination method known as Sanger sequencing (Sanger et al., 1977).

Table 9. pipetting scheme for sequencing sample

Volume [µl]	Compound
6	Primer
x	Plasmid (0.7 – 1.2 ng)[2]
Ad to 15	H_2O

Genome sequencing

To identify mutations, amplifications, and gene deletions in suppressor mutants, cDNAs underwent whole-genome sequencing. Genome library preparation and sequencing were conducted by GENEWIZ in Leipzig, Germany, utilizing the Illumina NovaSeq X method for next-generation sequencing of bacterial genomes. Unless otherwise specified, the reads were paired-end (2 x 150 bp) and aligned to the *B. subtilis* SP1 reference genome NC_000964 from GenBank (Barbe et al., 2009), following established protocols (Widderich et al., 2016) using the Geneious software package (Geneious Prime 2024.1.1) (Kearse et al., 2012). Single nucleotide polymorphisms (SNPs) were considered significant when the total coverage depth exceeded 30 reads with a frequency variance of > 90%. SNPs were validated by Sanger sequencing. The amplification level of a genomic region was determined by dividing the average coverage of the amplified region by the average coverage of the entire genome.

Calculating mutation frequency

To calculate the mutation frequency in bacterial strains exhibiting different phenotypes or growth advantages compared to their parental strain, three cultures of 4 ml each were prepared from an overnight culture of the specific strain in a complex medium such as LB. The following day, the cells were collected by centrifugation and washed twice with saline solution to remove any remaining traces of the complex medium. The optical density at 600 nm (OD_{600}) of each culture was adjusted to 1.0. Subsequently, 100 µl aliquots of each culture were separately plated on media that either allowed for selection or screened for suppressor mutations. The plates were then incubated at 37°C for a defined period. After incubation, the number of colonies appearing on each plate was counted visually, and the mutational frequency was estimated as the average of the colony numbers from all three plates. The mutational frequency is estimated based on the concentration of *B. subtilis* cells, which can vary depending on the strain and growth conditions. A commonly used estimate is that an optical density at 600 nm (OD_{600}) of 1 corresponds roughly to 10×10^7 colony-forming units (CFUs) per milliliter. This estimation is derived from the relationship between the optical density of a bacterial culture at 600

[2] For PCR product (18 ng per 100 bp) is recommended

nm and the number of viable cells present in the culture (D. E. Lea & Coulson, 1949; Gunka et al., 2012).

β-Galactosidase assay

This enzyme assay is a quantitative method used to measure the activity of a promoter *in vivo*. This method involves the fusion of the promoter with a reporter gene, typically the *lacZ* gene. When the fused promoter is activated, it drives the expression of β-galactosidase, an enzyme that catalyzes the hydrolysis of lactose or chromogenic substrates such as o-nitrophenyl-β-D-galactopyranoside (ONPG). The enzymatic reaction results in the formation of o-nitrophenol, which absorbs light at a wavelength of 420 nm. The amount of o-nitrophenol produced within a specific time period is directly proportional to the activity of the promoter (Griffith & Wolf, 2002). Single colonies of the desired *B. subtilis* strains were used to inoculate 4 ml of SM minimal medium supplemented with appropriate antibiotics and histidine (final concentration 0.1%) as the sole source of carbon and nitrogen. The inoculated cultures were then incubated overnight at 28°C with agitation to establish a pre-culture. The following day, 10 ml of the same medium were inoculated using the pre-culture, with an initial OD_{600} of 0.1, and incubated at 37°C for several hours with agitation until reaching an OD_{600} of 0.5 – 0.8. Subsequently, cells from 1.5 to 2 ml of the main culture were harvested by centrifugation at 4°C, and the β-galactosidase activity was determined as described in the literature (Kunst & Rapoport, 1995; Stannek et al., 2015).

Determination of α-amylase activity

The α-amylase, encoded by the *amyE* gene, hydrolysis of α bonds in large, α-linked polysaccharides, such as starch, resulting in the production of shorter chains, dextrins, and maltose. The activity of α-amylase can be assessed using the iodine–starch test, where iodine reacts with starch to produce an intensely blue-black color. The *amyE* locus, located on the *B. subtilis* chromosome, can serve as a site for the integration of promoter-reporter gene fusions via double-homologous recombination at the 5’ and 3’ ends. To achieve this, the desired promoter or gene is fused to a reporter gene present in plasmids such as pAC5 and pAC7 (Weinrauch et al., 1991; Martin-Verstraete et al., 1994; Stülke et al., 1997). Integration of these plasmids into the *B. subtilis* chromosome leads to disruption and inactivation of the *amyE* gene, resulting in the absence of α-amylase activity. To detect α-amylase activity, a single colony of the *B. subtilis* transformants and a positive control (wild-type strain SP1) were streaked in separate lines on top of the starch-agar plates and incubated overnight at 37°C. The next day, 5 ml of diluted Lugol solution (1x) was applied on the surface of the plates. Strains harboring the *amyE* gene exhibit α-amylase activity, leading to the hydrolysis of starch and the formation of a halo

around the bacteria. Conversely, strains lacking the *amyE* gene do not hydrolyze starch and consequently do not exhibit halo formation.

Preparation of samples for metabolome analysis

To quantify the concentration of metabolites in a specific *B. subtilis* strain, the cells were initially cultured in the 4 ml of SM minimal medium. After culturing overnight at 37°C with agitation, a pre-culture is inoculated the next day using the overnight culture in 10 ml of SM medium with a starting OD_{600} of 0.1. This pre-culture is then incubated for 6 hours at 37°C and 200 rpm. Following incubation, a small sample of the culture is taken to measure the OD_{600}, which is used to calculate the volume of culture required to collect approximately 0.5 mg of biomass (625 µl of culture with an OD_{600} of 1.0 is roughly equivalent to 0.5 mg of biomass). Subsequently, 0.5 mg of biomass from each strain is loaded separately onto Durapore® 0.45 µm PVDF membrane filters and filtered to remove the medium and collect the cells. The filters are then immediately transferred with tweezers into pre-cooled quenching solution in glass vials, ensuring the filters are fully submerged. The vials are kept at -20°C for at least 30 minutes. Afterwards, 1 ml of the mixtures is transferred to 1.5 ml reaction tubes and centrifuged at -9°C and 13000 rpm for 15 minutes to remove remaining particles from cell disruption. Finally, 400 µl of the supernatants are stored in a new 1.5 ml tube at -80°C until LC-MS analysis is performed.

Overexpression of recombinant proteins in *E. coli*

To produce proteins on a large scale, expression plasmids were introduced into suitable *E. coli* strains (*E. coli* BL21). To perform this task, plasmids pGP172 for N-terminally Strep-tag fusion and pGP574 for C-terminally Strep-tag fusion were used, as described by Jonathan Rosenberg in his PhD thesis (2018), to construct pBP641 and pBP642, respectively. Both plasmids share the same vector backbone and are controlled by a *lac*-inducible promoter, which prevents protein expression in the absence of the artificial inducer IPTG. Following introduction of the expression plasmid into *E. coli* BL21, 50 ml LB medium supplemented with appropriate antibiotics were inoculated with a fresh colony and cultured overnight at 37°C with agitation. The following day, 500 ml of preheated LB medium were inoculated with the overnight culture to achieve a starting OD_{600} of 0.1. The culture was then incubated until reaching an OD_{600} of 0.8 – 1.0. Subsequently, IPTG was added to a final concentration of 1 mM to initiate protein expression. After 2 – 3 hours of induction, the culture was harvested by centrifugation at 5000 rpm for 15 minutes at 4°C. The cells were briefly washed with 15 ml of Buffer W (1x) and pelleted again by centrifugation at 8500 rpm for 15 minutes at 4°C. The resulting pellets were stored at -20°C until further processing.

Cell Disruption

The French pressure cell, often referred to as the French press, was named after its inventor Charles Stacy French from the Carnegie Institution of Washington. It is a widely used method for cell disruption, necessary for subsequent experiments such as protein purification or protein-protein interaction studies. In this method (using French press machine from G. HEINEMANN HTU-DIGI-Press), cells were first resuspended in an appropriate buffer and poured into a pre-cooled cylinder, sealed on the top with a movable piston. At the bottom, there is a narrow hole with a valve through which the cell suspension is pressed. This process generates a pressure of approximately 18,000 psi, causing the cells to disrupt as shear forces occur due to the smaller release opening. The resulting cell lysate was collected, and the process was typically repeated at least once for Gram-negative bacteria and twice for Gram-positive bacteria to ensure thorough disruption. The lysed bacteria were then centrifuged at 8,500 rpm for 15 minutes at 4°C, followed by a subsequent centrifugation at 35,000 rpm for 1 hour at 4°C using an ultracentrifuge. Finally, the supernatant containing the desired proteins was separated from the cell debris and stored at 4°C for further experiments.

Affinity chromatography

There are various methods for protein purification, with affinity chromatography being one of the most widely used. In this method, affinity tags, which are specific sequences of amino acids that exhibit binding specificity for certain materials, are fused to one end of the target protein (either the N- or C-terminal). To perform affinity chromatography, the bacterial crude extract containing the tagged protein is applied to an affinity column filled with immobilized affinity molecules. Only proteins containing the specific amino acid sequence bind to the column, while others remain in the liquid phase and are washed away. Once the protein is bound to the column, elution is achieved by adding a ligand with higher affinity to the stationary phase, allowing the protein to be released and collected for further use.

Purification of Strep-tagged proteins by affinity chromatography

The Strep-tag II is a short peptide (8 amino acids, WSHPQFEK) that can be fused to one end of a target protein, allowing it to bind with high specificity to Strep-Tactin®, an engineered form of streptavidin. According to the manufacturer, the binding affinity of Strep-tag II to Strep-Tactin® (KD = 1 mM) is nearly 100 times higher than its affinity to streptavidin. Additionally, Strep-tag II is more resistant to SDS and proteases. The natural ligand for streptavidin is biotin, but a biotin derivative, desthiobiotin, is used for eluting the protein. Desthiobiotin offers reversible binding, allowing for easy elution under mild conditions by competing with free desthiobiotin. Furthermore, using desthiobiotin helps reduce nonspecific or background binding that may occur with biotin, as desthiobiotin does not bind as tightly to endogenous biotin-binding proteins. To perform affinity

chromatography, an affinity column was filled with 1 ml of 50% Strep-Tactin® (IBA Lifescience) suspension per 1 liter of cell culture and equilibrated with 5 ml of buffer W. The crude extract (CE), obtained after cell lysis, was loaded onto the column, and the flow-through was collected (FT). The column was then washed five times with 1.25 ml of buffer W (W1 – W5) before elution commenced by adding four times 0.5 ml of buffer E (E1 – E4).

Protein-pulldown experiment

The protein-pulldown experiment is a method used to study *in vitro* protein-protein interactions. In this experiment, specific amounts of a purified protein were added to the crude extract of a *B. subtilis* strain, which may contain unknown interaction partners. The mixture is then incubated at 37°C for 30 minutes and loaded onto a Strep-Tactin® affinity column. Subsequently, the column is washed as described in the respective purification protocol. Finally, after elution, the different elution fractions are checked using an SDS gel with subsequent silver staining.

Determination of protein concentration

One fast and simple method to measure the concentration of proteins is the Bradford assay. The Bradford reagent can be used for solutions, and the mechanism relies on the formation of a complex between Coomassie brilliant blue G-250 and the proteins (Bradford, 1976). The absorption increases with increasing protein amount and vice versa. This assay can be used for the determination of protein concentrations ranging from 0.1 to 1.4 mg.

In this assay, 1 ml of Bradford reagent (1x) is mixed with 2–20 µl of protein solution, and the OD_{595} is measured in relation to a blank containing only Bradford reagent and elution buffer/dialysis buffer. A calibration curve is then plotted, showing the linear relation between the amount of protein and the absorption at OD_{595}. The slope of the calibration curve is typically around 0.0536 and is used as the standard value for further measurements.

To calculate the amount of protein in the sample, the following equation is used:

$$c = \frac{OD_{595}}{V \times 0.0536}$$

Where *V* is the volume of the protein solution in microliters used for the measurement and *c* is the protein concentration in the tested solution. The resultant unit is µg/µl.

SDS polyacrylamide gel electrophoresis

Polyacrylamide gel electrophoresis (PAGE) is a method developed to separate proteins by their molecular weight. It employs a discontinuous polyacrylamide gel composed of

two distinct regions: a stacking gel and a running gel. Both gels contain acrylamide, water, Tris-HCl buffer, ammonium persulfate (APS), and N,N'-Methylenebisacrylamide, with the addition of the radical initiator TEMED. The inclusion of APS and TEMED initiates radical polymerization, causing acrylamide molecules to crosslink with N,N'-Methylenebisacrylamide. This results in the formation of the gel matrix. Similar to the agarose gels, the percentage of acrylamide in the gel determines the size range of proteins that can be separated. In this study, 12% gels were used to separate proteins ranging from 10 to 180 kDa.

SDS-PAGE is a specialized variant of polyacrylamide gel electrophoresis (PAGE) that utilizes sodium dodecyl sulfate (SDS), an anionic, negatively charged detergent, to denature and linearize proteins (Laemmli, 1970). SDS coats the proteins uniformly, imparting a negative charge to each protein molecule and disrupting the native protein structure. When an electric field is applied, the negatively charged proteins migrate towards the positively charged electrode. The rate of migration is determined by the size of the protein molecules, with larger proteins moving more slowly through the gel matrix due to increased steric hindrance.

In SDS-PAGE, the gel consists of two parts: the stacking gel and the running gel. The stacking gel, which has a lower percentage of acrylamide and a pH near 7, allows proteins to concentrate and form a tight band at the interface between the stacking and running gels. The running gel, with a higher pH (usually around 8.8), provides the appropriate environment for protein separation based on size.

To prepare the gel, the running gel solution was poured into a gel casting apparatus, such as a Mini-PROTEAN® system (Bio-Rad), and overlaid with isopropanol (or simply water) to exclude oxygen and facilitate polymerization. Once polymerized, the stacking gel was applied, and a comb was inserted to create sample wells. After removing the comb, protein samples (up to 15 µl) mixed with 2.5 µl of 6 x loading dye were incubated for 10 minutes at 95°C. This step helps to denature and linearize the protein samples, ensuring uniform binding of the SDS detergent and facilitating accurate protein separation during electrophoresis. Subsequently, the mixtures were loaded into the wells along with a pre-stained protein marker for size reference. The gel was then subjected to electrophoresis at a constant voltage, typically around 160 V, until the bromophenol blue dye in the loading buffer reaches the bottom of the gel, indicating that the smallest proteins have migrated sufficiently.

Table 10. Pipetting scheme of a 12% SDS running gel

Volume [ml]	Compound
3.3	H_2O
4	Acrylamide
2.5	Tris-HCl pH 8.8 (1.5 M)
0.1	SDS (10% w/v)

0.1	APS (10% w/v)
0.010	TEMED

Table 11. Pipetting scheme of a separation gel

Volume [ml]	Compound
6.83	H_2O
1.5	Acrylamide
0.87	Tris-HCl pH 8.8 (1.5 M)
0.1	SDS (10% w/v)
0.1	APS (10% w/v)
0.010	TEMED

Coomassie staining

To fix and visualize the separated proteins by gel electrophoresis, the Coomassie Brilliant Blue staining method was employed in this study. This method is fast, easy, and commonly used for detecting proteins. Initially, the gel was immersed in a fixation solution and incubated for at least 10 minutes at room temperature with gentle agitation. Following fixation, the gel was covered with Coomassie Brilliant Blue staining solution for 10 to 20 minutes at room temperature with gentle agitation. Finally, to remove background staining from the SDS gel, it was incubated overnight in a destaining solution.

Silver staining

Since silver staining is a highly sensitive technique, capable of detecting even small amounts of proteins (sensitivity 5 - 30 ng per protein band), it is commonly used for applications such as pull-downs or protein-protein interaction experiments. In this technique, amino acid residues such as glutamate, aspartate, and cysteine form complexes with silver ions, leading to the reduction of silver ions to metallic silver. Unlike Coomassie staining, silver staining cannot be used for quantitative determination of proteins because the level of staining depends heavily on the amount of these specific residues present (Winkler et al., 2007). The silver staining procedure follows the method described by Nesterenko, Tilley, and Upton (Nesterenko et al., 1994).

Table 12. Protocol of silver protein staining

Step	Solution	Time
Fixing	Fixation solution	1 – 24 h

Washing	EtOH (50% w/v)	20 min	3x
Reduction	Thiosulfate solution	1.5 min	
Washing	Deion. H_2O	20 s	3x
Staining	Impregnator	15 – 25 min	
Washing	Deion. H_2O	20 s	3x
Development	Developer	Until sufficient stained	
Washing	Deion. H_2O	20 s	2x
Stop	Stop solution	5 min	

Dialysis

To remove unnecessary molecules and salts from elution fractions containing Strep-tagged proteins, dialysis is performed. This process involves placing the elution fraction into a dialysis tube, such as the Thermo Scientific™ SnakeSkin™ Dialysis Tubing with a molecular weight cutoff (MWCO) of 10 KDa and an inner diameter of 22 mm. This tubing consists of a semi-permeable membrane that allows the passage of smaller molecules and ions while retaining larger molecules like proteins.

Before placing the protein solution into the dialysis tube, the tube is boiled in deionized water for 10 minutes to ensure proper sterilization. Once sterilized, the protein solution is transferred into the dialysis tube, and both ends are sealed with clips to prevent leakage. The sealed tube is then submerged in dialysis buffer (buffer W), which is the desired buffer for subsequent reactions, at a ratio of 1000-fold excess of buffer volume to protein solution volume. The tube is left to dialyze overnight with gentle stirring to facilitate the diffusion of small molecules through the semi-permeable membrane and achieve equilibration. After dialysis, the protein is free from excess molecules and salts and is ready for further experimentation.

Results

Restoration of glutamate prototrophy of a *gltAB* mutant by genomic adaptation

At the outset of the present PhD thesis, the concept was to establish an interspecies cross-feeding community to identify novel players in vitamin B6 metabolism. In this community, the *B. subtilis gltAB* mutant and the *C. glutamicum pdxST* mutant were positioned on opposite ends, while *B. subtilis* presumed to produce and release vitamin B6 required by *C. glutamicum*, and *C. glutamicum* reciprocating by producing and releasing L-glutamate to feed *B. subtilis*. For this purpose, *C. glutamicum* required its specialized minimal medium called CGXII, which is also compatible with the growth of *B. subtilis*.

The role of the GOGAT, GltAB, as the primary enzyme responsible for glutamate biosynthesis in *B. subtilis* was elucidated in 1989 (Bohannon & Sonenshein, 1989). It was widely believed that GOGAT-GS was the sole pathway for glutamate production in the cell. Therefore, we decided to delete the *gltAB* genes, which encode GOGAT, in the background of the *B. subtilis* SP1 (a strain derived from the laboratory-commonly used *B. subtilis* 168 (*trpC2*) but not auxotrophic for tryptophan like its parental strain).

To achieve this, competent *B. subtilis* SP1 cells were transformed with cDNA from *B. subtilis* GP807 (*trpC2 gltAB*::*tet*), a 168-derivative strain with *gltAB* deleted and replaced with a tetracycline resistance cassette (*tet* cassette). The transformants were screened on LB agar plates supplemented with tetracycline.

To confirm that the newly obtained transformant, named BP261, was only auxotrophic for glutamate and not tryptophan, it was cultivated alongside *B. subtilis* SP1, 168, and GP807 as controls. This was done on plates of C-Glc medium supplemented with and without tryptophan (0.5% w/v), as well as CE glucose medium supplemented with and without tryptophan. The results revealed that unlike the other named strains, BP261, regardless of the presence of tryptophan, was able to grow only when glutamate was present in the medium (Fig. 6A).

BP261 (*gltAB*) was then propagated on CGXII plates, a medium commonly used for growth and maintenance of *C. glutamicum*, containing glucose as a sole carbon source and ammonium/urea as a nitrogen source (Keilhauer et al., 1993). After leaving the plates at room temperature for one week, several single colonies of potential suppressor mutants emerged. Several suppressor mutants were isolated, but it was decided to proceed with only two of them, designated as BP364 (M1) and BP365 (M2), for further studies. They were propagated on the same medium supplemented with tetracycline, alongside their parental strain BP261 as a control. Incubation at 37°C for 48 hours

revealed that only the suppressor mutants BP364 and BP365 were able to grow, while no growth was observed for BP261 (Fig. 6B).

To confirm the clean deletion of the *gltAB* genes by the *tet* resistance cassette, a PCR was performed using primers targeting the *tet* gene (FC363) and *gltC* (the upstream gene of the *gltAB* locus) (MD56) on the cDNA of BP364 (M1) and BP365 (M2), compared to GP807 (*trpC2 gltAB*::*tet*) as a control. Results of the gel electrophoresis confirmed that the *gltAB* genes were completely replaced by the *tet* resistance cassette (Fig. 6C). Additionally, to investigate if there was a genetic link between the suppressor mutations and the *gltAB* locus, competent cells of *B. subtilis* SP1 were separately transformed with cDNA from both suppressor mutants BP364 and BP365. The growth of the resulting transformants, T1 and T2, was compared to M1 and M2 on CGXII plates with and without glutamate. The inability of the transformants to growth on CGXII plate without supplementation with glutamate indicated that there was no genetic connection between the gain of prototrophy in M1 and M2 and the *gltAB* locus (Fig. 6D).

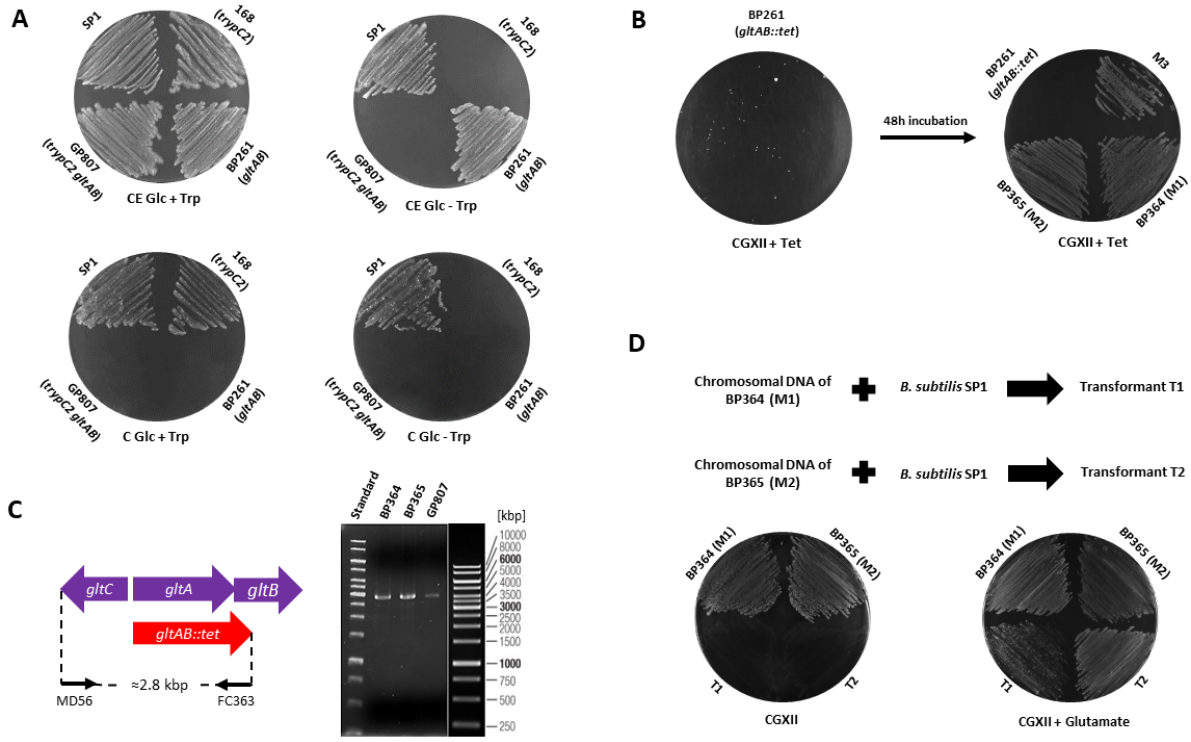

Figure 6. Serendipitous mutations relieve glutamate auxotrophy of a *gltAB* mutant and are not linked to the *gltAB* locus.
A) Growth experiment of BP261 (*gltAB*) alongside the parental strain GP807 (*trpC2 gltAB*), SP1 and 168 (*trpC2*) on C-Glc medium and CE glucose medium with and without tryptophan at 37°C for 48h. **B)** Emergence of serendipitous suppressor mutants from BP261 on CGXII medium after 48h incubation at 37°C and comparing the growth of 3 of them (M1, M2, M3) with their parental strain on the same medium. **C)** Verification PCR on cDNA of BP364 (M1), BP365 (M2) and GP807 (*trpC2 gltAB*) using the primers binding to the *tet* and *gltC* genes. **D)** Comparing the growth of transformed SP1 with cDNA of BP364 and BP365, T1 and T2, with BP364 and BP365 on plates of CGXII and CGXII plus glutamate. (Figure adapted from Mardoukhi et al., 2024)

Mutations in *ansR* and *citG* genes are responsible for relieving glutamate auxotrophy of a *gltAB* mutant

After confirming that the mutants were not linked to the *gltAB* locus, the cDNA of both suppressor mutants BP364 and BP365 was extracted and sent for whole-genome sequencing. Analysis of the data revealed that in both cases, the *ansR* and *citG* genes are affected (Tab. 13). The *ansR* gene encodes AnsR, a transcriptional repressor of an operon consisting of two other genes, *ansA* and *ansB*. This operon is involved in the degradation of L-aspartate and L-asparagine. The *ansA* gene encodes L-asparaginase AnsA, which, along with the main L-asparaginase enzyme AnsZ, catalyzes the degradation of L-asparagine to L-aspartate and a released ammonium group. The *ansB* gene codes for L-aspartase AnsB, which degrades L-aspartate to fumarate (Sun & Setlow, 1991; Fisher & Wray, 2002).

Mutations in *ansR*, which appear to lead to the expression of a non-functional protein due to amino acid replacements close to the turn-helix-turn motif responsible for DNA attachment and the dimerization domain, essential for the functional activity of AnsR (C57R in BP364 and L101P in BP365, respectively), disrupt its capability to bind to the promoter of *ansAB* (Fig. 7A). Consequently, the *ansAB* operon is de-repressed which allows fumarate from the TCA cycle to be converted to L-aspartate by the enzymatic action of AnsB. This reaction, which is energy-free, assimilates nitrogen. Subsequently, through a transamination reaction catalyzed by aspartate transaminase AspB, the ammonium group is transferred from aspartate to α-ketoglutarate, resulting in the synthesis of one molecule of L-glutamate and one molecule of oxaloacetate. The oxaloacetate can then enter the TCA cycle. The transamination reaction mediated by AspB is also energy-free (Dajnowicz et al., 2017).

In the suppressor mutant BP364 (M1), a deletion of approximately 10.7 kbp region (coordinates 3381391 to 3392113) results in the removal of a significant portion of the *citG* gene, which encodes the TCA cycle enzyme fumarase CitG, responsible for conversion of fumarate to malate (Moir et al., 1984; Miles & Guest, 1985; Feavers et al., 1988). Similarly, in suppressor mutant BP365 (M2), a single nucleotide insertion at position 62 causes premature termination of translation, resulting in a truncated and non-functional protein. In both cases, the inactivation of fumarase leads to the accumulation of fumarate. This accumulation likely exerts further pressure to channel fumarate through aspartase, resulting in the synthesis of L-aspartate. Subsequently, L-aspartate can be converted to glutamate through the action of aspartate transaminase.

Based on the mutations observed in M1 and M2, it can be inferred that *B. subtilis* lacking the *gltAB* gene can overcome glutamate auxotrophy through just two genomic alterations. Firstly, the loss of DNA-binding activity in AnsR allows *B. subtilis* to synthesize glutamate via the reversible reactions catalyzed by AnsB and AspB (Toney, 2014; Viola, 2000). These enzymes convert fumarate and ammonium to L-aspartate, which is then further converted to L-glutamate. In addition, the metabolic flux from the

TCA cycle to the newly established aspartase-aspartate transaminase glutamate biosynthesis bypass is enhanced by the inactivation of fumarase CitG (Fig. 7B).

Table 13. Identified mutations in the BP261 (*gltAB*) mutants by NGS

Strain	Mutant	Phenotype	Affected gene, mutations	Amino acid exchanges, effect on the protein
BP364	M1	Growth on CGXII	*ansR* T302C, 10.7 kbp deletion including *citG*	AnsR L101P, CitG not synthesized
BP365	M2	Growth on CGXII	*ansR* T169C, *citG* Δ62G	AnsR C57R, CitG ΔC43

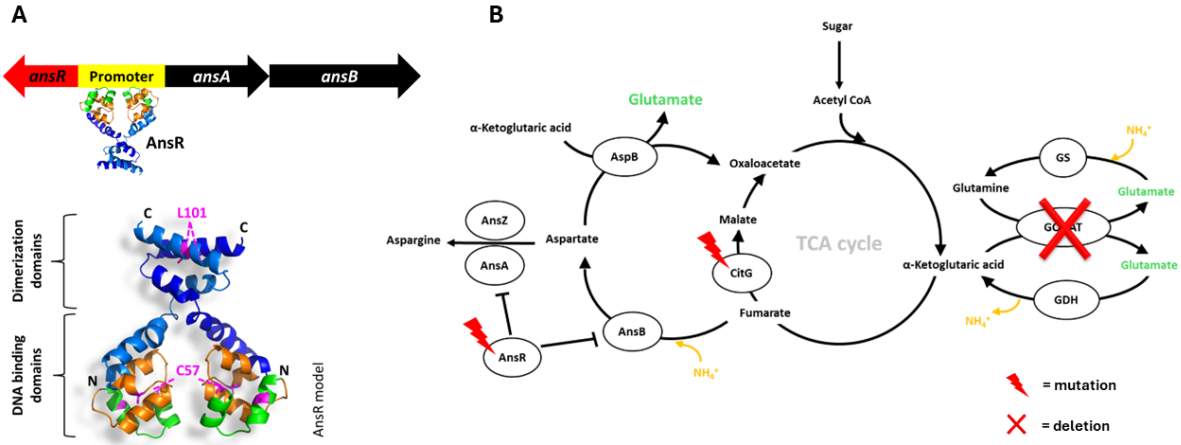

Figure 7. Only two genomic alterations in the *ansR* and *citG* genes relieve glutamate auxotrophy from the *B. subtilis gltAB* strain.
A) AnsR, a transcriptional repressor of the *ansAB* operon, has its repressive effect nullified by single point mutations in the DNA binding domain and dimerization domain. This leads to the deactivation of AnsR, allowing for the expression of the *ansAB* operon (the structural homology model of AnsR was constructed by SWISS-MODEL server based on EspR structure from *Mycobacterium tuberculosis*, (PDB-id: 3QF3) (Blasco et al., 2011). **B)** The *B. subtilis gltAB* mutant overcomes glutamate auxotrophy by acquiring inactivating mutations in the *citG* and *ansR* genes, enabling the production of glutamate through a non-canonical pathway (aspartate-aspartate transaminase pathway).

Design a screening system for identifying and classifying of the *gltAB* suppressor mutants

To determine if inactivation of *ansR* is sufficient to overcome glutamate auxotrophy in the *gltAB* mutant, a selection and screening system was established. For this reason, it was decided to fuse the promoter of *ansAB* to the *lacZ* gene and insert the constructed translational P_{ansAB}-*lacZ* into the *gltAB* mutant (Fig. 8A). Subsequently, the newly constructed strain designated as BP265 (*gltAB* P_{ansAB}-*lacZ*) was grown on CGXII agar plates supplemented with the chromogenic substrate X-Gal.

First, the promoter region of *ansAB* was amplified by PCR from the cDNA of *B. subtilis* 168 using F_{oligo} SM1 and R_{oligo} SM2 primers, which carry the *Eco*RI and *Bam*HI restriction sites, respectively. Subsequently, the promoter segment was fused to the *lacZ* gene inside plasmid pAC7. This plasmid is designed for constructing translational *lacZ* fusions and can be integrated at the *amyE* locus. Also, it does not replicate in *B. subtilis* and so needs to be first cloned inside *E. coli* (Weinrauch et al., 1991). Both the PCR product and the plasmid were digested with the respective enzymes and then ligated together. The ligation sample was used to transform *E. coli* XL1-Blue. The resulting construct, designated as pBP1110 (P_{ansAB}-*lacZ*), was then transformed into competent *E. coli* XL1-Blue and selected on LB plates supplemented with ampicillin and X-Gal. To confirm the correct insertion of the *ansAB* promoter segment into the pAC7, plasmids were extracted from blue colonies of *E. coli* and subjected to Sanger sequencing using primer IS37.

After confirming the correct construction of the plasmid, competent cells of BP261 (*gltAB*) were transformed with pBP1110 and selected on LB agar supplemented with kanamycin and X-Gal. Afterward, a starch assay was performed with 4 single blue colonies of the newly constructed strain BP265 (*gltAB* P_{ansAB}-*lacZ*) to ensure the correct integration of the plasmid into the *amyE* locus.

Next, BP265 was cultured overnight in LB. The following day, cells were washed two times with saline solution and propagated on CGXII plate supplemented with X-Gal. After 3 days of incubation at 37°C, several blue colonies appeared, indicating inactivation mutations in *ansR*. Further incubation led to the emergence of white suppressor mutants, which could arise from either loss-of-function mutations in *citG* or amplification of the genomic segment containing the *ansAB* locus, as reported in other studies (Dormeyer et al., 2017; Richts et al., 2021).

Analysis of *gltAB* blue suppressors

First, to identify and characterize the blue suppressor mutants, two separate colony PCR experiments were conducted on 10 of the isolated blue colonies, designated as BP281 to BP290 (Fig. 8B). In the first PCR, primer pairs SM2 and SM18 were used to amplify the *ansR* gene and its promoter region, while in the second PCR, primers SM3 and SM4 were employed to amplify the *citG* gene. Subsequently, the PCR products were subjected to Sanger sequencing (Tab. 14). The results confirmed our hypothesis, as all 10 suppressor mutants exhibited mutations related to *ansR*. Among these mutants, 8 showed insertions at the same position (A36), which could be considered a mutational hotspot leading to truncated and non-functional proteins. Additionally, one mutant displayed a large deletion (365 bp), and another exhibited a mutation in the ribosome-binding site of the *ansR* promoter. Regarding suppressor mutations in *citG*, only 4 of the mutants showed alterations in this gene.

In conclusion, the inactivation of *ansR* or reduced expression of *ansR* is necessary to relieve repression on the *ansAB* genes and open up the AnsB/AspB pathway for

glutamate synthesis. Furthermore, mutations in *citG* that inactivate fumarase activity or decrease its activity likely contribute to redirecting metabolic flux toward the aspartate-dependent pathway.

Table 2. Identified mutations in the BP265 (*gltAB* P_{ansAB}-*lacZ*) by Sanger sequencing

Strain	Mutant	Phenotype	Affected gene, mutations	Amino acid exchanges, effect on the protein
BP281	B1	Growth on CGXII, blue colony	*ansR* +A36, *citG* +G917	AnsR ΔC11, CitG ΔC310
BP282	B2	Growth on CGXII, blue colony	*ansR* Δ2456934-2457298	AnsR ΔC16
BP283	B3	Growth on CGXII, blue colony	*ansR* +A36, *citG* C1226A	AnsR ΔC11, CitG A409E
BP284	B4	Growth on CGXII, blue colony	*ansR* +A36	AnsR ΔC11
BP285	B5	Growth on CGXII, blue colony	*ansR* +A36	AnsR ΔC11
BP286	B6	Growth on CGXII, blue colony	*ansR* +A36	AnsR ΔC11
BP287	B7	Growth on CGXII, blue colony	P_{ansAB} (G-10A), *citG* T876A	Enhanced *ansAB* expression, CitG D292E
BP288	B8	Growth on CGXII, blue colony	*ansR* +A36	AnsR ΔC11
BP289	B9	Growth on CGXII, blue colony	*ansR* +A36 *citG,* Δ3390211-3390276	AnsR ΔC11, CitG not synthesized
BP290	B10	Growth on CGXII, blue colony	*ansR* +A36	AnsR ΔC11

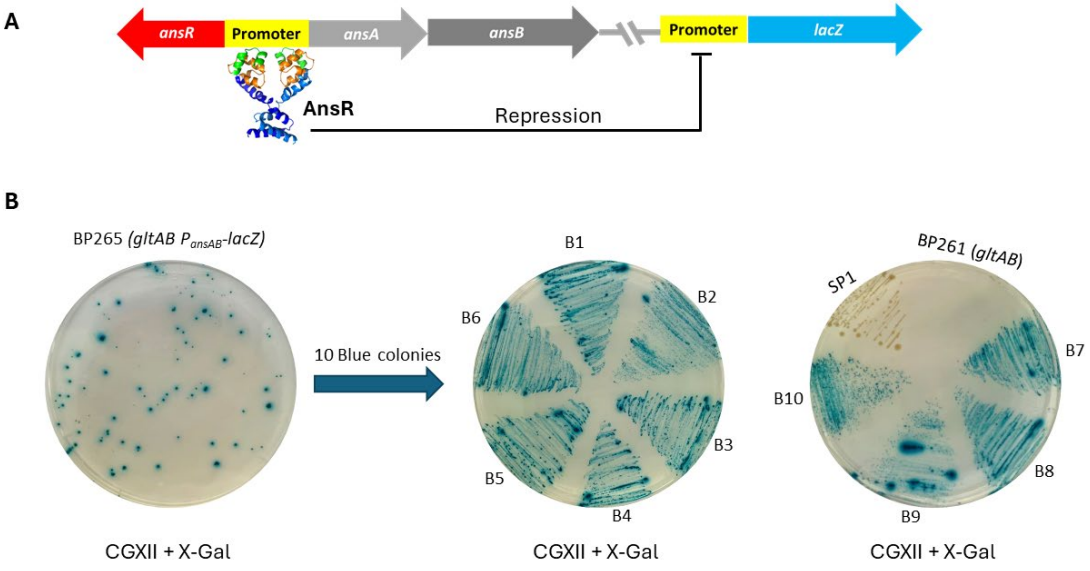

Figure 8. Schematic illustration of the screening system and emergence of blue suppressor mutants derived from BP265 (*gltAB* P_{ansAB}-*lacZ*) on CGXII plates supplemented with X-Gal. **A)** Screening-reporter system constructed from the fused of *ansAB* promoter to *lacZ* reporter gene. **B)** Emergence of blue suppressor mutants from BP265 (*gltAB* P_{ansAB}-*lacZ*) by cultivation on CGXII plates supplemented with X-Gal for 3 days at 37°C.

Analysis of *gltAB* white suppressors

To identify and characterize the white suppressor mutants, incubation of the CGXII plates carrying BP265 (*gltAB* P_{ansAB}-*lacZ*) was extended to 8 days at 37°C, resulting in the anticipated appearance of numerous small white suppressor mutants. One such single white colony, designated as BP298, was isolated (Fig. 9A) and subsequently propagated three times on CGXII + X-Gal plates. Then, cDNA from BP298 was extracted and subjected to Illumina sequencing. Analysis of the sequencing data revealed a substantial amplification within a genomic segment approximately 25.3 kbp in size, encompassing the *ansAB* locus (Fig. 9B). By evaluating the average coverage of the amplified region compared to the entire genome, revealing a 5-fold increase in amplification dosage, it becomes apparent that despite the persistent activity of AnsR within the cell, these findings suggest that enhancing the expression of *ansAB* could provide an alternative mechanism for *B. subtilis* to alleviate glutamate auxotrophy in the *gltAB* mutant strain. This may be accomplished by upregulating the expression of the *ansAB* locus to a degree where its entire promoter region is no longer susceptible to repression by AnsR.

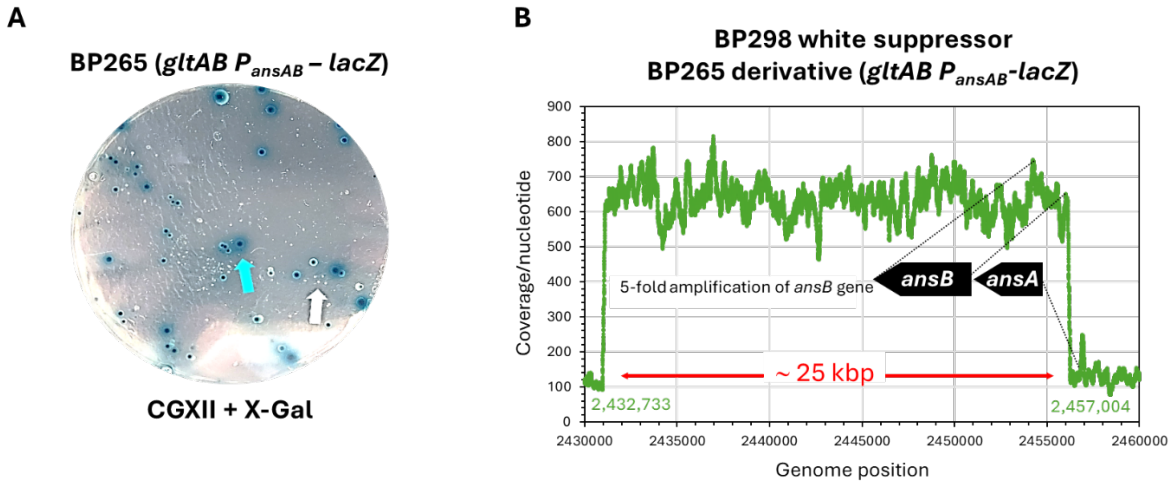

Figure 9. White suppressor mutants derived from BP265 (*gltAB* P_{ansAB}-*lacZ*) carrying *lacZ* fusion. **A)** Extended incubation of CGXII plates containing BP265 at 37°C up to 8 days resulted in the appearance of small white colonies. Blue and white arrows point to the blue and white colonies, respectively. **B)** a 5-fold amplification in a region approximately 25.3 kbp in size where *ansAB* genes are located enhances 5 times more expression of *ansAB* genes. (Figure adapted from Mardoukhi et al., 2024)

Effect of additional copy of *ansR* on the genomic stability of the *gltAB* mutants

Following the characterization of blue and white suppressor mutants of BP265 (*gltAB* P_{ansAB}-*lacZ*), an investigation was conducted to determine whether the presence of an additional copy of *ansR* alongside the native copy would alter the mutational frequency and distribution of blue and white colonies. For this purpose, PCR amplification was performed on the cDNA of *B. subtilis* SP1 using F_{oligo} SM36 and R_{oligo} SM2 primers, which contain *Eco*RI and *Bam*HI restriction sites, respectively. This PCR targeted the *ansR* gene and its promoter region. Subsequently, the purified and digested PCR product was ligated into the pAC7 plasmid, which had been digested with the same restriction enzymes. The newly constructed plasmid, designated as pBP1111, was initially cloned using *E. coli* XL1-Blue. Following plasmid extraction, it was introduced into competent *B. subtilis* BP261 (*gltAB*), resulting in the construction of the new strain BP294 (*gltAB ansR*-P_{ansAB}-*lacZ*).

Subsequently, cells from overnight cultures of BP265 and BP294 grown in LB medium were washed twice with saline solution, and their OD_{600} was adjusted to 1.0. Finally, 100 µl of each cell suspension was spread onto three plates of CGXII supplemented with X-Gal and incubated at 37°C for up to 12 days. The number of suppressor mutants was enumerated based on their color in the subsequent days.

Observations suggest that *B. subtilis* strain BP294 (*gltAB ansR*-P_{ansAB}-*lacZ*), harboring two copies of the *ansR* gene (one native and one integrated into the *amyE* locus), exhibited decreased mutational frequency in *ansR* (which is already reported in the previous experiment that typically leads to the emergence of blue color colonies). This reduced mutational frequency is attributed to the decreased likelihood of mutations occurring simultaneously in both copies of *ansR*, compared to the scenario where only one copy is present (BP265 (*gltAB* P_{ansAB}-*lacZ*)) (Fig. 10A). Consequently, BP294 predominantly forms fewer and only white suppressor mutants (Fig. 10B). Thus, it can be inferred that inactivation of *ansR* is pivotal in facilitating the utilization of the AnsB-AspB glutamate synthesis pathway, thereby retaining glutamate prototrophy in *gltAB* mutants.

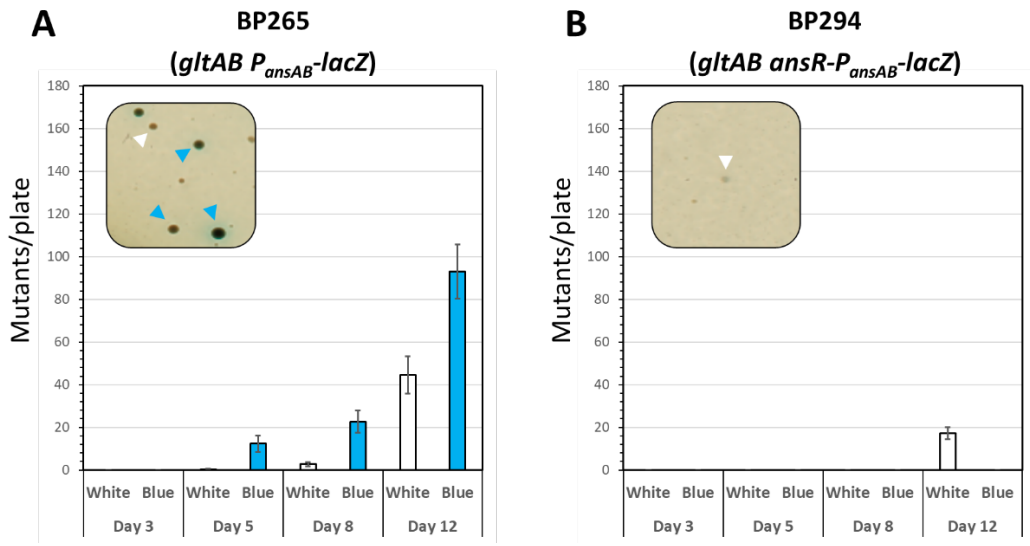

Figure 10. Blue-white colony screening with the *B. subtilis gltAB* mutant strains carrying one or two copies of *ansR* gene.
A) BP265 (*gltAB* P_{ansAB}-*lacZ*), with only one copy of the *ansR* gene, is more susceptible to loss-of-function mutations in *ansR*, leading to the emergence of numerous blue and white suppressor mutants. **B)** BP294 (*gltAB ansR-*P_{ansAB}-*lacZ*), possessing two copies of *ansR*, predominantly forms white colonies only in significantly lower numbers. After an overnight cultivation in LB and 2 time washing the cells, 100 µl of both strain with OD_{600} = 1.0 were cultured on CGXII plates supplemented with X-Gal and incubated at 37°C for up to 12 days. All the experiments were carried out three times independently (*N* = *3*). (Figure adapted from Mardoukhi et al., 2024)

Inactivation of *ansR* alleviates aspartate dependency of an *aspB* mutant

In *B. subtilis*, L-aspartate is synthesized through amino transformation from L-glutamate to oxaloacetate, yielding α-ketoglutarate and L-aspartate facilitated by the enzymatic activity of aspartate transaminase AspB. A study in 2018 demonstrated that *B. subtilis* lacking *aspB* is auxotrophic for aspartate and asparagine (H. Zhao et al., 2018). Additionally, examination of Fig. 2C in the mentioned paper revealed some heterogeneity in colony morphology in the *aspB*-deficient strain, suggesting potential genetic instability when growing on a plate without supplementation of L-aspartate. It is hypothesized that this genetic instability may be related to the inactivation of *ansR* and the restoration of aspartate prototrophy through ammonium assimilation via the reversible activity of L-aspartase AnsB, converting fumarate to L-aspartate. To test this hypothesis, the *aspB* gene was first replaced with the spectinomycin resistance cassette *aad9* in the genome of *B. subtilis* SP1 using LFH-PCR resulting in a new strain named as BP270 (*aspB*::*aad9*). Subsequently, the strain BP264 (P_{ansAB}-*lacZ*), carrying the *lacZ* fusion was transformed with cDNA from BP270 which resulted in the construction of a new strain designated as BP279 (*aspB* P_{ansAB}-*lacZ*).

Analysis of *aspB* blue suppressors

After overnight incubation of BP279 (*aspB* P_{ansAB}-*lacZ*) in LB medium, the cells were washed twice and the OD_{600} was adjusted to 1.0. Subsequently, 100 µl of the cells were spread onto three CGXII plates supplemented with X-Gal and incubated for 3 days at 37°C. As anticipated, blue colonies emerged. cDNA was extracted from these colonies, and two PCR reactions were performed on them. One PCR utilized primers SM2 and SM18 to amplify the *ansR* gene and its promoter site, while the other PCR employed primers SM3 and SM4 to amplify the *citG* gene. Subsequently, the PCR products underwent Sanger sequencing, revealing loss-of-function mutations in *ansR* in all three suppressor mutants, leading to the de-repression of *ansAB* operon (Tab. 15). Interestingly, none of the three suppressor mutants exhibited mutations in *citG*, suggesting that the inactivation of only *ansR* appears to be sufficient to overcome the auxotrophy in the *aspB*-deficient strain.

Analysis of *aspB* white suppressors

Further incubation of the plates led to the emergence of white color suppressor mutants, two of which were designated as BP296 (W1) and BP297 (W2). Their cDNA was subsequently sent for whole-genome sequencing. The results revealed mutations in *citG* in both suppressors, apparently resulting in lower expression of CitG and accumulation of fumarate. This accumulation of fumarate may act as a force to direct metabolites towards the aspartase pathway. Additionally, both mutants exhibited amino acid replacements in the L-asparaginase AnsA, which likely serve as an *ansA* activity reducer affecting the production of L-asparagine from L-aspartate (Tab. 16). This production of L-asparagine is necessary for the *aspB* mutant to regain aspartate prototrophy.

Table 15. Identified mutations in the BP279 (*aspB* P_{ansAB}-*lacZ*) by Sanger sequencing

Strain	Mutant	Phenotype	Affected gene, mutations	Amino acid exchanges, effect on the protein
BP366	B1	Growth on CGXII, blue colony	*ansR* C171A	AnsR ΔC56
BP367	B2	Growth on CGXII, blue colony	*ansR* G3A	AnsR M1I
BP368	B3	Growth on CGXII, blue colony	*ansR* G94C	AnsR A32P

Table 16. Identified mutations in the BP279 (*aspB* P_{ansAB}-*lacZ*) by NGS

Strain	Mutant	Phenotype	Affected gene, mutations	Amino acid exchanges, effect on the protein
BP296	W1	Growth on CGXII, white colony	*ansA* T43A, *citG* C686T	AnsA S15T, CitG A229V
BP297	W2	Growth on CGXII, white colony	*ansA* T43A, *citG* C312G	AnsA S15T, CitG N104K

Effect of additional copy of *ansR* on the genomic stability of the *aspB* mutants

Following the same experimental procedure as with BP294 (*gltAB ansR-*P_{ansAB}*-lacZ*) (harboring 2 copies of *ansR* in a background of a deleted *gltAB* strain), it was decided to introduce an additional copy of *ansR* into the background of an *aspB*-deleted strain to observe the effect. Initially, *B. subtilis* SP1 was transformed with plasmid pBP1111 carrying the promoter of *ansR* and the *ansR* gene fused into the front of *lacZ*, which integrated at the *amyE* locus. The resulting strain was named BP282 (*ansR-*P_{ansAB}*-lacZ*). Subsequently, the cDNA of BP270 (*aspB*) was introduced into competent BP282 cells, resulting in a new strain designated as BP283 (*aspB ansR-*P_{ansAB}*-lacZ*), which carried one native *ansR* copy and one additionally-introduced copy of *ansR* in the background of *aspB* deletion.

In the next step, cells from overnight cultures of BP279 (*aspB* P_{ansAB}*-lacZ*) and BP283 (*aspB ansR-*P_{ansAB}*-lacZ*) in LB were collected and washed twice. The OD_{600} was adjusted to 1.0 and 100 µl of the mixture of both strains was separately propagated onto three plates of CGXII + X-Gal. The plates were then incubated for up to 12 days at 37°C, during which colony numbers were counted.

The results clearly indicate that the number of colonies in BP283 (Fig. 11B), containing 2 copies of *ansR*, is much lower than in BP279 (Fig. 11A), which has only one native copy of *ansR*. Most of the colonies derived from both strains are white. Based on these data, it can be concluded that the chance of mutations occurring simultaneously in both copies of *ansR* is much lower than for one copy alone. Furthermore, this provides further evidence that a strain lacking *aspB* requires inactivation of *ansR* to remove the repression force on *ansB* and overcome the auxotrophy for L-aspartate by allowing to conversion of fumarate to L-aspartate.

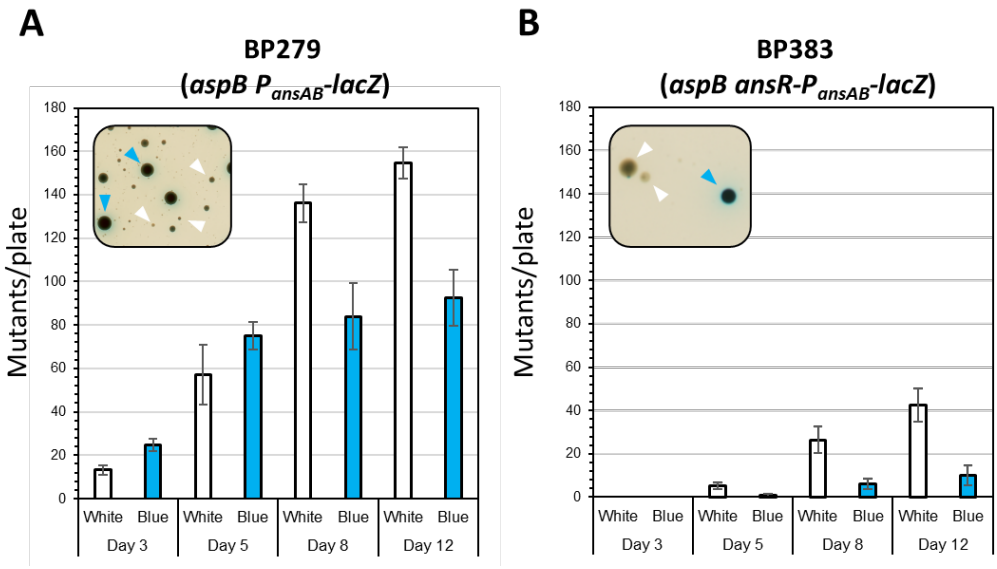

Figure 11. Blue-white colony screening in *B. subtilis* strains carrying one or two copies of *ansR* gene in a strain lacking *aspB* gene.
A) The significantly higher number of blue and white colonies in BP279 (*aspB* P_{ansAB}-*lacZ*) **B)** compared to BP283 (*aspB ansR*-P_{ansAB}-*lacZ*) can be attributed to the difference in the copy number of *ansR* in each strain. After an overnight cultivation in LB and 2 time washing the cells, 100 µl of both strain with OD_{600} = 1.0 were cultured on CGXII plates supplemented with X-Gal and incubated at 37°C for up to 3 days. All the experiments were carried out three times independently (*N* = *3*). (Figure adapted from Mardoukhi et al., 2024)

Analyzing additional or externally-introduced copies of *ansR* on the regulation of the P_{ansAB} promoter

As part of this study, investigating the impact of additional copies of the *ansR* gene on the activity of the P_{ansAB}-*lacZ* screening system, Janina Berg conducted an analysis in her master's thesis (2022) titled "Functional characterization and analysis of the Xre-family transcription factor AnsR from *B. subtilis*." The activity of the *ansAB* promoter was examined in three different strains: BP264 (P_{ansAB}-*lacZ*), BP271 (*ansR* P_{ansAB}-*lacZ*), and BP293 (*ansR ansR*-P_{ansAB}-*lacZ*), under three different conditions: C-Glc minimal medium, C-Glc minimal medium supplemented with 0.5% (w/v) L-glutamate, and C-Glc minimal medium supplemented with 0.5% (w/v) L-asparagine. It is important to note that the *ansR* gene was introduced into the chromosomal *amyE* locus in strain BP293 (Fig. 12A).

Berg performed a β-galactosidase assay on all samples and observed that strain BP271 (*ansR*-deleted strain) exhibited approximately a 48-fold increase in promoter activity compared to the wild-type BP264 (carrying *ansR* in the native locus) and approximately a 39-fold increase compared to the constructed complementation strain BP293 (carrying one copy of *ansR* in the *amyE* locus) when grown in C-Glc minimal medium without supplementation. Under the same condition, BP293 showed a similar value compared to the wild type BP264, with 10 and 8 U/mg of protein, respectively (Fig. 12A).

The results of the β-galactosidase assay for growth in media supplemented with glutamate showed almost similar outcomes and ratios as in the non-supplemented condition, with only slightly higher values observed in all strains: BP264 (19 U/mg), BP271 (570 U/mg), and BP293 (17 U/mg) (Fig. 12A).

In conditions supplemented with L-asparagine, the promoter activity in all strains, specifically BP264 (P_{ansAB}-*lacZ*) and BP293 (*ansR ansR*-P_{ansAB}-*lacZ*), dramatically increased to 204 and 104 U/mg, respectively. This indicates the inducer effect of L-asparagine on the *ansAB* promoter, suggesting that the transcriptional repressor effect of AnsR on the P_{ansAB}-*lacZ* is removed in the presence of L-asparagine. This result is entirely consistent with a previous study published in 2002 (Fig. 12A; Fisher & Wray, 2002).

Subsequently, the effect of the presence of a non-integrated *ansR* gene in the chromosome of *B. subtilis* on the activity of the P_{ansAB}-*lacZ* screening system was analyzed in this study. Plasmid pGP873 (constructed in the Jörg Stülke's lab), which contains *ansR* inserted into the backbone of plasmid pBQ200 (Martin-Verstraete et al., 1994), was used to introduce one copy of *ansR* into BP271 (*ansR* P_{ansAB}-*lacZ*), creating a strain designated as BP295 (*ansR*$^+$ *ansR* P_{ansAB}-*lacZ*). In parallel, the empty pBQ200 plasmid was introduced into BP271, resulting in the construction of a new strain named BP300 (BP271 + pBQ200) as a negative control strain. These two newly constructed strains, BP295 and BP300, along with the wild-type strain BP264 (P_{ansAB}-*lacZ*), were cultured in two different media: SM minimal medium and SM minimal medium supplemented with L-asparagine to a final concentration of 0.5% (w/v). This process was independently repeated three times. The activity of the promoter was measured using the β-galactosidase assay, and the average of all three measurements was calculated (Fig. 12B).

The results indicated that the promoter activity in BP264 (P_{ansAB}-*lacZ*) and BP295 (*ansR*$^+$ *ansR* P_{ansAB}-*lacZ*), grown in medium without supplementation, was close to zero (2 and 3, respectively), indicating the repressor activity of AnsR, irrespective of the location of the *ansR* gene, whether integrated into the chromosome or present on a non-integrated plasmid. As expected, the promoter activity in BP300 (*ansR* P_{ansAB}-*lacZ*) in the same medium was high, at 383 U/mg of protein (Fig. 12B).

When cultivated under supplementation with L-asparagine, BP300, which lacks *ansR*, showed almost the same promoter activity as observed in SM medium without supplementation, at 387 U/mg and 383 U/mg, respectively. However, the promoter activity in BP264 increased to 200 U/mg, and in BP295, it rose to 226 U/mg of protein. Although the promoter activity in BP264, which harbors an *ansR* copy in the native chromosomal locus, is slightly lower than in BP295, which carries an *ansR* copy on a non-integrated plasmid, it could be assumed that there is no meaningful relationship between the location of *ansR* and the promoter activity of the *lacZ* fusion. This slight difference may arise from the possibility that during growth, some of the BP295 cells lost

their plasmid carrying *ansR*, resulting in a lower copy number of *ansR* (Fig. 12B; Leonhardt & Alonso, 1991; Inoue, 1997; Wein et al., 2019).

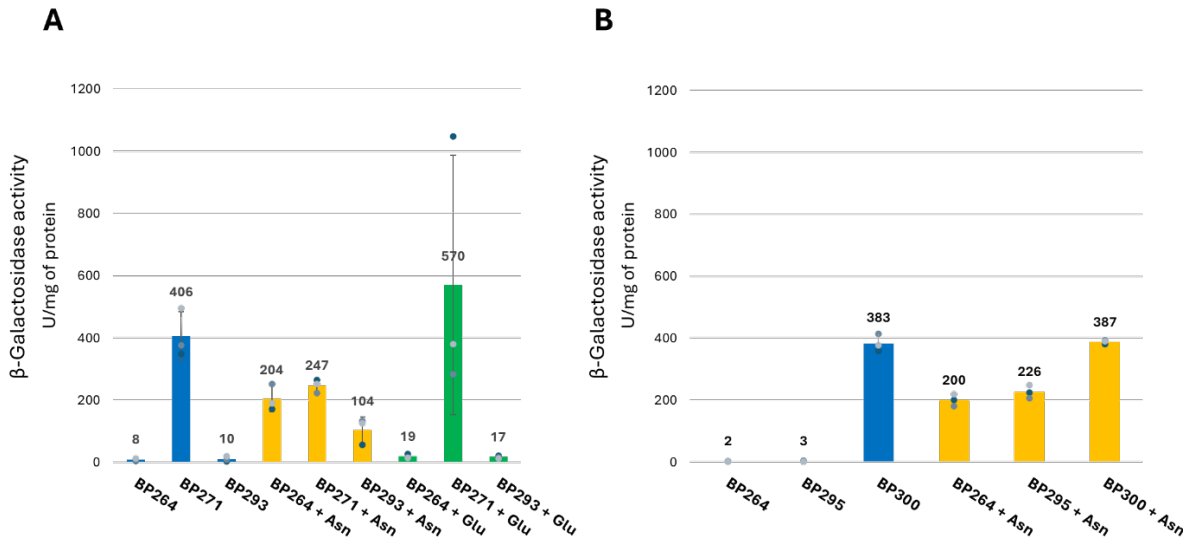

Figure 12. Analyzing the effect of additional copies of *ansR*, whether integrated or non-integrated, on the expression level of the P_{ansAB}-*lacZ* reporter system.
A) The results of the β-galactosidase assay conducted by Janina Berg for three *B. subtilis* strains, BP264 (P_{ansAB}-*lacZ*), BP271 (*ansR* P_{ansAB}-*lacZ*), and BP293 (*ansR ansR*-P_{ansAB}-*lacZ*) under three different conditions: C-Glc minimal medium, C-Glc minimal medium supplemented with 0.5% (w/v) glutamate (Glu), and C-Glc minimal medium supplemented with 0.5% (w/v) asparagine (Asn). **B)** The results of the β-galactosidase assay performed in this study for three *B. subtilis* strains, BP264 (P_{ansAB}-*lacZ*), BP295 (*ansR*$^+$ *ansR* P_{ansAB}-*lacZ*), and BP300 (*ansR* P_{ansAB}-*lacZ*) under two different conditions: C-Glc minimal medium, and C-Glc minimal medium supplemented with 0.5% (w/v) asparagine. All the experiments were carried out three times independently ($N = 3$).

Reconstruction and characterization of the AnsB-AspB pathway

To investigate the newly discovered glutamate pathway and how L-glutamate biosynthesis is accruing through it, it is imperative to delete essential genes involved in both the GS-GOGAT and AnsB-AspB pathways and observe the resulting consequences. To achieve this, a series of mutant strains were constructed, each carrying different arrangements of gene deletions, and their ability to grow in liquid and on solid minimal medium with and without supplementation of L-glutamate, L-aspartate and L-asparagine, were assessed.

In the background of the SP1 strain, gene deletions were performed using LFH-PCR (the oligo primers used in this section are listed in the primer list in the appendix). Specifically, *citG* and *ansAB* were replaced with the *ermC* (erythromycin resistance cassette), while *ansR* was replaced with the *cat* (chloramphenicol resistance cassette). These deletions were combined with BP265 (*gltAB* P_{ansAB}-*lacZ*) and BP279 (*aspB* P_{ansAB}-*lacZ*) mutations from previous experiments mentioned before to generate the strains

outlined in Tab. 17. Subsequently, the growth behavior of all mutant strains was monitored on CGXII plates supplemented with X-Gal, with and without L-glutamate, L-aspartate and L-asparagine, during incubation for 2 days at 37°C (Fig. 13A). For liquid culture experiments, the strains were initially grown overnight in LB medium. Subsequently, the following day, the cells were washed twice and inoculated into minimal medium supplemented with or without L-glutamate, L-aspartate, and L-asparagine. Incubation was carried out for 24h at 37°C (Fig. 13B).

Comparing the growth behavior of all strains on CGXII plates where ammonium serves as the sole nitrogen source, inactivation of *ansR* appears to be pivotal for mutant strains to utilize the aspartase-aspartate transaminase pathway, thereby overcoming glutamate auxotrophy in BP273 and BP276, as well as aspartate auxotrophy in BP292, in contrast to their parental strains BP265, BP274, and BP279, respectively. Even in liquid medium under the same conditions, growth is observed upon inactivation of the *ansR*, *citG*, and *ansR* genes in strains lacking *gltAB* and *aspB*, respectively. Notably, comparison of BP273 (*gltAB ansR* P_{ansAB}-*lacZ*) and BP274 (*gltAB citG* P_{ansAB}-*lacZ*) reveals that deletion of *citG* in a *gltAB ansR* strain enhances growth due to the redirection of metabolites into the AnsB-AspB pathway. Addition of L-glutamate to the medium enables growth in all strains except for BP279 (*aspB* P_{ansAB}-*lacZ*), which is aspartate auxotrophic. However, its derivative strain BP292 (*ansR aspB* P_{ansAB}-*lacZ*), lacking the *ansR* gene, regains aspartate prototrophy. Although supplementation with both L-aspartate and L-asparagine supports growth in all strains, it appears that L-aspartate serves as a superior nitrogen source compared to L-asparagine in both solid and liquid media which later will be discussed in more detail. It is worth mentioning that although strains BP274 (*gltAB citG* P_{ansAB}-*lacZ*) and BP276 (*gltAB ansR citG* P_{ansAB}-*lacZ*), both lacking the *citG* gene, exhibited a growth defect on a plate supplemented with L-asparagine, BP276 displayed normal growth in liquid medium (Fig. 13B).

Table 17. Constructed strains

Strain	genotype
BP265	*gltAB* P_{ansAB}-*lacZ*
BP273	*gltAB ansR* P_{ansAB}-*lacZ*
BP274	*gltAB citG* P_{ansAB}-*lacZ*
BP276	*gltAB ansR citG* P_{ansAB}-*lacZ*
BP278	*gltAB ansR citG aspB* P_{ansAB}-*lacZ*
BP279	*aspB* P_{ansAB}-*lacZ*
BP280	*gltAB ansAB*
BP291	*ansR citG aspB* P_{ansAB}-*lacZ*
BP292	*ansR aspB* P_{ansAB}-*lacZ*
BP395	*ansAB aspB*

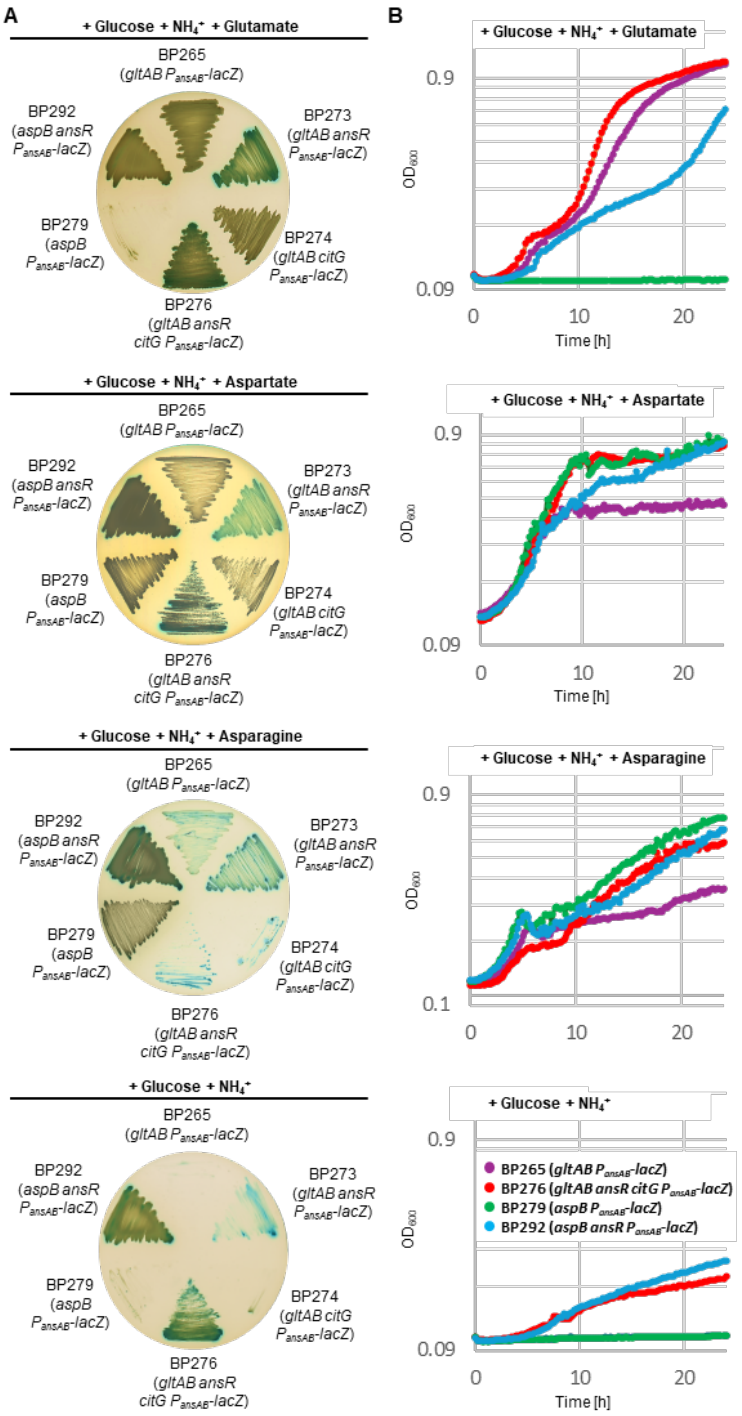

Figure 13. Growth characterisation of the strains lacking *citG*, *ansR* or both genes. **A)** The growth of all constructed mutant strains was monitored on CGXII plates supplemented with X-Gal, both with and without L-glutamate, L-aspartate, and L-asparagine at the final concentration of 0.5% (w/v). Plate were incubated for 2 days at 37°C. **B)** The growth of all strains was evaluated in liquid CGXII medium supplemented with and without L-glutamate, L-aspartate, and L-asparagine at the final concentration of 0.5% (w/v). The growth was monitors for 24h at 37°C. All the experiments in liquid media were carried out three times independently (*N* = *3*). (Figure adapted from Mardoukhi et al., 2024)

In the final stage, based on the outcomes of previous experiments, it was hypothesized that a strain lacking essential genes for both L-glutamate and L-aspartate biosynthesis pathways should not be able to grow without an additional source of L-glutamate and L-aspartate. In other words, these strains should be genetically stable and auxotroph for L-glutamate and L-aspartate.

So, with the combination of the deleted genes, new strains designated as BP386 (*gltAB ansAB* P_{ansAB}*-lacZ*) and BP278 (*gltAB citG ansR aspB*) were constructed, which were expected to be auxotroph for L-glutamate, and BP395 (*ansAB aspB*) for L-aspartate.

Subsequently, they were cultivated on plates with and without supplementation of L-glutamate and L-aspartate, separately and incubated at 37°C for up to 15 days. The results clearly demonstrated that none of the strains were capable of growth without external supplementation of L-glutamate and L-aspartate, thus confirming the hypothesis (Fig. 14). As observed, BP278 is unable to grow without supplementation with L-glutamate because there is no pathway available to convert L-aspartate to L-glutamate, unlike its parental strain BP276 (Fig. 14A). Furthermore, BP386 can only grow in the presence of L-glutamate or L-aspartate in the medium because the aspartate transaminase AspB in its background is intact and can convert L-glutamate or L-aspartate to one another (Fig. 14B). Considering BP395, it exhibits a dependency on the supplementation with L-aspartate for growth. This reliance stems from its capability to synthesize L-glutamate; however, it remains incapable of converting L-glutamate into L-aspartate. (Fig. 14B, C).

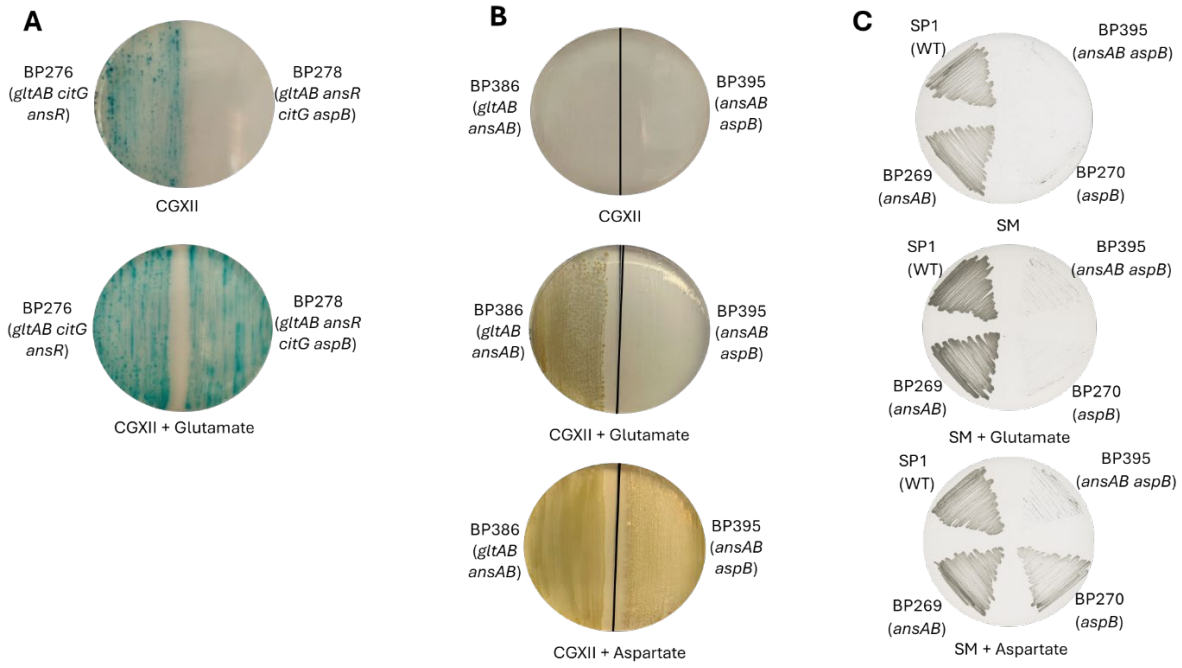

Figure 14. Deletion of key genes in both glutamate biosynthesis pathways GS-GOGAT and AnsB-AspB, resulting in genetically stable auxotrophy for L-glutamate and L-aspartate. **A)** BP276 (*gltAB ansR citG* P_{ansAB}-*lacZ*), utilizing the fumarate-aspartate dependent pathway, is capable of growth on minimal medium CGXII, whereas BP278 (*gltAB ansR citG aspB* P_{ansAB}-*lacZ*), with an additional deletion in *aspB*, exhibits auxotrophy for L-glutamate. **B)** BP386 (*gltAB ansAB*) demonstrates an inability to grow without external supplementation of L-glutamate or L-aspartate, while BP395 (*ansAB aspB*) requires only L-aspartate for growth. **C)** Comparison of the growth of BP395 (*ansAB aspB*) with its parental strains and wild-type SP1. All the plates were incubated at 37°C for 2 days.

High amount of nitrogen is toxic for the *gltAB* mutant

After the initial discovery in 1989 by Bohannon and Sonenshein that the *gltAB* genes encode for GOGAT in *B. subtilis* (Bohannon & Sonenshein, 1989), most laboratories that work with *B. subtilis* have utilized TSS and specially C-Glc medium as a minimal medium. However, despite several days of incubation of a *gltAB*-deficient strain, no suppressor mutants had been reported prior to this study, suggesting the absence of an alternative glutamate biosynthesis route.

As elucidated in the beginning of the results section, owing to the establishment of a cross-feeding community between *B. subtilis* and *C. glutamicum*, the decision was made to employ CGXII minimal medium. The CGXII medium, frequently employed for *C. glutamicum* cultivation and upkeep, incorporates glucose as the carbon source and either ammonium or urea as the nitrogen source (Keilhauer et al., 1993). Upon the initial observation of suppressor mutant emergence of BP261 (*gltAB*) on CGXII, it raised the question of why CGXII supports the emergence of suppressor mutations but not C-Glc medium. To address this question, all components of CGXII, with the same exact amounts, were separately added to C-Glc medium. BP265 (*gltAB* P_{ansAB}-*LacZ*) cells, cultured overnight in LB and washed twice with saline solution, were then propagated onto the plates supplemented with X-Gal for better visualization of the emergence of possible suppressor mutants.

Comparison of the ammonium sulfate content in both media revealed that CGXII contains 0.134 M ammonium sulfate, whereas C-Glc has only 0.025 M (5.36 times more ammonium sulfate in CGXII compared to C-Glc). Furthermore, only CGXII contains urea, with a concentration of approximately 0.074 M. The remaining components present in both media are in micro and nanomolar amounts, which do not have a considerable effect on growth (Fig. 15A). As depicted in Fig. 15B, after 3 days of incubation at 37°C, suppressor mutants appeared on plates supplemented with ammonium sulfate, urea, and CGXII basic solution. In contrast, even after up to 8 days of incubation, there was no growth observed on C-Glc and C-Glc plus biotin plates. Notably, the highest number and largest colonies were observed on the CGXII plates including CGXII basic solution which contains urea and ammonium sulfate as a standard amount in the CGXII medium. Thus, based on the growth experiment on plates and calculation of the ingredient concentration, it can be concluded that the excessive amount of nitrogen in CGXII medium acts as a driving force for *gltAB*-deficient strains to form suppressors with mutations in *ansR* and *citG* genes, thereby recovering from auxotrophy for L-glutamate.

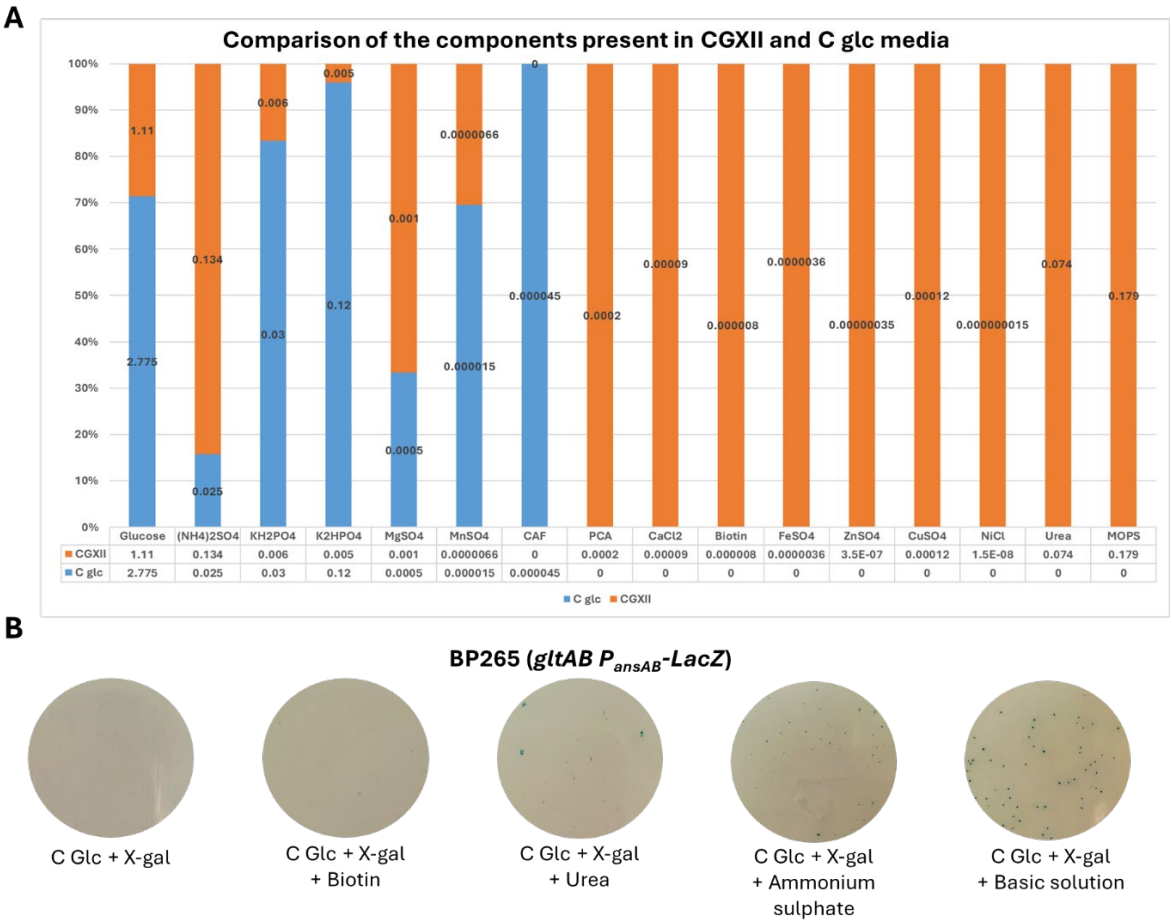

Figure 15. The comparison of CGXII and C-Glc minimal media.
A) The amount of each component in each medium is illustrated based on a 100% stacked diagram, with the actual amount of each component also shown in molar units in a table on the X-axis. **B)** By systematically adding each individual component of CGXII medium to C-Glc medium, it becomes evident that plates containing urea, ammonium sulfate, and basic solution showed the emergence of suppressor mutants of BP265 (*gltAB* P_{ansAB}-*lacZ*). All the plates were incubated up to 8 days at 37°C. (Figure adapted from Mardoukhi et al., 2024)

Assessment of the efficiency of ammonium assimilation in *gltAB citG ansR* and *aspB ansR* strains

To assess the efficiency of ammonium assimilation by the L-aspartase AnsB in strains BP276 (*gltAB ansR citG* P_{ansAB}-*lacZ*) and BP292 (*aspB ansR* P_{ansAB}-*lacZ*), it is required to use a medium which the amount of nitrogen source could be easily manipulated. Therefore, it was decided to utilize SM minimal medium, which contains ammonium sulfate as the sole source of nitrogen. Both strains, along with the wild-type strain BP264 (P_{ansAB}-*lacZ*) as a control, were initially incubated overnight in 4 ml LB at 28°C. The following day, a pre-culture was prepared by inoculating 4 ml of SM medium supplemented with ammonium sulfate with 200 µl of the overnight cultures, then incubated at 37°C for several hours. Using 96-well plates and a plate reader machine, the growth behavior of the three strains were monitored for 24 hours in SM medium

supplemented with increasing amounts of ammonium sulfate, ranging from 0.0% to 4.0% w/v (0–302.7 mM). Each measurement was assessed three times independently.

The results indicated that, in the absence of a nitrogen source, there was no growth observed in all strains, as expected. Strains BP264 (P_{ansAB}-*lacZ*) and BP292 (*aspB ansR* P_{ansAB}-*lacZ*) showed minimal differences in growth with increasing amounts of ammonium, while the growth behavior of strain BP276 (*gltAB ansR citG* P_{ansAB}-*lacZ*) clearly changed from low to high with increasing ammonium concentration in the medium (Fig. 16A). This suggests a greater dependency on ammonium in BP276. Additionally, based on growth rate calculations, it can be concluded that the efficiency of ammonium assimilation by AnsB is limited and lower than that of ammonium assimilation via the GS-GOGAT pathway (Fig. 16B). Furthermore, the reduced reliance on ammonium observed in strain BP292 could be attributed to the fact that ammonium assimilation catalyzed by L-aspartase may only be necessary for the *de novo* synthesis of L-aspartate and L-asparagine in this genetic background of an AspB-deficient strain. In contrast, ammonium assimilation in the background of the *gltAB* mutant (BP276) is required not only for the biosynthesis of L-glutamate, the most abundant and major amino group donor in the cell, but also for L-aspartate and L-asparagine production (Fig. 24A).

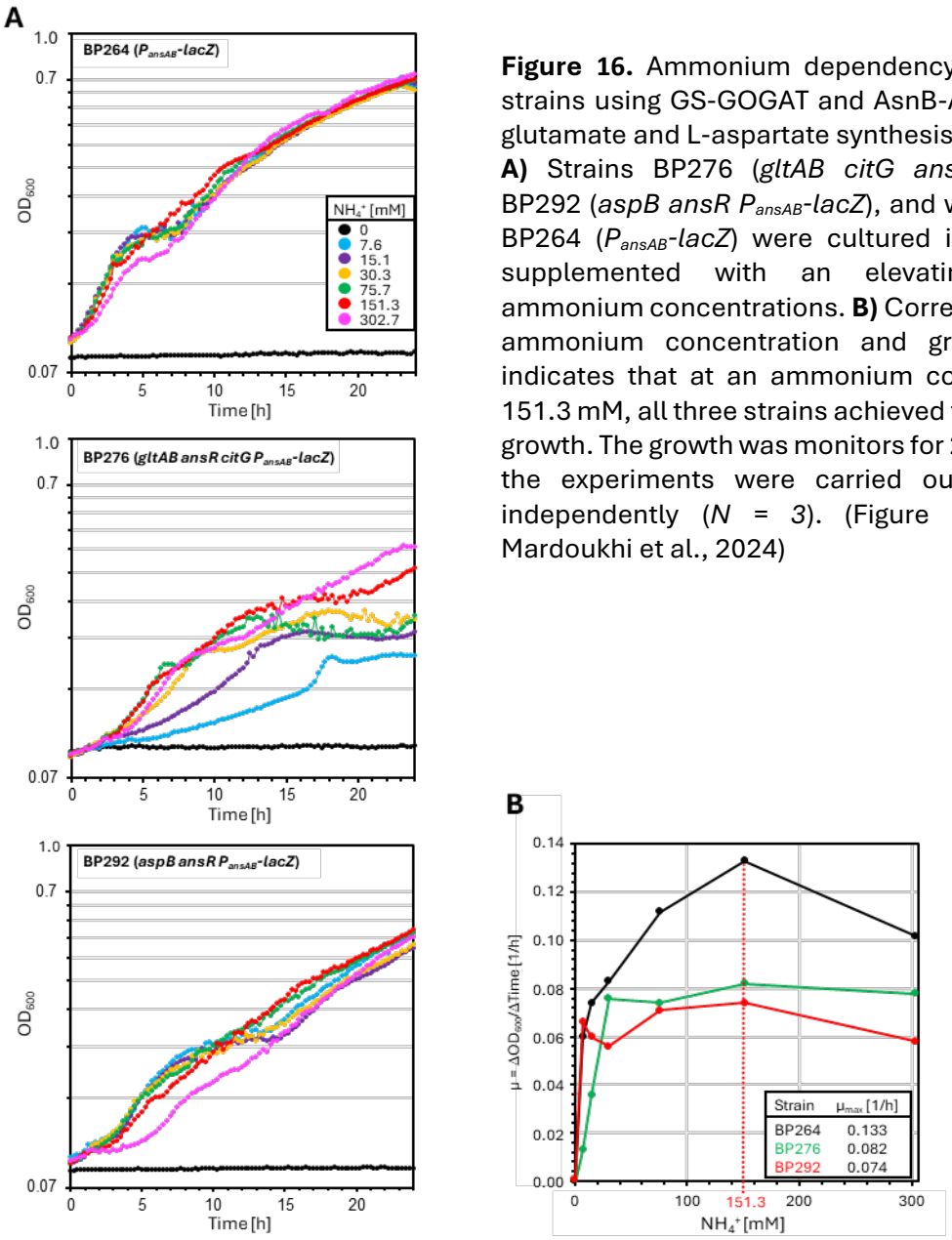

Figure 16. Ammonium dependency of *B. subtilis* strains using GS-GOGAT and AsnB-AspB for the L-glutamate and L-aspartate synthesis.
A) Strains BP276 (*gltAB citG ansR* P_{ansAB}-*lacZ*), BP292 (*aspB ansR* P_{ansAB}-*lacZ*), and wild-type strain BP264 (P_{ansAB}-*lacZ*) were cultured in SM medium supplemented with an elevating range of ammonium concentrations. **B)** Correlation between ammonium concentration and growth rate (μ) indicates that at an ammonium concentration of 151.3 mM, all three strains achieved their maximum growth. The growth was monitors for 24h at 37°C. All the experiments were carried out three times independently (*N* = 3). (Figure adapted from Mardoukhi et al., 2024)

Growth of *gltAB citG ansR* and *aspB ansR* strains under hyperosmotic conditions

As discussed in the introduction section, L-proline serves as the compatible solute for *B. subtilis*, aiding in its ability to withstand hyperosmotic pressure in varying growth conditions. L-proline is synthesized from L-glutamate as a precursor. Therefore, it can be inferred that a higher capacity to adapt to salt stress reflects a greater synthesis of L-proline and, consequently, higher production of L-glutamate.

To investigate this hypothesis, strains BP276 (*gltAB ansR citG* P_{ansAB}-*lacZ*) and BP292 (*aspB ansR* P_{ansAB}-*lacZ*), alongside the wild-type strain BP264 (P_{ansAB}-*lacZ*), were cultured overnight in LB at 28°C. The following day, all strains were transferred and cultured in SM

minimal medium supplemented with increasing amounts of sodium chloride (NaCl) within a 96-well plate. Their growth was monitored by a plate reader at 37°C for 48 hours. Each measurement was independently assessed three times.

Comparing the growth of both mutant strains with the wild-type, they exhibited significant tolerance against elevated salinity in the medium; however, there was a slight difference observed (Fig. 17A). Despite experiencing considerable salt stress at higher concentrations of NaCl which led to growth impairment, both BP276 and BP292 strains synthesized a considerable amount of L-glutamate (Fig. 17B).

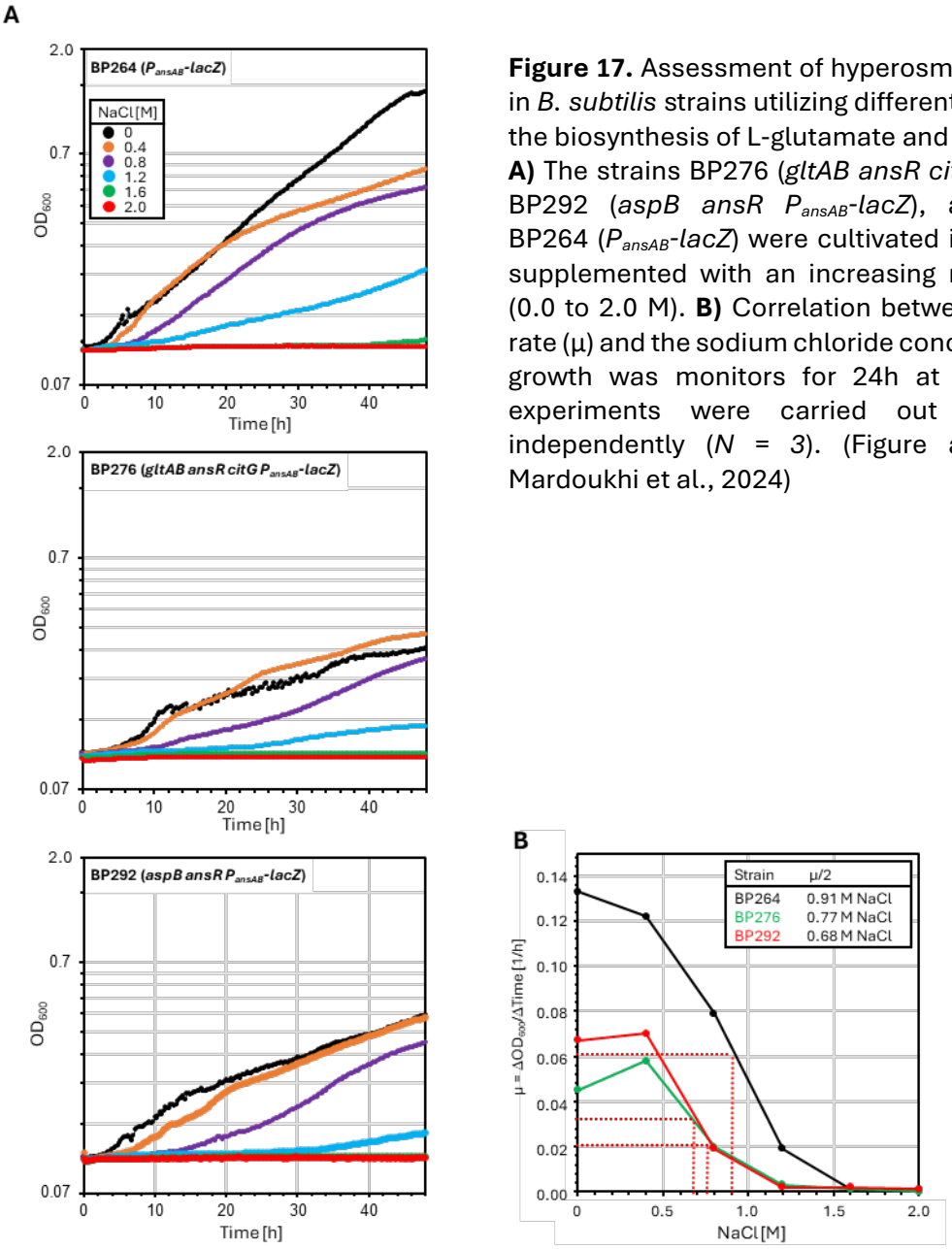

Figure 17. Assessment of hyperosmotic tolerance in *B. subtilis* strains utilizing different pathways for the biosynthesis of L-glutamate and L-aspartate. **A)** The strains BP276 (*gltAB ansR citG* P_{ansAB}-*lacZ*), BP292 (*aspB ansR* P_{ansAB}-*lacZ*), and wild-type BP264 (P_{ansAB}-*lacZ*) were cultivated in SM medium supplemented with an increasing range of NaCl (0.0 to 2.0 M). **B)** Correlation between the growth rate (μ) and the sodium chloride concentration. The growth was monitors for 24h at 37°C. All the experiments were carried out three times independently (*N* = 3). (Figure adapted from Mardoukhi et al., 2024)

Metabolite synthesis via GS-GOGAT and AnsB-AspB routes

To investigate how the levels of metabolites change when utilizing the fumarate-based ammonium assimilation pathway to overcome L-glutamate and L-aspartate/L-asparagine auxotrophy of BP276 (*gltAB citG ansR* P_{ansAB}-*lacZ*) and BP292 (*aspB ansR* P_{ansAB}-*lacZ*) compared to the native GS-GOGAT pathway in the background of the wild-type *B. subtilis* BP264 (P_{ansAB}-*lacZ*), metabolome analysis was performed. Samples were prepared in triplicate and sent for LC/MS analysis at the group of Professor Dr. Hannes Link (Interfaculty Institute for Microbiology and Infection Medicine Tübingen, University of Tübingen, Tübingen, Germany). The analysis reported the levels of L-glutamate, L-glutamine, L-aspartate, L-asparagine, and TCA cycle intermediates citrate, succinate, and malate. Then, the data was normalized based on the concentration levels of metabolites in the wild-type BP264, with the threshold zero line indicating the concentration of metabolites in the BP264 strain. As shown in Fig. 18, the concentration levels of citrate, L-glutamate, L-glutamine, and L-asparagine were almost the same in the strains BP276 and BP292. Considering the succinate concentration, which was higher in BP276 compared to BP292, it could be the result of deficient fumarase CitG, leading to the accumulation of fumarate and, consequently, succinate as well. The alteration in cellular aspartate concentration, observed to diminish in BP292 while augmenting in BP276, suggests that the deletion of *citG* and the subsequent accumulation of fumarate indeed forces the metabolite to serve as a substrate for L-aspartase AnsB, facilitating its conversion into L-aspartate. This observation is consistent with the reduction of malate due to the deficient conversion of fumarate to malate.

In conclusion, although the metabolite levels changed in both strains compared to the wild-type native status, the assimilation of ammonium via L-aspartase AnsB appears to be sufficiently efficient to support growth.

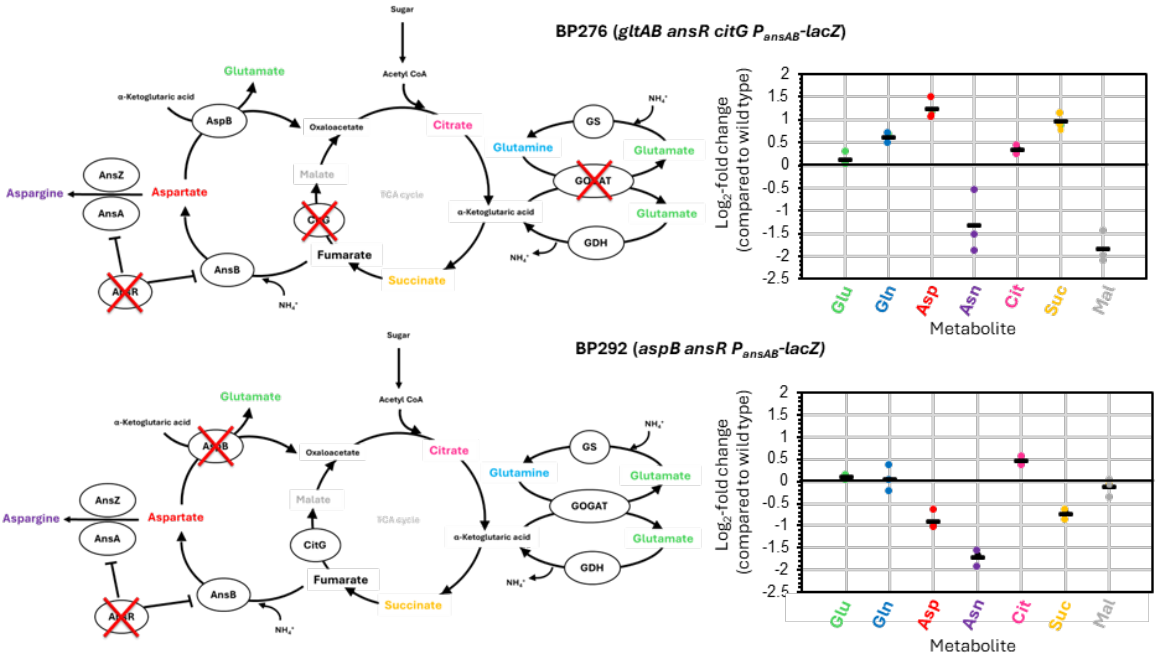

Figure 18. The concentration of metabolites in BP276 (*gltAB citG ansR* P_{ansAB}*-lacZ*) and BP292 (*aspB ansR* P_{ansAB}*-lacZ*), utilizing the L-aspartase AnsB for ammonium assimilation to synthesize L-glutamate and L-aspartate, was compared to the wild-type GS-GOGAT pathway in BP264 (P_{ansAB}*-lacZ*). Initially, metabolome samples were prepared from disrupted cells obtained from the cultivation of all strains in SM minimal medium at 37°C, repeated three times independently. Subsequently, the concentration of metabolites was measured using LC/MS, and the $\log_2$-fold changes were calculated relative to the wild-type strain BP264 (zero threshold). (Figure adapted from Mardoukhi et al., 2024)

Evolution of strains lacking fumarase CitG in rich medium

During the initial stages of construction, it was noted that strains lacking fumarase CitG, such as BP275 (*citG ansR* P_{ansAB}*-lacZ*) and BP276 (*gltAB citG ansR* P_{ansAB}*-lacZ*), exhibited poor growth on rich media like LB agar. To elucidate the underlying cause of this phenotype and ascertain whether it is linked to the biosynthesis of L-glutamate and L-aspartate/L-asparagine through the newly discovered fumarate-aspartate bathway, or simply due to the deletion of the *citG* gene, reconstituted strains BP276 (*gltAB citG ansR* P_{ansAB}*-lacZ*) and BP292 (*aspB ansR* P_{ansAB}*-lacZ*) comparing with wild-type BP264 (P_{ansAB}*-lacZ*) were cultivated in liquid LB and BHI with and without glucose supplementation (0.5% w/v). Their growth behavior was then monitored at 37°C for 24 hours.

As depicted in Fig. 19, the only strain exhibiting a growth defect in both LB and BHI media was BP276. However, this growth defect was relieved upon the addition of glucose. Hence, it can be inferred that the deactivation of fumarase CitG is the primary reason for the growth defect observed in BP276. This phenomenon may arise due to a block in the TCA cycle, potentially impeding the efficient consumption of other amino acids present in the rich media by the cells.

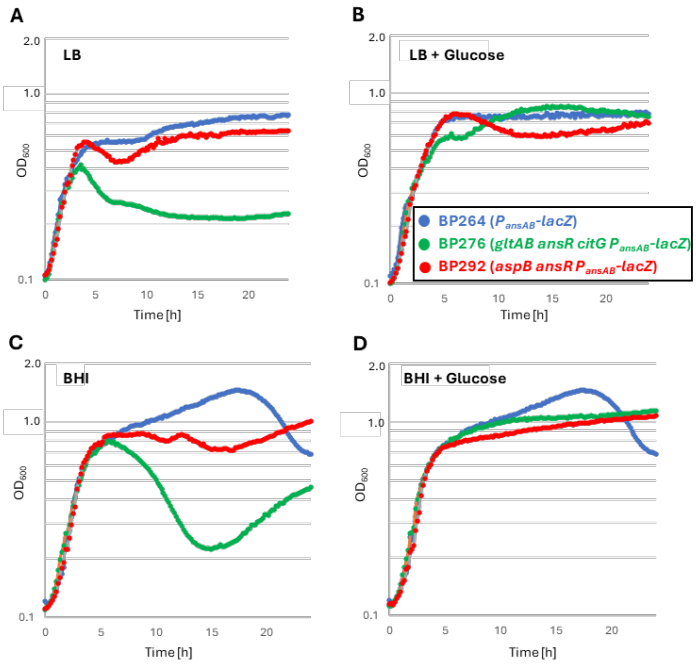

Figure 19. Growth defect of strains lacking *citG* in rich media. BP276 (*gltAB citG ansR* P_{ansAB}-*lacZ*), BP292 (*aspB ansR* P_{ansAB}-*lacZ*) and wild-type BP264 (P_{ansAB}-*lacZ*) were cultivated in LB and BHI with and without glucose supplementation (0.5% w/v) for 24 h at 37°C. All the experiments were carried out three times independently (*N* = *3*). (Figure adapted from Mardoukhi et al., 2024)

In the subsequent experiment, it was aimed to assess whether strains lacking *citG* could adapt to rich medium conditions. To this end, strains BP275 (*citG ansR* P_{ansAB}-*lacZ*) and BP276 (*gltAB citG ansR* P_{ansAB}-*lacZ*), along with the wild-type BP264 (P_{ansAB}-*lacZ*), underwent a short-term evolution test in LB medium. Initially, 10 ml LB medium was inoculated separately with fresh colonies of all three strains. After exactly 24 hours incubation at 37°C with agitation, the OD_{600} was measured. Subsequently, a fresh LB medium was inoculated with 100 µl of the culture from the measured culture, and this process was repeated for 10 days (Fig. 20A). Cells from the final day were then cultivated on LB plates and compared to their parental strains. Additionally, cDNA from the evolved strains, designated as BP384 (BP264 derivative), BP369 (BP275 derivative), and BP370 (BP276 derivative), were extracted and sent for whole genome sequencing analysis.

A comparison of the growth of the evolved strains with their parental strain on LB plates and LB liquid revealed that the evolved strain BP384 showed the same phenotype like the parental strain BP264. However, both evolved CitG-deficient strains, BP369 and BP370, formed larger and more stable colonies compared to their parental strains. Notably, the growth deficiencies observed in the parental strains BP275 and BP276 were no longer apparent in the evolved strains, which exhibited the ability to thrive on LB medium (Fig. 20B, C).

Furthermore, the results of whole genome sequencing from the evolved strains indicated that in strains lacking the *citG* gene, bacteria had reactivated the cryptic version of GDH, *gudB*^{CR}, by deleting an exact 9 bp sequence, which is tandemly repeated in the open reading frame of the *gudB* gene and effectively deactivate the expressed protein (Belitsky & Sonenshein, 1998; Gunka et al., 2012) (Tab. 18). This suggests that the growth defect

observed in strains lacking fumarase CitG can be partially overcome by the increased activity of GDH. This likely leads to enhanced degradation of glutamate-family amino acids and more efficient utilization of these amino acids by the cells which later will be examined and discussed.

Table 6. Identified mutations in the evolved BP275 (*citG ansR* P_{ansAB}-*lacZ*) and BP276 (*gltAB citG ansR* P_{ansAB}-*lacZ*) in LB by NGS

Strain	Mutant	Phenotype	Affected gene, mutations	Amino acid exchanges, effect on the protein
BP384	LBW	Growth on LB	-	-
BP369	LB1	Growth on LB	*gudB* ΔG279-C287	Synthesis of GudB1
BP370	LB2	Growth on LB	*gudB* ΔG279-C287	Synthesis of GudB1

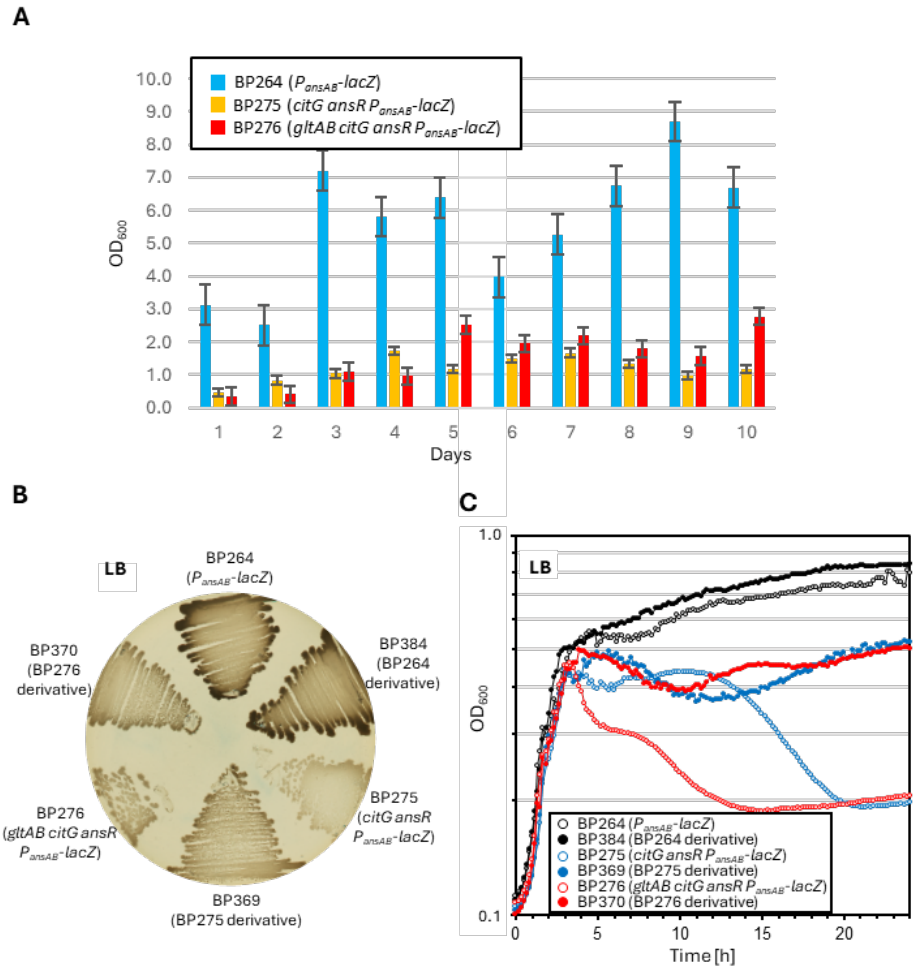

Figure 20. Adaptation of the *B. subtilis* strains synthesis L-glutamate and L-aspartate through GS-GOGAT and AnsB-AspB pathways.
A) Measured OD_{600} every 24h from the evolution test in LB medium for 10 days at 37°C with strains BP264 (P_{ansAB}-*lacZ*), BP275 (*citG ansR* P_{ansAB}-*lacZ*) and BP276 (*gltAB citG ansR* P_{ansAB}-*lacZ*). **B)** Comparing the growth of strains BP264, BP275 and BP276 with their evolved derivatives strains BP384, BP369, and BP370, respectively on LB agar at 37°C for 24h. **C)** Monitoring the growth of BP264, BP275 and BP276 and their derivatives BP384, BP369, and

BP370 in liquid LB medium for 24h at 37°C. Experiments in section C were carried out three times independently (*N* = *3*). (Figure adapted from Mardoukhi et al., 2024)

Adaptation of fumarase mutants to toxic levels of L-arginine

As mentioned in the introduction, arginine is a member of the glutamate amino acids family, which can be degraded to glutamate in catabolic process. However, in *B. subtilis* strains lacking the ability to degrade L-glutamate due to inactivation of genes *rocG* and *gudB*, arginine becomes toxic due to L-glutamate accumulation (Belitsky & Sonenshein, 1998). L-arginine uptake occurs through permeases RocC and RocE, followed by conversion to L-glutamate by the series enzymatic activity of RocF, RocD and RocA (Calogero et al., 1994; Gardan et al., 1995; Belitsky & Sonenshein, 1998). This study aimed to assess whether a functional TCA cycle is crucial to prevent the accumulation of L-glutamate and TCA cycle intermediates in the presence of L-arginine.

To investigate this, the growth behavior of various *B. subtilis* strains was monitored on media containing L-arginine. Strains wild-type BP264 (P_{ansAB}-*lacZ*), BP265 (*gltAB* P_{ansAB}-*lacZ*), BP271 (*ansR* P_{ansAB}-*lacZ*), BP275 (*citG ansR* P_{ansAB}-*lacZ*), BP276 (*gltAB citG ansR* P_{ansAB}-*lacZ*), BP279 (*aspB* P_{ansAB}-*lacZ*), and BP292 (*aspB ansR* P_{ansAB}-*lacZ*) were cultivated on SM minimal medium supplemented with glucose, only L-arginine (0.5% w/v), glucose plus L-arginine (0.5% w/v), and LB agar as a control, then incubated for 24 hours at 37°C.

As also shown in previous experiment (Fig. 20), strains BP275 and BP276 lacking fumarase CitG exhibited a growth defect on LB plates (Fig. 21A). These strains also failed to grow on SM plates containing only L-arginine as the sole source of nitrogen and carbon, presumably due to L-glutamate or TCA cycle intermediate accumulation. However, the addition of glucose to the media eliminated the toxicity of L-arginine, allowing both strains to grow normally. Glucose serves as a preferred carbon source, facilitating faster growth and increased demand for L-glutamate derived from L-arginine degradation, thereby mitigating L-arginine toxicity (Fig. 21A; Belitsky & Sonenshein, 1998; Commichau, Wacker, et al., 2006).

In the subsequent experiment, SM plates containing only L-arginine were further incubated for up to 10 days at 37°C to observe whether strains lacking the *citG* gene (BP275 and BP267) would evolve to adapt to the arginine toxicity. Surprisingly, among all strains, only these mentioned strains produced suppressor mutants with two distinct phenotypes: small and large colonies (Fig. 21B). Subsequently, two small and two large colonies from each strain were selected and cultured on SM plates containing glucose and L-arginine (0.5% w/v), as well as plates containing only L-arginine, alongside their parental strains BP275 (*citG ansR* P_{ansAB}-*lacZ*), BP276 (*gltAB citG ansR* P_{ansAB}-*lacZ*), and wild-type BP264 (P_{ansAB}-*lacZ*) as controls. After 48 hours of incubation at 37°C, while all strains grew well as expected on SM media supplemented with glucose and L-arginine, derivative suppressor mutants designated as BP371-BP374 (derived from BP275) and BP375-BP378 (derived from BP276) exhibited slight but significant growth on minimal

media containing only L-arginine. "S" stands for small colonies and "B" for big colonies, based on their morphology (Fig. 21C).

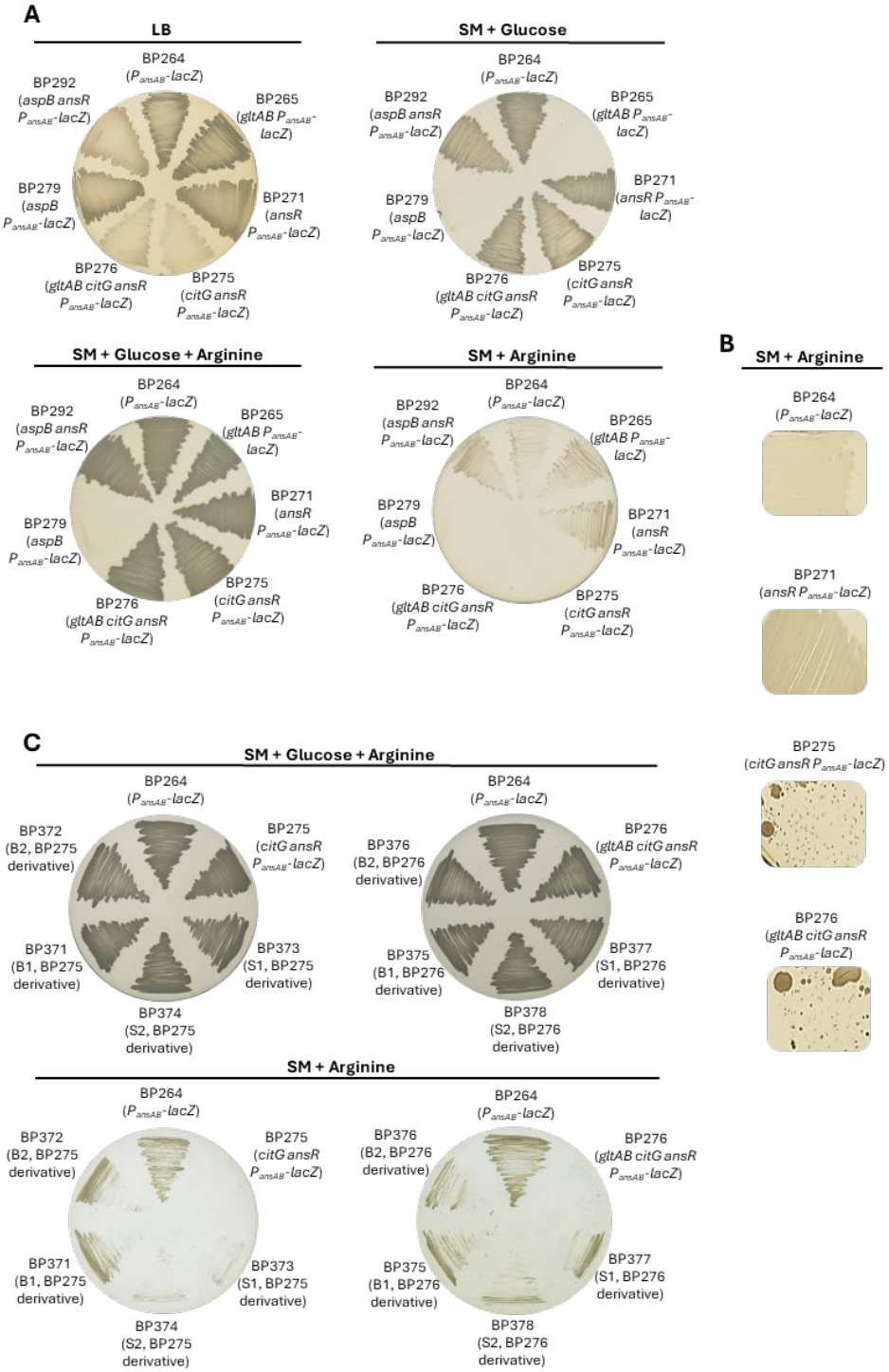

Figure 21. Adaptation of fumarase mutants to toxic levels of L-arginine.
A) Growth monitoring of BP264 (*P*$_{ansAB}$-*lacZ*), BP265 (gltAB *P*$_{ansAB}$-*lacZ*), BP271 (*ansR P*$_{ansAB}$-*lacZ*), BP275 (*citG ansR P*$_{ansAB}$-*lacZ*), BP276 (*gltAB citG ansR P*$_{ansAB}$-*lacZ*), BP279 (*aspB P*$_{ansAB}$-*lacZ*), and BP292 (*aspB ansR P*$_{ansAB}$-*lacZ*) on LB and SM minimal media supplemented with glucose, both glucose and L-arginine, and only L-arginine (final concentration of glucose and arginine = 0.5% (w/v)) for 24h at 37°C. **B)** Popping up of suppressor mutants derived from BP275 and

BP276 on SM media supplemented with L-arginine as the sole source of carbon and nitrogen compared with BP264 and BP271, which did not exhibit any mutations during 10 days of incubation at 37°C. **C)** Comparison of the growth of BP275 and BP276 with their derivative suppressor mutants BP371-BP374 and BP375-BP278, respectively, alongside BP264 as the wild-type positive control. Plates were incubated at 37°C for 48h. (Figure adapted from Mardoukhi et al., 2024)

In the subsequent step, cDNA from all derivative suppressor mutant strains BP371-BP378 was extracted and subjected to whole-genome sequencing (Tab. 19). Next-generation sequencing analysis revealed that in three of the big colonies, BP371, BP372, and BP376, a genomic region containing the *aspB* gene was amplified, likely resulting in increased expression of *aspB*. This suggests higher levels of aspartate transaminase within the cells, leading to increased degradation of L-glutamate derived from L-arginine catabolism and reducing the toxic levels of L-glutamate (Fig. 22A). In strain BP375, a single point mutation occurred in the promoter region of the *dinG* gene, which is also located upstream of the *ypmA*, *ypmB*, and *aspB* genes. This mutation may enhance the expression of all these genes, particularly *aspB*, resulting in increased AspB levels. Consequently, there is more conversion of L-glutamate and oxaloacetate to L-aspartate and α-ketoglutarate, thereby preventing the accumulation of L-glutamate to toxic levels. Interestingly, in 2011, Flórez et al. demonstrated that glutamate can serve as the sole source of carbon and nitrogen for a strain lacking GDH activity and AnsR, utilizing the catabolic activity of aspartate transaminase AspB (Flórez et al., 2011). Two of the small suppressor mutants, BP373 and BP374 (derived from BP275), exhibited mutations in the *rocC* gene, which encodes the L-arginine permease RocC. In BP373, a proline-to-leucine substitution occurred at amino acid position 411 within the RocC structure, situated in the transmembrane helix. This alteration likely reduces the permease activity of RocC. In BP374, a single nucleotide insertion caused a frameshift mutation in *rocC*, resulting in the production of an inactive-truncated protein (Tab. 19; Fig. 22C). Hence, it can be inferred that in bacteria with an inactivated *citG* background, two distinct solutions can be adopted to counteract the toxic effects of L-arginine: 1) overexpression of *aspB*, leading to increased L-glutamate degradation, and 2) reduction in L-arginine uptake via RocC permease activity.

In suppressor mutant BP373, it remains unclear why the *acpA* gene, responsible for encoding an essential protein involved in fatty acid biosynthesis, harbored a mutation (Schujman et al., 2003). Additionally, in the small suppressor mutants BP377 and BP378 (both derived from BP276), mutations associated with *odhA* were identified (Tab. 19). In BP377, a 176 bp deletion within the *odhA* gene resulted in its inactivation, consequently affecting the activity of the entire 2-oxoglutarate dehydrogenase complex (PdhAB-PdhD) (Fig. 22D; Resnekov et al., 1992). Conversely, in BP378, a mutation in the promoter site of *odhA* likely reduced the expression of the *odhA* gene. However, it is worth noting that a 2017 study demonstrated that the growth of a strain lacking *odhA* significantly improved during growth in minimal medium (Koo et al., 2017). Therefore, the inactivation or alteration of *odhA* expression may not be directly relevant to the adaptation to L-

arginine toxicity. Additionally, mutations affecting the essential *pyrH* gene, which codes for uridylate kinase PyrH, were observed in both strains BP377 and BP378 (Tab. 19; Fig. 22E; Quinn et al., 1991). Although these mutations may seem irrelevant to bacterial tolerance to toxic levels of L-arginine based on current knowledge, further investigation into the effects of *odhA* and *pyrH* gene mutations is warranted in future studies.

Table 19. Identified mutations in the BP275 (*citG ansR* P_{ansAB}-*lacZ*) and BP276 (*gltAB citG ansR* P_{ansAB}-*lacZ*) on SM plates supplemented with L-arginine (0.5% w/v) by NGS

Strain	Mutant	Parental strain	Phenotype	Affected gene, mutations	Amino acid exchanges, effect on the protein
BP371	B1	BP275 (*citG ansR* P_{ansAB}-*lacZ*)	Growth on SM+Arg, big colonies	5.2 kbp amplification including *aspB*	Enhanced AnsB synthesis
BP372	B2	BP275 (*citG ansR* P_{ansAB}-*lacZ*)	Growth on SM+Arg, big colonies	5.2 kbp amplification including *aspB*	Enhanced AnsB synthesis
BP373	S1	BP275 (*citG ansR* P_{ansAB}-*lacZ*)	Growth on SM+Arg, small colonies	*acpA* G55T, *rocC* C1232T	AcpA D19Y, RocC P411L
BP374	S2	BP275 (*citG ansR* P_{ansAB}-*lacZ*)	Growth on SM+Arg, small colonies	*rocC* +T698	RocC Δ*C270*
BP375	B1	BP276 (*gltAB citG ansR* P_{ansAB}-*lacZ*)	Growth on SM+Arg, big colonies	P_{dinG} (C-63T)	Enhanced AspB synthesis
BP376	B2	BP276 (*gltAB citG ansR* P_{ansAB}-*lacZ*)	Growth on SM+Arg, big colonies	34.7 kbp amplification including *aspB*	Enhanced AnsB synthesis
BP377	S1	BP276 (*gltAB citG ansR* P_{ansAB}-*lacZ*)	Growth on SM+Arg, small colonies	*odhA* ΔT175-A351, *pyrH* A433C	OdhA not synthesized, PyrH T145P
BP378	S2	BP276 (*gltAB citG ansR* P_{ansAB}-*lacZ*)	Growth on SM+Arg, small colonies	P_{odhA} (G-189A), *pyrH* A433C	changed *odhA* expression? PyrH T145P

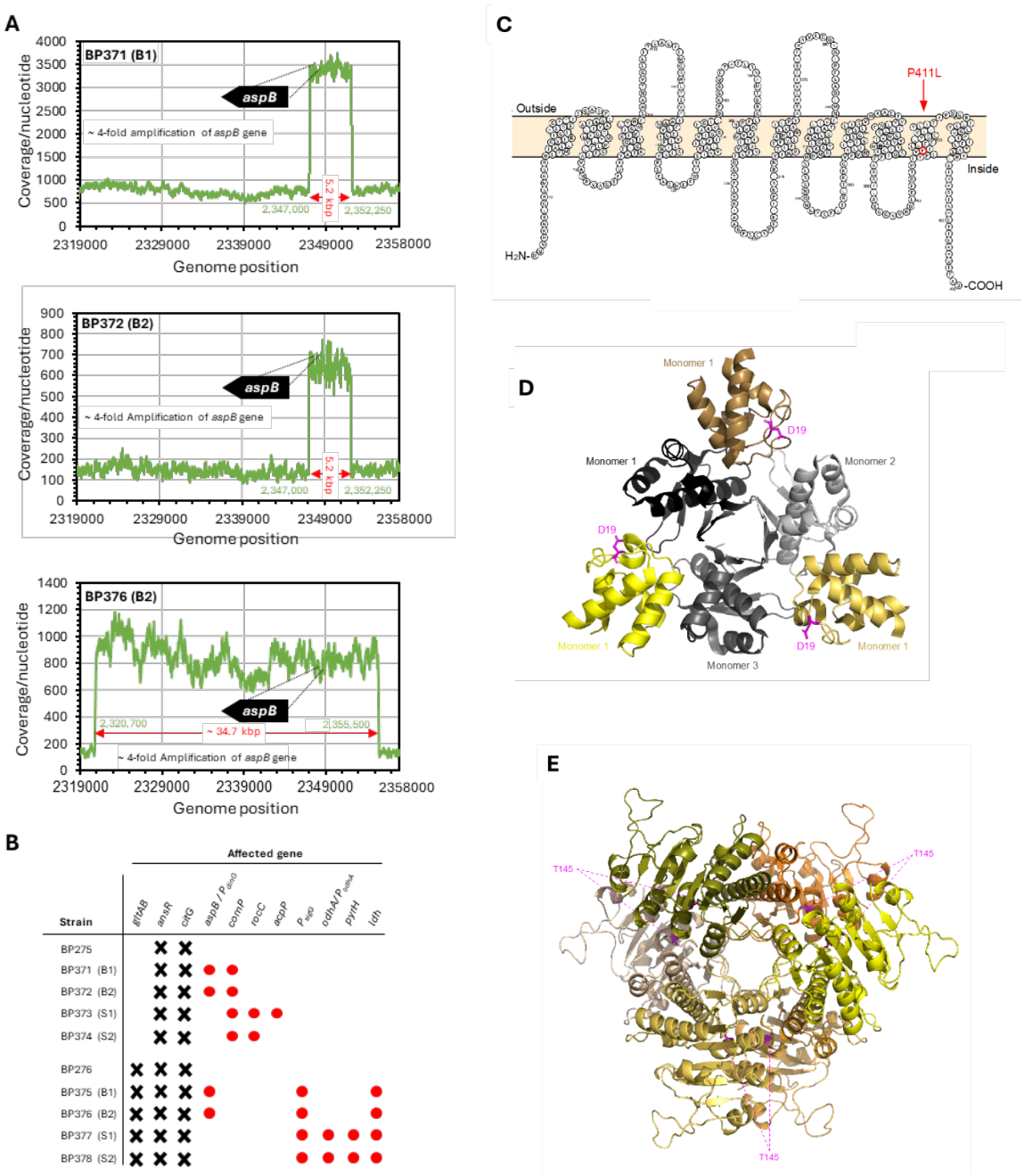

Figure 22. Adaptation of fumarase-deficient *B. subtilis* strains to toxic levels of L-arginine at the genomic scale and localization of the amino acid exchanges in the structure of RocC, AcpA-AcpS complex and PyrH.

A) Coverage of the reads of the genomic segment containing amplification regions from 2,319,000 to 2,358,000 bp. Based on the comparison of the reads coverage of the whole genome and the reads coverage of the amplified region, it can be observed that a 5.2 kbp and 34.7 bp region were 4-times amplified, which includes the *ansB* gene. This indicates that suppressor mutants BP371 (derived from BP275), BP372 (derived from BP275), and BP376 (derived from BP276) harbor 4 copies of any genes located in the amplified region, specifically the *aspB* gene. **B)** Deleted genes and affected (mutated) genes in the suppressor mutants emerging from L-arginine adaptation are depicted as black crosses and red circles, respectively, compared to the parental strains. **C)** Location of P411L exchange in RocC structure belongs to the suppressor mutant BP373. The topology model for RocC was constructed with Protter (Omasits et al., 2014). **D)** & **E)** Location of amino acid exchanges in the 3D-structure model of the AcpA-AcpS complex and of PyrH, respectively. The models

were generated using Swiss-model server for homology modeling of protein structures (Waterhouse et al., 2018) based on the structures of *B. subtilis* AcpA-AcpS (PDBid: 1F80) (Parris et al., 2000) and the *E. coli* UMP kinase (PDBid: 2V4Y) (Meyer et al., 2008) as templates. (Figure adapted from Mardoukhi et al., 2024)

Presence of fumarase-based ammonium assimilation in other bacteria

To investigate the prevalence of the newly discovered ammonium assimilation pathway via AnsB-AspB in other bacterial species, two distinct approaches were taken. The first method was laboratory experiments which were conducted with *C. glutamicum*, representing another Gram-positive bacterial species (constructed and delivered from the Institute of Bio- and Geosciences (IBG) – Jülich). These bacterial strains pose a clean deletion of GOGAT, GHD, and potential homologous genes encoding proteins similar to L-aspartase AnsB and aspartate transaminase AspB. Subsequently, the ability of the modified strains to grow in minimal media both with and without supplementation of L-glutamate was tested. These experiments aimed to determine whether the ammonium assimilation pathway mediated by AnsB-AspB is present and functional in this organism; The second method was bioinformatics analysis which was conducted on bacterial genomes available in public databases to identify strains harboring enzymes involved in the AnsB/AspB-based ammonium assimilation pathway.

Investigation of the fumarase-based ammonium assimilation route in *C. glutamicum*

Previous studies have demonstrated that a *C. glutamicum* strain lacking GOGAT/GDH still is able to grow on a minimal medium containing only glucose and ammonium as the sole sources of carbon and nitrogen, respectively (Rehm et al., 2010). According to the FASTA alignment, the potential protein homolog for AnsB in *C. glutamicum* is the aspartate ammonia-lyase (aspartase, AspA). This protein exhibits an overall sequence identity of 46.9% with the L-aspartase AnsB from *B. subtilis*. Moreover, AspA catalyzes the same reaction as AnsB, which involves the degradation of L-aspartate to fumarate while releasing one molecule of ammonium, and vice versa (Galperin et al., 2021). Additionally, the aspartate transaminase in *C. glutamicum* is referred to as AspT.

A growth test was conducted on CGXII minimal medium plates with and without supplementation of L-glutamate (0.5% w/v) and casamino acid (CAA, 0.1% w/v) using the following *C. glutamicum* strains: WT (ATCC13032), *gltB gdh*, *gltB gdh aspA*, and *gltB gdh aspT*. The plates were incubated at 30°C for 48 hours. Results in Fig. 23 indicate that wild-type strain and *gltB gdh* double deletion could grow on all plates as expected, so it must be another pathway for assimilation of ammonium and synthesis of L-glutamate. The strain lacking *gltB gdh aspT* was unable to grow under any of the conditions tested. This suggests that this strain is likely auxotrophic not only for L-aspartate and L-asparagine but also maybe for L-glutamate. However, the triple deletion strain *gltB gdh aspA*, which was expected not to grow on the CGXII plate without any supplementation,

surprisingly exhibited growth. This suggests that AspA may not be involved in the fumarate-based ammonium assimilation pathway in *C. glutamicum*. It is possible that there is an alternative ammonium assimilation route in *C. glutamicum* that is yet unknown. Alternatively, there may be other homologous enzymes capable of fulfilling the role of AspA in its absence (Fig. 23).

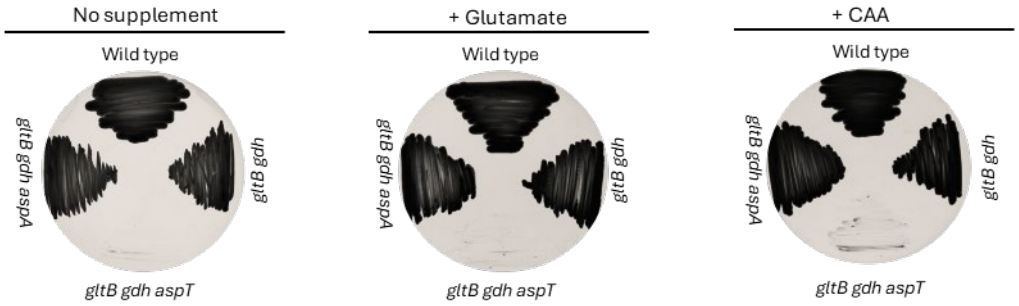

Figure 23. Monitoring the growth of *C. glutamicum* WT, *gltB gdh*, *gltB gdh aspA*, and *gltB gdh aspT* on CGXII minimal medium plates with and without supplementation of glutamate (0.5% w/v) and casamino acid (CAA, 0.1% w/v) for 48h at 30°C. (Figure adapted from Mardoukhi et al., 2024)

Bioinformatics analysis to identify bacterial strains using the AnsB-AspB pathway for ammonium assimilation

Nowadays, genomic databases contain a vast number of whole genome sequences from various bacterial species, facilitating investigations into the prevalence of the newly discovered ammonium assimilation pathway via the AnsB-AspB enzymes across bacterial taxa. Two potential pathways for the synthesis of L-glutamate, L-aspartate, and L-asparagine were considered: one involving the general pathway of L-glutamate synthase-L-glutamine synthetase (GOGAT-GS), and the other involving the AnsB-AspB pathway facilitated by CitG, AnsB, and AspB enzymes (Fig. 24A).

A dataset comprising all available bacterial genomes was retrieved from RefSeq, totaling 14,954 genomes as of April 13, 2022. Subsequently, BLASTP analysis was employed to identify genomes lacking the GltAB subunits (required for the GlnA-GltAB cycle) but possessing CitG, AnsB, and AspB enzymes (required for the alternative ammonium assimilation route via fumarate). Bacterial genomes were queried using the GltAB subunits from *B. subtilis*, considering the enzyme to be absent if neither subunit yielded a significant BLASTP hit. An e-value threshold of e^{-50} was applied, validated through testing on various bacterial species.

Among the analyzed genomes, 2,791 lacked GltAB and were subsequently screened to identify CitG, AnsB, and AspB homologs using *B. subtilis* protein queries (e-value < e-50). Ultimately, 1,642 genomes were identified as lacking GltAB but possessing CitG, AnsB, and AspB homologs. The taxonomic lineage of these genomes was determined using

taxonomic identification numbers (taxIDs) obtained from NCBI and analyzed using ETE3 (Fig. 24B).

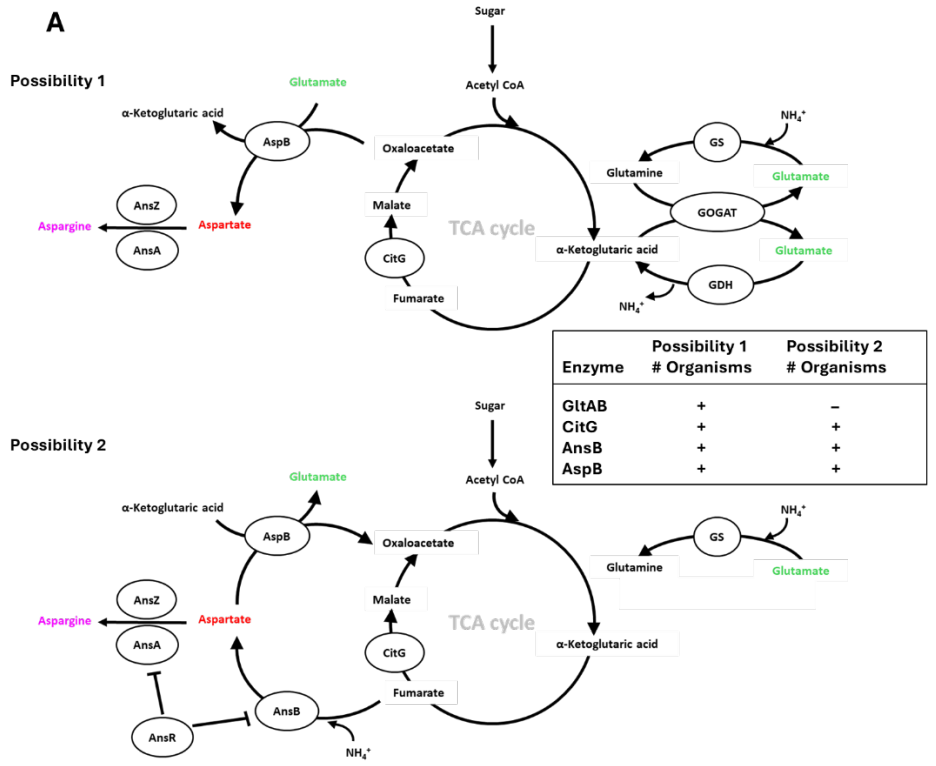

Enzyme	Possibility 1 # Organisms	Possibility 2 # Organisms
GltAB	+	–
CitG	+	+
AnsB	+	+
AspB	+	+

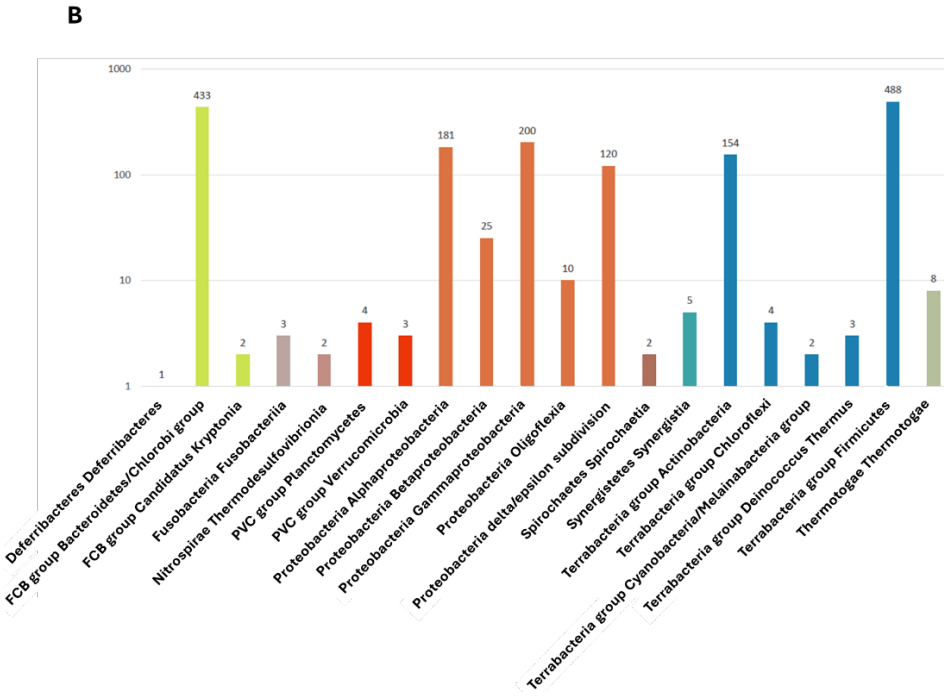

Figure 24. Bioinformatics analysis on the prevalence of bacteria relying on the fumarate-dependent pathway for biosynthesis of L-glutamate, L-aspartate, and L-asparagine.
A) Two possibilities of ammonium assimilation: Possibility 1. α-ketoglutarate-dependent biosynthesis of L-glutamate and oxaloacetate/L-glutamate-dependent biosynthesis of L-aspartate/L-asparagine; Possibility 2. fumarate-dependent biosynthesis of L-glutamate, L-aspartate, and L-asparagine. **B)** Taxonomic distribution of bacterial species lacking GltA and GltB homologs while possessing AnsB, AspB, and CitG homologs suggesting a possible fumarate-based ammonium assimilation bypass. (Figure adapted from Mardoukhi et al., 2024)

Amino acids that support growth of the *gltAB ansAB* mutant

As described above, *B. subtilis* lacking *gltAB* is genetically unstable and acquires the ability to synthesize L-glutamate either by *citG ansR* inactivation or by amplification of the *ansAB* genes which rewire the metabolic flux. Strains harboring combinations of gene inactivation involving *gltAB ansAB*, *gltAB aspB*, or *ansB aspB* demonstrate an incapacity to proliferate in the absence of exogenous supplementation with either L-glutamate, L-glutamate and L-aspartate, or solely L-aspartate, respectively. Consequently, the selection of BP386 (*gltAB ansAB* P_{ansAB}-*lacZ*) was undertaken due to its singular auxotrophic requirement solely for L-glutamate. This choice was made to elucidate the capacity of the twenty proteinogenic amino acids to serve as only nitrogen sources, or both carbon and nitrogen sources, thereby facilitating the restoration of L-glutamate prototrophy.

For the initial experiment, the objective was to delineate the amino acids capable of solely serving as a nitrogen source. Accordingly, strain BP386 was cultured overnight in 4 ml of LB liquid with agitation at 30°C. Subsequently, the following day, the cells underwent two rounds of washing with saline solution, after which the growth experiment commenced. This experiment was conducted in two distinct SM minimal media: one containing ammonium sulfate and the other lacking it. Each medium was supplemented individually with one of the twenty L-amino acids at a final concentration of 0.5% (w/v). Subsequent growth kinetics were monitored for 24h and 37°C in a 96-well plate utilizing a plate reader machine.

The data obtained from the experiment reveals that amino acids belonging to the glutamate family, encompassing L-glutamate, L-glutamine, L-arginine, L-proline, and L-aspartate, exhibit the ability to support bacterial growth irrespective of the presence of ammonium in the media. This suggests their capacity to be degraded to L-glutamate by *B. subtilis*, thereby serving as proficient nitrogen sources (Fig. 25; Gunka & Commichau, 2012; Zhao et al., 2018; Stecker et al., 2022; Warneke et al., 2023; Mardoukhi et al., 2024). Conversely, the remaining amino acids fail to sustain bacterial growth, likely due to their inability to be degraded to glutamate or potentially reaching a toxic concentration of 0.5% (w/v) for the cells, a hypothesis requiring further experimental validation.

Upon consideration of amino acid degradation pathways and growth test results, two amino acids exhibited noteworthy characteristics. Firstly, L-asparagine demonstrated

toxicity towards the *gltAB ansAB* double mutant. As depicted in Fig. 13, its growth-supporting capability was inferior to that of L-aspartate or L-glutamate, potentially attributed to its degradation to L-aspartate by L-asparaginase AnsZ and subsequent accumulation, rendering it toxic for the cells (Fisher & Wray, 2002). Intriguingly, after approximately 20 hours of incubation in both SM media, whether supplemented with or without an ammonium source but including L-asparagine, a resurgence of growth was observed towards the end of the growth curve (indicated with yellow arrow) (Fig. 25). This resurgence probably hints at the emergence of adaptive suppressor mutations, a phenomenon warranting further exploration.

Secondly, L-histidine displayed unusual behavior, as hypothesized to support the growth of BP386, yet not reflected in the growth data. This discrepancy may stem from the cryptic nature of GDH, GudB, which, within the genetic background of *B. subtilis* 168 or SP1 (the parental strain for all *B. subtilis* strains utilized in this study), only allows for the activity of RocG (Belitsky & Sonenshein, 1998; Gunka et al., 2012). This single enzyme may not suffice for the efficient degradation of L-glutamate, leading to its accumulation and subsequent cellular toxicity (Gunka & Commichau, 2012). Alternatively, repression by CcpA, because of the presence of glucose in the media, on the *hut* operon and *rocG* gene, responsible for histidine degradation to glutamate and eventually to α-ketoglutarate, could contribute to the observed phenomenon (Wray & Fisher, 1994; Belitsky et al., 2004). Moreover, it is noteworthy that further investigation into the effects of L-histidine, which has been conducted in subsequent sections, merits detailed study.

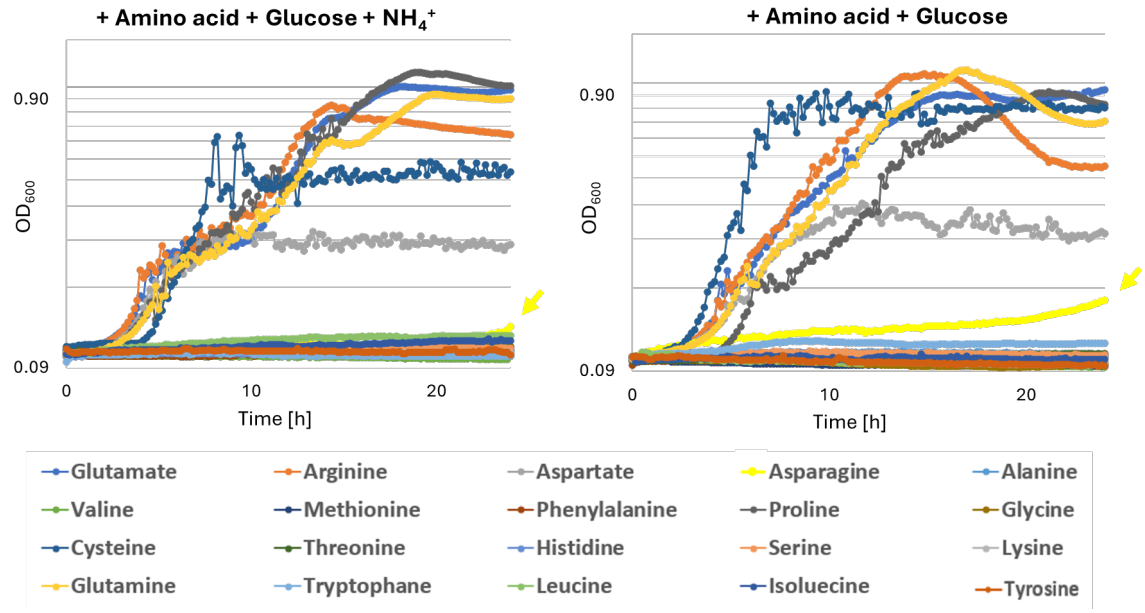

Figure 25. Growth experiment to identify a set of amino acids capable of restoring growth to the genetically-stable glutamate auxotroph strain BP386 (*gltAB ansAB* P_{ansAB}-*lacZ*).
BP386 was cultivated in SM minimal medium with and without ammonium, supplemented individually with one of the twenty proteinogenic L-amino acids at a final concentration of 0.5% (w/v). Cells were incubated at 37°C for 24h. Each experiment was independently repeated as triplet (*N* = 3).

Adaptation of the glutamate auxotroph strain *gltAB ansAB* to toxic levels of L-asparagine

Initially, the aim was to evaluate the toxic impact of L-asparagine on the genetically-stable auxotrophic strain for glutamate, BP386 (*gltAB asnAB* P_{ansAB}-*lacZ*), when cultivated with L-asparagine, a condition previously observed to be detrimental for BP386 as depicted in Fig. 25. To achieve this objective, BP386 was cultured in both LB broth (as a complex medium) and SM minimal medium, with and without supplementation of L-asparagine at a final concentration of 0.5% (w/v) equal to 38 mM. Incubation was carried out at 37°C for 48 hours with agitation. The choice of an extended incubation period was made to facilitate a clearer observation of potential emergence of adaptive suppressor mutants throughout the growth curve. For comparative purposes, the growth of the wild-type SP1 strain and the parental strains BP265 (*gltAB* P_{ansAB}-*lacZ*) and BP269 (*ansAB*) were concurrently monitored alongside BP386.

The results of the growth test revealed distinct outcomes between LB medium supplemented with L-asparagine and without supplementation. In LB medium supplemented with L-asparagine at the final concentration of 0.5% (w/v), all strains failed to grow due to the toxic effects of L-asparagine, but in the LB medium without L-asparagine, growth was observed in all strains except BP269 (*ansAB*), which exhibited growth later after 37 hours incubation, indicating the emergence of suppressor mutants. With prolonged incubation, it is likely that other strains could also develop suppressor mutants (Fig. 26A).

In the SM minimal medium, wild-type SP1 and BP269 (*ansAB*) demonstrated immediate growth owing to their non-auxotrophic nature. BP265 (*gltAB*), an unstable glutamate auxotroph, exhibited slow growth after approximately 10 hours of incubation, highly likely due to mutations in *ansR* or *citG* or amplification in the *ansAB* operon as previously discussed. In SM medium supplemented with L-asparagine, SP1 and BP265 (*gltAB*) grew without issue, while BP269 (*ansAB*) and BP386 (*gltAB asnAB*) exhibited delayed growth after about 20 hours, suggesting the occurrence of mutations (Fig. 26B).

It can be inferred that the toxic effects observed in LB medium were likely exacerbated by the presence of traces of L-asparagine or other amino acids capable of degradation to L-asparagine or L-glutamate, surpassing the final concentration of 0.5% (w/v), particularly impacting SP1 and BP269 (Fig. 26A). However, a higher tolerance was observed in the SM medium plus L-asparagine (Fig. 26B). Furthermore, the emergence of suppressor mutations in SM medium supplemented with L-asparagine, specifically in strains where *ansAB* is deleted (BP269 and BP386), suggests a potential association with the *ansAB* gene, warranting further detailed investigation.

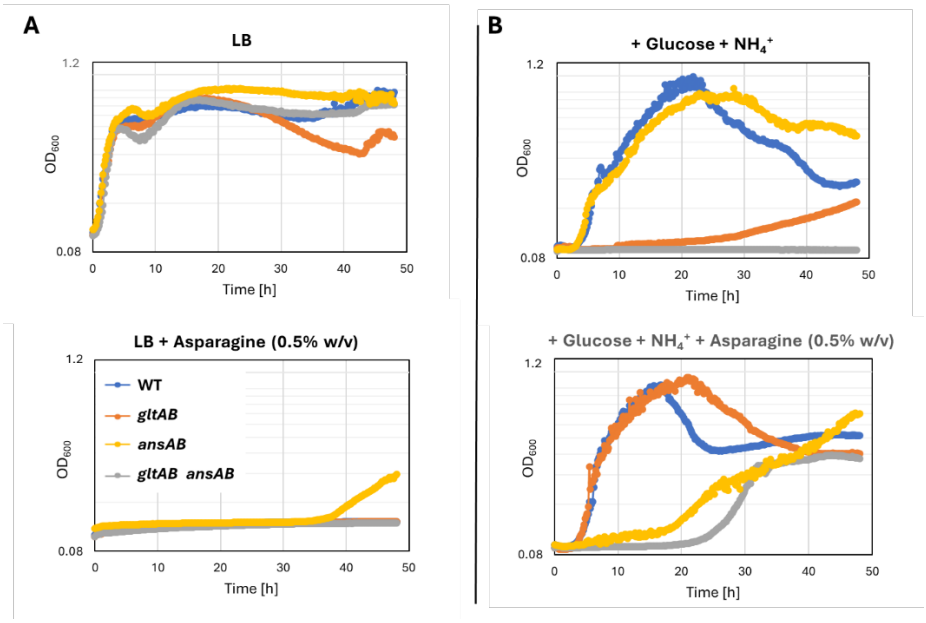

Figure 26. Assessment of the toxic effect of asparagine.
Monitoring the growth of BP264 (WT), BP265 (*gltAB*), BP269 (*ansAB*) and BP386 (*gltAB asnAB*) at 37°C for 48 hours in **A)** LB with and without supplementation of L-asparagine at the final concentration of 0.5% (w/v); and **B)** SM minimal medium with and without supplementation of L-asparagine at the final concentration of 0.5% (w/v) = 38 mM. Each experiment was independently repeated as triplet (*N* = *3*).

Determination of L-asparagine toxicity level in complex and minimal medium

To investigate the tolerance threshold of *B. subtilis* strains to asparagine and to determine the point at which it becomes toxic for the double deletion strain BP386 (*gltAB ansAB* P_{ansAB}-*lacZ*) compared to the BP264 (P_{ansAB}-*lacZ*) as wild-type strain, a growth experiment was conducted in LB complex medium and SM minimal medium with varying concentrations of L-asparagine. Both strains were cultured overnight in 4 ml LB at 30°C, followed by two washing steps with saline solution. Subsequently, the cells were inoculated into LB and SM media supplemented with L-asparagine at concentrations ranging from 0% to 4.0% (w/v) and incubated at 37°C for 48 hours.

The growth graph revealed that although both strains tolerated up to 0.12% (w/v) (9.1 mM)of L-asparagine in LB medium without issues, the growth curve in 0.25% (w/v) (19 mM) concentration indicated the emergence of suppressor mutants with a delay of approximately 10 hours and 30 hours for BP264 and BP386, respectively (Fig. 27A). In SM minimal medium, the wild-type BP264 demonstrated greater tolerance to L-asparagine, up to 1.0% (w/v) (76 mM), beyond which no growth was observed within the 48-hour experiment. Interestingly, in the SM medium, BP386 exhibited the emergence of adaptive mutations between 20 to 30 hours of incubation, enabling tolerance to L-asparagine concentrations of up to 1.0% (w/v) (76 mM), similar to BP264 (Fig. 27B). It is worth noting that the BP264 strain does not require L-asparagine for growth in LB and SM media as it is a prototrophic strain. In contrast, BP386 (*gltAB ansAB* P_{ansAB}-*lacZ*), being a strain

auxotrophic for glutamate, relies on asparagine intake from minimal medium and its subsequent degradation to glutamate to support growth.

In conclusion, the highest tolerated concentration of asparagine by both strains was 1.0% (w/v), coinciding with the emergence of suppressor mutants. Additionally, it is evident that traces of asparagine or other amino acids capable of degradation to asparagine or glutamate in LB media contribute to increased toxicity with additional asparagine supplementation.

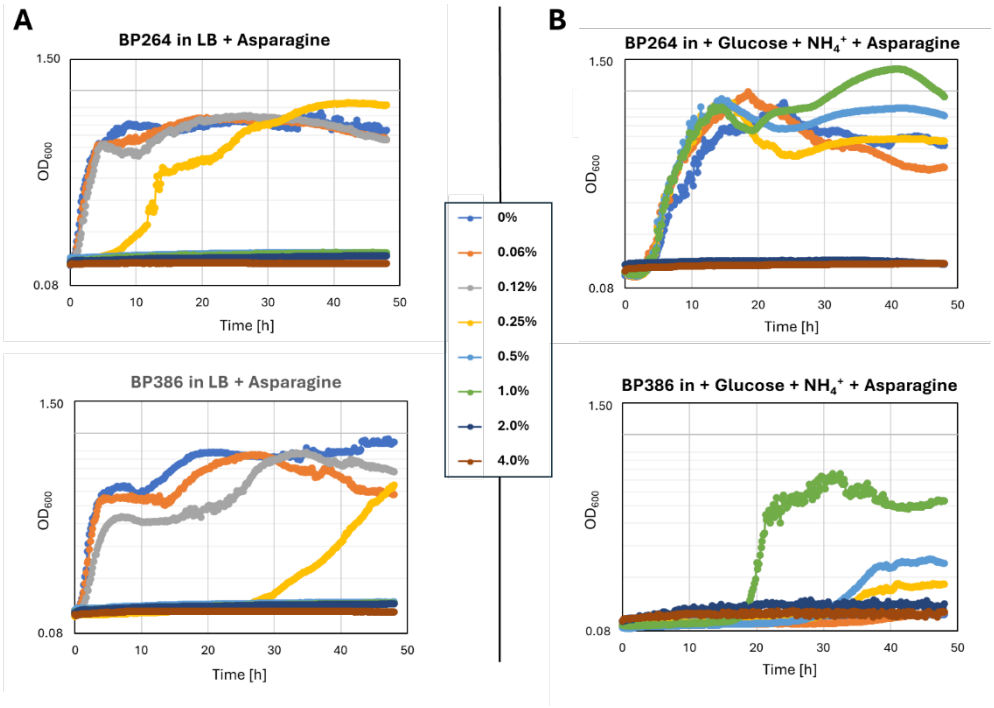

Figure 27. Assessment of L-asparagine toxicity levels in complex and minimal medium.
Growth experiment with *B. subtilis* wild-type BP264 (P_{ansAB}-*lacZ*) and BP386 (*gltAB asnAB* P_{ansAB}-*lacZ*) at 37°C for 48 hours in **A)** LB; and **B)** SM minimal medium, with and without supplementation of L-asparagine at the final concentration of 0%, 0.06%, 0.12%, 0.25%, 0.5%, 1.0%, 2.0% and 4.0% (w/v). Each experiment was independently repeated as triplet (*N* = *3*).

Mutations in *azlB* and *aimA* are responsible for tolerating the toxicity of L-asparagine

After conducting several growth experiments in both complex and minimal media supplemented with L-asparagine, it became evident that L-asparagine exerts a toxic effect on *B. subtilis*, prompting the formation of suppressor mutants as an adaptation mechanism (Fig. 26, Fig. 27). Consequently, it was decided to culture BP264 (as wild type), BP269 (*ansAB*) and BP386 (*gltAB ansAB* P_{ansAB}-*lacZ*) on plates in order to isolate these suppressor mutants and elucidate the genomic basis of the adaptation process. LB and SM plates supplemented with L-asparagine at final concentrations of 0.25% and 0.5% (w/v) were utilized to cultivate cells that had been grown overnight and washed twice. The incubation process was conducted for 7 days at 37°C. Suppressor mutants

that emerged from each strain were isolated and subsequently subjected to next-generation sequencing for genomic analysis (Fig. 28A).

Whole-genome sequencing analysis, reported in Tab. 20, unveiled inactivation mutations in the *azlB* gene among all four suppressors of BP386, designated as BP387 to BP390. As elucidated in the introduction section, *azlB* functions as a transcriptional repressor for the *azlB-azlC-azlD* operon, responsible for encoding the AzlCD amino acid exporter complex. This complex facilitates the export of various branched-chain amino acids, histidine, and 2,3-diaminopropionic acid (Meißner et al., 2022).

Furthermore, in the BP390 derivative of BP386, a 58.8 Kbp long deletion was identified, including *aimA*, which encodes AimA, a general amino acid importer with low affinity symporter for H^+ with glutamate, serine, glycine, 2,3-diaminopropionic acid, alanine, and ß-alanine (Errasti-Murugarren et al., 2019; Klewing et al., 2020; Krüger et al., 2021; Warneke et al., 2024). Moreover, the BP269 (*ansAB*) suppressor mutants, denoted as BP291 and BP292, exhibited insertions in *aimA*, resulting in the deactivation of the final product through truncation and alteration of the amino acid sequences.

In both suppressor mutants BP393 and BP394 derived from the wild-type BP264, the *malP* gene displayed a point mutation and elongation in the final expression product, respectively. MalP acts as a maltose-specific permease facilitating the diffusion of maltose molecules into the cell (Yamamoto et al., 2001; Schönert et al., 2006). While direct evidence linking MalP to L-asparagine tolerance is lacking, investigating its effects remains imperative for future research, especially considering the potential overlap with other permeases and transporters in amino acid transport.

Additionally, *srfAA* and *srfAB*, encoding surfactin synthetase, are part of a larger regulon responsible for surfactin synthesis (Nakano et al., 1991; Y. Xu et al., 2023). Given the mutations observed in *srfAA* and *srfAB* genes in only one of the suppressor mutants (BP387) and their role in surfactin synthesis, their involvement in adapting to L-asparagine toxicity seems improbable.

However, the genome sequences of BP388 and BP391 also revealed point mutations in *yrhJ* and *yetL*, respectively, whose functions are not fully characterized yet. It is proposed that their products may act as an NADPH-cytochrome P450 reductase and a transcriptional repressor of the YetL regulon, respectively (Palmer et al., 1999; Hirooka et al., 2009), although the complete role of the YetL regulon remains unclear (Palmer et al., 1999; Hirooka et al., 2009).

In all four mutants BP387 to BP390, derived from BP386, a point mutation (C-44T) occurred in the downstream region of the *reoM* gene. ReoM functions as an effector protein in MurAA degradation, contributing to peptidoglycan precursor biosynthesis (Kock et al., 2004; Wamp et al., 2020). It was intriguing to investigate whether this point mutation enhanced the expression of *reoM* and if it had any effect on the adaptation to L-asparagine toxicity in *B. subtilis*. To address this, a reporter system was designed and constructed to assess the impact of the mutation in the *reoM* downside. The

downstream regions of the wild-type version and the *reoM* with the C-44T point mutation were amplified by PCR from cDNA of BP387 and SP1 as templates, using oligo primers SM68 and SM69, containing *Eco*RI and *Bam*HI cutting sites, respectively. Subsequently, the PCR products were separately inserted into plasmid pAC7 in front of the *lacZ* gene. The resulting plasmids, namely pBP1122 (P_{reoM}-*lacZ*) and pBP1123 ($P_{reoM\,(C\text{-}44T)}$-*lacZ*), were then introduced into *B. subtilis* SP1 and newly constructed strains designated as BP574 and BP575, respectively. Finally, both strains were cultivated on LB plates supplemented with X-Gal, but no blue-colored colonies were observed, indicating two potential reasons. First, it is possible that the promoter of *reoM* is not situated in the region where the point mutation occurred, as the exact location of the *reoM* promoter is unclear. It is conceivable that *reoM* shares its promoter with *alaS*, the first downstream gene after *reoM*. Second, the observed point mutation may not affect the expression of *reoM*. Thus, it can be inferred that the mutation downstream of *reoM* likely occurred spontaneously and may not be directly correlated with L-asparagine detoxification, suggesting that this mutation can be disregarded.

In mutants BP393 and BP394, derived from the wild-type strain BP264 (P_{ansAB}-*lacZ*), inactivation mutations in *cpaA* and the promoter of *sigG* were also observed. CpaA is a well-studied K^+/H^+ antiporter, and it is highly unlikely to be involved in facilitating the tolerance of L-asparagine toxicity (Lee et al., 2013; Stülke & Krüger, 2020). However, further studies in the future may be necessary to fully elucidate its role. On the other hand, *sigG*, which encodes the sigma factor SigG, aids RNA polymerase in transcribing sporulation genes during the late forespore phase (Wang et al., 2006). The correlation between SigG and tolerating toxic levels of L-asparagine can be excluded due to the different phases of expression and growth of the host bacteria.

As a final conclusion depicted in Fig. 28B, it can be inferred that the inactivation mutation in *azlB*, resulting in continuous expression of the *azlCD* operon, not only facilitates the detoxification of L-histidine by exporting it to the extracellular space, as previously reported, but also assists in detoxifying high concentrations of L-asparagine. This is because AzlCD functions as a broad-spectrum amino acid exporter. Conversely, the inactivation of AimA, observed in several suppressor mutants as a means to tolerate toxic levels of L-asparagine, serves to reduce the import of L-asparagine through a non-specific or promiscuous amino acid transporter. These findings have been reported in recently published collaboration with Jörg Stülke's group (Meißner et al., 2024).

Table 20. Identified mutations in the BP264, BP269 (*ansAB*) and BP386 (*gltAB ansAB*) on LB and SM plates supplemented with asparagine (0.5% and 0.25% w/v) by NGS

Strain	Mutant	Parental strain	Phenotype	Affected gene, mutations	Amino acid exchanges, effect on the protein
BP387	S3	BP386 (*gltAB ansAB* P_{ansAB}-*lacZ*)	Growth on SM+Asn	*srfAA* ΔG9236-10764A, *srfAB* ΔA1-T9059, *azlB* T194G, P_{reoM} C-44T	SrfAA is deactivated, SrfAB is not synthesized, AzlB I65S, changed ReoM expression?
BP388	S5	BP386 (*gltAB ansAB* P_{ansAB}-*lacZ*)	Growth on SM+Asn	*azlB* T194G, *yrhJ* C461T, P_{reoM} C-44T	AzlB I65S, YrhJ T154M, changed ReoM expression?
BP389	S7	BP386 (*gltAB ansAB* P_{ansAB}-*lacZ*)	Growth on SM+Asn	*azlB* T194G, P_{reoM} C-44T	AzlB I65S, changed ReoM expression?
BP390	S14	BP386 (*gltAB ansAB* P_{ansAB}-*lacZ*)	Growth on SM+Asn	58.8 Kbp deletion Δ225622-284415 including *aimA*, *azlB* Δ139G, P_{reoM} C-44T	AimA is not synthesized, AzlB is deactivated, changed ReoM expression?
BP391	S1	BP269 (*ansAB*)	Growth on LB+Asn	*aimA* +CTA194, *yetL* G287T	AimA is deactivated, YetL A96E
BP392	S2	BP269 (*ansAB*)	Growth on LB+Asn	*aimA* +G213	AimA is deactivated
BP393	S1	BP264 (P_{ansAB}-*lacZ*)	Growth on LB+Asn	*malP* A194C, P_{sigG} G+78A	MalP Q65P, Changed SigG expression?
BP394	S2	BP264 (P_{ansAB}-*lacZ*)	Growth on LB+Asn	*cpaA +T153, malP +A1571*	CpaA is deactivated, MalP is deactivated

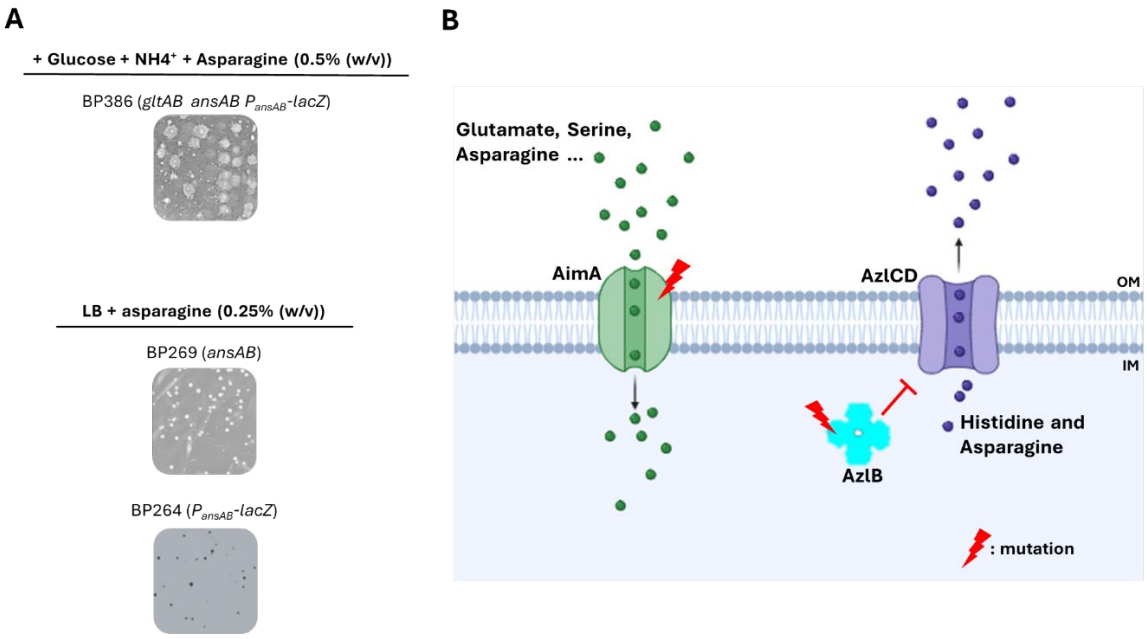

Figure 28. Asparagine detoxification via mutation in *azlB* and *aimA*.
A) *B. subtilis* strain wild-type BP264 (P_{ansAB}-*lacZ*), BP269 (*ansAB*), and BP386 (*gltAB ansAB* P_{ansAB}-*lacZ*) were cultivated overnight, washed twice, and then propagated on LB and SM minimal medium supplemented with 0.25% and 0.5% (w/v) L-asparagine. The cultures were then incubated for 7 days at 37°C. **B)** Schematic illustration depicting mutations in *azlB* and *aimA*, which contribute to the tolerance of toxic levels of L-asparagine.

Adaptation of the *gltAB ansAB* mutant to toxic levels of L-histidine

Another amino acid with surprising results was L-histidine Fig. 25. Previous research and the catabolic pathway discussed in the introduction section indicate that *B. subtilis* can uptake L-histidine from the environment via histidine permease HutM and degrade it to L-glutamate through the enzymatic reaction of four enzymes: HutH, HutU, HutI, and HutG, encoded by genes located in a single operon, *hutHUIG*, controlled by transcriptional antiterminator HutP (Wray & Fisher, 1994; Bender, 2012). Therefore, cultivation of the double deletion strain BP280 (*gltAB ansAB*) in a minimal medium supplemented with L-histidine would be expected to result in growth. However, as shown in Fig. 25, this was not the case.

To investigate this further, it was decided to determine if L-histidine could serve as the sole source of carbon and nitrogen and restore growth to the glutamate auxotroph strain BP280 (*gltAB ansAB*). Initially, BP280 (*gltAB ansAB*) and wild-type SP1 were incubated overnight in 4 ml LB broth. The following day, after washing the cells twice, they were inoculated into two different minimal media supplemented with L-histidine at a final concentration of 0.5% (w/v). In one medium, histidine was the only source of nitrogen, while in the other, histidine served as the sole source of carbon and nitrogen. The growth of both strains was monitored in both media for 48 hours at 37°C.

In the medium containing glucose (Fig. 29A), L-histidine was solely required as a nitrogen source. Consequently, the wild-type strain began to grow immediately. However, after approximately 25 hours of incubation, BP280 underwent mutation and suddenly initiated growth, unlike in the medium where L-histidine was expected to serve as both a carbon and nitrogen source, in which BP280 did not grow in 48 hours of the test at all (Fig. 29B). SP1 was indeed capable of growth without glucose supplementation but exhibited initial struggle, possibly indicating the emergence of suppressor mutants adapting to the L-histidine concentration of 0.5% (w/v) after about 12 hours and ultimately failing to reach high levels of growth (Fig. 29B).

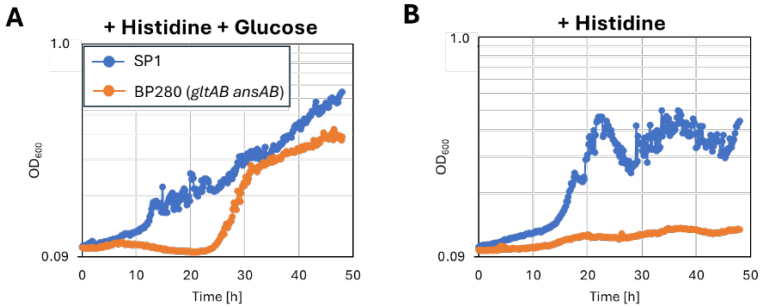

Figure 29. Growth experiment in minimal medium supplemented with L-histidine. Wild-type SP1 and BP280 (*gltAB ansAB*) were cultivated for 48 h at 37°C in SM minimal medium supplemented with **A)** glucose and L-histidine (0.5% w/v) and **B)** only L-histidine (0.5% w/v). Each experiment was independently repeated as triplet (*N* = *3*).

Determination of L-histidine toxicity level in minimal medium

Previous experiment raises the question of whether the wild type and *gltAB ansAB* strains are capable of utilizing L-histidine as a nitrogen source but not as a carbon source until mutation occurs. To address this question, it was necessary to evaluate the toxicity level of L-histidine in the minimal medium. Subsequently, conducting long-term growth experiments on solid media and isolating potential suppressor mutants would likely provide insights and answers to the question at hand.

After incubating overnight in LB liquid and washing twice with saline solution, cells of SP1 and BP280 (*gltAB ansAB*) were cultured in SM minimal medium supplemented with a spectrum of L-histidine concentrations ranging from 0 to 1.0% (w/v), both with and without glucose. The growth experiment was conducted at 37°C for 48 hours.

Results clearly indicated that as the concentration of L-histidine in the media increased, SP1 exhibited a longer lag phase regardless of the presence of glucose. However, when grown with glucose, SP1 was able to reach the log phase and achieve higher OD_{600} values more quickly. Interestingly, even at the lowest L-histidine concentration, 0.005% (w/v), SP1 demonstrated growth, but delays in growth were observed at concentrations of 0.5% and 1.0% (w/v), possibly due to the emergence of suppressor mutants (Fig. 30).

Analyzing the growth curve of BP280 (*gltAB ansAB*) revealed that without glucose supplementation, L-histidine could not serve as both a carbon and nitrogen source for the bacteria. Minimal growth was observed within 48 hours of incubation, suggesting that this strain either cannot effectively uptake and utilize L-histidine as a carbon and nitrogen source, or the uptake and degradation processes are insufficient to support growth (Fig. 30B). Conversely, when L-histidine served as the sole nitrogen source, the growth curves of BP280 remained relatively constant at concentrations higher than 0.005% (w/v), with no significant differences observed (Fig. 30B). This suggests that the process of releasing the amino group from L-histidine during catabolism is more efficient, and that glucose is a superior carbon source compared to L-histidine.

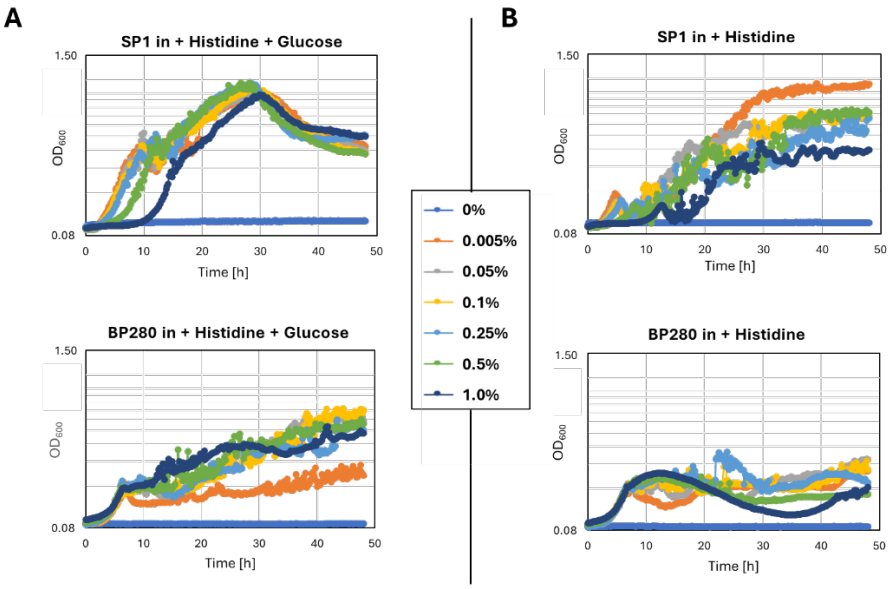

Figure 30. Assessment of histidine toxicity level minimal medium. Growth experiment with wild-type SP1 and BP280 (*gltAB asnAB*) at 37°C for 48 hours in SM minimal medium supplemented with histidine at the final concentration of 0%, 0.005%, 0.05%, 0.1%, 0.25%, 0.5%, 1.0% (w/v), **A)** with glucose; and **B)** without glucose. Each experiment was independently repeated as triplet (*N* = *3*).

Mutations in *gudB* and *hutP* are responsible for tolerating the toxicity of histidine

Based on the preceding experiment, it became evident that both strains of *B. subtilis*, namely SP1 (wild type) and the glutamate auxotroph BP280 (*gltAB ansAB*), which exhibits genetic stability, are capable of generating suppressor mutants to thrive in liquid minimal medium supplemented with 0.5% (w/v) L-histidine (Fig. 29, Fig. 30). To isolate these suppressor mutants, each strain was cultured separately on plates of SM minimal medium supplemented with L-histidine at a final concentration of 0.5% (w/v), both with and without glucose. Incubation of the plates was conducted at 37°C for 7 days to allow for the emergence of mutant colonies.

Following the 7-day incubation period, it was observed that while SP1 produced mutants in the form of conspicuously large colonies on SM medium containing L-histidine and glucose, on the SM plates supplemented solely with L-histidine, a bacterial lawn developed without the formation of distinct colonies. Consequently, it was only feasible to isolate colonies from the glucose-containing medium (Fig. 31A). Conversely, BP280 yielded suppressor mutants on both media, with and without glucose, albeit in significantly fewer numbers compared to SP1. It is noteworthy that the BP280 mutants appearing on the SM plates containing only L-histidine as the sole source of carbon and nitrogen exhibited diminutive size. Furthermore, upon isolation and subsequent recultivation on the same medium, suppressor mutants displayed poor growth. However, after an extended incubation period, it became evident that these mutants were unstable and gave rise to forward mutants. Four of these forward mutants were also isolated, and intriguingly, they exhibited robust and stable growth on the same medium (SM + histidine) in comparison to their parental strain (Fig. 31A).

After isolation of the emerged colonies from the suppressor mutants, following three rounds of propagation to ensure the purity of the mutants, cDNA from two suppressor mutants in each case was extracted and subjected to next-generation sequencing (Tab. 21).

Table 21. Identified mutations in the SP1, and BP280 (*gltAB ansAB*) on SM plates supplemented with L-histidine (0.5% w/v) by NGS

Strain	Mutant	Parental strain	Phenotype	Affected gene, mutations	Amino acid exchanges, effect on the protein
BP581	H2	SP1 (wild type)	Growth on SM+His+Glc	*yhxA* -T346, *cwlO* G535A, *hutP* C174T	YhxA is deactivated, CwlO E179K, HutP (no effect)
BP582	H4	SP1 (wild type)	Growth on SM+His+Glc	*yhxA* -T338, *hutP* C174T	YhxA is deactivated, HutP (no effect)
BP583	E1	BP280 (*gltAB ansAB*)	Growth on SM+His+Glc	*ansR* C107A, *hutP* C174T	AnsR is deactivated, HutP (no effect)
BP584	E4	BP280 (*gltAB ansAB*)	Growth on SM+His+Glc	*ansR* C107A, *hutP* C174T	AnsR is deactivated, HutP (no effect)
BP585	D3	BP280 (*gltAB ansAB*)	Growth on SM+His	P_{ppsA} C+81T, *ansR* C107A, *hutP* C174T	Changed PpsA expression?, AnsR is deactivated, HutP (no effect)
BP586	D4	BP280 (*gltAB ansAB*)	Growth on SM+His	*ansR* C107A, *hutP* C174T	AnsR is deactivated, HutP (no effect)
BP587	FD2	BP280-D2 (*gltAB ansAB*)	Growth on SM+His	P_{ppsA} C+81T, *ansR* C107A, *hutP* T162C, *gudB* ΔG279-C287	Changed PpsA expression?, AnsR is deactivated, HutP (no effect), Synthesis of GudB1

BP588	FD4	BP280-D4 (*gltAB ansAB*)	Growth on SM+His	*rpoC* C3038T, P_{srfAA} C+415T, *ansR* C107A, *hutP* C174T, *gudB* ΔG279-C287	RpoC A1013V, Changed SrfaA expression?, AnsR is deactivated, HutP (no effect), Synthesis of GudB1

Interestingly, all the suppressor mutants, derived from different parental strains, showed single point mutation C174T in *hutP* gene except mutant strain BP587, which showed mutation in the same gene but different position (T162C).

Surprisingly, based on the codon sequence table, none of these mutations in *hutP* have any effect on the final expressed protein but still cannot be easily excluded because the mutation could possibly affect RNA stability and thus HutP synthesis. Also, HutP is an RNA-binding protein that exists as a hexamer and binds to cis-acting regulatory sequences of the transcript in response to the presence of L-histidine and Mg^{2+}. The mechanism of HutP acting model proposed in which HutP prevents the transcription termination of the *hut* operon by binding to the anti-terminator on the *hut* mRNA, thus stabilizing the anti-terminator, which then inhibits the formation of the downstream terminator (Oda et al., 2000). Given that the anti-terminator sequence resides upstream of the *hutP* gene, it is plausible to assume that a single point mutation in *hutP* could potentially affect the structural formation of the anti-terminator. Consequently, this could facilitate or hinder the read-through of RNA polymerase and transcription of the entire upstream *hut* operon. Given that glucose is a preferred carbon source of *B. subtilis* and many other bacteria, the *hut* operon is subject to carbon catabolite repression (CCR) by CcpA (Wray & Fisher, 1994). Therefore, the point mutations identified in suppressor mutants BP581 to BP584 (Tab. 21), which exhibit growth on SM minimal medium supplemented with L-histidine and glucose, where the *hut* operon is already repressed, can theoretically be interpreted as facilitators or enhancers of *hut* operon expression. This enhanced expression could lead to increased uptake of L-histidine, which serves as the sole source of nitrogen in this condition. Additionally, the emergence of suppressor mutants BP585 to BP588 on SM medium supplemented solely with L-histidine as the sole source of carbon and nitrogen can be viewed as secondary evidence supporting the necessity for L-histidine uptake, which is likely augmented by the point mutation in the *hutP* gene.

Forward mutant strains BP587 (FD2) and BP588 (FD4), derived from BP280-D2 (not sequenced, only depicted in Fig. 31A) and BP586 (D4), respectively, exhibit a 9-bp deletion (ΔG279-C287) in the *gudB* gene encoding GDH, GudB, leading to its decryption into a functional variant, GudB1 (Belitsky & Sonenshein, 1998; Gunka et al., 2012; Gunka & Commichau, 2012), alongside an apparent nonsense mutation in *hutP*. The comparison of the increased stability and faster growth rate observed in BP587 and BP588 compared to their parental strain on minimal medium plates suggests that the

mutation in *hutP*, although not resulting in any alteration to the protein product, likely influences the expression of the *hut* operon. This modulation appears to enhance the expression of the entire *hut* operon by affecting the stabilization of the anti-termination structure, thereby shifting it from a stable to an unstable state. Consequently, this instability leads to higher expression levels of the entire *hut* operon (Fig. 31A). Also, the uptake of L-histidine, in order to be used as the only source of carbon and nitrogen, may increase due to the higher expression level of histidine permease HutM. Furthermore, in the subsequent genomic adaptation level, in the forward mutants BP587 (FD2) and BP588 (FD4), the decryption of GudB facilitates the degradation of accumulated L-glutamate resulting from L-histidine catabolism via HutHUIG, thereby channeling it into the TCA cycle as 2-oxoglutarate. This process aids in the detoxification of L-glutamate accumulation arising from elevated L-histidine concentrations (Fig. 31B). Notably, it has been previously reported that the function of GDH, GudB is essential for facilitating the growth of *B. subtilis* NCIB 3610 in minimal media wherein L-histidine or other amino acids metabolized through glutamate, serve as the sole carbon source. (Jayaraman et al., 2022).

To assess the impact of the observed point mutations in *hutP* on the expression level of the *hut* operon, a reporter system was devised. This involved placing both the native and mutated versions of the *hutP* gene, along with its upstream region (encompassing the promoter of the *hut* operon and the region where the terminator stem-loop structure forms), in front of the *lacZ* gene within the integrative plasmid pAC5. These constructs were then introduced separately into the *B. subtilis* SP1 (wild-type) and the *hutP*-deleted strain BP396 (*hutP::aphAIII*). Subsequently, β-Galactosidase activity, indicative of any alterations in *hut* operon expression, could be measured.

To accomplish this, segments comprising the *hutP* gene and its upstream region (between *hutP* and *hutH*) were amplified via PCR using oligo primers SM76 and SM77, utilizing cDNA templates from *B. subtilis* SP1, BP581 (C174T), and BP587 (T162C). These amplifications were employed to construct plasmids designated as pBP1126, pBP1127, and pBP1128, respectively. Subsequently, all constructed plasmids were introduced to *B. subtilis* SP1 and BP396 (*hutP*) to construct the final strains BP397 (*hutP* P_{hutP}-*hutP*-*lacZ*), BP398 (*hutP hutP*$^{(C176T)}$-P_{hutP}-*lacZ*), BP399 (*hutP hutP*$^{(T162C)}$-P_{hutP}-*lacZ*), BP578 (*hutP*-P_{hutP}- *lacZ*), BP579 (*hutP*$^{(C176T)}$-P_{hutP}-*lacZ*) and BP580 (*hutP*$^{(T162C)}$-P_{hutP}-*lacZ*). In the next step, initial β-Galactosidase measurements from all strains growing in SM minimal medium supplemented solely with L-histidine as the sole source of carbon and nitrogen indicated the functionality of the system (data not shown). However, further investigations are warranted to delve deeper into this experiment and narrow down its scope.

In addition to the mutations in *hutP* and *gudB*, which exhibit the highest relevance to the phenotype of the suppressor mutants, whole-genome sequencing has revealed additional mutations (Tab. 21). Among these, a nucleotide alteration in the *ansR* gene is consistently observed in all suppressor mutants derived from BP280 (*gltAB ansAB*), resulting in the C-terminal truncation of AnsR and deactivation of the encoded protein.

However, it is established that AnsR functions as a transcriptional repressor of the *ansA-ansB* operon. Given that the *ansAB* gene is already replaced with an *ermC* cassette in the genome of the parental strain BP280, it can be inferred that mutations in *ansR* do not exert any discernible effect on the emergence of suppressor mutants.

Furthermore, inactivation mutations in *yhxA*, which shares similarity with adenosylmethionine-8-amino-7-oxononanoate aminotransferase, although its precise function remains elusive, along with amino acid replacements in CwlO, an autolysin involved in cell wall synthesis, mutations in the promoter site of the *ppsA* gene encoding the antibacterial compound plipastatin, single nucleotide changes in the *rpoC* gene encoding the RNA polymerase beta' subunit, and mutation in downstream of *srfAA,* responsible for the production of surfactin synthetase enzyme, have been identified through whole-genome sequencing analysis.

In theory, while mutations in *hutP* and *gudB* are the primary candidates conferring *B. subtilis* with the ability to detoxify L-histidine and utilize it as a sole source of nitrogen or both carbon and nitrogen, further experimental investigation is warranted to conclusively elucidate the impact of the remaining mutations.

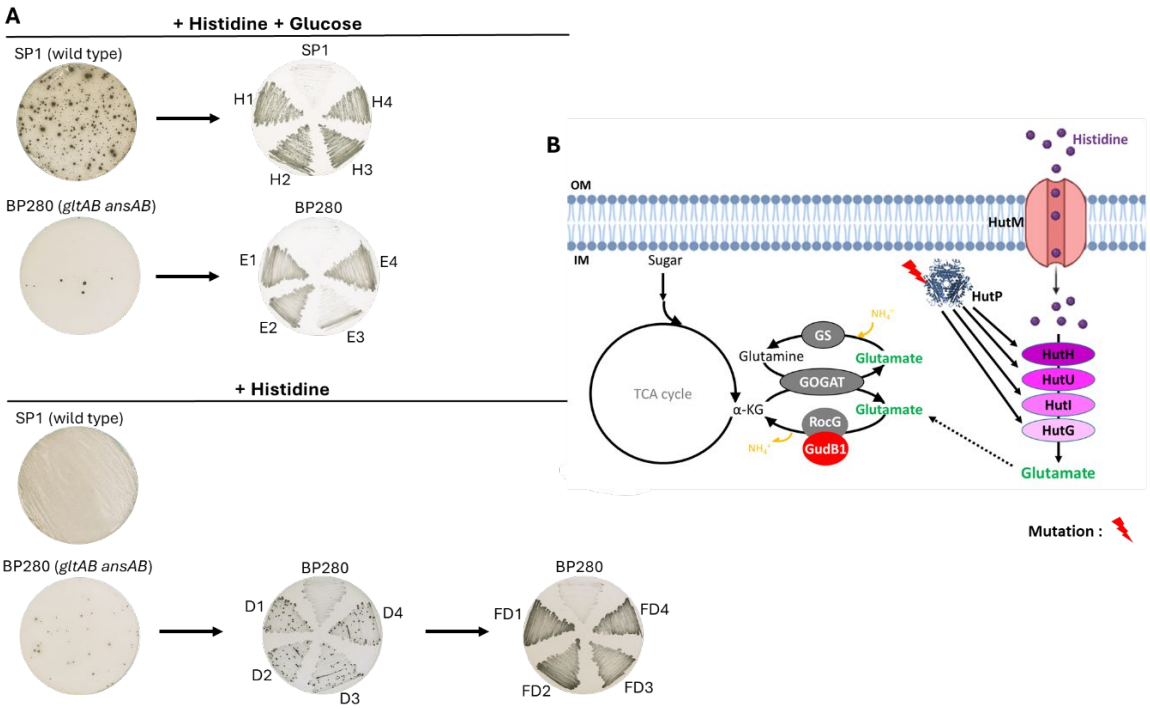

Figure 31. L-Histidine detoxification through mutation in *hutP* and decryptification of *gudB*. **A)** The *B. subtilis* strains SP1 and BP280 (*gltAB ansAB*) were incubated overnight in LB medium, followed by two rounds of cell washing and propagation on SM minimal medium plates supplemented with L-histidine and glucose, as well as plates containing histidine alone. Then, plates were incubated at 37°C for 7 days. **B)** Genomic-based schematic illustration of mutations in *hutP* and *gudB* which enable the detoxification of L-histidine and its utilization as a sole source of carbon or both carbon and nitrogen.

Amino acids serving as a carbon and nitrogen source for the *gltAB ansAB* mutant

Based on previously published studies and growth experiments involving L-arginine and L-histidine in this investigation (Belitsky & Sonenshein, 1998; Gunka & Commichau, 2012; Jayaraman et al., 2022; Mardoukhi et al., 2024), it has been deduced that in *B. subtilis* laboratory strain SP1 or 168, wherein one of the two GDH enzymes is inactivated, experiences insufficient degradation of L-glutamate, leading to its toxic accumulation from certain amino acids degradation. Consequently, the reactivation/decryptification of the *gudB* gene becomes imperative to alleviate this toxicity. So, it was decided to engineer two new strains wherein the GDH, GudB, is functional. These strains are intended to be constructed in the genetic backgrounds of both wild-type SP1 and the glutamate auxotroph strain BP280 (*gltAB ansAB*). Subsequently, all twenty amino acids can be introduced into minimal medium, and the growth of *B. subtilis* strains can be monitored to ascertain their capability to serve as sources of carbon and nitrogen, thereby supporting bacterial growth.

To construct strains harboring both active GDHs, GudB and RocG, *B. subtilis* strains SP1 and BP280 (*gltAB ansAB*) were first incubated overnight in LB medium. Subsequently, after two rounds of cell washing, the cells were inoculated onto the surface of C minimal medium plates where L-glutamate served as the sole carbon source. In this setup, L-glutamate needed to be degraded by GDH into 2-oxoglutarate, which could then enter the TCA cycle to be used as a carbon source and support bacterial growth. However, the activity of the GDH, RocG, alone was found to be insufficient for adequate L-glutamate degradation. Hence, the decryptification of the second GDH gene, GudB1, provides significant benefits. Strains harboring both active forms of GDH were characterized by the formation of larger colonies and faster growth on media containing amino acids from the glutamate family (Belitsky & Sonenshein, 1998; Gunka et al., 2012; Gunka & Commichau, 2012). Following a 4-day incubation period at 37°C, several colonies emerged, a subset of which was isolated and subjected to three consecutive rounds of propagation on the same medium to obtain pure suppressor mutant colonies. Subsequently, cDNA was extracted from two isolated colonies of each strain. PCR amplification of the *gudB* gene was then performed using oligo primers LS64 and MD86. The PCR products were expected to reveal a 9-bp deletion indicative of *gudB* decryptification in the suppressor mutants. Sanger sequencing of the PCR products confirmed the precise deletion.

In the subsequent step, *B. subtilis* strains SP1 and BP280, now harboring the functional GudB1 enzyme, were designated as BP576 (*gudB1*) and BP577 (*gltAB ansAB gudB1*), respectively. Concurrently, their parental strains were included for comparison purposes. Growth experiments involving all twenty proteinogenic amino acids were conducted, wherein the amino acids served as the sole source of carbon, nitrogen, or both. Initially, all four strains were cultured overnight in 4 ml of LB medium. Following two rounds of washing, the cells were inoculated into SM minimal medium

supplemented with each of the twenty amino acids individually, at a final concentration of 0.1% (w/v). Each growth experiment was replicated three times and conducted at 37°C for 48 hours.

As anticipated, amino acids belonging to the glutamate family consisting L-glutamate, L-glutamine, L-aspartate, L-proline, and L-arginine, could serve as nitrogen sources for both the SP1 (wild type) and BP280 (*gltAB ansAB*) strains when glucose was present in the media, thereby serving as the nitrogen source (Fig. 32A, C). Furthermore, these amino acids were capable of supporting the growth of BP576 (*gudB1*) and BP577 (*gltAB ansAB gudB1*) strains when employed as the sole source of carbon. This can be attributed to the activity of GudB1, which efficiently degrades L-glutamate to α-ketoglutarate (Fig. 32B, D).

In accordance with findings from a previously published study (Jayaraman et al., 2022), *B. subtilis* strains harboring both active GDHs, BP576 and BP577, exhibited the ability to utilize L-histidine as the sole source of both carbon and nitrogen (Fig. 32B, D). Conversely, their parental strains, SP1 and BP280, were incapable of doing so.

The growth data with L-asparagine, as also depicted in Fig. 27B, further supports the notion that at a final concentration of 0.1% (w/v), L-asparagine is insufficient to sustain the growth of BP280 (*gltAB ansAB*), likely due to inadequate conversion of L-asparagine to L-aspartate, and subsequently to L-glutamate, or due to an insufficient final pool of L-glutamate to alleviate glutamate auxotrophy and support growth. Conversely, in the presence of the active version of GudB (GudB1) in the background of the same strain, BP577 (*gltAB ansAB gudB1*) exhibited slight growth when L-asparagine served as the sole source of carbon or both carbon and nitrogen. This suggests that L-asparagine could be converted into L-aspartate, and subsequently into L-glutamate, which could then enter the TCA cycle as α-ketoglutarate, facilitated by the enzymatic activity of GudB1 and RocG (Fig. 32C, D). It should be mention that, both the wild-type strain SP1 and its derivative BP576 (*gudB1*) were able to utilize L-asparagine as a single source of carbon or both carbon and nitrogen, although the growth rates did not reach high levels (Fig. 32A, B).

Examining the growth graphs of L-cysteine and L-alanine reveals that both amino acids could sustain the growth of SP1 and BP576 (*gudB1*) strains as a single source of carbon, nitrogen, or both carbon and nitrogen (Fig. 32A, B). This suggests a possible mechanism wherein L-cysteine is taken up by *B. subtilis* in its cystine form, the oxidized dimer and more stable variant of cysteine. Subsequently, through the action of an unidentified enzyme, cystine may be cleaved into two molecules of L-cysteine. These molecules then undergo enzymatic transformations via O-succinylhomoserine lyase MetI and cystathionine beta-lyase MetC/PatB, ultimately leading to the synthesis of homocysteine and later L-methionine. During this process, one molecule of pyruvate and one molecule of ammonium are released (Auger et al., 2002, 2005; Oudega et al., 1997). Pyruvate can serve as a source of carbon, while the ammonium group contributes to the nitrogen pool. However, no growth was observed in the case of glutamate auxotroph strains BP280 (*gltAB ansAB*) and BP577 (*gltAB ansAB gudB*$^{+}$), indicating a lack of capability to convert

L-cysteine to L-glutamate. This inference is supported by a long-term growth experiment on SM minimal medium plates supplemented with L-cysteine as the sole source of carbon, nitrogen, or both carbon and nitrogen in final concentrations of 0.1%, 0.25%, 0.5% (w/v), which did not result in growth or the emergence of suppressor mutants (data not shown). Similar growth patterns were observed when using L-alanine, suggesting that the action of L-alanine dehydrogenase Ala releases one molecule of pyruvate and one molecule of ammonium (Siranosian et al., 1993). These compounds subsequently enter the TCA cycle and nitrogen pool, supporting the growth of wild-type strains but not the glutamate auxotroph strains (Fig. 32).

Other amino acids, including L-valine, L-leucine, L-isoleucine, L-lysine, L-serine, L-tyrosine, L-tryptophan, L-glycine, L-phenylalanine, L-threonine, and L-methionine, were unable to support the growth of any of the strains when applied as the sole source of carbon or both carbon and nitrogen. For wild-type strains SP1 and BP576 (*gudB1*), it appears that these amino acids cannot efficiently enter the TCA cycle and be utilized as a carbon source. In the case of glutamate auxotroph strains BP280 (*gltAB ansAB*) and BP577 (*gltAB ansAB gudB1*), the inability of these amino acids to support growth suggests that they are not directly or indirectly (but insufficiently) converted to L-glutamate to alleviate glutamate auxotrophy. It is noteworthy that these amino acids, except L-serine which seems to be toxic in this concentration, surprisingly could serve as the sole source of nitrogen for wild type strains when glucose was provided as the carbon source. This finding presents a challenge, as it implies the presence of enzymatic activity capable of releasing nitrogen from the amino acids, a phenomenon not reported in existing literature. Hence, further investigation is imperative to determine whether the nitrogen source supporting growth originates from the catabolism of the mentioned amino acids by *B. subtilis* or results from the breakdown of amino acids in the media due to pH or temperature changes or other unidentified factors. Clarifying this aspect of the study and refining its scope in future research is essential.

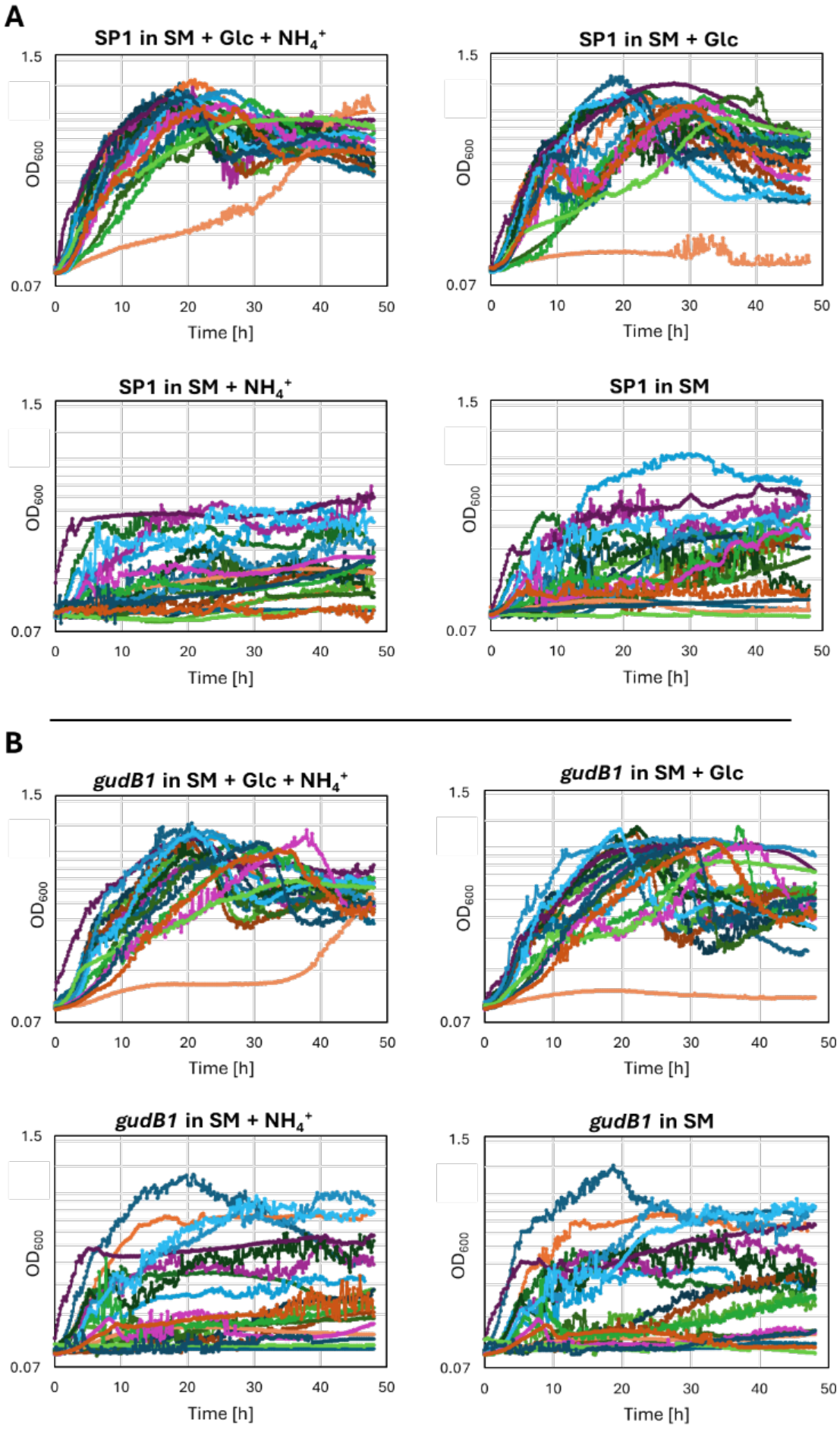
A
SP1 in SM + Glc + NH4+
SP1 in SM + Glc
SP1 in SM + NH4+
SP1 in SM
B
gudB1 in SM + Glc + NH4+
gudB1 in SM + Glc
gudB1 in SM + NH4+
gudB1 in SM
OD600
Time [h]
1.5
0.07
0
10
20
30
40
50

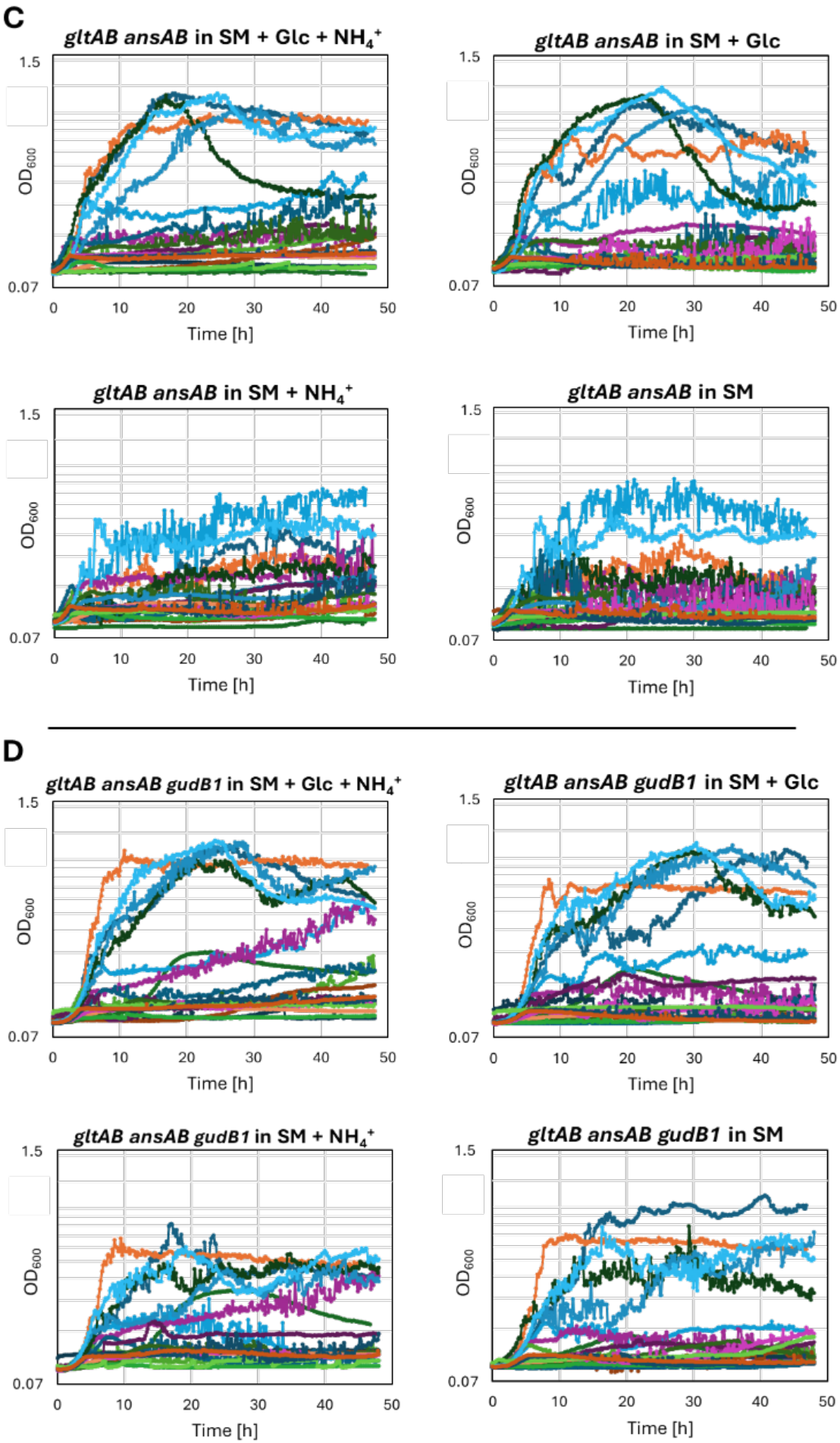
C
gltAB ansAB in SM + Glc + NH4+
gltAB ansAB in SM + Glc
gltAB ansAB in SM + NH4+
gltAB ansAB in SM
D
gltAB ansAB gudB1 in SM + Glc + NH4+
gltAB ansAB gudB1 in SM + Glc
gltAB ansAB gudB1 in SM + NH4+
gltAB ansAB gudB1 in SM
OD600
Time [h]
1.5
0.07
0
10
20
30
40
50

Figure 32. Monitoring the growth of B. subtilis SP1 (wild type), BP576 (*gudB1*), BP280 (*gltAB ansAB*) and BP577 (*gltAB ansAB gudB1*) in minimal medium supplemented with all 20 proteinogenic amino acids, separately. Following overnight incubation in LB medium, cells were subjected to two rounds of washing and subsequently inoculated into SM minimal medium supplemented separately with glucose and ammonium, glucose only, and ammonium only. Additionally, all twenty amino acids were provided each as supplements at the final concentration of 0.1% (w/v). The growth of the cultures was monitored for 48 hours at 37°C. Each experiment was independently repeated as triplet ($N = 3$).

Discussion

As previously explained, glutamate serves a critical metabolite/substrate in all living cells as a primary nitrogen donor/an amino group provider, an osmoprotectant, and a counterion (Magasanik, 2003; Saum et al., 2006; Gunka & Commichau, 2012; Mardoukhi et al., 2024). Given these indispensable functions, maintaining elevated intracellular levels of glutamate is essential. This can be achieved either through environmental uptake, if available, or through biosynthesis via a highly efficient and tightly regulated pathway. Since the discovery of the responsible *gltAB* genes, for glutamate biosynthesis in *B. subtilis* in 1989 (Bohannon & Sonenshein, 1989), it has been widely accepted that the GS-GOGAT pathway is the principal and sole route for glutamate biosynthesis in *B. subtilis* (Fig. 2; Commichau et al., 2008). This study, however, demonstrates that the inactivation of the *ansR* and *citG* genes or overexpression of *ansB* gene enables *B. subtilis* lacking GOGAT activity to overcome glutamate auxotrophy by re-routing ammonium assimilation through a non-canonical fumarate-based pathway (Tab. 13, 22; Fig. 7B; Mardoukhi et al., 2024). Inactivation of *ansR* results in the de-repression of L-aspartase *ansB* gene, while inactivation of *citG* gene redirects the metabolic flux towards L-aspartate production, which is subsequently converted to L-glutamate by the enzymatic activity of aspartate transaminase AspB. Besides, overexpression of the *ansB* gene, achieved through the amplification of its copy number on genome, effectively counteracts the repressive effects of the *ansR* regulatory protein. This de-repression facilitates the robust expression of L-aspartase AnsB, enabling the enzymatic conversion of fumarate to L-aspartate to proceed efficiently. Then, L-aspartate, as explained above, will be converted to L-glutamate (Fig. 7B).

A

Canonical glutamate-based ammonium assimilation pathway

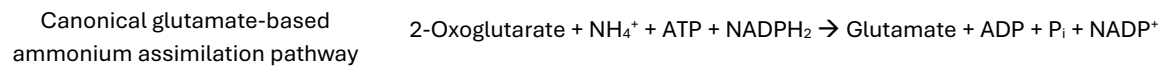

B

Non-canonical fumarate-based ammonium assimilation pathway

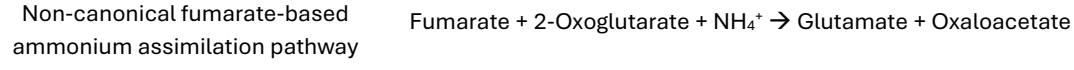

Figure 33. Ammonium assimilation in canonical and non-canonical glutamate biosynthesis pathways.
A) In the GOGAT-GS pathway, ammonium is assimilated with 2-oxoglutarate to produce one molecule of L-glutamate. This process requires energy in the form of ATP and $NADPH_2$. **B)** In the AnsB-AspB pathway, ammonium is assimilated with fumarate to generate L-aspartate. Subsequently, the ammonium group from L-aspartate is transferred to 2-oxoglutarate, ultimately yielding one molecule of L-glutamate and one molecule of oxaloacetate. Notably, this pathway does not require energy input.

Moreover, the inactivation of *ansR* alone is sufficient to alleviate the aspartate auxotrophy of an *aspB* mutant (Mardoukhi et al., 2024). It should be noted that this newly identified pathway compensates not only for glutamate auxotrophy but also for aspartate and asparagine auxotrophy. It is plausible to hypothesize that the absence of AnsR alone permits the growth of the *aspB* mutant strain, which is an aspartate auxotroph, whereas overcoming the glutamate auxotrophy in a strain lacking active *gltAB* genes requires the combined inactivation of AnsR and CitG. This is likely because the cell demands significantly less aspartate than glutamate. This hypothesis is supported by the fact that glutamate is indeed the predominant cellular metabolite in both prokaryotes and eukaryotes (Bennett et al., 2009).

Numerous studies have demonstrated that when a genetic alteration results in the glutamate auxotrophy in *B. subtilis*, the bacterium can adapt genomically to resolve the issue and restore prototrophy. In 1997, Belitsky and Sonenshein revealed that glutamate auxotrophy resulting from the inactivation of the *gltC* gene can be restored by a gain-of-function mutation in the *gltR* gene (Belitsky & Sonenshein, 1997). As already explained, the *gltC* gene encodes the transcriptional regulator GltC, which is essential for activating the transcription of *gltAB* genes in the absence of glutamate (Fig. 3A). Therefore, in the absence of glutamate and inactive GltC, the active LysR-type transcription factor GltR (specifically, GltR24) of unknown function initiates the transcription of *gltAB* genes, thereby restoring glutamate prototrophy (Tab. 22; Belitsky & Sonenshein, 1997). Additionally, a 2017 study by Dormeyer et al. demonstrated two alternative mechanisms in three different classes of mutants by which the same glutamate auxotrophy, caused by inactivation of the *gltC* gene, can be restored (Tab. 22). In one class of mutants, a mutation in the promoter region of the *gltAB* operon led to GltC-independent initiation of transcription of the *gltAB* genes. In the second class of mutants, they found another gain-of-function mutation in the *gltR* gene encoding the transcription factor GltR24. In the third class of mutants, a genome amplification of the region containing the *gltAB* genes resulted in an increased copy number of these genes, despite their poor expression (Dormeyer et al., 2017).

Another example is inactivating mutations in the *ccpA* gene, which encodes carbon catabolite control protein (CcpA), result in glutamate auxotrophy in *B. subtilis* (Reuß et al., 2018). CcpA is crucial in regulating glucose metabolism. In the presence of glucose, CcpA represses the GDH, *rocG* gene, thereby preventing glutamate degradation (Wacker et al., 2003; Belitsky et al., 2004; Commichau, et al., 2006). However, when the *ccpA* gene is inactivated through a mutation or deletion, *rocG* is de-repressed. The resulting RocG protein binds to and inactivates GltC, leading to insufficient expression of the *gltAB* genes, which are responsible for synthesizing glutamate to support bacterial growth (Belitsky et al., 2004). Under these conditions, *B. subtilis* restores glutamate prototrophy by accumulating mutations in the *topA* gene, which encodes DNA topoisomerase I (TopA) (Tab. 22; Reuß et al., 2018). TopA is involved in relaxing negatively supercoiled DNA behind RNA polymerase (Dasgupta et al., 2020). These suppressor mutations result in TopA variants with enhanced activity, improving DNA relaxation and reducing

supercoiling. This enhancement boosts the expression of the *gltAB* operon, thereby increasing the production of GOGAT. This adaptation involves a substantial reorganization of the global transcription network and a re-routing of metabolic pathways. Ultimately, the expression of the *gltAB* genes leads to the inactivation of GDH (Reuß et al., 2018).

Table 22. Mutations compensating for the lack of *gltAB* expression or *gltAB* genes.

Genotype parental strain	Suppressor mutations	Mechanism of suppression
gltC	*gltR24*	Constitutive *gltAB* expression achieved by GltR24
	P_{gltA}*	Constitutive *gltAB* expression due to promoter-up mutation
	Amplification of *gltAB* genes	Increased dosage of *gltAB* genes
ccpA	*topA**	Constitutive *gltAB* expression due to altered DNA topology
gltAB	*ansR citG*	Glutamate biosynthesis via aspartase AnsB and aspartate transaminase AspB
	Amplification of *ansB* gene	Increased dosage of *ansB* gene

Wild-type *B. subtilis* 168 is unable to grow on a minimal medium supplemented with ammonium and succinate as the sole sources of nitrogen and carbon, respectively. This condition leads to glutamate limitation, which can eventually be alleviated by spontaneous inactivating mutations in the *rocG* gene (Commichau et al., 2007). These mutations result in the deactivation of the strictly catabolically active GDH, RocG. In these suppressor mutants, the synthesis of RocG, a glutamate-degrading enzyme, is halted. Consequently, the transcription regulator GltC can constitutively activate the transcription of the GOGAT, *gltAB* genes, thereby restoring glutamate synthesis, refill the glutamate pool and allowing the bacteria to grow under these restrictive conditions (Commichau et al., 2007; Commichau et al., 2008; Dormeyer et al., 2017).

As previously noted, when grown in minimal medium supplemented with glutamate or arginine (amino acids that are part of the glutamate family) as the sole sources of carbon and nitrogen, *B. subtilis* 168/SP1 promptly activates the cryptic GDH gene, *gudB*, synthesizing the enzymatically active GudB1 (Belitsky & Sonenshein, 1998; Gunka et al., 2012). The *gudB* gene is cryptic due to a perfect direct repeat of 9 base pairs (G279-C287) in its coding sequence, causing a duplication of three amino acids within its active site. This duplication destabilizes the protein's structure, leading to rapid proteolytic degradation (Gerth et al., 2008; Gunka et al., 2012). Precise deletion of these 9 base pairs results in the activation of the gene (Belitsky & Sonenshein, 1998; Commichau et al., 2006; Gunka et al., 2012; Dormeyer et al., 2017). The reactivated GudB1, alongside the existing GDH, RocG, facilitates the degradation of glutamate, releasing its amino group to be used as a nitrogen source and providing the carbon backbone as α-ketoglutarate

to the TCA cycle for use as a carbon source. Thus, even high concentrations of a critical metabolite like glutamate, which can be toxic to the cell, can be managed through genomic alterations in *B. subtilis*.

Furthermore, a similar decryptification of the *gudB* gene was observed in another study involving a *B. subtilis* strain lacking the *rocG* gene grown in rich media (Belitsky & Sonenshein, 1998). In this case, the decryptified *gudB* gene encodes the functional GDH, GudB1, which completely compensates for the absence of RocG and prevents the accumulation of glutamate during growth (Stannek et al., 2015).

Not only *B. subtilis*, but also other bacterial species like *E. coli* respond to fluctuations in glutamate homeostasis at the genomic level. Studies have shown that an *E. coli* strain lacking the GOGAT, *gltBD* genes, is unable to synthesize sufficient glutamate for rapid growth in a nitrogen-limited medium. However, mutations in the promoter region of the GDH, *gdhA* gene, compensate for the deficiency by enhancing the anabolic activity of GDH, resulting in increased expression. It is important to note that in many bacterial strains, such as *E. coli* and *C. glutamicum*, GDH functions both catabolically and anabolically *in vivo*, unlike in *B. subtilis* (Reitzer, 2003; Yan, 2007).

Rewiring of the metabolism pathways was also reported in the other microorganism. A recent study conducted in 2022 aimed to investigate potential bypasses for the Embden-Meyerhof-Parnas (EMP) glycolysis pathway in *E. coli* (Iacometti et al., 2022). By deleting the enzymes that block the pathway, the researchers identified two alternative routes: one proceeding via methylglyoxal and the other via serine biosynthesis and degradation. Furthermore, they demonstrated which of these routes is favored by natural selection. The results showed that evolved mutants preferentially used the serine shunt (Iacometti et al., 2022). This finding highlights the flexible repurposing of metabolic pathways, wherein enzymes from different metabolic pathways are recruited to create new metabolite links, effectively rewiring central metabolism.

Under stressful conditions, bacteria adapt by modulating their cellular metabolism to mitigate the adverse effects. In *E. coli*, loss-of-function mutations in specific genes can enhance ethanol tolerance through metabolic alterations. For example, the inactivation of the *slt* gene, which encodes a soluble lytic transglycosylase involved in the recycling of peptidoglycan, enhances ethanol tolerance by restructuring the bacterial cell wall (Engel et al., 1991; Goodarzi et al., 2010; Hottes et al., 2013). This demonstrates how reorganization of metabolic pathways enables cellular adaptation to ethanol-enriched environments.

One potential solution to compensate for a lesion in a metabolic pathway is enzyme promiscuity (Khersonsky & Tawfik, 2010). This phenomenon occurs when enzymes exhibit activities other than those for which they originally evolved. So, enzymatic reaction that is absent due to a gene deletion can be circumvented by recruiting a promiscuous enzyme that catalyzes the missing reaction. For example, in *B. subtilis*, L-proline, which serves as a building block or compatible solute during osmotic stress, is

synthesized from L-glutamate through two distinct pathways. One pathway (ProB-ProA-ProI) operates under non-osmotic stress conditions, while the other pathway (ProJ-ProA-ProH) is active under salinity stress (Fig. 4; Bremer & Krämer, 2019). In both pathways, the enzyme glutamate-5-semialdehyde dehydrogenase ProA plays a central and crucial role. Inactivation of ProA results in strict proline dependency. However, when a ProA-deficient strain is propagated in minimal medium without any external proline source, suppressor mutants eventually emerge. These mutants overexpress the *rocD* gene, which encodes ornithine transaminase RocD. Interestingly, despite the lack of sequence similarity between the *proA* and *rocD* genes, both enzymes catalyze the same reaction product (Zaprasis et al., 2014; Stecker et al., 2022).

Another example of enzyme promiscuity in *B. subtilis* has been observed where the overexpression of threonine synthase ThrC enables the growth of an *ilvA* mutant, which lacks the major threonine dehydratase IlvA (Rosenberg et al., 2016). Due to sequence homology and similar catalytic mechanisms, it has been suggested that threonine dehydratase and threonine synthase evolved from a common ancestral enzyme (Parsot, 1986). However, since ThrC possesses only minor threonine dehydratase activity, a *B. subtilis ilvA* mutant overexpressing the *thrC* gene can grow only in the presence of threonine (Rosenberg et al., 2016).

Another study conducted on *Pseudomonas aeruginosa* revealed that the loss of a key enzyme in the TCA cycle, citrate synthase GltA, which typically prevents cell growth, can be rapidly mitigated through enzyme promiscuity and regulatory network rewiring (Dolan et al., 2022). *P. aeruginosa* can swiftly adapt to the loss of GltA function by acquiring loss-of-function mutations in a transcriptional repressor, leading to the de-repression of *prpC* gene and synthesize 2-methylcitrate synthase PrpC, which can substitute for GltA. The PrpC, an enzyme involved in the propionate pathway, shares significant structural similarity with GltA. It is noteworthy that *P. aeruginosa* is known for its exceptional metabolic flexibility, allowing it to thrive in diverse environments (Dolan et al., 2022). This metabolic plasticity also contributes to its resistance to antibiotics and drugs targeting central metabolic pathways, complicating efforts to combat this bacterium (Gil-Gil et al., 2020; Lopatkin et al., 2021).

Recent advancements in understanding the biosynthesis pathway of vitamin B6 in *E. coli*, facilitated by bioinformatics predictions and subsequent experimental validation, have revealed that overexpression of *thiG* in a Δ*pdxB* mutant effectively suppresses growth defects observed on minimal medium. Furthermore, mutations in the predicted active site residues of ThiG abolish this suppressive effect. The enzyme 1-deoxy-D-xylulose 5-phosphate:thiol sulfurtransferase ThiG is involved in the synthesis of the thiazole moiety of thiamine, while erythronate-4-phosphate dehydrogenase PdxB catalyzes the second reaction in the pyridoxal 5'-phosphate (vitamin B6) biosynthesis I pathway (Vander Horn et al., 1993; G. Zhao et al., 1995). These findings highlight the promiscuous activity of ThiG, allowing it to compensate for the genetic disruption in the vitamin B6 biosynthesis pathway (Oberhardt et al., 2016).

In a study conducted on *Acinetobacter baylyi* in 2022, the bacterium was engineered to lack the *panD* gene, disabling its canonical pathway for synthesizing β-alanine, an essential precursor for coenzyme A biosynthesis. Novel enzymatic intermediates synthesized by 2,4-diaminobutyrate aminotransferase Dat and 2,4-diaminobutyrate decarboxylase Ddc compensated for the lost function of *panD* gene. Remarkably, through adaptive evolution, the *A. baylyi* developed compensatory mechanisms to reroute this biosynthetic pathway. These changes included mutations that activated alternative enzymes capable of catalyzing novel steps in β-alanine synthesis. The adaptations showcased the organism's ability to exploit the inherent flexibility of its metabolic network, using previously untapped enzymatic functions to bypass genetic disruptions (Perchat et al., 2022). This work highlights the evolutionary capacity of bacteria to sustain essential metabolic functions under genetic constraints and emphasizes the role of enzyme promiscuity in facilitating such adaptations.

In the present study, the results demonstrate that ammonium assimilation for L-glutamate biosynthesis in *B. subtilis* is achievable not only through the GOGAT-GS pathway but also via a non-canonical fumarate-based pathway (Fig. 33; Mardoukhi et al., 2024). This prompts inquiry into whether the GOGAT-GS pathway predominates in glutamate biosynthesis across nature and the prevalence of the novel pathway among other organisms, particularly noting that the non-canonical fumarate-based ammonium assimilation pathway operates independently of ATP and $NADPH_2$ (Fig. 33B). Recent findings indicate that in *E. coli*, similar to *B. subtilis*, overexpression of native L-aspartase facilitates ammonium assimilation through the fumarate-based pathway, potentially substituting for the canonical glutamate-based pathway in GOGAT/GDH-deficient *E. coli* strains (Schulz-Mirbach et al., 2022). Furthermore, a 2010 study demonstrated the viability of a GOGAT/GDH-deficient *C. glutamicum* strain to grow using glucose and ammonium as sole sources of carbon and nitrogen, respectively (Rehm et al., 2010).

The remarkable growth capability of the *C. glutamicum* triple deletion strain *gltB gdh aspA* on minimal medium supplemented with glucose and ammonium as the only source of carbon and nitrogen, respectively, suggests the presence of an additional, yet unidentified route for glutamate biosynthesis in this organism (Fig. 23). Despite the fact that L-aspartase AspA, sharing 46.7% overall sequence identity with AnsB from *B. subtilis*, is not implicated in the fumarate-based ammonium assimilation pathway, the possibility of an alternative ammonium assimilation route in *C. glutamicum* remains plausible. Alternatively, there may exist other homologous or promiscuous enzymes capable of assuming the role of AspA in its absence which needs to be discovered.

In this study, employing bioinformatics analysis, I aimed to identify bacterial strains utilizing the AnsB-AspB pathway for ammonium assimilation (Mardoukhi et al., 2024). Ultimately, genome data analysis revealed 1,642 genomes lacking GltAB but harboring homologs of CitG, AnsB, and AspB (Fig. 24B). It would be intriguing to further investigate experimentally whether the AnsB-AspB pathway serves as the primary glutamate

biosynthesis pathway in these identified species and how efficient this pathway is in order to produce glutamate in comparison to the GOGAT-GS pathway.

Considering the energy expenditure associated with the biosynthesis of a single molecule of L-glutamate via the conventional GOGAT-GS pathway, starting from one molecule of pyruvate as the initial substrate entering the TCA cycle, as detailed below:

1) Conversion of pyruvate to acetyl-CoA by pyruvate dehydrogenase complex (Patel et al., 2014):
   Pyruvate + CoA + NAD^+ ⟶ Acetyl-CoA + CO_2 + NADH

2) Conversion of isocitrate to α-ketoglutarate by isocitrate dehydrogenase enzyme (Singh et al., 2002):
   Isocitrate + NAD^+ ⟶ α-Ketoglutarate + NADH + CO_2

3) Conversion of α-ketoglutarate to L-glutamate by GOGAT-GS (Gunka & Commichau, 2012; Mardoukhi et al., 2024):
   α-Ketoglutarate + NH_4^+ (Glutamine) + ATP + $NADPH_2$ ⟶ Glutamate + ADP + P_i + $NADP^+$

Conversely, for the biosynthesis of one molecule of glutamate via the non-canonical fumarate-based pathways, starting from one molecule of pyruvate as the initial substrate, the steps mentioned in 1 and 2 (above) remain consistent. However, the TCA cycle progresses three steps further to generate fumarate (as the precursor for L-aspartate which is the ammino doner to synthesis of L-glutamate), as described below:

4) Conversion of α-ketoglutarate to succinyl-CoA by 2-oxoglutarate dehydrogenase complex (Rex Sheu & Blass, 1999; Blencke et al., 2003):
   α-ketoglutarate + NAD^+ + CoA ⟶ Succinyl CoA + CO_2 + NADH

5) Conversion of succinyl-CoA to succinate by succinyl-CoA synthetase complex (Blencke et al., 2003):
   Succinyl CoA + P_i + GDP ⟶ Succinate + CoA + GTP

6) Conversion of succinate to fumarate by succinate dehydrogenase complex (Hederstedt, 2002):
   Succinate + FAD ⟶ Fumarate + $FADH_2$

From fumarate to L-aspartate and ultimately L-glutamate, there is no additional energy expenditure involved in the glutamate biosynthesis process (Mardoukhi et al., 2024):

7 and 8) Fumarate + α-ketoglutarate + NH_4^+ ⟶ Glutamate + Oxaloacetate

The biosynthesis of one molecule of L-glutamate from pyruvate via the GOGAT-GS pathway results in the production of 2 NADH, while consuming 1 ATP and 1 $NADPH_2$. Each NADH molecule can subsequently yield approximately 2.5 ATP through the electron transport chain (ETC) and oxidative phosphorylation (Dill, 1991). Although $NADPH_2$ is primarily generated through other metabolic pathways, such as the pentose phosphate pathway (PPP), its utilization in this context represents an energy cost, as $NADPH_2$ serves

as a crucial reducing equivalent for biosynthetic reactions (Zamboni, 2003; Shimizu, 2013; Stincone et al., 2015). In many bacteria including *B. subtilis*, $NADPH_2$ is predominantly produced via the PPP, with an associated indirect ATP cost of approximately 0.5 ATP per $NADPH_2$ molecule synthesized (Zamboni, 2003).

In summary, the net potential ATP yield for the biosynthesis of one molecule of L-glutamate via the GOGAT-GS pathway is approximately 3.5 ATPs. Conversely, for the biosynthesis of one molecule of L-glutamate via the non-canonical fumarate-based pathways, 1 GTP (equivalent to 1 ATP), 3 NADH, and 1 $FADH_2$ are produced. The $FADH_2$ molecule further yields approximately 1.5 ATP through the ETC and oxidative phosphorylation (Lodish, 2013; Shimizu, 2013). This pathway does not incur any additional energy consumption, leading to a total potential ATP yield of approximately 10 ATP molecules. Overall, a general comparative analysis of ATP synthesis from the different L-glutamate biosynthesis pathways reveals that the AnsB-AspB pathway is more energy-efficient than the GOGAT-GS pathway, producing 2.5 times more ATP molecules (10 ATP versus 3.5 ATP).

This study also reveals that *B. subtilis* strains relying on the non-canonical fumarate-based pathway for glutamate biosynthesis exhibit growth defects on both rich medium and minimal medium supplemented with L-arginine (an amino acid from the glutamate family) (Fig. 22). This growth inhibition can be mitigated by reducing the uptake of L-arginine (through deactivation of the arginine transporter RocC), increasing the degradation of glutamate derived from arginine catabolism (via increasing synthesis of AspB synthesis), and decreasing flux through the TCA cycle (by inactivating 2-oxoglutarate dehydrogenase OdhA) (Tab. 19).

Growth experiments with all 20 amino acids in this study demonstrate that amino acids from the glutamate family including glutamate, glutamine, arginine, proline, and aspartate can serve as sole nitrogen sources for both wild-type and *gltAB ansAB* mutant strains when glucose is present as the preferred carbon source (Fig. 32A, C). Additionally, these amino acids supported the growth of *gudB1* and *gltAB ansAB gudB1* strains when used as sole sources of carbon and nitrogen. This growth is attributed to the activity of GDH, GudB1, which efficiently degrades L-glutamate to α-ketoglutarate, feeding into the TCA cycle and preventing toxic accumulation of glutamate (Fig. 32B, D). Moreover, *B. subtilis* strains with active GDHs, RocG/GudB1, demonstrated the ability to utilize L-histidine and L-asparagine (albeit to a lesser extent) as sole sources of both carbon and nitrogen (Fig. 32B, D). In contrast, without GudB1, both amino acids were toxic to wild-type and *gltAB ansAB* mutant strains (Fig. 32A, C).

This study also shows that *B. subtilis* employs novel strategies to combat the toxicity of certain amino acids. In the case of L-asparagine toxicity, two new approaches were observed for the first time (Fig. 28): 1) Deactivation of AzlB: This leads to continuous expression of the *azlCD* operon. The AzlCD complex functions as a broad-spectrum amino acid exporter, capable of exporting not only L-histidine but also L-asparagine to the extracellular space, thereby detoxifying excessive intracellular concentrations of L-

asparagine (Meißner et al., 2024). 2) Deactivation of AimA: In several suppressor mutants, the promiscuous amino acid transporter AimA was found to be deactivated. By reducing the import of L-asparagine, *B. subtilis* lowers its intracellular concentration, thereby reducing toxicity (Meißner et al., 2024).

Regarding L-histidine toxicity, *B. subtilis* uses two distinct strategies in this study (Fig. 31): 1) Mutation in the *hutP* gene: This mutation probably alters the regulatory mechanism of HutP (transcriptional antiterminator of the *hut* operon), facilitating higher expression of the *hut* operon. The enhanced expression may lead to increased uptake of L-histidine by the histidine permease HutM, allowing L-histidine to serve as the sole source of carbon and nitrogen in the minimal medium (Oda et al., 2000; Wray & Fisher, 1994). However, this hypothesis requires further experimental validation. 2) Decryptification of the *gudB* gene: This leads to the expression of an active version of the GDH, GudB1 (Commichau et al., 2008; Gunka et al., 2012), which can effectively degrade the glutamate derived from the catabolism of histidine, thereby mitigating L-histidine toxicity.

At the beginning of this study, the use of a different minimal medium, CGXII minimal medium instead of C-Glc medium, with a much higher concentration of nitrogen source led to the discovery of the glutamate synthesis pathway through AnsB-AspB (Fig. 15). It would be intriguing to investigate how this new route could evolve under varying concentrations of nitrogen sources and demonstrate robust growth under both nitrogen-limited and nitrogen-excess conditions. Understanding the adaptability and efficiency of the AnsB-AspB pathway in different nitrogen environments could provide insights into its evolutionary potential and practical applications in optimizing bacterial growth and glutamate production. Also, given that the entry points of carbon sources for glutamate synthesis differ between the two glutamate biosynthesis pathways, GOGAT-GS and AnsB-AspB, one potential approach could be to test various carbon sources to observe their effects on the glutamate synthesis yield of the AnsB-AspB pathway. Additionally, examining the further evolution of this pathway with different carbon sources could provide valuable insights.

Similar to *B. subtilis*, in plants, GDHs are not significantly involved in the biosynthesis of glutamate (Lea & Miflin, 2003; Commichau et al., 2008). Instead, plants possess two types of GOGATs: one dependent on $NADH_2$ and the other dependent on ferredoxin (Fd). These enzymes play distinct roles in various plant tissues and are expressed during different phases of growth and development (Suzuki & Knaff, 2005). It has been reported that under non-photorespiratory conditions, overexpression of the Fd-dependent GOGAT in *Arabidopsis thaliana* results in higher synthesis of glutamate and several other amino acids (Ishizaki et al., 2010). This indicates that manipulating the expression levels of these enzymes could potentially enhance amino acid production in plants. From the present study, it is understood that deactivating AnsR in *B. subtilis* lifts the transcriptional repression on the *ansAB* genes (specifically *ansB*), thereby allowing ammonium assimilation. In other words, the deactivation of AnsR is crucial for activating

the new glutamate pathway via the L-aspartase/L-aspartate transaminase-dependent route (Mardoukhi et al., 2024). One potential experiment could involve deactivating AnsR in the background of the wild-type strain, thereby activating both glutamate synthesis pathways. Additionally, placing a high-expression promoter, such as the artificial promoter P_{alf4} (Gundlach et al., 2017; Kohm et al., 2023), in front of the *ansAB* operon could be explored. By conducting metabolome analysis, it could be determined whether this genetic modification leads to an increase in glutamate synthesis due to the importance of glutamate as a major amino group donors for all nitrogen-containing compounds. It holds significant potential for biotechnological applications aimed at increasing the production of glutamate. This approach could also offer valuable insights into the regulation and optimization of glutamate production in *B. subtilis* due to the fact that the cell maintains amino acid homeostasis by tightly regulating intracellular amino acid concentrations. As is well established, the excessive accumulation of certain amino acids can have toxic effects on the cell (Meißner et al., 2024; Warneke et al., 2024). Therefore, it is plausible that *B. subtilis* employs previously unidentified mechanisms to counteract the overproduction of glutamate, in addition to the regulatory pathways already known (Gunka & Commichau, 2012; Mardoukhi et al., 2024). Understanding these regulatory mechanisms could inform strategies to enhance glutamate production while preventing toxicity. Additionally, exploring these potential mechanisms could reveal novel strategies for maintaining cellular homeostasis under conditions of elevated glutamate synthesis.

One critical avenue for future research is to investigate the activity of the non-canonical ammonium assimilation pathway in *B. subtilis* under native environmental conditions regulated by the nitrogen regulatory system. To explore this, a system could be designed in which the *gltAB* genes are replaced with the *ansB-aspB* operon at their native locus. This replacement would enable the study of glutamate biosynthesis regulation through a P_{gltAB}-*lacZ* fusion. By monitoring the expression levels of this reporter, it would be possible to assess the cellular response to the gene replacement and potential glutamate limitation. If the *ansB-aspB* operon fails to fully compensate for glutamate biosynthesis, the activity of the P_{gltAB}-*lacZ* fusion should increase compared to the wild-type strain. This is because under glutamate-limited conditions, *gltC* expression would rise, activating the P_{gltAB} promoter and thereby increasing *lacZ* expression (Commichau et al., 2008; Gunka & Commichau, 2012; Mardoukhi et al., 2024). This activity can be quantified using a β-galactosidase assay, providing a direct measure of the operon's functional efficiency and regulatory impact (Mardoukhi et al., 2024).

Since the *ansB-aspB* operon is placed under the control of P_{gltAB}, its expression will also be influenced by environmental conditions. For example, in a medium where glucose is the sole carbon source, expression of *ansB-aspB* genes is expected to increase, promoting glutamate biosynthesis. Conversely, in the presence of glutamate family amino acids, such as L-arginine, the *rocG* gene would be expressed. The active GDH, RocG, could bind to GltC, inhibiting its transcriptional activation of the P_{gltAB}-*ansB-aspB*

operon, thereby suppressing glutamate production (Commichau et al., 2006; Gunka & Commichau, 2012; Stannek et al., 2015).

Moreover, examining this regulatory mechanism in the context of the wild-type strain versus the *B. subtilis* SP1 strain, which natively lacks active GudB, could provide additional insights. In the wild-type strain, where both GDHs, RocG and GudB, are functional, replacing *gltAB* with the *ansB-aspB* operon would remove the repressive effect of GltA on GudB, potentially resulting in enhanced glutamate degradation. However, in the *B. subtilis* SP1 background, where GudB is inactivated, such an effect is not expected, as RocG would remain the sole active GDH (Commichau et al., 2007; Gunka & Commichau, 2012; Jayaraman et al., 2022; Mardoukhi et al., 2024).

Based on this rationale, it might be helpful to performe the gene replacement in the SP1 background, where only one functional GDH is present. This approach would simplify the regulatory network, facilitating clearer interpretation of the non-canonical pathway's role and the regulatory influence of *ansB-aspB* under different environmental and metabolic conditions.

This study suggests that enabling the fumarate-based glutamate biosynthesis pathway in a *gltAB*-deletion background requires overcoming the repressive effects of AnsR on *ansAB* gene expression. This could be achieved by either deactivating the *ansR* gene or amplifying the *ansAB* locus to bypass AnsR-mediated repression (Mardoukhi et al., 2024). Therefore, it could be interesting to implement the replacement of the *gltAB* genes with the *ansB-aspB* operon in an *ansR*-deleted strain. This strategy would eliminate the repression of *ansB* expression, facilitating the conversion of fumarate to L-aspartate by AnsB, and subsequently to L-glutamate by the aminotransferase activity of AspB. This approach would optimize the utilization of the fumarate-based pathway for efficient L-glutamate biosynthesis.

References

A. Slusarchyk, W., Dejneka, T., M. Gordon, E., R. Weaver, E., & H. Koster, W. (1984). Monobactams: Ring Activating N-1-Substituents in Monocyclic b-Lactam Antibiotics. *Heterocycles*, 21(1).

Abe, S., Takayama, K. I., & Kinoshita, S. (1967). Taxonomical studies on glutamic acid-producing bacteria. *The Journal of General and Applied Microbiology*, 13(3).

Abendroth, J., McCormick, M. S., Edwards, T. E., Staker, B., Loewen, R., Gifford, M., Rifkin, J., Mayer, C., Guo, W., Zhang, Y., Myler, P., Kelley, A., Analau, E., Hewitt, S. N., Napuli, A. J., Kuhn, P., Ruth, R. D., & Stewart, L. J. (2010). X-ray structure determination of the glycine cleavage system protein H of *Mycobacterium tuberculosis* using an inverse Compton synchrotron X-ray source. *Journal of Structural and Functional Genomics*, 11(1).

Abraham L. Sonenshein, James A. Hoch, & Richard Losick. (1993). *Bacillus subtilis* and Other Gram-Positive Bacteria: Biochemistry, Physiology, and Molecular Genetics. *Bacillus subtilis and Other Gram-Positive Bacteria,* 10(1128).

Advances in Protein Chemistry. (1953). *Nature*, 171(4346).

Aizawa, S. I. (2001). Bacterial flagella and type III secretion systems. *FEMS Microbiology Letters* 202(2).

Amorim Franco, T. M., & Blanchard, J. S. (2017). Bacterial Branched-Chain Amino Acid Biosynthesis: Structures, Mechanisms, and Drugability. In *Biochemistry* (Vol. 56, Issue 44).

Arnold, H. H. (1977). Initiation of protein synthesis in *Bacillus subtilis* in the presence of trimethoprim or aminopterin. *BBA Section Nucleic Acids And Protein Synthesis*, 476(1).

Atkinson, M. R., Wray, L. V., & Fisher, S. H. (1990). Regulation of histidine and proline degradation enzymes by amino acid availability in *Bacillus subtilis*. *Journal of Bacteriology*, 172(9).

Auger, S., Gomez, M. P., Danchin, A., & Martin-Verstraete, I. (2005). The PatB protein of *Bacillus subtilis* is a C-S-lyase. *Biochimie*, 87(2).

Auger, S., Yuen, W. H., Danchin, A., & Martin-Verstraete, I. (2002). The *metIC* operon involved in methionine biosynthesis in *Bacillus subtilis* is controlled by transcription antitermination. *Microbiology*, 148(2).

Ayad, F., Ayad, N., Vazquez, J., Zhang, Y. P., Mateo, L. R., & Cummins, D. (2018). Use of a toothpaste containing 8% arginine and calcium carbonate for immediate and lasting relief of dentin hypersensitivity: A simple and effective in-office procedure. *American Journal of Dentistry*, 31(3).

Babitzke, P., Lai, Y. J., Renda, A. J., & Romeo, T. (2019). Posttranscription initiation control of gene expression mediated by bacterial RNA-binding proteins. *Annual Review of Microbiology,* 73(5).

Barbe, V., Cruveiller, S., Kunst, F., Lenoble, P., Meurice, G., Sekowska, A., Vallenet, D., Wang, T., Moszer, I., Médigue, C., & Danchin, A. (2009). From a consortium sequence to a

unified sequence: The *Bacillus subtilis* 168 reference genome a decade later. *Microbiology*, 155(6).

Becker, J., Schäfer, R., Kohlstedt, M., Harder, B. J., Borchert, N. S., Stöveken, N., Bremer, E., & Wittmann, C. (2013). Systems metabolic engineering of *Corynebacterium glutamicum* for production of the chemical chaperone ectoine. *Microbial Cell Factories*, 12(1).

Belitsky, B. R. (2011). Indirect repression by *Bacillus subtilis* CodY via displacement of the activator of the proline utilization operon. *Journal of Molecular Biology*, 413(2).

Belitsky, B. R. (2015). Role of branched-chain amino acid transport in *Bacillus subtilis* CodY activity. *Journal of Bacteriology*, 197(8).

Belitsky, B. R., Kim, H. J., & Sonenshein, A. L. (2004). CcpA-dependent regulation of *Bacillus subtilis* glutamate dehydrogenase gene expression. *Journal of Bacteriology*, 186(11).

Belitsky, B. R., & Sonenshein, A. L. (1995). Mutations in GltC that increase *Bacillus subtilis gltA* expression. *Journal of Bacteriology*, 177(19).

Belitsky, B. R., & Sonenshein, A. L. (1997). Altered transcription activation specificity of a mutant form of *Bacillus subtilis* GltR, a LysR family member. *Journal of Bacteriology*, 179(4).

Belitsky, B. R., & Sonenshein, A. L. (1998). Role and regulation of *Bacillus subtilis* glutamate dehydrogenase genes. *Journal of Bacteriology*, 180(23).

Belitsky, B. R., & Sonenshein, A. L. (2004). Modulation of activity of *Bacillus subtilis* regulatory proteins GltC and TnrA by glutamate dehydrogenase. *Journal of Bacteriology*, 186(11).

Belitsky, B. R., Wray, J., Fisher, S. H., Bohannon, D. E., & Sonenshein, A. L. (2000). Role of TnrA in nitrogen source-dependent repression of *Bacillus subtilis* glutamate synthase gene expression. *Journal of Bacteriology*, 182(21).

Bender, R. A. (2012). Regulation of the Histidine Utilization (Hut) System in Bacteria. *Microbiology and Molecular Biology Reviews*, 76(3).

Bennett, B. D., Kimball, E. H., Gao, M., Osterhout, R., Van Dien, S. J., & Rabinowitz, J. D. (2009). Absolute metabolite concentrations and implied enzyme active site occupancy in *Escherichia coli*. *Nature Chemical Biology*, 5(8).

Berg, J., Tymoczko, J., & Stryer, L. (2002). Biochemistry. *New York: W H Freeman*. 5th Edition.

Blasco, B., Stenta, M., Alonso-Sarduy, L., Dietler, G., Peraro, M. D., Cole, S. T., & Pojer, F. (2011). Atypical DNA recognition mechanism used by the EspR virulence regulator of *Mycobacterium tuberculosis*. *Molecular Microbiology*, 82(1).

Blencke, H. M., Homuth, G., Ludwig, H., Mäder, U., Hecker, M., & Stülke, J. (2003). Transcriptional profiling of gene expression in response to glucose in *Bacillus subtilis*: Regulation of the central metabolic pathways. *Metabolic Engineering*, 5(2).

Bohannon, D. E., & Sonenshein, A. L. (1989). Positive regulation of glutamate biosynthesis in *Bacillus subtilis*. *Journal of Bacteriology*, 171(9).

Borriss, R., Danchin, A., Harwood, C. R., Médigue, C., Rocha, E. P. C., Sekowska, A., & Vallenet, D. (2018). *Bacillus subtilis*, the model Gram-positive bacterium: 20 years of annotation refinement. *Microbial Biotechnology*, 11(1).

Boyle, J. (2005). Lehninger principles of biochemistry (4th Edition): Nelson, D., and Cox, M. *Biochemistry and Molecular Biology Education*, 33(1).

Bradford, M. M. (1976). A rapid and sensitive method for the quantitation of microgram quantities of protein utilizing the principle of protein-dye binding. *Analytical Biochemistry*, 72(2).

Bremer, E. (2014). Adaptation to Changing Osmolanty. *Bacillus subtilis* and Its Closest Relatives. *ASM Press*. (pp. 385–391)

Bremer, E., & Krämer, R. (2019). Responses of microorganisms to osmotic stress. *Annual Review of Microbiology,* 73(2).

Brill, J., Hoffmann, T., Bleisteiner, M., & Bremer, E. (2011). Osmotically controlled synthesis of the compatible solute proline is critical for cellular defense of *Bacillus subtilis* against high osmolarity. *Journal of Bacteriology*, 193(19).

Brill, J., Hoffmann, T., Putzer, H., & Bremer, E. (2011). T-box-mediated control of the anabolic proline biosynthetic genes of *Bacillus subtilis*. *Microbiology*, 157(4).

Brosnan, J. T. (2003). Interorgan Amino Acid Transport and its Regulation. *The Journal of Nutrition*, 133(6).

Brown, G., Singer, A., Proudfoot, M., Skarina, T., Kim, Y., Chang, C., Dementieva, I., Kuznetsova, E., Gonzalez, C. F., Joachimiak, A., Savchenko, A., & Yakunin, A. F. (2008). Functional and structural characterization of four glutaminases from *Escherichia coli* and *Bacillus subtilis*. *Biochemistry*, *47*(21).

Caldwell, R., Sapolsky, R., Weyler, W., Maile, R. R., Causey, S. C., & Ferrari, E. (2001). Correlation between *Bacillus subtilis scoC* phenotype and gene expression determined using microarrays for transcriptome analysis. *Journal of Bacteriology*, 183(24).

Calogero, S., Gardan, R., Glaser, P., Schweizer, J., Rapoport, G., & Debarbouille, M. (1994). RocR, a novel regulatory protein controlling arginine utilization in *Bacillus subtilis*, belongs to the NtrC/NifA family of transcriptional activators. *Journal of Bacteriology*, 176(5).

Chakraborty, B., & Burne, R. A. (2017). Effects of arginine on *Streptococcus* mutans growth, virulence gene expression, and stress tolerance. *Applied and Environmental Microbiology*, 83(15).

Chen, D., Ruzicka, F. J., & Frey, P. A. (2000). A novel lysine 2,3-aminomutase encoded by the *yodO* gene of *Bacillus subtilis*: Characterization and the observation of organic radical intermediates. *Biochemical Journal*, 348(3).

Chen, S., Xu, X. L., & Grant, G. A. (2012). Allosteric activation and contrasting properties of l-serine dehydratase types 1 and 2. *Biochemistry*, 51(26).

Chenier, P. J. (2002). Survey of Industrial Chemistry. Survey of Industrial Chemistry. *Springer US,* 10(4).

Choi, S. K., & Saier, M. H. (2005). Regulation of *sigL* expression by the catabolite control protein CcpA involves a roadblock mechanism in *Bacillus subtilis*: Potential connection between carbon and nitrogen metabolism. *Journal of Bacteriology*, 187(19).

Comai, L., Sen, L. C., & Stalker, D. M. (1983). An altered *aroA* gene product confers resistance to the herbicide glyphosate. *Science*, 221(4608).

Commichau, F. M., Alzinger, A., Sande, R., Bretzel, W., Reuß, D. R., Dormeyer, M., Chevreux, B., Schuldes, J., Daniel, R., Akeroyd, M., Wyss, M., Hohmann, H. P., & Prágai, Z. (2015). Engineering *Bacillus subtilis* for the conversion of the antimetabolite 4-hydroxy-l-threonine to pyridoxine. *Metabolic Engineering*, 29(5).

Commichau, F. M., Forchhammer, K., & Stülke, J. (2006a). Regulatory links between carbon and nitrogen metabolism. *Current Opinion in Microbiology,* 9(2).

Commichau, F. M., Forchhammer, K., & Stülke, J. (2006b). Regulatory links between carbon and nitrogen metabolism. *Current Opinion in Microbiology,* 9(2).

Commichau, F. M., Gunka, K., Landmann, J. J., & Stülke, J. (2008). Glutamate metabolism in *Bacillus subtilis*: Gene expression and enzyme activities evolved to avoid futile cycles and to allow rapid responses to perturbations of the system. *Journal of Bacteriology*, 190(10).

Commichau, F. M., Herzberg, C., Tripal, P., Valerius, O., & Stülke, J. (2007). A regulatory protein-protein interaction governs glutamate biosynthesis in *Bacillus subtilis*: The glutamate dehydrogenase RocG moonlights in controlling the transcription factor GltC. *Molecular Microbiology*, 65(3).

Commichau, F. M., Wacker, I., Schleider, J., Blencke, H. M., Reif, I., Tripal, P., & Stülke, J. (2006). Characterization of *Bacillus subtilis* mutants with carbon source-independent glutamate biosynthesis. *Journal of Molecular Microbiology and Biotechnology*, 12(1–2).

Csonka, L. N., Ikeda, T. P., Fletcher, S. A., & Kustu, S. (1994). The accumulation of glutamate is necessary for optimal growth of *Salmonella typhimurium* in media of high osmolality but not induction of the *proU* operon. *Journal of Bacteriology*, 176(20).

Cuevas, J. (2019). Neurotransmitters and Their Life Cycle. *Reference Module in Biomedical Sciences*.

Dajnowicz, S., Parks, J. M., Hu, X., Gesler, K., Kovalevsky, A. Y., & Mueser, T. C. (2017). Direct evidence that an extended hydrogen-bonding network influences activation of pyridoxal 5'-phosphate in aspartate aminotransferase. *Journal of Biological Chemistry*, 292(14).

Dasgupta, T., Ferdous, S., & Tse-Dinh, Y. C. (2020). Mechanism of type IA topoisomerases. In *Molecules,* 25(20).

de Lorenzo, V., Sekowska, A., & Danchin, A. (2015). Chemical reactivity drives spatiotemporal organisation of bacterial metabolism. In *FEMS Microbiology Reviews,* 39(1).

Debarbouille, M., Gardan, R., Arnaud, M., & Rapoport, G. (1999). Role of *bkdR*, a transcriptional activator of the SigL-dependent isoleucine and valine degradation pathway in *Bacillus subtilis*. *Journal of Bacteriology*, 181(7).

Débarbouillé, M., Martin-Verstraete, I., Kunst, F., & Rapoport, G. (1991). The *Bacillus subtilis sigL* gene encodes an equivalent of σ54 from Gram-negative bacteria. *Proceedings of the National Academy of Sciences of the United States of America*, 88(20).

Dill, K. (1991). Biochemistry (Mathews, Christopher K, van Holde, K.E.). *Journal of Chemical Education*, 68(1).

Dolan, S. K., Wijaya, A., Kohlstedt, M., Gläser, L., Brear, P., Silva-Rocha, R., Wittmann, C., & Welch, M. (2022). Systems-Wide Dissection of Organic Acid Assimilation in *Pseudomonas aeruginosa* Reveals a Novel Path To Underground Metabolism. *MBio*, 13(6).

Dormeyer, M., Lübke, A. L., Müller, P., Lentes, S., Reuß, D. R., Thürmer, A., Stülke, J., Daniel, R., Brantl, S., & Commichau, F. M. (2017). Hierarchical mutational events compensate for glutamate auxotrophy of a *Bacillus subtilis gltC* mutant. *Environmental Microbiology Reports*, 9(3).

Dritter Beitrag zur Erkenntniss grosser Organisation in der Richtung des ... - Christian Gottfried Ehrenberg - Google Books. (n.d.). Retrieved December 7, 2023, from https://books.google.de/books/about/Dritter_Beitrag_zur_Erkenntniss_grosser.html?id=9jXptwAACAAJ&redir_esc=y

Dubnau, D. (1991). The regulation of genetic competence in *Bacillus subtilis*. *Molecular Microbiology,* 5(1).

Eggeling, L., & Bott, M. (2005). Handbook of Corynebacterium glutamicum. *CRC Press*.

Elzanowski, Andrzej (Anjay), J. O. (2010). The Genetic Codes. *National Center for Biotechnology Information (NCBI)*.

Engel, H., Kazemier, B., & Keck, W. (1991). Murein-metabolizing enzymes from *Escherichia coli*: sequence analysis and controlled overexpression of the *slt* gene, which encodes the soluble lytic transglycosylase. *Journal of Bacteriology*, 173(21).

Epstein, W. (2003). The Roles and Regulation of Potassium in Bacteria. *Progress in Nucleic Acid Research and Molecular Biology,* 75(1).

Errasti-Murugarren, E., Fort, J., Bartoccioni, P., Díaz, L., Pardon, E., Carpena, X., Espino-Guarch, M., Zorzano, A., Ziegler, C., Steyaert, J., Fernández-Recio, J., Fita, I., & Palacín, M. (2019). L amino acid transporter structure and molecular bases for the asymmetry of substrate interaction. *Nature Communications*, 10(1).

Errington, J., & Wu, L. J. (2017). Cell cycle machinery in *Bacillus subtilis*. *Sub-Cellular Biochemistry*, 84(5).

Feavers, I. M., Price, V., & Moir, A. (1988). The regulation of the fumarase (*citG*) gene of *Bacillus subtilis* 168. *MGG Molecular & General Genetics*, 211(3).

Fedorova, K., Kayumov, A., Woyda, K., Ilinskaja, O., & Forchhammer, K. (2013). Transcription factor TnrA inhibits the biosynthetic activity of glutamine synthetase in *Bacillus subtilis*. *FEBS Letters*, 587(9).

Fisher, S. H., & Wray, L. V. (2002). *Bacillus subtilis* 168 contains two differentially regulated genes encoding L-asparaginase. *Journal of Bacteriology*, 184(8).

Flórez, L. A., Gunka, K., Polanía, R., Tholen, S., & Stülke, J. (2011). SPABBATS: A pathway-discovery method based on Boolean satisfiability that facilitates the characterization of suppressor mutants. *BMC Systems Biology*, 5(2).

Floyd, D. M., Fritz, A. W., & Cimarusti, C. M. (1982). Monobactams. Stereospecific Synthesis of (S)-3-Amino-2-oxoazetidine-1-sulfonic Acids. *Journal of Organic Chemistry,* 47(1).

Forlani, G., Nocek, B., Chakravarthy, S., & Joachimiak, A. (2017). Functional characterization of four putative δ1-pyrroline-5-carboxylate reductases from *Bacillus subtilis*. *Frontiers in Microbiology*, 8(4).

Frank, C., Hoffmann, T., Zelder, O., Felle, M. F., & Bremer, E. (2021). Enhanced Glutamate Synthesis and Export by the Thermotolerant Emerging Industrial Workhorse *Bacillus methanolicus* in Response to High Osmolarity. *Frontiers in Microbiology*, 12(3).

Galperin, M. Y., Wolf, Y. I., Makarova, K. S., Alvarez, R. V., Landsman, D., & Koonin, E. V. (2021). COG database update: Focus on microbial diversity, model organisms, and widespread pathogens. *Nucleic Acids Research*, 49(1).

Garattini, S. (2000). Glutamic acid, twenty years later. *Journal of Nutrition*, 130(4).

Gardan, R., Rapoport, G., & Débarbouillé, M. (1995). Expression of the *rocDEF* operon involved in arginine catabolism in *Bacillus subtilis*. *Journal of Molecular Biology*, 249(5).

Gardan, R., Rapoport, G., & Débarbouillé, M. (1997). Role of the transcriptional activator RocR in the arginine-degradation pathway of *Bacillus subtilis*. *Molecular Microbiology*, 24(4).

Garnett, J. A., Baumberg, S., Stockley, P. G., & Phillips, S. E. V. (2007). Structure of the C-terminal effector-binding domain of AhrC bound to its corepressor L-arginine. *Acta Crystallographica Section F: Structural Biology and Crystallization Communications*, 63(11).

Genchi, G. (2017). An overview on d-amino acids. *Amino Acids,* 49(9).

Gerth, U., Kock, H., Kusters, I., Michalik, S., Switzer, R. L., & Hecker, M. (2008). Clp-dependent proteolysis down-regulates central metabolic pathways in glucose-starved *Bacillus subtilis*. *Journal of Bacteriology*, 190(1).

Gil-Gil, T., Corona, F., Martínez, J. L., & Bernardini, A. (2020). The Inactivation of enzymes belonging to the central carbon metabolism is a novel mechanism of developing antibiotic resistance. *MSystems*, 5(3).

Goelzer, A., Bekkal Brikci, F., Martin-Verstraete, I., Noirot, P., Bessières, P., Aymerich, S., & Fromion, V. (2008). Reconstruction and analysis of the genetic and metabolic regulatory networks of the central metabolism of *Bacillus subtilis*. *BMC Systems Biology*, 2(2).

Goodarzi, H., Bennett, B. D., Amini, S., Reaves, M. L., Hottes, A. K., Rabinowitz, J. D., & Tavazoie, S. (2010). Regulatory and metabolic rewiring during laboratory evolution of ethanol tolerance in *E. coli*. *Molecular Systems Biology*, 6(1).

Greenwich, J., Reverdy, A., Gozzi, K., Di Cecco, G., Tashjian, T., Godoy-Carter, V., & Chai, Y. (2019). A decrease in serine levels during growth transition triggers biofilm formation in *Bacillus subtilis*. *Journal of Bacteriology*, 201(15).

Griffith, K. L., & Wolf, R. E. (2002). Measuring β-galactosidase activity in bacteria: Cell growth, permeabilization, and enzyme assays in 96-well arrays. *Biochemical and Biophysical Research Communications*, 290(1).

Griffith, L. J., Ostrander, W. E., Mullins, C. G., & Beswick, D. E. (1965). Drug antagonism between lincomycin and erythromycin. *Science*, 147(3659).

Guérout-Fleury, A. M., Shazand, K., Frandsen, N., & Stragier, P. (1995). Antibiotic-resistance cassettes for *Bacillus subtilis*. *Gene*, 167(2).

Gundlach, J., Commichau, F. M., & Stülke, J. (2018). Perspective of ions and messengers: an intricate link between potassium, glutamate, and cyclic di-AMP. *Current Genetics,* 64 (1).

Gundlach, J., Herzberg, C., Kaever, V., Gunka, K., Hoffmann, T., Weiß, M., Gibhardt, J., Thürmer, A., Hertel, D., Daniel, R., Bremer, E., Commichau, F. M., & Stülke, J. (2017). Control of potassium homeostasis is an essential function of the second messenger cyclic di-AMP in *Bacillus subtilis*. *Science Signaling*, 10(475).

Gunka, K., & Commichau, F. M. (2012). Control of glutamate homeostasis in *Bacillus subtilis*: A complex interplay between ammonium assimilation, glutamate biosynthesis and degradation. *Molecular Microbiology,* 85 (2).

Gunka, K., Stannek, L., Care, R. A., & Commichau, F. M. (2013). Selection-driven accumulation of suppressor mutants in *Bacillus subtilis*: The apparent high mutation frequency of the cryptic *gudB* gene and the rapid clonal expansion of *gudB*+ suppressors are due to growth under selection. *PLoS ONE*, 8(6).

Gunka, K., Tholen, S., Gerwig, J., Herzberg, C., Stülke, J., & Commichau, F. M. (2012). A high-frequency mutation in *Bacillus subtilis*: Requirements for the decryptification of the *gudb* glutamate dehydrogenase gene. *Journal of Bacteriology*, 194(5).

Hamoen, L. W., Venema, G., & Kuipers, O. P. (2003). Controlling competence in *Bacillus subtilis*: Shared use of regulators. In *Microbiology,* 149(1).

He, H., Li, Y., Zhang, L., Ding, Z., & Shi, G. (2023). Understanding and application of *Bacillus* nitrogen regulation: A synthetic biology perspective. In *Journal of Advanced Research* 49(1).

Hederstedt, L. (2002). Succinate:quinone oxidoreductase in the bacteria *Paracoccus denitrificans* and *Bacillus subtilis*. *Biochimica et Biophysica Acta – Bioenergetics,* 1553(1).

Helling, R. B. (1998). Pathway choice in glutamate synthesis in *Escherichia coli*. *Journal of Bacteriology*, 180(17).

Henkin, T. M. (1996). The role of the CcpA transcriptional regulator in carbon metabolism in *Bacillus subtilis*. In *FEMS Microbiology Letters,* 135(1).

Higgins, D., & Dworkin, J. (2012). Recent progress in *Bacillus subtilis* sporulation. In *FEMS Microbiology Reviews,* 36(1).

Hirooka, K., Danjo, Y., Hanano, Y., Kunikane, S., Matsuoka, H., Tojo, S., & Fujita, Y. (2009). Regulation of the *Bacillus subtilis* divergent *yetL* and *yetM* genes by a transcriptional repressor, YetL, in response to flavonoids. *Journal of Bacteriology*, 191(11).

Hoffmann, T., Bleisteiner, M., Sappa, P. K., Steil, L., Mäder, U., Völker, U., & Bremer, E. (2017). Synthesis of the compatible solute proline by *Bacillus subtilis*: point mutations rendering the osmotically controlled proHJ promoter hyperactive. *Environmental Microbiology*, 19(9).

Hoffmann, T., von Blohn, C., Stanek, A., Moses, S., Barzantny, H., & Bremer, E. (2012). Synthesis, release, and recapture of compatible solute proline by osmotically stressed *Bacillus subtilis* cells. *Applied and Environmental Microbiology*, 78(16).

Holtmann, G., Bakker, E. P., Uozumi, N., & Bremer, E. (2003). KtrAB and KtrCD: Two K+ uptake systems in *Bacillus subtilis* and their role in adaptation to hypertonicity. *Journal of Bacteriology*, 185(4).

Hong, H. A., Khaneja, R., Tam, N. M. K., Cazzato, A., Tan, S., Urdaci, M., Brisson, A., Gasbarrini, A., Barnes, I., & Cutting, S. M. (2009). *Bacillus subtilis* isolated from the human gastrointestinal tract. *Research in Microbiology*, 160(2).

Hoppe, B. (1983). Die Biologie der Mikroorganismen von F. J. Cohn (1828-1898). Ent- wicklung aus Forschungen über mikrospopische Pflanzen und Tiere. *Sudhoffs Archiv; Zeitschrift Fur Wissenschaftsgeschichte*, 67(2).

Hottes, A. K., Freddolino, P. L., Khare, A., Donnell, Z. N., Liu, J. C., & Tavazoie, S. (2013). Bacterial Adaptation through Loss of Function. *PLoS Genetics*, 9(7).

Huang, S. C., Lin, T. H., & Shaw, G. C. (2011). PrcR, a PucR-type transcriptional activator, is essential for proline utilization and mediates proline-responsive expression of the proline utilization operon *putBCP* in *Bacillus subtilis*. *Microbiology*, 157(12).

Hughes, C. A., Beard, H. S., & Matthews, B. F. (1997). Molecular cloning and expression of two cDNAs encoding asparagine synthetase in soybean. *Plant Molecular Biology*, 33(2).

Humbert, R., & Simoni, R. D. (1980). Genetic and biochemical studies demonstrating a second gene coding for asparagine synthetase in *Escherichia coli*. *Journal of Bacteriology*, 142(1).

Iacometti, C., Marx, K., Hönick, M., Biletskaia, V., Schulz-Mirbach, H., Dronsella, B., Delmas, V. A., Berger, A., Dubois, I., Bouzon, M., Döring, V., Noor, E., Bar-Even, A., & Lindner, S. N. (2022). Activating silent glycolysis bypasses in *Escherichia coli*. *BioDesign Research,* 6(1)**.**

Ikeda, M. (2003). Amino Acid Production Processes. *Adv Biochem Eng Biotechnol,* 79(35).

Inoue, Y. (1997). Spontaneous Loss of Antibiotic-Resistant Plasmids Transferred to *Escherichia coli* in Experimental Chronic Bladder Infection. *International Journal of Urology*, 4(3).

Ishizaki, T., Ohsumi, C., Totsuka, K., & Igarashi, D. (2010). Analysis of glutamate homeostasis by overexpression of Fd-GOGAT gene in *Arabidopsis thaliana*. *Amino Acids*, 38(3).

Ivanova, N., Sorokin, A., Anderson, I., Galleron, N., Candelon, B., Kapatral, V., Bhattacharyya, A., Reznik, G., Mikhailova, N., Lapidus, A., Chu, L., Mazur, M., Goltsman, E., Larsen, N., D'Souza, M., Walunas, T., Grechkin, Y., Pusch, G., Haselkorn, R., … Kyrpides, N. (2003). Genome sequence of *Bacillus cereus* and comparative analysis with *Bacillus anthracis*. *Nature*, 423(6935).

Iyidoğan, N. F., & Bayindirli, A. (2004). Effect of l-cysteine, kojic acid and 4-hexylresorcinol combination on inhibition of enzymatic browning in Amasya apple juice. *Journal of Food Engineering*, 62(3).

Jayaraman, V., Lee, D. J., Elad, N., Vimer, S., Sharon, M., Fraser, J. S., & Tawfik, D. S. (2022). A counter-enzyme complex regulates glutamate metabolism in *Bacillus subtilis*. *Nature Chemical Biology*, 18(161).

Johansson, L., Gafvelin, G., & Arnér, E. S. J. (2005). Selenocysteine in proteins - Properties and biotechnological use. *Biochimica et Biophysica Acta - General Subjects,* 1726(1).

Kaminskas, E., Kimhi, Y., & Magasanik, B. (1970). Urocanase and N-formimino-L-glutamate formiminohydrolase of *Bacillus subtilis*, two enzymes of the histidine degradation pathway. *Journal of Biological Chemistry*, 245(14).

Kearse, M., Moir, R., Wilson, A., Stones-Havas, S., Cheung, M., Sturrock, S., Buxton, S., Cooper, A., Markowitz, S., Duran, C., Thierer, T., Ashton, B., Meintjes, P., & Drummond, A. (2012). Geneious Basic: An integrated and extendable desktop software platform for the organization and analysis of sequence data. *Bioinformatics*, 28(12).

Keilhauer, C., Eggeling, L., & Sahm, H. (1993). Isoleucine synthesis in *Corynebacterium glutamicum*: Molecular analysis of the *ilvB-ilvN-ilvC* operon. *Journal of Bacteriology*, 175(17).

Kempf, B., & Bremer, E. (1998). Uptake and synthesis of compatible solutes as microbial stress responses to high-osmolality environments. In *Archives of Microbiology* 170 (5).

Kendrick, K. E., & Wheelis, M. L. (1982). Histidine dissimilation in *Streptomyces coelicolor*. *Journal of General Microbiology*, 128(9).

Khersonsky, O., & Tawfik, D. S. (2010). Enzyme promiscuity: A mechanistic and evolutionary perspective. *Annual Review of Biochemistry,* 79(1).

Klewing, A., Koo, B. M., Krüger, L., Poehlein, A., Reuß, D., Daniel, R., Gross, C. A., & Stülke, J. (2020). Resistance to serine in *Bacillus subtilis*: identification of the serine transporter YbeC and of a metabolic network that links serine and threonine metabolism. *Environmental Microbiology*, 22(9).

Klingel, U., Miller, C. M., North, A. K., Stockley, P. G., & Baumberg, S. (1995). A binding site for activation by the *Bacillus subtilis* AhrC protein, a repressor/activator of arginine metabolism. *MGG Molecular & General Genetics*, 248(3).

Kobayashi, K., Ehrlich, S. D., Albertini, A., Amati, G., Andersen, K. K., Arnaud, M., Asai, K., Ashikaga, S., Aymerich, S., Bessieres, P., Boland, F., Brignell, S. C., Bron, S., Bunai, K., Chapuis, J., Christiansen, L. C., Danchin, A., Débarbouillé, M., Dervyn, E., … Ogasawara, N. (2003). Essential *Bacillus subtilis* genes. *Proceedings of the National Academy of Sciences of the United States of America*, 100(8).

Kock, H., Gerth, U., & Hecker, M. (2004). MurAA, catalysing the first committed step in peptidoglycan biosynthesis, is a target of Clp-dependent proteolysis in *Bacillus subtilis*. *Molecular Microbiology*, *51*(4).

Kohm, K., Jalomo-Khayrova, E., Basu, S., Steinchen, W., Bange, G., Hertel, R., Commichau, F. M., & Czech, L. (2023). Structural and functional analysis of YopR and identification of an additional key component of the SPβ phage lysis-lysogeny management system. *Nucleic Acids Research*, 51(17).

Koide, A., & Hoch, J. A. (1994). Identification of a second oligopeptide transport system in *Bacillus subtilis* and determination of its role in sporulation. *Molecular Microbiology*, 13(3).

Koo, B. M., Kritikos, G., Farelli, J. D., Todor, H., Tong, K., Kimsey, H., Wapinski, I., Galardini, M., Cabal, A., Peters, J. M., Hachmann, A. B., Rudner, D. Z., Allen, K. N., Typas, A., & Gross, C. A. (2017). Construction and Analysis of Two Genome-Scale Deletion Libraries for *Bacillus subtilis*. *Cell Systems*, 4(3).

Koonin, E. V., & Novozhilov, A. S. (2009). Origin and evolution of the genetic code: The universal enigma. *IUBMB Life*, 61(2).

Kostrzewa, R. M., Nowak, P., Kostrzewa, J. P., Kostrzewa, R. A., & Brus, R. (2005). Peculiarities of L-DOPA treatment of Parkinson's disease. *Amino Acids*, 28(2).

Krüger, L., Herzberg, C., Rath, H., Pedreira, T., Ischebeck, T., Poehlein, A., Gundlach, J., Daniel, R., Völker, U., Mäder, U., & Stülke, J. (2021). Essentiality of c-di-AMP in *Bacillus subtilis*: Bypassing mutations converge in potassium and glutamate homeostasis. *PLoS Genetics*, 17(1).

Krüger, L., Herzberg, C., Warneke, R., Poehlein, A., Stautz, J., Weiß, M., Daniel, R., Hänelt, I., & Stülke, J. (2020). Two ways to convert a low-affinity potassium channel to high affinity: Control of *Bacillus subtilis ktrCD* by glutamate. *Journal of Bacteriology*, 202(12).

Kuhlmann, A. U., & Bremer, E. (2002). Osmotically regulated synthesis of the compatible solute ectoine in *Bacillus pasteurii* and related *Bacillus* spp. *Applied and Environmental Microbiology*, 68(2).

Kunst, F., Ogasawara, N., Moszer, I., Albertini, A. M., Alloni, G., Azevedo, V., Bertero, M. G., Bessières, P., Bolotin, A., Borchert, S., Borriss, R., Boursier, L., Brans, A., Braun, M., Brignell, S. C., Bron, S., Brouillet, S., Bruschi, C. V., Caldwell, B., … Danchin, A. (1997). The complete genome sequence of the gram-positive bacterium *Bacillus subtilis*. *Nature*, 390(6657).

Kunst, F., & Rapoport, G. (1995). Salt stress is an environmental signal affecting degradative enzyme synthesis in *Bacillus subtilis*. *Journal of Bacteriology*, 177(9).

Kvenvolden, K., Lawless, J., Pering, K., Peterson, E., Flores, J., Ponnamperuma, C., Kaplan, I. R., & Moore, C. (1970). Evidence for Extraterrestrial Amino-acids and Hydrocarbons in the Murchison Meteorite. *Nature*, 228(5275).

Lachowicz, T. M., Morzejko, E., Panek, E., & Piątkowski, J. (1996). Inhibitory Action of Serine on Growth of Bacteria of the Genus *Bacillus* on Mineral Synthetic Media. *Folia Microbiologica*, 41(1).

Laemmli, U. K. (1970). Cleavage of structural proteins during the assembly of the head of bacteriophage T4. *Nature*, 227(5259).

Lea, D. E., & Coulson, C. A. (1949). The distribution of the numbers of mutants in bacterial populations. *Journal of Genetics*, 49(3).

Lea, P. J., & Miflin, B. J. (2003). Glutamate synthase and the synthesis of glutamate in plants. *Plant Physiology and Biochemistry*, 41(6).

Lee, C., Kang, H. J., Von Ballmoos, C., Newstead, S., Uzdavinys, P., Dotson, D. L., Iwata, S., Beckstein, O., Cameron, A. D., & Drew, D. (2013). A two-domain elevator mechanism for sodium/proton antiport. *Nature*, 501(7468).

Lee, N. K., Kim, W. S., & Paik, H. D. (2019). *Bacillus* strains as human probiotics: characterization, safety, microbiome, and probiotic carrier. *Food Science and Biotechnology,* 28(5).

Lee, P. Y., Costumbrado, J., Hsu, C. Y., & Kim, Y. H. (2012). Agarose gel electrophoresis for the separation of DNA fragments. *Journal of Visualized Experiments*, 62(1).

Leiman, S. A., May, J. M., Lebar, M. D., Kahne, D., Kolter, R., & Losick, R. (2013). D-Amino acids indirectly inhibit biofilm formation in *Bacillus subtilis* by interfering with protein synthesis. *Journal of Bacteriology*, 195(23).

Leonhardt, H., & Alonso, J. C. (1991). Parameters affecting plasmid stability in *Bacillus subtilis*. *Gene*, 103(1).

Leuchtenberger, W., Huthmacher, K., & Drauz, K. (2005). Biotechnological production of amino acids and derivatives: Current status and prospects. In *Applied Microbiology and Biotechnology,* 69(1).

Liu, P., Liu, H., Semenec, L., Yuan, D., Yan, S., Cain, A. K., & Li, M. (2022). Length-based separation of Bacillus subtilis bacterial populations by viscoelastic microfluidics. *Microsystems and Nanoengineering*, 8(1).

Lodish. (2013). Molecular Cell Biology - Lodish. *Journal of Petrology,* 369(1).

Lopatkin, A. J., Bening, S. C., Manson, A. L., Stokes, J. M., Kohanski, M. A., Badran, A. H., Earl, A. M., Cheney, N. J., Yang, J. H., & Collins, J. J. (2021). Clinically relevant mutations in core metabolic genes confer antibiotic resistance. *Science*, 371(6531).

López, D., & Kolter, R. (2010). Extracellular signals that define distinct and coexisting cell fates in *Bacillus subtilis*. *FEMS Microbiology Reviews,* 34(2).

Lorca, G. L., Barabote, R. D., Zlotopolski, V., Tran, C., Winnen, B., Hvorup, R. N., Stonestrom, A. J., Nguyen, E., Huang, L. W., Kim, D. S., & Saier, M. H. (2007). Transport capabilities of eleven gram-positive bacteria: Comparative genomic analyses. *Biochimica et Biophysica Acta – Biomembranes,* 1768(6).

Magasanik, B. (2003). Ammonia assimilation by *Saccharomyces cerevisiae*. *Eukaryotic Cell,* 2(5).

Magasanik, B., & Bowser, H. R. (1955). The degradation of histidine by *Aerobacter aerogenes*. *The Journal of Biological Chemistry*, 213(2).

Magnuson, B. A., Burdock, G. A., Doull, J., Kroes, R. M., Marsh, G. M., Pariza, M. W., Spencer, P. S., Waddell, W. J., Walker, R., & Williams, G. M. (2007). Aspartame: A safety evaluation based on current use levels, regulations, and toxicological and epidemiological studies. *Critical Reviews in Toxicology,* 37(8).

Mandal, M., Lee, M., Barrick, J. E., Weinberg, Z., Emilsson, G. M., Ruzzo, W. L., & Breaker, R. R. (2004). A glycine-dependent riboswitch that uses cooperative binding to control gene expression. *Science*, 306(5694).

Marciniak, B. C., Pabijaniak, M., de Jong, A., Duhring, R., Seidel, G., Hillen, W., & Kuipers, O. P. (2012). High- and low-affinity *cre* boxes for CcpA binding in *Bacillus subtilis* revealed by genome-wide analysis. *BMC Genomics*, 13(1).

Mardoukhi, M. S. Y., Rapp, J., Irisarri, I., Gunka, K., Link, H., Marienhagen, J., de Vries, J., Stülke, J., & Commichau, F. M. (2024). Metabolic rewiring enables ammonium assimilation via a non-canonical fumarate-based pathway. *Microbial Biotechnology*, 17(3).

Martin-Verstraete, I., Débarbouillé, M., Klier, A., & Rapoport, G. (1992). Mutagenesis of the *Bacillus subtilis* "-12, -24" promoter of the levanase operon and evidence for the existence of an upstream activating sequence. *Journal of Molecular Biology*, 226(1).

Martin-Verstraete, I., Débarbouillé, M., Klier, A., & Rapoport, G. (1994). Interactions of wild-type and truncated LevR of *Bacillus subtilis* with the upstream activating sequence of the levanase operon. *Journal of Molecular Biology*, 241(2).

Mathiopoulos, C., Mueller, J. P., Slack, F. J., Murphy, C. G., Patankar, S., Bukusoglu, G., & Sonenshein, A. L. (1991). A *Bacillus subtilis* dipeptide transport system expressed early during sporulation. *Molecular Microbiology*, 5(8).

McLaggan, D., Naprstek, J., Buurman, E. T., & Epstein, W. (1994). Interdependence of K+ and glutamate accumulation during osmotic adaptation of *Escherichia coli*. *Journal of Biological Chemistry*, 269(3).

McNaught, A. D., & Wilkinson, A. (1997). IUPAC. Compendium of Chemical Terminology, 2nd ed. (the "Gold Book"). *IUPAC Compendium of Chemical Terminology*.

Meißner, J., Königshof, M., Wrede, K., Warneke, R., Mardoukhi, M. S. Y., Commichau, F. M., & Stülke, J. (2024). Control of asparagine homeostasis in *Bacillus subtilis*: identification of promiscuous amino acid importers and exporters. *Journal of Bacteriology*, 260(23).

Meißner, J., Schramm, T., Hoßbach, B., Stark, K., Link, H., & Stülke, J. (2022). How To Deal with Toxic Amino Acids: The Bipartite AzlCD Complex Exports Histidine in *Bacillus subtilis*. *Journal of Bacteriology*, 204(12).

Meldrum, B. S. (2000). Glutamate as a Neurotransmitter in the Brain: Review of Physiology and Pathology. *The Journal of Nutrition*, 130(4).

Meyer, P., Evrin, C., Briozzo, P., Joly, N., Bârzu, O., & Gilles, A. M. (2008). Structural and functional characterization of *Escherichia coli* UMP kinase in complex with its allosteric regulator GTP. *Journal of Biological Chemistry*, 283(51).

Michal, G., & Schomburg, D. (2013). Biochemical Pathways: An Atlas of Biochemistry and Molecular Biology: Second Edition.

Miles, J. S., & Guest, J. R. (1985). Complete nucleotide sequence of the fumarase gene (*citG*) of *Bacillus subtilis* 168. *Nucleic Acids Research*, 13(1).

Miller, C. M., Baumberg, S., & Stockley, P. G. (1997). Operator interactions by the *Bacillus subtilis* arginine repressor/activator, AhrC: Novel positioning and DNA-mediated assembly of a transcriptional activator at catabolic sites. *Molecular Microbiology*, 26(1).

Moir, A. (1990). Bacillus subtilis: Molecular biology and industrial application. *Trends in Biotechnology*, 8(1).

Moir, A., Feavers, I. M., & Guest, J. R. (1984). Characterization of the fumarase gene of *Bacillus subtilis* 168 cloned and expressed in *Escherichia coli* K12. *Journal of General Microbiology*, 130(11).

Montgomery, M. W. (1983). Cysteine as an Inhibitor of Browning in Pear Juice Concentrate. *Journal of Food Science*, 48(3).

Morawska, L. P., Detert Oude Weme, R. G. J., Frenzel, E., Dirkzwager, M., Hoffmann, T., Bremer, E., & Kuipers, O. P. (2022). Stress-induced activation of the proline biosynthetic pathway in *Bacillus subtilis*: a population-wide and single-cell study of the osmotically controlled *proHJ* promoter. *Microbial Biotechnology*, 15(9).

Moses, S., Sinner, T., Zaprasis, A., Stöveken, N., Hoffmann, T., Sonenshein, B. R. B., Boris, R. B., & Bremer, E. (2012). Proline utilization by *Bacillus subtilis*: Uptake and catabolism. *Journal of Bacteriology*, 194(4).

Nakamura, L. K. (1989). Taxonomic relationship of black-pigmented *Bacillus subtilis* strains and a proposal for *Bacillus atrophaeus* sp. nov. *International Journal of Systematic Bacteriology*, 39(3).

Nakano, M. M., Xia, L., & Zuber, P. (1991). Transcription initiation region of the *srfA* operon, which is controlled by the *comP-comA* signal transduction system in *Bacillus subtilis*. *Journal of Bacteriology*, 173(17).

Naylor, S. L., Busby, L. L., & Klebe, R. J. (1976). Biochemical selection systems for mammalian cells: The essential amino acids. *Somatic Cell Genetics*, 2(2).

Nesterenko, M. V., Tilley, M., & Upton, S. J. (1994). A simple modification of Blum's silver stain method allows for 30 minutes detection of proteins in polyacrylamide gels. *Journal of Biochemical and Biophysical Methods*, 28(3).

Nicolas, P., Mäder, U., Dervyn, E., Rochat, T., Leduc, A., Pigeonneau, N., Bidnenko, E., Marchadier, E., Hoebeke, M., Aymerich, S., Becher, D., Bisicchia, P., Botella, E., Delumeau, O., Doherty, G., Denham, E. L., Fogg, M. J., Fromion, V., Goelzer, A., … Noirot, P. (2012). Condition-dependent transcriptome reveals high-level regulatory architecture in *Bacillus subtilis*. *Science*, 335(6072).

Noda-Garcia, L., Romero Romero, M. L., Longo, L. M., Kolodkin-Gal, I., & Tawfik, D. S. (2017). *Bacilli* glutamate dehydrogenases diverged via coevolution of transcription and enzyme regulation. *EMBO Reports*, 18(7).

O Duke, S., & B Powles, S. (2008). Glyphosate: a once-in-a-century herbicide. *Pest Management Science*, 63(11).

Oberhardt, M. A., Zarecki, R., Reshef, L., Xia, F., Duran-Frigola, M., Schreiber, R., Henry, C. S., Ben-Tal, N., Dwyer, D. J., Gophna, U., & Ruppin, E. (2016). Systems-Wide Prediction of Enzyme Promiscuity Reveals a New Underground Alternative Route for Pyridoxal 5'-Phosphate Production in *E. coli*. *PLOS Computational Biology*, 12(1).

Oda, M., Kobayashi, N., Ito, A., Kurusu, Y., & Taira, K. (2000). cis-Acting regulatory sequences for antitermination in the transcript of the *Bacillus subtilis* hut operon and histidine-dependent binding of HutP to the transcript containing the regulatory sequences. *Molecular Microbiology*, 35(5).

Oda, M., Sugishita, A., & Furukawa, K. (1988). Cloning and nucleotide sequences of histidase and regulatory genes in the *Bacillus subtilis hut* operon and positive regulation of the operon. *Journal of Bacteriology*, 170(7).

Oh, Y. K., Palsson, B. O., Park, S. M., Schilling, C. H., & Mahadevan, R. (2007). Genome-scale reconstruction of metabolic network in *Bacillus subtilis* based on high-throughput phenotyping and gene essentiality data. *Journal of Biological Chemistry*, 282(39).

Omasits, U., Ahrens, C. H., Müller, S., & Wollscheid, B. (2014). Protter: Interactive protein feature visualization and integration with experimental proteomic data. *Bioinformatics*, 30(6).

Oudega, B., Koningstein, G., Rodrigues, L., Ramon, M. D. S., Hilbert, H., Düsterhöft, A., Pohl, T. M., & Weitzenegger, T. (1997). Analysis of the *Bacillus subtilis* genome: Cloning and nucleotide sequence of a 62 kb region between 275°(*rrnB*) and 284°(*pai*). *Microbiology*, 143(8).

Palmer, C. N. A., Gustafsson, M. C. U., Dobson, H., Von Wachenfeldt, C., & Wolf, C. R. (1999). Adaptive responses to fatty acids are mediated by the regulated expression of cytochromes P450. *Biochemical Society Transactions*, 27(4).

Parris, K. D., Lin, L., Tam, A., Mathew, R., Hixon, J., Stahl, M., Fritz, C. C., Seehra, J., & Somers, W. S. (2000). Crystal structures of substrate binding to *Bacillus subtilis* holo-(acyl carrier protein) synthase reveal a novel trimeric arrangement of molecules resulting in three active sites. *Structure*, 8(8).

Parsot, C. (1986). Evolution of biosynthetic pathways: a common ancestor for threonine synthase, threonine dehydratase and D-serine dehydratase. *The EMBO Journal*, 5(11).

Patel, M. S., Nemeria, N. S., Furey, W., & Jordan, F. (2014). The pyruvate dehydrogenase complexes: Structure-based function and regulation. *Journal of Biological Chemistry,* 289(24).

Paul, S. I., Rahman, M. M., Salam, M. A., Khan, M. A. R., & Islam, M. T. (2021). Identification of marine sponge-associated bacteria of the Saint Martin's island of the Bay of Bengal emphasizing on the prevention of motile *Aeromonas septicemia* in *Labeo rohita*. *Aquaculture*, 545(1).

Pelley, J. W. (2012). Protein Synthesis and Degradation. *Elsevier's Integrated Review Biochemistry,* 52(1).

Perchat, N., Dubois, C., Mor-Gautier, R., Duquesne, S., Lechaplais, C., Roche, D., Fouteau, S., Darii, E., & Perret, A. (2022). Characterization of a novel β-alanine biosynthetic pathway consisting of promiscuous metabolic enzymes. *Journal of Biological Chemistry*, 298(7).

Perego, M., Higgins, C. F., Pearce, S. R., Gallagher, M. P., & Hoch, J. A. (1991). The oligopeptide transport system of *Bacillus subtilis* plays a role in the initiation of sporulation. *Molecular Microbiology*, 5(1).

Petroff, O. A. C. (2002). GABA and glutamate in the human brain. *Neuroscientist,* 8(6).

Picossi, S., Belitsky, B. R., Sonenshein A. L. (2007). Molecular mechanism of the regulation of *Bacillus subtilis gltAB* expression by GltC. *J Mol Biol*, 365(5)

Piggot, P. J. (2009). Encyclopedia of Microbiology. *Encyclopedia of Microbiology*, 14(2)

Priest, F. G. (2014). Systematics and Ecology of *Bacillus*. *Bacillus subtilis and Other Gram-Positive Bacteria*, 124(12).

Quentin, Y., Fichant, G., & Denizot, F. (1999). Inventory, assembly and analysis of *Bacillus subtilis* ABC transport systems. *Journal of Molecular Biology*, 287(3).

Quinn, C. L., Stephenson, B. T., & Switzer, R. L. (1991). Functional organization and nucleotide sequence of the *Bacillus subtilis* pyrimidine biosynthetic operon. *Journal of Biological Chemistry*, 266(14).

Rahman, M. M., Paul, S. I., Akter, T., Tay, A. C. Y., Foysal, M. J., & Islam, M. T. (2020). Whole-Genome Sequence of *Bacillus subtilis* WS1A, a Promising Fish Probiotic Strain Isolated from Marine Sponge of the Bay of Bengal. *Microbiology Resource Announcements*, 9(39).

Reeds, P. J. (2000). Dispensable and Indispensable Amino Acids for Humans. *The Journal of Nutrition*, 130(7).

Rehm, N., & Burkovski, A. (2011). Engineering of nitrogen metabolism and its regulation in *Corynebacterium glutamicum*: Influence on amino acid pools and production. *Applied Microbiology and Biotechnology*, 89(2).

Rehm, N., Georgi, T., Hiery, E., Degner, U., Schmiedl, A., Burkovski, A., & Bott, M. (2010). L-glutamine as a nitrogen source for *Corynebacterium glutamicum*: Derepression of the AmtR regulon and implications for nitrogen sensing. *Microbiology*, 156(10).

Reitzer, L. (2003). Nitrogen Assimilation and Global Regulation in *Escherichia coli*. *Annual Review of Microbiology,* 57(1).

Reitzer, L. J., & Magasanik, B. (1982). Asparagine synthetases of *Klebsiella aerogenes*: Properties and regulation of synthesis. *Journal of Bacteriology*, 151(3).

Resnekov, O., Melin, L., Carlsson, P., Mannerlöv, M., von Gabain, A., & Hederstedt, L. (1992). Organization and regulation of the *Bacillus subtilis odhAB* operon, which encodes two of the subenzymes of the 2-oxoglutarate dehydrogenase complex. *MGG Molecular & General Genetics*, 234(2).

Reuß, D. R., Altenbuchner, J., Mäder, U., Rath, H., Ischebeck, T., Sappa, P. K., Thürmer, A., Guérin, C., Nicolas, P., Steil, L., Zhu, B., Feussner, I., Klumpp, S., Daniel, R., Commichau, F. M., Völker, U., & Stülke, J. (2017). Large-scale reduction of the *Bacillus subtilis* genome: Consequences for the transcriptional network, resource allocation, and metabolism. *Genome Research*, 27(2).

Reuß, D. R., Commichau, F. M., Gundlach, J., Zhu, B., & Stülke, J. (2016). The Blueprint of a Minimal Cell: MiniBacillus. *Microbiology and Molecular Biology Reviews*, 80(4).

Reuß, D. R., Rath, H., Thürmer, A., Benda, M., Daniel, R., Völker, U., Mäder, U., Commichau, F. M., & Stülke, J. (2018). Changes of DNA topology affect the global transcription landscape and allow rapid growth of a *Bacillus subtilis* mutant lacking carbon catabolite repression. *Metabolic Engineering*, 45(2).

Rex Sheu, K., & Blass, J. P. (1999). The α-Ketoglutarate Dehydrogenase Complex. *Annals of the New York Academy of Sciences*, 893(1).

Richts, B., Lentes, S., Poehlein, A., Daniel, R., & Commichau, F. M. (2021). A *Bacillus subtilis* Δ*pdxT* mutant suppresses vitamin B6 limitation by acquiring mutations enhancing *pdxS* gene dosage and ammonium assimilation. *Environmental Microbiology Reports*, 13(2).

Riley, E. P., Schwarz, C., Derman, A. I., & Lopez-Garrido, J. (2021). Milestones in *Bacillus subtilis* sporulation research. In *Microbial Cell,* 8(1).

Rosenberg, J., Müller, P., Lentes, S., Thiele, M. J., Zeigler, D. R., Tödter, D., Paulus, H., Brantl, S., Stülke, J., & Commichau, F. M. (2016). ThrR, a DNA-binding transcription factor involved in controlling threonine biosynthesis in *Bacillus subtilis*. *Molecular Microbiology*, 101(5).

Rosenow, E. C. (1919). Studies on Elective Localization Focal Infection with Special Reference to Oral Sepsis'. *Journal of Dental Research*, 1(3).

Rother, M., & Krzycki, J. A. (2010). Selenocysteine, pyrrolysine, and the unique energy metabolism of methanogenic archaea. *Archaea,* 2010(1).

Rudner, D. Z., LeDeaux, J. R., Ireton, K., & Grossman, A. D. (1991). The *spo0K* locus of *Bacillus subtilis* is homologous to the oligopeptide permease locus and is required for sporulation and competence. *Journal of Bacteriology*, 173(4).

Saiki, R. K., Scharf, S., Faloona, F., Mullis, K. B., Horn, G. T., Erlich, H. A., & Arnheim, N. (1985). Enzymatic amplification of β-globin genomic sequences and restriction site analysis for diagnosis of sickle cell anemia. *Science*, 230(4732).

Samtiya, M., Samtiya, S., Badgujar, P. C., Puniya, A. K., Dhewa, T., & Aluko, R. E. (2022). Health-Promoting and Therapeutic Attributes of Milk-Derived Bioactive Peptides. In *Nutrients,* 14(15).

Sanger, F., Nicklen, S., & Coulson, A. R. (1977). DNA sequencing with chain-terminating inhibitors. *Proceedings of the National Academy of Sciences of the United States of America*, 74(12).

Satomura, T., Shimura, D., Asai, K., Sadaie, Y., Hirooka, K., & Fujita, Y. (2005). Enhancement of glutamine utilization in *Bacillus subtilis* through the GlnK-GlnL two-component regulatory system. *Journal of Bacteriology*, 187(14).

Saum, S. H., Sydow, J. F., Palm, P., Pfeiffer, F., Oesterhelt, D., & Müller, V. (2006). Biochemical and molecular characterization of the biosynthesis of glutamine and glutamate, two major compatible solutes in the moderately halophilic bacterium *Halobacillus halophilus*. *Journal of Bacteriology*, 188(19).

Schallmey, M., Singh, A., & Ward, O. P. (2004). Developments in the use of *Bacillus* species for industrial production. *Canadian Journal of Microbiology,* 50(1).

Schirmer, F., Ehrt, S., & Hillen, W. (1997). Expression, inducer spectrum, domain structure, and function of MopR, the regulator of phenol degradation in *Acinetobacter calcoaceticus* NCIB8250. *Journal of Bacteriology*, 179(4).

Schmidt, A., Sivaraman, J., Li, Y., Larocque, R., Barbosa, J. A. R. G., Smith, C., Matte, A., Schrag, J. D., & Cygler, M. (2001). Three-dimensional structure of 2-amino-3-ketobutyrate CoA ligase from *Escherichia coli* complexed with a PLP-substrate intermediate: Inferred reaction mechanism. *Biochemistry*, 40(17).

Schönert, S., Seitz, S., Krafft, H., Feuerbaum, E. A., Andernach, I., Witz, G., & Dahl, M. K. (2006). Maltose and maltodextrin utilization by *Bacillus subtilis*. *Journal of Bacteriology*, 188(11).

Schreier, H. J., Brown, S. W., Hirschi, K. D., Nomellini, J. F., & Sonenshein, A. L. (1989). Regulation of *Bacillus subtilis* glutamine synthetase gene expression by the product of the *glnR* gene. *Journal of Molecular Biology*, 210(1).

Schuirbach, H., Müller, A., Wu, T., Pfister, P., Aslan, S., von Borzyskowski, L. S., Erb, T. J., Bar-Even, A., & Lindner, S. N. (2022). On the flexibility of the cellular amination network in *E. coli*. *ELife*, 11(10).

Schujman, G. E., Paoletti, L., Grossman, A. D., & de Mendoza, D. (2003). FapR, a bacterial transcription factor involved in global regulation of membrane lipid biosynthesis. *Developmental Cell*, 4(5).

Scofield, M. A., Lewis, W. S., & Schuster, S. M. (1990). Nucleotide sequence of *Escherichia coli asnB* and deduced amino acid sequence of asparagine synthetase B. *Journal of Biological Chemistry*, 265(22).

Seif, Y., Choudhary, K. S., Hefner, Y., Anand, A., Yang, L., & Palsson, B. O. (2020). Metabolic and genetic basis for auxotrophies in Gram-negative species. *Proceedings of the National Academy of Sciences of the United States of America*, 117(11).

Sezonov, G., Joseleau-Petit, D., & D'Ari, R. (2007). *Escherichia coli* physiology in Luria-Bertani broth. *Journal of Bacteriology*, 189(23).

Sheng, Q., Wu, X. Y., Xu, X., Tan, X., Li, Z., & Zhang, B. (2021). Production of L-glutamate family amino acids in *Corynebacterium glutamicum*: Physiological mechanism, genetic modulation, and prospects. In *Synthetic and Systems Biotechnology,* 6(4).

Shimizu, K. (2013). Regulation Systems of Bacteria such as *Escherichia coli* in Response to Nutrient Limitation and Environmental Stresses. *Metabolites*, 4(1).

Sidiq, K. R., Chow, M. W., Zhao, Z., & Daniel, R. A. (2021). Alanine metabolism in *Bacillus subtilis*. *Molecular Microbiology*, 115(4).

Simoni, R. D., Hill, R. L., & Vaughan, M. (2002). The Discovery of the Amino Acid Threonine: The Work of William C. Rose. *Journal of Biological Chemistry*, 277(37).

Singh, S. K., Miller, S. P., Dean, A., Banaszak, L. J., & Laporte, D. C. (2002). *Bacillus subtilis* isocitrate dehydrogenase. A substrate analogue for *Escherichia coli* isocitrate dehydrogenase kinase/phosphatase. *Journal of Biological Chemistry*, 277(9).

Siranosian, K. J., Ireton, K., & Grossman, A. D. (1993). Alanine dehydrogenase (*ald*) is required for normal sporulation in *Bacillus subtilis*. *Journal of Bacteriology*, 175(21).

Slack, F. J., Serror, P., Joyce, E., & Sonenshein, A. L. (1995). A gene required for nutritional repression of the *Bacillus subtilis* dipeptide permease operon. *Molecular Microbiology*, *15*(4).

Sonenshein, A. L. (2007). Control of key metabolic intersections in *Bacillus subtilis*. In *Nature Reviews Microbiology,* 5(12).

Sonenshein, A. L., Hoch, J. A., & Losick, R. (2002). *Bacillus subtilis* and its closest relatives: from genes to cells. *Bacillus subtilis and Its Closest Relatives*.

Spiegelhalter, F., & Bremer, E. (1998). Osmoregulation of the *opuE* proline transport gene from *Bacillus subtilis*: Contributions of the sigma A- and sigma B-dependent stress-responsive promoters. *Molecular Microbiology*, 29(1).

Stannek, L., Thiele, M. J., Ischebeck, T., Gunka, K., Hammer, E., Völker, U., & Commichau, F. M. (2015). Evidence for synergistic control of glutamate biosynthesis by glutamate dehydrogenases and glutamate in *Bacillus subtilis*. *Environmental Microbiology*, 17(9).

Stecker, D., Hoffmann, T., Link, H., Commichau, F. M., & Bremer, E. (2022). L-Proline synthesis mutants of *Bacillus subtilis* overcome osmotic sensitivity by genetically adapting L-Arginine metabolism. *Frontiers in Microbiology*, 13(1).

Stein, T. (2005). *Bacillus subtilis* antibiotics: Structures, syntheses and specific functions. *Molecular Microbiology,* 56(4).

Stephens, C. (1998). Bacterial sporulation: A question of commitment? *Current Biology,* 8(2).

Stincone, A., Prigione, A., Cramer, T., Wamelink, M. M. C., Campbell, K., Cheung, E., Olin-Sandoval, V., Grüning, N. M., Krüger, A., Tauqeer Alam, M., Keller, M. A., Breitenbach, M., Brindle, K. M., Rabinowitz, J. D., & Ralser, M. (2015). The return of metabolism: Biochemistry and physiology of the pentose phosphate pathway. *Biological Reviews*, 90(3).

Stülke, J. (2023). *Bacillus subtilis* — Topmodel für Forschung, Gesundheit und Biotechnologie. *BIOspektrum*, 29(1).

Stülke, J., Grüppen, A., Bramkamp, M., & Pelzer, S. (2023). *Bacillus subtilis*, a Swiss Army Knife in Science and Biotechnology. In *Journal of Bacteriology,* 205(5).

Stülke, J., & Krüger, L. (2020). Cyclic di-AMP Signaling in Bacteria. In *Annual Review of Microbiology,* 74(1).

Stülke, J., Martin-Verstraete, I., Zagorec, M., Rose, M., Klier, A., & Rapoport, G. (1997). Induction of the *Bacillus subtilis ptsGHI* operon by glucose is controlled by a novel antiterminator, GlcT. *Molecular Microbiology*, 25(1).

Sudhagar Scholar, S., Rami Reddy, P., Nagalakshmi Scholar, G., Sudhagar, S., & Nagalakshmi, G. (2017). Influence of elevation in structuring the gut bacterial communities of Apis cerana. *Journal of Entomology and Zoology Studies*, 5(3).

Sun, D., & Setlow, P. (1991). Cloning, nucleotide sequence, and expression of the *Bacillus subtilis ans* operon, which codes for L-asparaginase and L-aspartase. *Journal of Bacteriology*, 173(12).

Sun, D., & Setlow, P. (1993). Cloning and nucleotide sequence of the *Bacillus subtilis ansR* gene, which encodes a repressor of the *ans* operon coding for L-asparaginase and L-aspartase. *Journal of Bacteriology*, 175(9).

Suzuki, A., & Knaff, D. B. (2005). Glutamate synthase: Structural, mechanistic and regulatory properties, and role in the amino acid metabolism. *Photosynthesis Research,* 83(2).

Tabor, H., & Hayaishi, O. (1952). The enzymatic conversion of histidine to glutamic acid. *The Journal of Biological Chemistry*, 194(1).

Takumi, K., Ziyatdinov, M. K., Samsonov, V., & Nonaka, G. (2017). Fermentative production of cysteine by *Pantoea ananatis*. *Applied and Environmental Microbiology*, 83(5).

Thorne, C. B., Gomez, C. G., & Housewright, R. D. (1955). Transamination of D-amino acids by *Bacillus subtilis*. *Journal of Bacteriology*, 69(3).

Tolner, B., Ubbink-Kok, T., Poolman, B., & Konings, W. N. (1995). Characterization of the proton/glutamate symport protein of *Bacillus subtilis* and its functional expression in *Escherichia coli*. *Journal of Bacteriology*, 177(10).

Toney, M. D. (2014). Aspartate aminotransferase: An old dog teaches new tricks. In *Archives of Biochemistry and Biophysics,* 544(1).

Tosa, T., Sato, T., Mori, T., & Chibata, I. (1974). Basic Studies for Continuous Production of L-Aspartic Acid by Immobilized Escherichia coli Cells. *Applied Microbiology*, 27(5).

Travis, B. A., Peck, J. V., Salinas, R., Dopkins, B., Lent, N., Nguyen, V. D., Borgnia, M. J., Brennan, R. G., & Schumacher, M. A. (2022). Molecular dissection of the glutamine synthetase-GlnR nitrogen regulatory circuitry in Gram-positive bacteria. *Nature Communications*, 13(1).

Van Heeke, G., & Schuster, S. M. (1989). Expression of human asparagine synthetase in *Escherichia coli*. *Journal of Biological Chemistry*, 264(10).

Van Heijenoort, J. (2001). Formation of the glycan chains in the synthesis of bacterial peptidoglycan. *Glycobiology*, 11(3).

Vander Horn, P. B., Backstrom, A. D., Stewart, V., & Begley, T. P. (1993). Structural genes for thiamine biosynthetic enzymes (*thiCEFGH*) in *Escherichia coli* K-12. *Journal of Bacteriology*, 175(4).

Vickery, H. B., & Schmidt, C. L. A. (1931). The history of the discovery of the amino acids. *Chemical Reviews*, 9(2).

Viola, R. E. (2000). L-aspartase: Newtricks from an old enzyme. *Advances in Enzymology and Related Areas of Molecular Biology*, 74(7).

Von Blohn, C., Kempf, B., Kappes, R. M., & Bremer, E. (1997). Osmostress response in *Bacillus subtilis*: Characterization of a proline uptake system (OpuE) regulated by high osmolarity and the alternative transcription factor sigma B. *Molecular Microbiology*, 25(1).

Wach, A. (1996). PCR-synthesis of marker cassettes with long flanking homology regions for gene disruptions in *S. cerevisiae*. *Yeast*, 12(3).

Wacker, I., Ludwig, H., Reif, I., Blencke, H. M., Detsch, C., & Stülke, J. (2003). The regulatory link between carbon and nitrogen metabolism in *Bacillus subtilis*: Regulation of the *gltAB* operon by the catabolite control protein CcpA. *Microbiology*, 149(10).

Walczak, R., Westhof, E., Carbon, P., & Krol, A. (1996). A novel RNA structural motif in the selenocysteine insertion element of eukaryotic selenoprotein mRNAs. *RNA*, 2(4).

Wamp, S., Rutter, Z. J., Rismondo, J., Jennings, C. E., Möller, L., Lewis, R. J., & Halbedel, S. (2020). Prka controls peptidoglycan biosynthesis through the essential phosphorylation of ReoM. *ELife*, 9(10).

Wang, S. T., Setlow, B., Conlon, E. M., Lyon, J. L., Imamura, D., Sato, T., Setlow, P., Losick, R., & Eichenberger, P. (2006). The forespore line of gene expression in *Bacillus subtilis*. *Journal of Molecular Biology*, 358(1).

Ward, J. B., & Zahler, S. A. (1973). Regulation of leucine biosynthesis in *Bacillus subtilis*. *Journal of Bacteriology*, 116(2).

Warneke, R., Garbers, T. B., Herzberg, C., Aschenbrandt, G., Ficner, R., & Stülke, J. (2023). Ornithine is the central intermediate in the arginine degradative pathway and its regulation in *Bacillus subtilis*. *Journal of Biological Chemistry*, 299(7).

Warneke, R., Herzberg, C., Daniel, R., Hormes, B., & Stülke, J. (2024). Control of three-carbon amino acid homeostasis by promiscuous importers and exporters in *Bacillus subtilis*: role of the “sleeping beauty” amino acid exporters. *MBio*, 15(23).

Waterhouse, A., Bertoni, M., Bienert, S., Studer, G., Tauriello, G., Gumienny, R., Heer, F. T., De Beer, T. A. P., Rempfer, C., Bordoli, L., Lepore, R., & Schwede, T. (2018). SWISS-MODEL: Homology modelling of protein structures and complexes. *Nucleic Acids Research*, 46(W1).

Wein, T., Hülter, N. F., Mizrahi, I., & Dagan, T. (2019). Emergence of plasmid stability under non-selective conditions maintains antibiotic resistance. *Nature Communications*, 10(1).

Weinrauch, Y., Msadek, T., Kunst, F., & Dubnau, D. (1991). Sequence and properties of *comQ*, a new competence regulatory gene of *Bacillus subtilis*. *Journal of Bacteriology*, 173(18).

Wendisch, V. F. (2016). Microbial Production of Amino Acid-Related Compounds. *Adv Biochem Eng Biotechnol*. 159(34).

Whatmore, A. M., Chudek, J. A., & Reed, R. H. (1990). The effects of osmotic upshock on the intracellular solute pools of *Bacillus subtilis*. *Journal of General Microbiology*, 136(12).

Whatmore, A. M., & Reed, R. H. (1990). Determination of turgor pressure in *Bacillus subtilis*: A possible role for K+ in turgor regulation. *Journal of General Microbiology*, 136(12).

Wicke, D., Schulz, L. M., Lentes, S., Scholz, P., Poehlein, A., Gibhardt, J., Daniel, R., Ischebeck, T., & Commichau, F. M. (2019). Identification of the first glyphosate transporter by genomic adaptation. *Environmental Microbiology*, 21(4).

Widderich, N., Rodrigues, C. D. A., Commichau, F. M., Fischer, K. E., Ramirez-Guadiana, F. H., Rudner, D. Z., & Bremer, E. (2016). Salt-sensitivity of σH and Spo0A prevents sporulation of *Bacillus subtilis* at high osmolarity avoiding death during cellular differentiation. *Molecular Microbiology*, 100(1).

Winkler, C., Denker, K., Wortelkamp, S., & Sickmann, A. (2007). Silver-and Coomassie-staining protocols: Detection limits and compatibility with ESI MS. *Electrophoresis*, *28*(12).

Wolosker, H., Dumin, E., Balan, L., & Foltyn, V. N. (2008). D-amino acids in the brain: D-serine in neurotransmission and neurodegeneration. *FEBS Journal,* 275(14).

Wray, L. V., & Fisher, S. H. (1994). Analysis of *Bacillus subtilis hut* operon expression indicates that histidine-dependent induction is mediated primarily by transcriptional antitermination and that amino acid repression is mediated by two mechanisms: Regulation of transcription initiation and inhibition of histidine transport. *Journal of Bacteriology*, 176(17).

Wray, L. V., Person, A. E., Rohrer, K., & Fisher, S. H. (1996). TnrA, a transcription factor required for global nitrogen regulation in *Bacillus subtilis*. *Proceedings of the National Academy of Sciences of the United States of America*, 93(17).

Wray, L. V., Zalieckas, J. M., & Fisher, S. H. (2001). *Bacillus subtilis* glutamine synthetase controls gene expression through a protein-protein interaction with transcription factor TnrA. *Cell*, 107(4).

Wu, G. (2009). Amino acids: metabolism, functions, and nutrition. *Amino Acids*, 37(1).

Xie, J., & Schultz, P. G. (2005). Adding amino acids to the genetic repertoire. *Current Opinion in Chemical Biology,* 9(6).

Wollaston, W. H, XIII. On cystic oxide, a new species of urinary calculus. (1810). *Philosophical Transactions of the Royal Society of London*, 100(1).

Xu, X. L., & Grant, G. A. (2013). Identification and characterization of two new types of bacterial l-serine dehydratases and assessment of the function of the ACT domain. *Archives of Biochemistry and Biophysics*, 540(1–2).

Xu, Y., Wu, J. Y., Liu, Q. J., & Xue, J. Y. (2023). Genome-Wide Identification and Evolutionary Analyses of SrfA Operon Genes in *Bacillus*. *Genes*, 14(2).

Yamaguchi, S., & Ninomiya, K. (2000). Umami and Food Palatability. *The Journal of Nutrition*, 130(4).

Yamamoto, H., Serizawa, M., Thompson, J., & Sekiguchi, J. (2001). Regulation of the *glv* operon in *Bacillus subtilis*: YfiA (GlvR) is a positive regulator of the operon that is repressed through CcpA and *cre*. *Journal of Bacteriology*, 183(17).

Yan, D. (2007). Protection of the glutamate pool concentration in enteric bacteria. *Proceedings of the National Academy of Sciences of the United States of America*, 104(22).

Yoshida -i., K., Sano, H., Seki, S., Oda, M., Fujimura, M., & Fujita, Y. (1995). Cloning and sequencing of a 29 kb region of the *Bacillus subtilis* genome containing the hut and *wapA* loci. *Microbiology*, 141(2).

Yoshida, K. I., Fujita, Y., & Ehrlich, S. D. (1999). Three asparagine synthetase genes of *Bacillus subtilis*. *Journal of Bacteriology*, 181(19).

Yu, J., Ge, J., Heuveling, J., Schneider, E., & Yang, M. (2015). Structural basis for substrate specificity of an amino acid ABC transporter. *Proceedings of the National Academy of Sciences of the United States of America*, 112(16).

Zamboni, N. (2003). Metabolic engineering of respiration for improved riboflavin production and elucidation of NADPH metabolism in *Bacillus subtilis*. *ETH Zürich*, 15118(1).

Zaprasis, A., Bleisteiner, M., Kerres, A., Hoffmann, T., & Bremer, E. (2015). Uptake of amino acids and their metabolic conversion into the compatible solute proline confers osmoprotection to *Bacillus subtilis*. *Applied and Environmental Microbiology*, 81(1).

Zaprasis, A., Hoffmann, T., Stannek, L., Gunka, K., Commichau, F. M., & Bremer, E. (2014). The γ-aminobutyrate permease GabP serves as the third proline transporter of *Bacillus subtilis*. *Journal of Bacteriology*, 196(3).

Zhang, L., Cao, Y., Tong, J., & Xu, Y. (2019). An alkylpyrazine synthesis mechanism involving L-threonine-3-dehydrogenase describes the production of 2,5-dimethylpyrazine and 2,3,5-trimethylpyrazine by *Bacillus subtilis*. *Applied and Environmental Microbiology*, 85(24).

Zhao, G., Pease, A. J., Bharani, N., & Winkler, M. E. (1995). Biochemical characterization of *gapB*-encoded erythrose 4-phosphate dehydrogenase of *Escherichia coli* K-12 and its possible role in pyridoxal 5'-phosphate biosynthesis. *Journal of Bacteriology*, 177(10).

Zhao, H., Roistacher, D. M., & Helmann, J. D. (2018). Aspartate deficiency limits peptidoglycan synthesis and sensitizes cells to antibiotics targeting cell wall synthesis in *Bacillus subtilis*. *Molecular Microbiology*, 109(6).

Appendix

Enzymes

Enzymes	Supplier
T4 DNA ligase	Thermo Scientific (Germany)
Phusion DNA polymerase	Thermo Scientific (Germany)
Lysozyme	Merck (Germany)
Restriction endonucleases	ThermoFischer (Germany)

Equipment

Device	Manufacturer
Synergy H1 plate reader	Agilent (USA)
Centrifuge 5424	Eppendorf (Germany)
Thermomixer 5436	Eppendorf (Germany)
Genesys 10S UV-Vis Spectrophotometer	Thermo Scientific (Germany)
T3 Thermocycler	Biometra (Germany)
PowerPac HC	Bio-Rad (USA)
Electronic scale Sartorius universal	Sartorius (Germany)
French pressure cell	G. Heinemann (Germany)
Nanodrop ND-1000	ThermoFischer (Germany)
SDS-PAGE glass plates	Bio-Rad (USA)
Water desalination plant	Millipore (Germany)

Commercial systems

System	Supplier
peqGOLD Bacterial DNA Kit	Peqlab (Germany)
PCR purification kit	Qiagen (Germany)
Monarch Plasmid Miniprep Kit	New England Biolabs (USA)
PageRulerTM Plus Prestained Protein Ladder	ThermoFischer (Germany)

Bacterial strains

Strain	Bacterium, mutant	Genotype	Reference, construction[a]
168	*B. subtilis*	*trpC2*	Laboratory strain collection
SP1	*B. subtilis*	Prototrophic derivative of strain 168	Richts et al., 2020
GP807	*B. subtilis*	*trpC2 gltAB::tet*	LFH → 168
GP1153	*B. subtilis*	*trpC2 ansAB::ermC*	LFH → 168
BP234	*B. subtilis*	*trpC gltP::cat*	Wicke et al., 2019
BP261	*B. subtilis*	*gltAB::tet*	cDNA GP807 → SP1
BP262	*B. subtilis*	*gltAB::tet amyE::*(P_{alf4}-*lacZ cat*)	pBP164 → BP261
BP263	*B. subtilis*	*amyE::*(P_{alf4}-*lacZ cat*)	pBP164 → SP1
BP264	*B. subtilis*	*amyE::*(P_{ansAB}-*lacZ aphA*)	pBP1110 → SP1
BP265	*B. subtilis*	*amyE::*(P_{ansAB}-*lacZ aphA*) *gltAB::tet*	pBP1110 → BP261

BP266	*B. subtilis*	*ansR::cat*	LFH → SP1
BP267	*B. subtilis*	*citG::ermC*	LFH → SP1
BP268	*B. subtilis*	*sdhA::aad9*	LFH → SP1
BP269	*B. subtilis*	*ansAB::ermC*	cDNA GP1153 → SP1
BP270	*B. subtilis*	*aspB::spc*	LFH → SP1
BP271	*B. subtilis*	*amyE::*(P_{ansAB}-*lacZ aphA*) *ansR::cat*	cDNA BP266 → BP264
BP272	*B. subtilis*	*amyE::*(P_{ansAB}-*lacZ aphA*) *citG::ermC*	cDNA BP267 → BP264
BP273	*B. subtilis*	*amyE::*(P_{ansAB}-*lacZ aphA*) *ansR::cat gltAB::tet*	cDNA BP266 → BP265
BP274	*B. subtilis*	*amyE::*(P_{ansAB}-*lacZ aphA*) *citG::ermC gltAB::tet*	cDNA BP267 → BP265
BP275	*B. subtilis*	*amyE::*(P_{ansAB}-*lacZ aphA*) *ansR::cat citG::ermC*	cDNA BP271 → BP272
BP276	*B. subtilis*	*amyE::*(P_{ansAB}-*lacZ aphA*) *ansR::cat citG::ermC*	cDNA BP273 → BP274
BP277	*B. subtilis*	*gltAB::tet amyE::*(P_{ansAB}-*lacZ aphA*) *ansR::cat citG::ermC sdhA::aad9*	cDNA BP268 → BP276
BP278	*B. subtilis*	*gltAB::tet amyE::*(P_{ansAB}-*lacZ aphAIII*) *ansR::cat citG::ermC aspB::aad9*	cDNA BP270 → BP276
BP279	*B. subtilis*	*amyE::*(P_{ansAB}-*lacZ aphA*) *aspB::spc*	cDNA BP270 → BP264
BP280	*B. subtilis*	*gltAB::tet ansAB::ermC*	cDNA BP269 → BP261
BP281	Suppressor of BP265	*amyE::*(P_{ansAB}-*lacZ aphA*) *gltAB::tet ansR* +A36 *citG* +G917	Selection
BP282	Suppressor of BP265	*amyE::*(P_{ansAB}-*lacZ aphA*) *gltAB::tet ansR* Δ2456934-2457298	Selection
BP283	Suppressor of BP265	*amyE::*(P_{ansAB}-*lacZ aphA*) *gltAB::tet ansR* +A36 *citG* C1226A	Selection
BP284	Suppressor of BP265	*amyE::*(P_{ansAB}-*lacZ aphA*) *gltAB::tet ansR* +A36	Selection
BP285	Suppressor of BP265	*amyE::*(P_{ansAB}-*lacZ aphA*) *gltAB::tet ansR* +A36	Selection
BP286	Suppressor of BP265	*amyE::*(P_{ansAB}-*lacZ aphA*) *gltAB::tet ansR* +A36	Selection
BP287	Suppressor of BP265	*amyE::*(P_{ansAB}-*lacZ aphA*) *gltAB::tet* P_{ansAB}(G-10A) *citG* T876A	Selection
BP288	Suppressor of BP265	*amyE::*(P_{ansAB}-*lacZ aphA*) *gltAB::tet ansR* +A36	Selection
BP289	Suppressor of BP265	*amyE::*(P_{ansAB}-*lacZ aphA*) *gltAB::tet ansR* +A36 *citG* Δ3390211-3390276	Selection
BP290	Suppressor of BP265	*amyE::*(P_{ansAB}-*lacZ aphA*) *gltAB::tet ansR* +A36	Selection
BP291	*B. subtilis*	*amyE::*(P_{ansAB}-*lacZ aphA*) *ansR::cat citG::ermC aspB::aad9*	cDNA BP270 → BP275
BP292	*B. subtilis*	*amyE::*(P_{ansAB}-*lacZ aphA*) *ansR::cat aspB::spc*	cDNA BP270 → BP271
BP293	*B. subtilis*	*amyE::*(*ansR*-P_{ansR}-*lacZ aphA*) *ansR::cat*	pBP1111 → BP266
BP294	*B. subtilis*	*amyE::*(*ansR*-P_{ansR}-*lacZ aphA*) *gltAB::tet*	pBP1111 → BP261
BP295	*B. subtilis*	*amyE::*(P_{ansAB}-*lacZ aphA*) *ansR::cat ansR ermC*	BP271 + pGP873
BP296	Suppressor of BP279	*amyE::*(P_{ansAB}-*lacZ aphA*) *aspB::spc citG* C686T *ansA* T43A	Selection
BP297	Suppressor of BP279	*amyE::*(P_{ansAB}-*lacZ aphA*) *aspB::spc citG* C312G *ansA* T43A	Selection

BP298	Suppressor of BP265	*amyE::*(P_{ansAB}-*lacZ aphA*) *gltAB::tet citG* A1033T 25.2 kbp amplification including *ansAB*	Selection
BP300	*B. subtilis*	*amyE::*(P_{ansAB}-*lacZ aphA*) *ansR::cat ermC*	BP271 + pBQ200
BP364	Suppressor of BP261	*gltAB::tet ansR* T302C 10.7 kbp deletion including *citG*	Selection
BP365	Suppressor of BP261	*gltAB::tet ansR* T169C *citG* ΔG62	Selection
BP366	Suppressor of BP279	*amyE::*(P_{ansAB}-*lacZ aphA*) *aspB::spc ansR* C171A	Selection
BP367	Suppressor of BP279	*amyE::*(P_{ansAB}-*lacZ aphA*) *aspB::spc ansR* G3A	Selection
BP368	Suppressor of BP279	*amyE::*(P_{ansAB}-*lacZ aphA*) *aspB::spc ansR* G94C	Selection
BP369	Derivative of BP275	*amyE::*(P_{ansAB}-*lacZ aphA*) *ansR::cat citG::ermC gudB* ΔG279-C287	Selection
BP370	Derivatives of BP276	*amyE::*(P_{ansAB}-*lacZ aphA*) *gltAB::tet ansR::cat citG::ermC gudB* ΔG279-C287	Selection
BP371	Suppressor of BP275	*amyE::*(P_{ansAB}-*lacZ aphA*) *ansR::cat citG::ermC* 5.2 kbp amplification including *aspB*	Selection
BP372	Suppressor of BP275	*amyE::*(P_{ansAB}-*lacZ aphA*) *ansR::cat citG::ermC* 5.2 kbp amplification including *aspB*	Selection
BP373	Suppressor of BP275	*amyE::*(P_{ansAB}-*lacZ aphA*) *ansR::cat citG::ermC rocC* C1232T	Selection
BP374	Suppressor of BP275	*amyE::*(P_{ansAB}-*lacZ aphA*) *ansR::cat citG::ermC rocC* + T698	Selection
BP375	Suppressor of BP276	*amyE::*(P_{ansAB}-*lacZ aphA*) *gltAB::tet ansR::cat citG::ermC* P_{dinG} (G-63A)	Selection
BP376	Suppressor of BP276	*amyE::*(P_{ansAB}-*lacZ aphA*) *gltAB::tet ansR::cat citG::ermC* 34.7 kbp amplification including *aspB*	Selection
BP377	Suppressor of BP276	*amyE::*(P_{ansAB}-*lacZ aphA*) *gltAB::tet ansR::cat citG::ermC odhA* ΔT175-A351	Selection
BP378	Suppressor of BP276	*amyE::*(P_{ansAB}-*lacZ aphA*) *gltAB::tet ansR::cat citG::ermC* P_{odhA} (G-189A)	Selection
BP279	*B. subtilis*	*gltAB::tet ansR::cat*	BP261 → BP266
BP280	*B. subtilis*	*gltAB::tet ansR::cat citG::ermC*	BP267 → BP379
BP281	*B. subtilis*	*ansR::cat aspB::aad9*	BP270 → BP266
BP382	*B. subtilis*	*amyE::*(*ansR*-P_{ansR}-*lacZ aphA*)	pBP1111 → SP1
BP383	*B. subtilis*	*amyE::*(*ansR*-P_{ansR}-*lacZ aphA*) *aspB::spc*	cDNA BP270 → BP382
BP384	Derivative of BP264	*amyE::*(P_{ansAB}-*lacZ aphA*)	Selection
BP385	*B. subtilis*	*amyE::*(P_{ansAB}- *ansR*-His(C)-*lacZ aphA*) *ansR::cat*	pBP1120 → BP266
BP386	*B. subtilis*	*amyE::*(*PansAB-lacZ aphA*) *gltAB::tet ansAB::ermC*	pBP1110 → BP280
BP387	Derivative of BP386	*amyE::*(P_{ansAB}-*lacZ aphA*) *gltAB::tet ansAB::ermC srfAA* ΔG9236-10764A *srfAB* ΔA1-T9059 *azlB* T194G P_{reoM} (C-44T)	Selection
BP388	Derivative of BP386	*amyE::*(P_{ansAB}-*lacZ aphA*) *gltAB::tet ansAB::ermC azlB* T194G *yrhJ* C461T P_{reoM} (C-44T)	Selection

BP389	Derivative of BP386	*amyE*::(P_{ansAB}-*lacZ aphA*) *gltAB*::*tet ansAB*::*ermC azlB* T194G P_{reoM} (C-44T)	Selection
BP390	Derivative of BP386	*amyE*::(P_{ansAB}-*lacZ aphA*) *gltAB*::*tet ansAB*::*ermC* 58.8 kbp deletion Δ225622-284415 *azlB* Δ139G P_{reoM} (C-44T)	Selection
BP391	Derivative of BP269	*ansAB*::*ermC aimA* +CTA194 *yetL* G287T	Selection
BP392	Derivative of BP269	*ansAB*::*ermC aimA* +G213	Selection
BP393	Derivative of SP1	*malP* A194C P_{sigG} (G+78A)	Selection
BP394	Derivative of SP1	*cpaA* +T153 *malP* +A1571	Selection
BP395	*B. subtilis*	*ansAB*::*ermC aspB*::*aad9*	cDNA BP270 → BP269
BP396	*B. subtilis*	*hutP*::*aphA*	cDNA BKK39340 → SP1
BP397	*B. subtilis*	*amyE*::(P_{hutP}-*hutP-lacZ cat*) *hutP*::*aphA*	pBP1126 → BP396
BP398	*B. subtilis*	*amyE*::(P_{hutP}-*hutP*(C176T)-*lacZ cat*) *hutP*::*aphA*	pBP1127 → BP396
BP399	*B. subtilis*	*amyE*::(P_{hutP}-*hutP*(T162C)-*lacZ cat*) *hutP*::*aphA*	pBP1128 → BP396
BP574	*B. subtilis*	*amyE*::(P_{reoM}-*lacZ aphA*)	pBP1122 → SP1
BP575	*B. subtilis*	*amyE*::(P_{reoM}(C-44T)-*lacZ aphA*)	pBP1123 → SP1
BP576	*B. subtilis*	*gudB* ΔC279-G287	Selection
BP577	*B. subtilis*	*gltAB*::*tet ansAB*::*erm gudB* ΔC279-G288	Selection
BP578	*B. subtilis*	*amyE*::(P_{hutP}-*hutP-lacZ cat*)	pBP1126 → SP1
BP579	*B. subtilis*	*amyE*::(P_{hutP}-*hutP*(C176T)-*lacZ cat*)	pBP1127 → SP1
BP580	*B. subtilis*	*amyE*::(P_{hutP}-*hutP*(T162C)-*lacZ cat*)	pBP1128 → SP1
BP581	Derivative of SP1	*yhxA* -T346 *cwlO* G535A *hutP C174T*	Selection
BP582	Derivative of SP1	*yhcX* G648A *yhxA* -T338 *hutP* C174T	Selection
BP583	Derivative of BP280	*ansR* C107A *hutP* C174T	Selection
BP584	Derivative of BP280	*ansR* C107A *hutP* C174T	Selection
BP585	Derivative of BP280	P_{ppsA} (C+81T) *ansR* C107A *hutP* C174T	Selection
BP586	Derivative of BP280	*ansR* C107A *hutP* C174T	Selection
BP587	Derivative of BP280	P_{ppsA} C+81T *ansR* C107A *hutP* T162C *gudB* ΔG279-C287	Selection
BP588	Derivative of BP280	*rpoC* C3038T P_{srfAA} C+415T *ansR* C107A *hutP* C174T *gudB* ΔG279-C287	Selection
BP647	*B. subtilis*	*trpC2 recN*::*ermC*	LFH → 168
BP1303	*B. subtilis*	*trpC gdpP*::*spc*	Schwedt et al., 2023
XL1-Blue	*E. coli* XL1-Blue	*recA1 endA1 gyrA96 thi-1 hsdR17 supE44 relA1 lac* [F′ *proAB, lacIqZΔM15* Tn*10* (Tet^r)]	Stratagene
Wild type	*C. glutamicum* ATCC13032	-	Abe et al., 1967
Δ*gdh* Δ*gltB*	*C. glutamicum* ATCC13032	Δ*gdh* Δ*gltB*	This study
Δ*gdh* Δ*gltB* Δ*aspA*	*C. glutamicum* ATCC13032	Δ*gdh* Δ*gltB* Δ*aspA*	This study
Δ*gdh* Δ*gltB* Δ*aspT*	*C. glutamicum* ATCC13032	Δ*gdh* Δ*gltB* Δ*aspT*	This study

Primers

Primer	Description[a]	Purpose
FC75	5‘-CGAGCGCCTACGAGGAATTTGTATCGGAAGTGGC GCGTGAAGTGGATC	Construction of the strain GP807
FC76	5‘-GGTTCTGACGGCGCGGGTATC	Construction of the strain GP807
FC350	5‘-CAGCGAACCATTTGAGGTGATAGGCGGCAATAGT TACCCTTATTATCAAG	Amplification of the *cat* gene
FC352	5‘-CGATACAAATTCCTCGTAGGCGCTCGGTTATAAAA GCCAGTCATTAGGCCTATC	Amplification of the *cat* gene
FC356	5‘-CAGCGAACCATTTGAGGTGATAGGGATCCTTTAA CTCTGGCAACCCTC	Amplification of the *ermC* gene
FC357	5‘-CGATACAAATTCCTCGTAGGCGCTCGGGCCGACT GCGCAAAAGACATAATCG	Amplification of the *ermC* gene
FC359	5‘-CAGCGAACCATTTGAGGTGATAGGGACTGGCTCG CTAATAACGTAACGTGACTGGCAAGAG	Amplification of the *spc* gene
FC361	5‘-CGATACAAATTCCTCGTAGGCGCTCGGTTTCCACC ATTTTTTCAATTTTTTTATAATTTTTTT	Amplification of the *spc* gene
FC363	5‘-CGATACAAATTCCTCGTAGGCGCTCGGGAACTCTC TCCCAAAGTTGATCCC	Verification of the integration of the *tet* gene
KG1	5‘-CCTATCACCTcaaatggttcgggccgattccgca tgcatcatgttc	Construction of the strain GP807
KG2	5‘-cattcgcggaaggcgcaagctc	Construction of the strain GP807
KG28	5‘-ATGGCTTGGACCCGTTATTGGGG	Construction of the strain GP1153
KG29	5‘-CCTATCACCTCAAATGGTTCGCTGGAGCCAGCCC ATTTTCCCCTTC	Construction of the strain GP1153
KG30	5‘-CCGAGCGCCTACGAGGAATTTGTATCGCGGCGCT GATCATCTTGTTGATG	Construction of the strain GP1153
KG31	5‘-AAGTCGGCACAACGCCTCCGG	Construction of the strain GP1153
MD56	5‘-AAAGTCGACTTATTGATACTGCTCCAGCTTAGAGA AAAATTGAATG	Verification of the integration of the *tet* gene
MD119	5‘-CCTATCACCTCAAATGGTTCGCTGGACTTAACGAA ACGCCATGC	Construction of strain BP267
MD120	5‘-ACCCGATTCTGTATTTGCCTTCT	Construction of strain BP267
MD121	5‘-CCGAGCGCCTACGAGGAATTTGTATCGCCGCGTT CAAAAGAAACCGT	Construction of strain BP267
MD122	5‘-AATCACGGGAGGAGACGGA	Construction of strain BP267
mls fwd (kan)	5‘-CAGCGAACCATTTGAGGTGATAGGGATCCTTTAAC TCTGGCAACCCTC	Amplification of the *ermC* gene
mls rev (kan)	5‘-CGATACAAATTCCTCGTAGGCGCTCGGG CCGACTGCGCAAAAGACATAATCG	Amplification of the *ermC* gene
SM1	5‘-TTTGAATTCGAACTTCCGCTCCTTTTTCACC	Construction of pBP1110
SM2	5‘-TTTGGATCCATACCATGCACCTCTTCACTGTATC	Construction of pBP1110, pBP1111, pBP1120
SM3	5‘-TTTATGGAATACAGAATTGAACGAGAC	Amplification of *citG*
SM4	5‘-TTTTACGCCTTTGGTTTTACCATG	Amplification of *citG*
SM5	5‘-TTTCTAGCGCCCACATCAATTTTGGC	Construction of strain BP266
SM6	5‘-TTTTCTTCGCCTTCTTCAAGACATTG	Construction of strain BP266
SM7	5‘-CCTATCACCTCAAATGGTTCGCTGGAACTTCCGCT CCTTTTTCACCTTGAG	Construction of strain BP266

SM8	5‘-CCGAGCGCCTACGAGGAATTTGTATCGATCTTTAG CTCACGGTTTAATTTTA	Construction of strain BP266
SM9	5‘-TTTTCATCTGGAAAATATCGCGAGCTTGACG	Construction of strain BP266
SM10	5‘-TTTCGCCAAAACATTAACGCTGGACAGAAT	Construction of strain BP266
SM11	5‘-TTTCCACACGGCCGTTAAACAGGG	Construction of strain BP267
SM12	5‘-TTTGCTGGATATTTTTAAGCCGCGCC	Construction of strain BP267
SM13	5‘-CCTATCACCTCAAATGGTTCGCTGTTATGTATCCC TCCATAACGGTTGCTTC	Construction of strain BP267
SM14	5‘-CCGAGCGCCTACGAGGAATTTGTATCGATAGGAA GAACGGCTGCTTTTTAAG	Construction of strain BP267
SM15	5‘-TTTTGGTCATATCCTAGCAGGCCTCCG	Construction of strain BP267
SM16	5‘-TTTCGTCCAATTCTCTCATTCTAGATTCACCCT	Construction of strain BP267
SM18	5‘-TTTGGATCCTTAACTCAGTTCCTCCTGTACTTTTCTT TTG	Amplification of *ansR*
SM19	5‘-TTTCAAGAGGAAACTTACGGGCGAG	Construction of strain BP268
SM20	5‘-TTTGCGTTCATTTCAATTTCTTTTAGGTTGTC	Construction of strain BP268
SM21	5‘-CCTATCACCTCAAATGGTTCGCTGGATAGCCCCT CTCCCTCTAGTAAT	Construction of strain BP268
SM22	5‘-CGAGCGCCTACGAGGAATTTGTATCGCCATACGA TTTATTATCACACGTCAAGATAC	Construction of strain BP268
SM23	5‘-TTTGCTTTTTAAAATAAGAAATCCGCACCTCC	Construction of strain BP268
SM24	5‘-TTTTCACATAGATGCGCAACTCTTCATAAGG	Construction of strain BP268
SM25	5‘-TTTAAATGTGAGCTTGCCCGCAAAAAAG	Construction of strain BP270
SM26	5‘-TTTAGACAAGGGAACGATTATTATATTGGACA	Construction of strain BP270
SM27	5‘-CCTATCACCTCAAATGGTTCGCTGCTTGAACTCC CCCTAATTCGTCTTAAG	Construction of strain BP270
SM28	5‘-CGAGCGCCTACGAGGAATTTGTATCGACAGATCA AAAAGCGGCTGACAGAAAAG	Construction of strain BP270
SM29	5‘-TTTTACGTAATTCTTGGGAACGGGGCT	Construction of strain BP270
SM30	5‘-TTTGTGATGAATACCGGTTTGTCATAATGTTC	Construction of strain BP270
SM36	5‘-TTTGAATTCTCATTAACTCAGTTCCTCCTGTACTTTT CTTTTTGTG	Construction of pBP1111
SM37	5‘-GTAAAACGACGGCCAGTG	Check forward pBQ200
SM38	5‘-GGAAACAGCTATGACCAT	Check reverse pBQ200
SM40	5‘-TTTGGATCCATGAATCTAGATCGTTTAACTGAATTG AGAAAAAAG	Construction of pBP1112
SM41	5‘-TTTAAGCTTTTAACTCAGTTCCTCCTGTACTTTTCTT TTG	Construction of pBP1112, pBP1118
SM42	5‘-TTTGGATCCATTAAAGAGGAGAAATTAACTAATGAA TCTAGATCGTTTAACTGAATTG	Construction of pBP1113
SM43	5‘-TTTGGTACCACTCAGTTCCTCCTGTACTTTTCTTTTT GG	Construction of pBP1113
SM44	5‘-AAAGAATTCTTGACAAGTGAAGGCGCGCTATGCTA TAATACAGCTTGGTTTAAAGGAGGAAACAATCATGGTG AGCAAGGGCGAGG	Construction of pBP1116
SM45	5‘-AAAGGATCCCTACTTGTACAGCTCGTCCATGCCGC CGG	Construction of pBP1116
SM46	5‘-AAAGAATTCTTGACAAGTGAAGGCGCGCTATGCTA TAATACAGCTTGGTTTAAAGGAGGAAACAATCATGGTG AGCAAGGGCGAGG	Construction of pBP1117
SM47	5‘-AAAGGATCCTTACTTGTACAGCTCGTCCATGCCG	Construction of pBP1117
SM48	5‘-TTTGTCGACATTAAAGAGGAGAAATTAACTATGAGA GG	Construction of pBP1118, pBP1119

SM49	5‘-TTTAAGCTTTTAGTGATGGTGATGGTGATGGGTACCAC	Construction of pBP1119
SM50	5‘-TTTGAATTCTTAGTGATGGTGATGGTGATGGGTACCACTCAGTTCCTCCTGTAC	Construction of pBP1120
SM51	5‘-ATTAAAGAGGAGAAATTAACTATGAGAGGATC	Construction of pBP1121
SM52	5‘-TTTGAATTCTTAACTCAGTTCCTCCTGTACTTTTC	Construction of pBP1121
SM53	5‘-GAGTATCAATTAAAGAGGAGAAATTAGAACTTCCGCTCCTTTTTCAC	Construction of pBP1121
SM54	5‘-TTTAGATCTACCATGCACCTCTTCACTG	Construction of pBP1121
SM55	5‘-TTTGGATCCTTACAGGACAACGTCATCAGC	Amplification of the *ansA* gene and P_{ansAB}
SM56	5‘-TTTCAATTGGAACTTCCGCTCCTTTTTCACC	Amplification of the *ansA* gene and P_{ansAB}
SM60	5‘-TTTGAATTCACTTTCTGTTTTGCGAATTTTAACAATTTTCG	Amplification of the P_{azlB}
SM61	5‘-TTTGGATCCATTTCACAACCCCCAATACAACTTAACAG	Amplification of the P_{azlB}
SM62	5‘-TTTCATATTTGATATTGAAAGAAAGAACAACCGC	LFH-PCR on the *azlB* gene
SM63	5‘-TTTGCGATTTCCACCTTATTACGCCG	LFH-PCR on the *azlB* gene
SM64	5‘-CCTATCACCTCAAATGGTTCGCTGTTCACAACCCCCCAATACAACTTAACAG	LFH-PCR on the *azlB* gene
SM65	5‘-CCGAGCGCCTACGAGGAATTTGTATCGGAGGTTGTTGATTTGAATAAAAATAAAGAATCG	LFH-PCR on the *azlB* gene
SM66	5‘-TTTACCAATTCAGGAATGCCATGACTTC	LFH-PCR on the *azlB* gene
SM67	5‘-TTTCCAATTGCACCAAAACCATATAAACAACG	LFH-PCR on the *azlB* gene
SM68	5‘-AAAGAATTCTTCGCCCATGTAGTGTAGAATGATG	Construction of pBP1122, pBP1123
SM69	5‘-TTTGGATCCATCGAGCTCACCGTTTTGCACC	Construction of pBP1122, pBP1123
SM70	5‘-TTTAGGCAACGTGGAAGCAGGAGCAATC	Check forward the *reoM* gene
SM71	5‘-TTTTCCAGCCCATTTCATCGCTCAGAG	Check reverse the *reoM* gene
SM72	5‘-AAAGACTTTCTGTTTTGCGAATTTTAACAATTTTCG	Check forward the *azlB* gene
SM73	5‘-AAAGCTAAATCCCAAAGAATGCATAAAGATC	Check reverse the *azlB* gene
SM74	5‘-AAAATGGCAGCCGATCGAAACACC	Check forward the *gudB* gene
SM75	5‘-AAATTATATCCAGCCTCTAAAACGCGAAG	Check reverse the *gudB* gene
SM76	5‘-AAAGAATTCTTCGTTGTCGGCGTTTTTTAAGATG	Construction of pBP1124, pBP1125, pBP1126, pBP1127, pBP1128
SM77	5‘-AAAGGATCCGTCACCATAAGCCCAACTCC	Construction of pBP1124, pBP1125, pBP1126, pBP1127, pBP1128
Tc fwd1 (kan)	5‘-CAGCGAACCATTTGAGGTGATAGGGCTTATCAACGTAGTAAGCGTGG	Amplification of the *tet* gene
Tc rev (kan)	5‘-CGATACAAATTCCTCGTAGGCGCTCGGGAACTCTCTCCCAAAGTTGATCCC	Amplification of the *tet* gene
KG201	5‘-AAACAATTGAAAGGAGGAAACAATCATGGATTCAATAGAAAAGGTAAGCGAATTTGC	Construction of pBP1114
KG208	5‘-TTTAGATCTtcattaCTTGTACAGCTCGTCCATGCCGA	Construction of pBP1114
KG199	5‘-AAACAATTGAAAGGAGGAAACAATCATGGTTTCAAAAGGCGAAGAACTGTTTACG	Construction of pBP1115
KG206	5‘-TTTAGATCTtcattaCTTATAAAGTTCGTCCATGCCAAGTGTAATG	Construction of pBP1115

Plasmids

Plasmid	Description	Reference, construction
pBQ200		
pAC7	For the construction of translational *lacZ* fusions, integration into the *amyE* locus	Weinrauch et al., 1991
pAC5	For the construction of translational *lacZ* fusions, integration into the *amyE* locus	(Martin-Verstraete et al., 1992)
pWH844	For the fusion of a His(6) tag to the N-terminus of the expressed protein in *E.coli*	Schirmer et al., 1997
pBP1110	pAC7::P_{ansAB}	Mardoukhi et al., 2024
pBP1111	pAC7::*ansR*-P_{ansAB}	Mardoukhi et al., 2024
pBP1112	pWH844::*ansR*	This study
pBP1113	pCHis::*ansR*	This study
pBP1114	pAC7::*yfp*	This study
pBP1115	pAC7::*cfp*	This study
pBP1116	pAC7::P_{alf1}-*mCherry*	This study
pBP1117	pAC7::P_{alf1}-*mVenus*(*SYFP2*)	This study
pBP1118	pBQ200::RBS-spacer-His(N)-*ansR*	This study
pBP1119	pBQ200::RBS-spacer-*ansR*-His(C)	This study
pBP1120	pAC7::P_{ansR}-*ansR*-His(C)	This study
pBP1121	pAC7::P_{ansR}-RBS-His(N)-*ansR*	This study
pBP1122	pAC7::P_{reoM}	This study
pBP1123	pAC7::P_{reoM} (C-44T)	This study
pBP1124	pAC7::P_{hutP}-*hutP*	This study
pBP1125	pAC7::P_{hutP}-*hutP* (C174T)	This study
pBP1126	pAC5::P_{hutP}-*hutP*	This study
pBP1127	pAC5::P_{hutP}-*hutP* (C174T)	This study
pBP1128	pAC5::P_{hutP}-*hutP* (T162C)	This study
pDG647	Template for the amplification of the *ermC* gene	Guérout-Fleury et al., 1995
pDG1514	Template for the amplification of the *tet* gene	Guérot-Fleury et al., 1995
pDG1726	Template for the amplification of the *spc* gene	Guérot-Fleury et al., 1995
pGEM-cat	Template for the amplification of the *cat* gene	Laboratory collection
pBP26	For the integration of a constitutively expressed y*fp,* integration into the *amyE* locus	Gunka et al., 2013
pBP27	For the integration of a constitutively expressed *cfp* into the *amyE* locus	Gunka et al., 2013
pJG08	For the integration of a constitutively expressed *mCherry* into the *amyE* locus	Greenwich et al., 2019
pJG09	For the integration of a constitutively expressed *mVenus* (*SYFP2*) into the *amyE* locus	Greenwich et al., 2019

Additional experiments

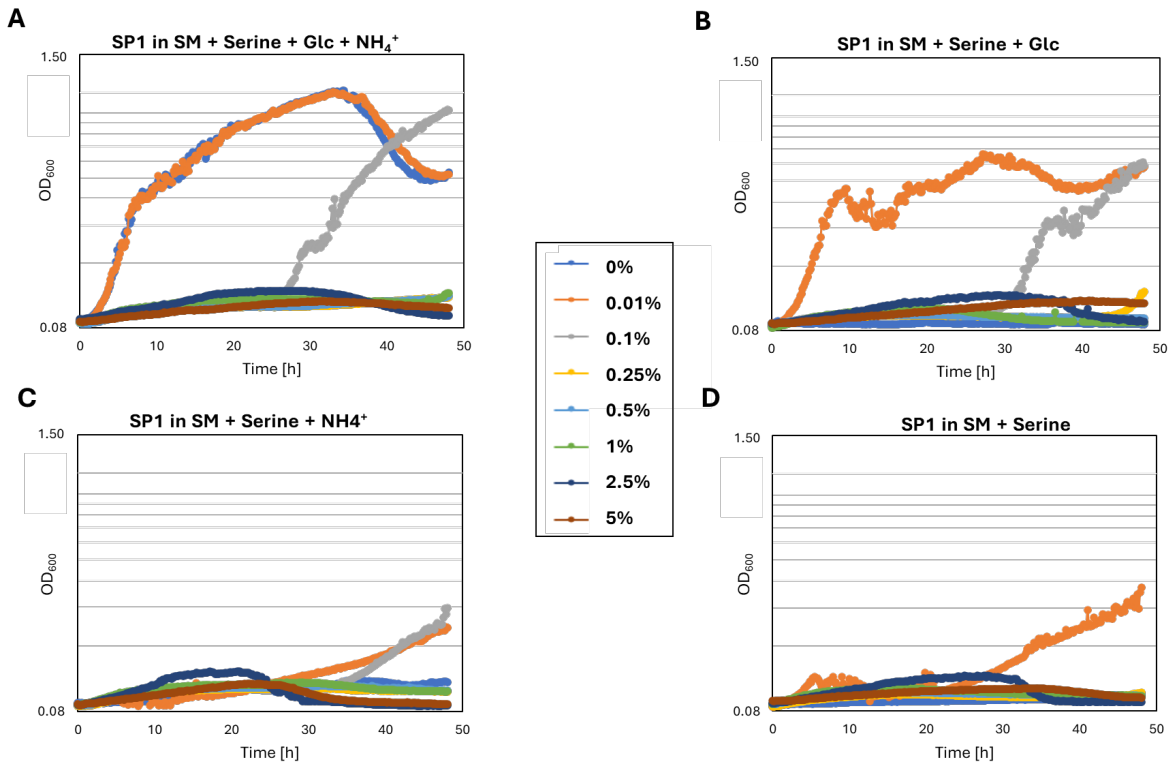

Figure S1. Monitoring the growth of *B. subtilis* SP1 (wild type) in SM minimal medium supplemented with L-serine at the final concentration ranging from 0% to 5% (w/v), **A)** with glucose and ammonium; **B)** with glucose; **C)** with ammonium; and **D)** without supplementation. Following overnight incubation in LB medium, cells were subjected to two rounds of washing and subsequently inoculated into SM minimal medium. The growth of the cultures was monitored for 48 hours at 37°C. Each experiment was independently repeated as triplet (*N* = *3*).

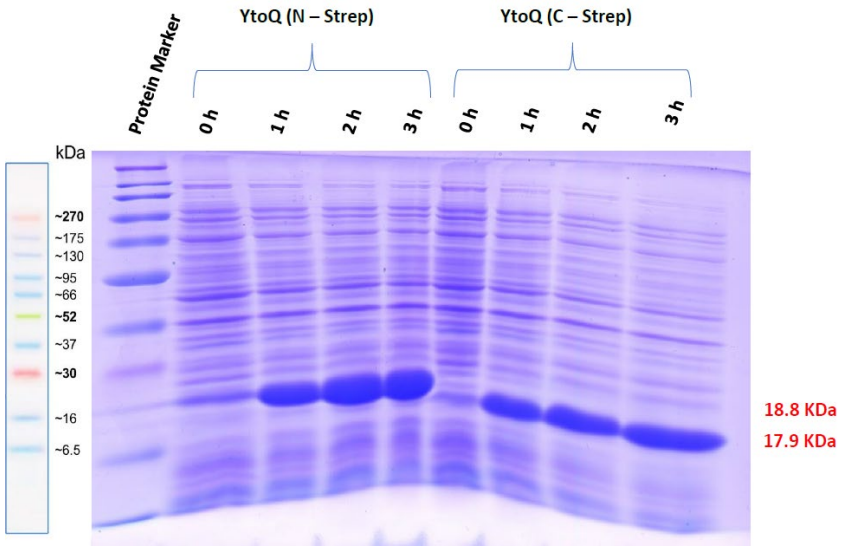

Figure S1. Expression analysis of YtoQ protein in *E. coli* BL21 on SDS-PAGE.

Expression levels of YtoQ protein were analyzed using two constructs: pBP641 (Strep-tagged YtoQ at the N-terminus) and pBP642 (Strep-tagged YtoQ at the C-terminus). Samples were collected from *E. coli* BL21 cultures at various time points—prior to induction (0 h) and post-induction at 1 h, 2 h, and 3 h—to evaluate the temporal expression profile. Visualization performed on SDS-PAGE 15%, followed by Coomassie staining.

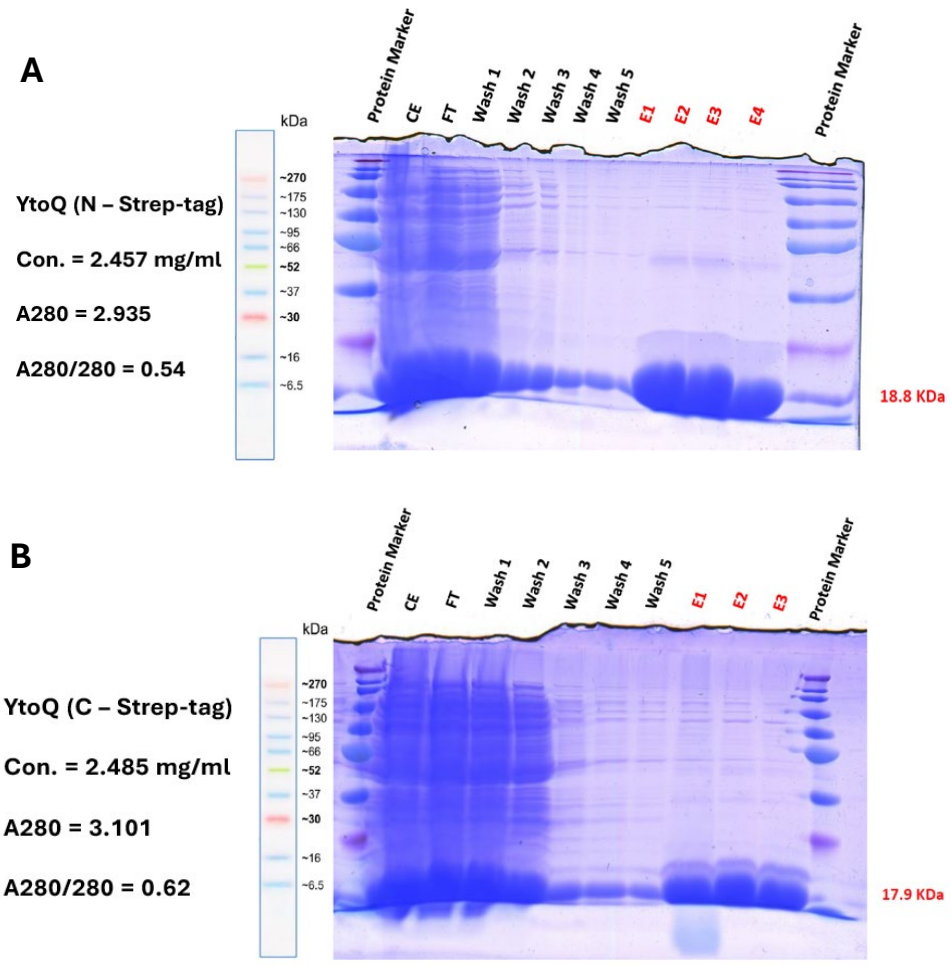

Figure S3. Purification of YtoQ protein by affinity chromatography.

YtoQ protein, expressed with **A)** an N-terminal Strep-tag (pBP641) or **B)** a C-terminal Strep-tag (pBP642), was purified using affinity chromatography. The purified proteins were subsequently dialyzed overnight against 1,000 volumes of Buffer W (1x). The purity of the samples was assessed by SDS-PAGE 15%, followed by Coomassie staining for visualization.

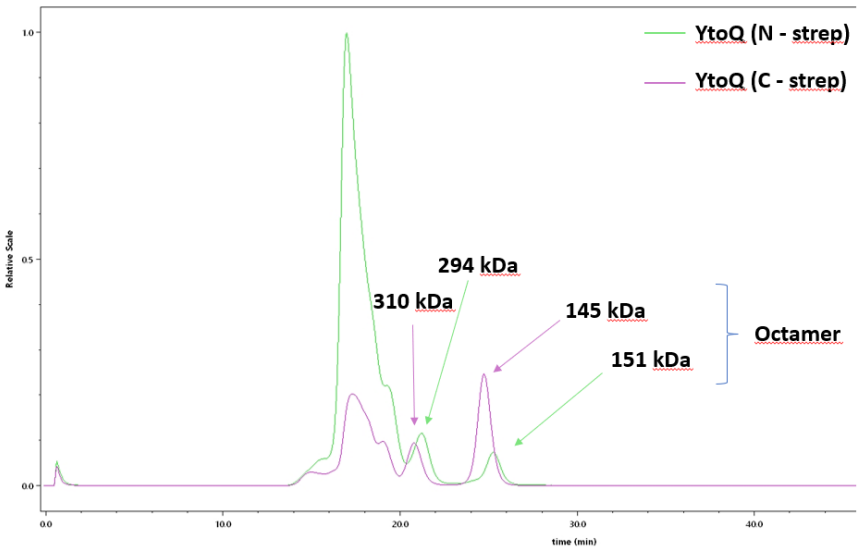

Normal conformation

	Peak 1				Peak 2				
	Mw (kDa)	Injected mass (µg)	Calculated mass (µg)	Mass recovery (%)	Mw (kDa)	Injected mass (µg)	Calculated mass (µg)	Mass recovery (%)	Mw (kDa)
20230421_YTOQ N terminal	151.3 (±0.3%)	112.00	14.91	13.3	310.5 (±0.1%)	112.00	12.24	10.9	479.5 (±0.0%)
20230421_YTOQ C terminal_Experiment6	145.3 (±0.1%)	112.00	51.53	46.0	294.0 (±0.2%)	112.00	9.94	8.9	757.1 (±0.2%)
Average	148.3	112.00	33.22	29.7	302.3	112.00	11.09	9.9	618.3
Standard deviation	4.2	0.00	25.89	23.1	11.7	0.00	1.63	1.5	196.3
% Standard deviation	2.9	0.00	77.95	78.0	3.9	0.00	14.71	14.7	31.7
Minimum	145.3	112.00	14.91	13.3	294.0	112.00	9.94	8.9	479.5
Maximum	151.3	112.00	51.53	46.0	310.5	112.00	12.24	10.9	757.1

Peak 3				Peak 4			
Mw (kDa)	Injected mass (µg)	Calculated mass (µg)	Mass recovery (%)	Mw (kDa)	Injected mass (µg)	Calculated mass (µg)	Mass recovery (%)
479.5 (±0.0%)	112.00	8.16	7.3	1153.3 (±0.1%)	112.00	42.95	38.4
757.1 (±0.2%)	112.00	18.31	16.3				
618.3	112.00	13.24	11.8	1153.3	112.00	42.95	38.4
196.3	0.00	7.18	6.4	n/a	n/a	n/a	n/a
31.7	0.00	54.23	54.2	n/a	n/a	n/a	n/a
479.5	112.00	8.16	7.3	1153.3	112.00	42.95	38.4
757.1	112.00	18.31	16.3	1153.3	112.00	42.95	38.4

Figure S4. SEC-MALS Analysis of YtoQ Protein.

Size exclusion chromatography coupled with multi-angle light scattering (SEC-MALS) was utilized to evaluate the molecular mass, hydrodynamic radius, and interaction properties of the YtoQ protein. A total of 500 µg of purified YtoQ protein was analyzed from two constructs: **A)** YtoQ with an N-terminal Strep-tag and **B)** YtoQ with a C-terminal Strep-tag. The experiments were conducted using a SEC-MALS-HPLC system with Buffer W (1x) as the mobile phase. The molecular characteristics were determined by measuring the intensity of scattered light.

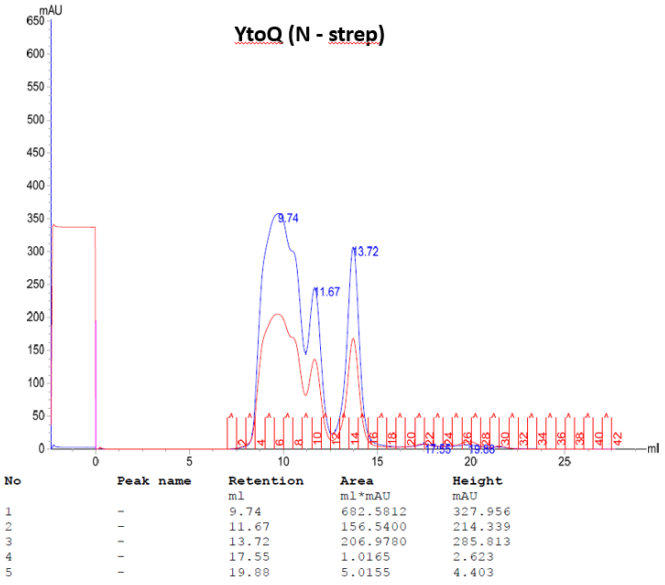

No	Peak name	Retention ml	Area ml*mAU	Height mAU
1	-	9.74	682.5812	327.956
2	-	11.67	156.5400	214.339
3	-	13.72	206.9780	285.813
4	-	17.55	1.0165	2.623
5	-	19.88	5.0155	4.403

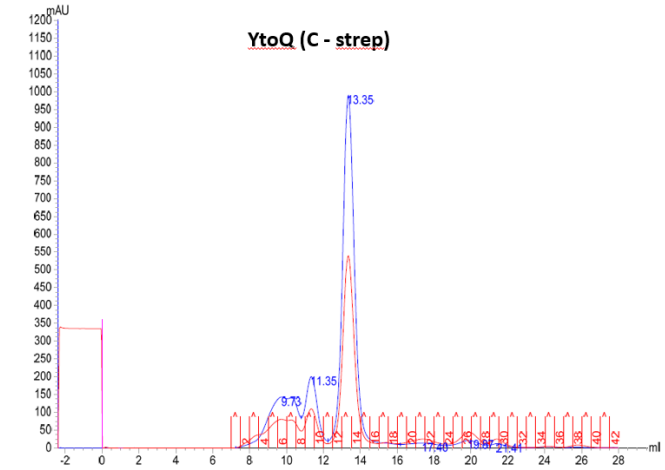

No	Peak name	Retention ml	Area ml*mAU	Height mAU
1	-	9.73	265.8214	143.250
2	-	11.35	158.9459	200.388
3	-	13.35	768.6967	989.819
4	-	17.40	27.3984	13.561
5	-	19.87	30.0785	21.668
6	-	21.41	11.7629	12.120

Figure S5. Size Exclusion Chromatography and Fraction Analysis of YtoQ Protein. Size exclusion chromatography was used to separate fractions of YtoQ protein. Fraction 14, from both the N-terminal Strep-tagged and C-terminal Strep-tagged constructs, was identified as the octameric and native functional form of the YtoQ protein.

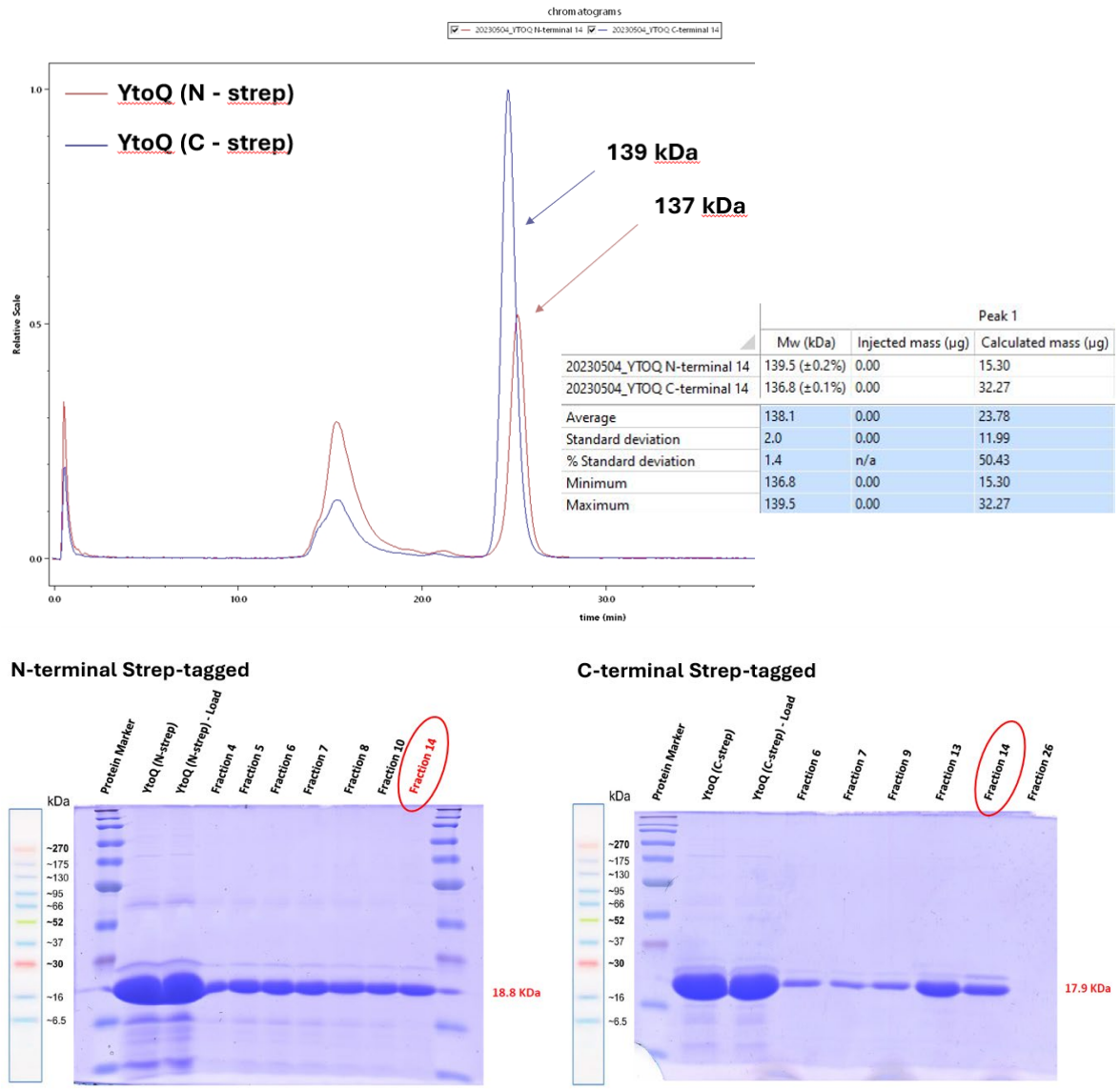

	Peak 1		
	Mw (kDa)	Injected mass (µg)	Calculated mass (µg)
20230504_YTOQ N-terminal 14	139.5 (±0.2%)	0.00	15.30
20230504_YTOQ C-terminal 14	136.8 (±0.1%)	0.00	32.27
Average	138.1	0.00	23.78
Standard deviation	2.0	0.00	11.99
% Standard deviation	1.4	n/a	50.43
Minimum	136.8	0.00	15.30
Maximum	139.5	0.00	32.27

Figure S6. SEC-MALS Analysis of Fraction 14 (Octameric YtoQ Protein). Fraction 14, representing the octameric form of the YtoQ protein, was analyzed using SEC-MALS to confirm its molecular mass. Both N-terminal Strep-tagged (pBP641) and C-terminal Strep-tagged (pBP642) constructs were assessed to provide a second validation of the molecular mass of the correctly assembled octameric format. Additionally, fraction 14 from both constructs was resolved on SDS-PAGE to evaluate protein purity and confirm the expected molecular weight.

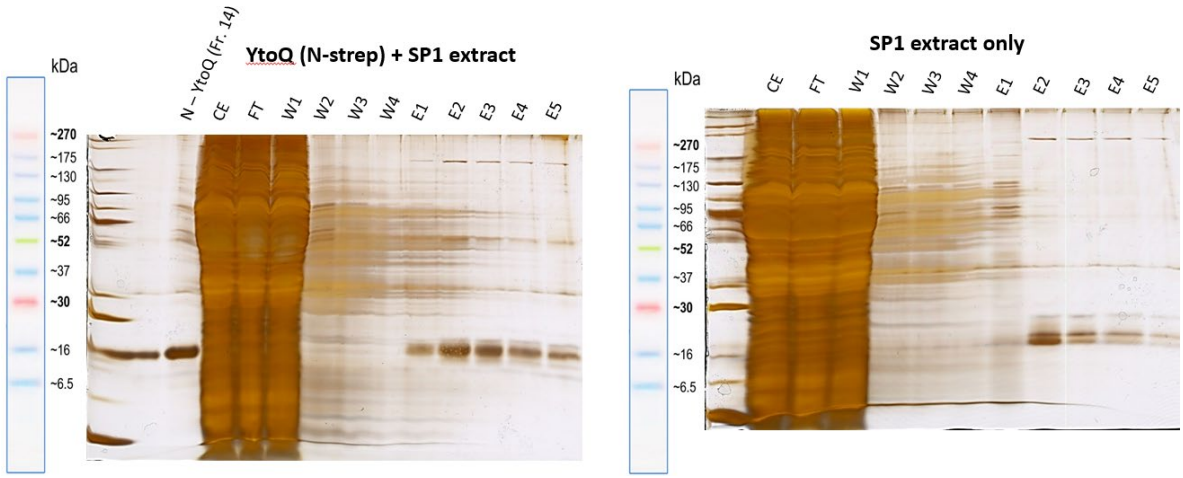

Figure S7. Identification of Potential YtoQ Interaction Partners Using *B. subtilis* Crude Extracts. A total of 200 µL of fraction 14, containing the N-terminal Strep-tagged variant of YtoQ protein, was mixed with 15 mL of cell-free crude extracts from *B. subtilis* SP1. The mixture was incubated at 37°C for 30 minutes. After incubation, the samples were subjected to SDS-PAGE analysis and visualized using silver staining to identify potential interaction partners of the YtoQ protein.